PRE-CLINICAL DEVELOPMENT OF VITAMIN B12 PHOTOACTIVATABLE THERAPEUTICS

Emilia M. Zywot

A dissertation submitted to the faculty at the University of North Carolina at Chapel Hill in partial fulfillment of the requirements for the degree of Doctor of Philosophy in the Division of Chemical Biology and Medicinal Chemistry in the Eshelman School of Pharmacy.

Chapel Hill
2021

Approved by:

David S. Lawrence

Shawn D. Hingtgen

Lindsey I. James

Michael B. Jarstfer

Teresa K. Tarrant

ABSTRACT

Emilia M. Zywot: Pre-Clinical Development of Vitamin B12 Photoactivatable Therapeutics
(Under the direction of David S. Lawrence)

Photoactivatable therapeutics are targeted light-activated drug delivery systems composed of a therapeutic cargo appended to a photoresponsive moiety, which releases the cargo upon illumination. These targeted therapeutics have the potential to diminish toxicity and improve efficacy of the therapeutic cargo due to the temporal and spatial control provided by external light controlled therapeutic release. The introduction of this dissertation describes the precedent set by clinically approved photodynamic therapy and currently available photoresponsive moieties. Together, this background contributes to the proposed pre-clinical development plan for photoactivatable therapeutics.

Vitamin B12, or cobalamin (Cbl), has shown exciting potential as a photoresponsive moiety with inherent photoresponsivity and minimal toxicity. Herein, two Cbl-based photoactivatable therapeutics encapsulated in red blood cells (RBCs) are developed. *In vivo* studies of a Cbl RBC chemotherapeutic and anti-inflammatory drug demonstrate localized delivery and efficacy comparable to standard of care respectively. Together, the advances contribute to the pre-clinical development plan for Cy5-Cbl photoactivatable therapeutics proposed in the conclusion. Overall, photoactivatable therapeutics, and Cy5-Cbl therapies specifically, are not far from first in human trials.

This work is dedicated to my family, who came to America to provide me with the endless opportunities I have had

ACKNOWLEDGEMENTS

The opportunity to pursue a Ph.D. at the University of North Carolina Chapel Hill and my resulting success would not have been possible without the support and mentorship of many. I would first like to thank my advisor, Dr. David S. Lawrence, for teaching me all that he could. I would also like to thank Dr. Teresa K. Tarrant for providing vital biological, animal, and clinical expertise to my dissertation work. I would like to thank my committee, Drs. Shawn Hingtgen, Lindsey James, Teresa Tarrant, and Michael Jarstfer, for being advocates of my abilities and fair critics of my research findings.

I would like to thank all the Lawrence lab members for their dedication to mentorship and to the community of support we foster together. To my research mentors, Drs. Christina Marvin and Lauren Haar, thank you for teaching me a range of skills from critical scientific thought, problem solving, to technical assay skills. Thank you for always supporting my passion and curiosity for science and helping me develop a resilience to failure and doubt. I would also like to thank the chemistry team, without your reliable syntheses we would never have been able to make the pre-clinical progress we have made: Dr. Song Ding, Dr. Qunzhao Wang, and Joshua Welfare. I would like to thank the co-authors of my first author publication for their meticulous work which contributed important findings to the manuscript: Dr. Natalia Orlova, Dr. Victoria Wickenheisser, Emily Rabjohns, and Rishi Rampersad. The findings highlighted in this dissertation work also include the hard-work and research advice of the UNC cores and other collaborators. Thank you for always being a pleasure to work with: Dr. Ramiro Diaz, Dr. Sebastien Coquery, and Dr. Nancy Fisher for teaching me flow cytometry, Mark Ross and Charlene Santos for all the help with animal handling, and Dr. William Zamboni and Dr. Allison Schorzman for our

pharmacokinetics collaboration. I would like to thank the current and previous lab members and our collaborators that provided me with research advice and mentorship: Dr. Marissa Berry, Dr. Natalia Orlova, Dr. Anwesha Goswami, Dr. Colin O'Banion, Dr. Qunzhao Wang, Dr. Song Ding, Dr. Brianna Vickerman, Joshua Welfare, Emily Rabjohns, and Rishi Rampersad. I would also like to thank the other members of the Lawrence lab who contribute to the supportive, friendly culture of our group: Dr. William Kinney, Dr. Fei Lou, Caylie McGlade, Gabby Gerlach, Joshua Welfare, Elizabeth Redding, and Ju-Sung Kim**.**

As the Ph.D. is a huge milestone in my professional development, I would be remiss to not mention the amazing people who have supported my career. I would like to thank my high school biology teacher, who initially promoted research to me and Dr. Amit Singh who provided me with my first research opportunity. I would also like to thank Dr. Terri Gustafson and Dr. Karl Werbovetz whose unending support during my undergraduate research established a foundation of scientific techniques, writing, and problem-solving skills. I would like to thank the intelligent, passionate women of our lab who have continued to support me and my career goals throughout my UNC years: Drs. Lauren Haar, Anwesha Goswami, Marissa Berry, Natalia Orlova, and Brianna Vickerman. Outside of the lab, I would like to thank the CCBTP community especially Dr. Adrienne Cox, Dr. Beka Layton, Dr. Michael Jarstfer, Dr. Craig Lee, and the UNC Blood Research team: Marcus Layer, Laura Finerty, Amy Brightwood, Brett Phillips, Dr. Raj Kasthuri, and Dr. Nigel Key. Thank you all for your professional mentorship and support in helping me achieve my career goals.

I would not have been successful without the people that brought love, laughter, and joy into my life. Thank you for always being a respite from the stress of graduate school: the board game community (especially Liz, David, Aly, Bryan, and Jacob: thank you for teaching me how to be comfortable with being different), the best co-chef Rachel, my D&D buddies, my concert friends, my biophysics colleagues, the board game designers community, my BBSP colleagues, the 2018 GSO team, and my CBMC colleagues. Also, a general thank you to all the people who have come and gone from my life, for being a part of my journey.

This work is dedicated to the people that have always provided me with kindness, guidance, and support. Thank you Reem Hakeem and Gabriella Budzieziewski for your scientific input on my work, for helping me believe justice is possible, and, of course, feeding me. Reem, thank you for helping me grow up during my first year of graduate school. I will forever admire and strive to achieve a comparable cool-headed power to that which you hold. Dr. Lauren Haar, thank you for always being an amazing mentor, teacher, and friend and for helping me believe we can contribute to something great. To my undergraduate friends who have continued to fill my life with a constancy of care and support: Ian Kirchner, Jared Duffy, and Varun Rao. To my aunts, uncles, and cousins in Europe, who have always welcomed me with open arms. Most of all, I would like to dedicate this to my closest family: Aluś, Mama, Tata, i Babcia. I will always strive to embody your never-ending belief in me and my potential. Tata, thank you for keeping me company the many, many late nights in lab. Your constant emotional support has helped me get through some of the worst struggles. Mama, thank you for always feeding me and for being an amazing travel partner who has strived to show me the world. Aluś, thank you for guidance through the hardest moments of my career and the mentorship you have provided me. I will forever use the skills you taught me. Babcia, dziękuje że zawsze byłaś jak moja druga matka. Nigdy nie zapomnę co to jest dobre jedzenie. Nie mogę się doczekać do następnego razu jak zjem twoja kuchnie.

TABLE OF CONTENTS

LIST OF SCHEMES

LIST OF FIGURES

LIST OF TABLES

LIST OF ABBREVIATIONS

ADC	antibody drug conjugate
ADME	absorption, distribution, metabolism, and excretion
ALA	5-aminolevulinic acid
AMD	age related macular degeneration
ANOVA	analysis of variance
AQ	amino-1,4-benzoquinones
ATP	adenosis 5'-triphosphate
AUC	area under the curve
Azo	azobenzene
BPDMA	benzoporphyrin derivative monoacid ring
bis-SorbPC	bis[10-(2′,4′-hexadienoyloxy)decanoyl]-sn-glycero-3-phosphocholine
BODIPY	boron-dipyrromethene
BSA	bovine serum albumin
ºC	degrees Celsius
CAIA	collagen antibody induced arthritis
Cbl	cobalamin
Cbl-CN	cyanocobalamin
CDT	1,1-carbonyldiiimidazole
CFSE	carboxyfluorescein succinimidyl ester
cm	centimeter
CMC	chemistry, manufacturing, and controls

CO	carbon monoxide
CO_2	carbon dioxide
CuOAc	copper (I) acetate
Cy5	cyanine 5 fluorophore dye
DASA	donor acceptor stenhouse adducts
DBU	diazabicycloundecene
DCM	dichloromethane
$DC_{8,9}PC$	1,2 bis(tricosa-10,12-diynoyl)-*sn*-glycero-3-phosphocholine
DDS	drug delivery system
Dex	dexamethasone
DMEM	Dulbecco's modified Eagle's medium
DMSO	dimethyl sulfoxide
DI	deionized
DiD	1,1-dioctadecyl-3,3,3,3-tetra-methylindodicarbocyanine
DiI	1,1-dioctadecyl-3,3,3,3-tetra-methylindocarbocyanine
DIPEA	diisopropylethylamine
DMF	dimethylformamide
DNA	deoxyribonucleic acid
DPBS	Dulbecco's phosphate buffered saline
ED_{50}/ EC_{50}	effective dose/ concentration 50%
EDA	ethylenediamine
EPR	enhanced permeation and retention
eq	equivalent(s)

ES-MS	electrospray ionization mass spectrometry
FBS	fetal bovine serum
FDA	Food and Drug Administration
FLS	fibroblast like synoviocyte
Fmoc	fluorenylmethyloxycarbonyl protecting group
Fmoc-OSu	9-fluorenylmethyl N-succinimidyl carbonate
FSC	forward light scatter
GBM	glioblastoma
GFP	green fluorescent protein
GLP	good laboratory practice
GMP	good manufacturing practice
GRα	glucocorticoid receptor α
h	hour
H_2O	water
H_2S	hydrogen sulfide
HABI	hexaarylbiimidazoles
HATU	hexafluorophosphate azabenzotriazole tertramethyl uronium
hct	hematocrit
HCTU	O-(1H-6-Chlorobenzotriazole-1-yl)-1,1,3,3-tetramethyluronium hexafluorophosphate
Hgb	hemoglobin
HPD	haematoporphyrin derivatives
HPLC	high-performance liquid chromatography

hRBC	human red blood cell
HTI	hemithioindigos
Hz	Herz
ICG	indocyanine green
IND	investigational new drug application
i.p.	intraperitoneal
IRB	institutional review board
J	joule
kDa	kilodalton
kg	kilogram
LASIK	laser-assisted *in situ* keratomileusis
L-15	Leibovitz's L-15 medium
LC-MS	liquid chromatography mass spectrometry
LD_{50}/ LC_{50}	lethal dose/ concentration 50%
LED	light-emitting diode
LSMEANS	least square means
M	molarity
MB	microbubbles
MCH	mean cell hemoglobin
MCHC	Mean cell hemoglobin concentration
MCV	mean cell volume
MeOH	methanol
mg	milligram

MHz	megahertz
min	minute
mJ	millijoule
mL	milliliter
mM	millimolar
mm	millimeter
MMAE	monomethyl auristatin E
mOsm	milliosmole
mRBC	mouse red blood cell
MRI	magnetic resonance imaging
MSN	mesoporous nanoparticles
MTD	maximum tolerated dose
mW	milliwatt
N_2	nitrogen gas
N-Deboc	N-Boc deprotection
NAMPT	nicotinamide phosphoribosyl transferase
NDA	new drug application
nm	nanometers
nM	nanomolar
NO	nitric oxide
NOAEL	no observed adverse effect Level
NOEL	no observed effect level
NH_4Br	ammonium bromide

NH_4OH	ammonium hydroxide
NIR	near infrared
NP	nanoparticle
NSC	neural stem cell
PACT	photoactivated chemotherapeutic
PAL	phenylalanine ammonia lyase
PBS	phosphate buffered saline
Pc	phthalocyanine
PD	pharmacodynamics
PDT	photodynamic therapy
PEG	polyethylene glycol
PhotoCORM	photoactivatable CO releasing molecule
PhotoNOD	photoactivatable nitric oxide donor
PK	pharmacokinetics
PPG	photolabile protecting groups
PS	photosensitizer
PSFD	photosensitizer fluorescence detection
RA	rheumatoid arthritis
RBC	red blood cell
RES	reticuloendothelial system
RMS	root mean square
ROS	reactive oxygen species
Ru	ruthenium

s	second
SD	standard deviation
SPION	superparamagnetic iron oxide nanoparticles
SiPc	silicon phthalocyanine
SSC	side light scatter
TAX	docetaxel
TFA	trifluoroacetic acid
TI	therapeutic index
TxRed	Texas red fluorophore
USA	United States of America
UV	ultraviolet
UV-Vis	ultraviolet visible
VEGF	vascular endothelial growth factor
W	Watt
Xe	xenon
3D	3 dimensional
^{1}H NMR	proton nuclear magnetic resonance
ε	extinction coefficient
#	number
Φ	quantum yield
μL	microliter
μM	micromolar

μs	microsecond
λ	wavelength
λ_{max}	maximum excitation wavelength

CHAPTER 1: SUCCESSFUL TRANSLATION OF PHOTOACTIVATED DRUG DELIVERY SYSTEMS INTO THE CLINIC

1.1 An Introduction to Personalized Medicine and the Advent of Externally Controlled Drug Delivery Systems (DDSs)

Since the 1950s, scientists and clinicians have observed substantial variability in patient response to therapeutics. With the mapping of the human genome in 2003, this variability was correlated to the uniqueness of each person's genome. This discovery birthed the field of pharmacogenomics which seeks to understand how the genetic variation (among other individual variations) affect patient response to therapeutics.[1] Since pharmacogenomics, personalized medicine has expanded with the development of targeted therapies, especially in the field of cancer. These therapies include monoclonal antibodies and drugs conjugated to antibodies (antibody drug conjugates, ADCs) that target specific cellular biomarkers based on a cell's expressed genetics.[2] Such targeted therapies have been extremely successful as they minimize toxicity and improve efficacy in the treatment of cancer.

However, therapies developed specifically for a patient's genome – or in the case of cancer, the cancer's mutated genome – can only be applied to a small number of patients and a small number of cancers.[3] These limitations, as well as current scientific limitations in understanding how pharmacogenomics relate to complex diseases, contribute to the development of targeted therapies that do not rely on a patient's genome. Instead these targeted therapies seek to optimize when, where, and how much therapeutic is delivered based on the patient's unique needs. Scientists developed stimuli-responsive drug delivery systems (DDSs) to achieve such control. Stimuli-responsive DDSs employ a small-molecule or nanomaterial carrier that releases therapeutic in a localized space in response to exposure to a specific stimulus.

Table 1-1 highlights many of the stimuli investigated for DDSs and provides a brief summation of limitations and advantages of each system.[4]

Externally controlled DDSs (with responsivity to heat, light, magnetics, ultrasound, or electrical stimuli) provide clinicians and patients with control over the location of therapeutic delivery, when therapeutic release occurs, and potentially what dosage of therapeutic is delivered by controlling the location of stimulation, when the stimulation is applied, and how long the stimulation is applied respectively. Externally controlled DDSs can therefore minimize therapeutic toxicity and maximize therapeutic efficacy by minimizing therapeutic exposure systemically and improving the pharmacokinetics (PK) of therapeutic exposure at the target site. Consequently, these improvements lead to targeted cellular uptake and effect (pharmacodynamics, PD).

The range of safety and efficacy of any given drug is quantified by its therapeutic index (TI). The TI is calculated by the ratio of the highest dose of drug that results in no toxicity (also known as maximum tolerated dose, MTD) to the required dose to produce the desired efficacy.[5] There are many ways to determine the therapeutic index between *in vitro* cellular endpoints, *in vivo* animal endpoints, and clinical endpoints in patients. It is important to note that toxicologists and the Food and Drug Administration (FDA) often discuss safety in terms of the "No Observed Adverse Effect Level" (NOAEL) that indicates the MTD and the "No Observed Effect Level" (NOEL) which indicates the highest dose that has no effect (efficacious or adverse) on the subject. These data points are commonly used to determine an initial starting dose for Phase I clinical trials and relate to measuring a drug's TI.[6, 7]

Externally stimulated DDSs improve the TI by minimizing therapeutic toxicity and maximizing therapeutic efficacy by localizing treatment delivery.

Table 1-1 Advantages and limitations of stimuli-responsive DDSs for personalized medicine. Reprinted with permission.[4]

Table 1. Advantages and limitations of closed- and open-loop on-demand drug-delivery systems.

Stimulus	Advantage(s)	Limitation(s)
Biomarker	High target specificity	Stability, potential leakage and possible immunogenicity of enzymes or antibodies used in the delivery system
pH	Small changes in pH can result in significant chemical and physical changes in drug carrier	Limited to the clinical conditions that alter local pH
Electrical	Iontophoresis devices make electrical fields accessible in the clinic	Risk of damage to healthy tissue from electric source needed for deep tissue penetration (attenuation of stimulus)
	Safe levels of electrical field strengths have been extensively studied	Electroresponsiveness is affected by many environmental factors (e.g., composition of aqueous medium, concentrations of electrolytes, presence of ionizable molecules)
Heat	Cancer cells are sensitive to hyperthermia (i.e., apoptosis, increased sensitivity to radiation and chemotherapeutics)	Risk of superficial tissue damage from external heating source needed for deep tissue penetration (attenuation of stimulus)
	Thermally responsive drug-delivery systems are in clinical trials	
Light	Ability to sequentially trigger multiple payloads	Questionable safety and/or biodegradability of materials
	High degree of spatiotemporal precision	Safety risks and low tissue penetration for UV-Vis light
Magnetic	In addition to triggered delivery, capable of magnetically guided drug targeting and can act as a contrast agent for imaging	Potential toxicity from iron oxide
	Magnetically responsive drug-delivery systems are in clinical trials	Requires complex equipment set-up for adequate focusing, intensity and penetration depth
Ultrasound	Minimal safety risks with low intensity and short exposures	Risk of damage to tissues with high intensity and long exposures
	High degree of spatiotemporal precision	Low drug carrier stability

1.2 Photoactivatable DDSs Advance Personalized Medicine

Photoactivatable, or light-activated, DDSs are poised to advance personalized medicine by enabling patient directed treatment and clinical theranostic control (the combination of imaging both treatment location and releasing therapeutic). Considering both the sensitivity and external devices for the technology currently under development in **Table 1-1,** light is currently the most sensitive and accessible DDS. There are many light-based FDA approved home devices, including simple laser pointers and light emitting diodes (LED) systems.[8] To feasibly develop patient-controlled stimuli-responsive DDSs, patients need to have access to devices sufficiently powerful to stimulate therapeutic delivery. Further, to feasibly develop clinician-controlled theranostic drug imaging and delivery, imaging technology needs to be clinically available. LED-based systems are FDA approved for superficial applications, as well as biomedical imaging.[9] Conversely, current heat-based systems under development require high intensity heat sources, while magnetic systems depend on magnetic nanomaterials for control.[10, 11]

Thus, light-based DDSs only require clinical approval of a photoresponsive therapeutic to the available home devices or a DDS that provides both photoresponsive imaging and therapeutic delivery detectable by the clinically approved imaging devices to advance personalized medicine. Patient-controlled treatments would further personalize medicine by allowing patients to dose themselves in response to symptom development with more localized control and safety than even an oral pill may provide. Photoactivatable DDSs can also further personalize medicine by providing clinicians with the ability to optimize therapeutic distribution before activation, potentially diagnose the diseased tissue with imaging, and immediately measure and deliver quantified therapeutic doses. Both systems are close to reaching human translation as *in vivo* animal studies are already underway.

Beyond these novel applications of photoactivatable DDSs, photoresponsive therapies have been already clinically established. For example, photodynamic therapy (PDT): a cancer

therapy in which an injected photosensitizer (PS) produces cytotoxic reactive oxygen species (ROS) after exposure to light.[12] FDA approved lasers and fiber optic devices are employed in PDT to provide very high spatial and temporal control over the cytotoxic effects of ROS. PDT has proven that long wavelength light in the near infrared (NIR) spectrum (600 - 950 nm) – also known as the optical window of tissue – can successfully penetrate tissue to cm depths. Other wavelengths, outside of the optical window of tissue, are predominantly absorbed by water and hemoglobin (**Figure 1.1**).[13, 14]

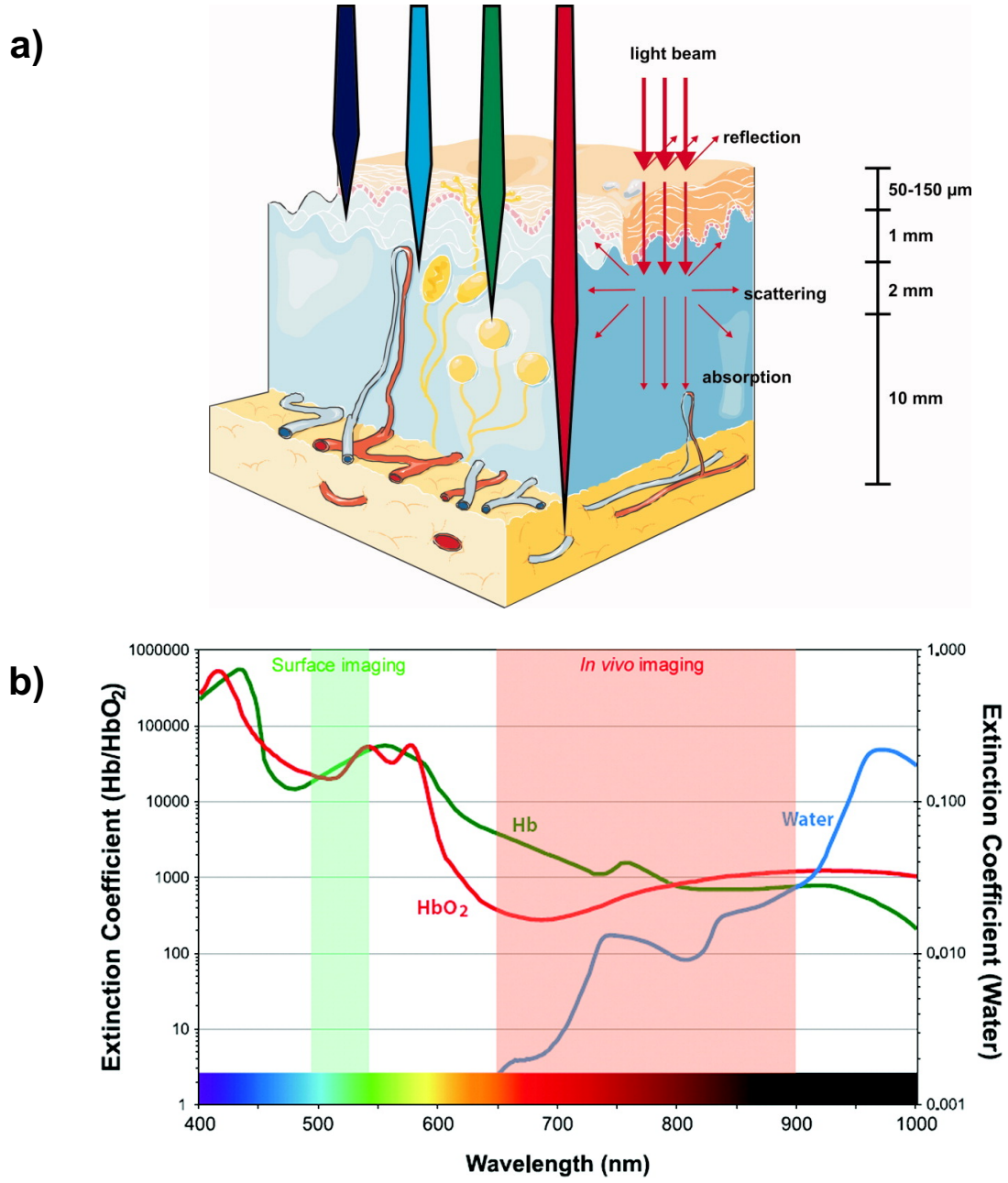

Figure 1.1 The optical window of tissue presented by **a)** a schematic of how different wavelengths of light propagate through tissue and **b)** absorbance of water, oxygenated hemoglobin, and deoxygenated hemoglobin, across the visible wavelength spectra. The optical window of tissue is highlighted in red. Both figures are reprinted with permission.[13, 14]

Photoactivatable DDSs and therapeutics differ from PDT, which are both included in the umbrella term “photoresponsive therapies”. Photoactivatable DDSs release and deliver therapeutic cargo upon illumination, while PDT PSs generate ROS species by reducing environmental oxygen upon illumination. Photoactivatable DDSs are composed of therapeutic cargo and a photoresponsive moiety, that releases the therapeutic in response to illumination which then proceeds to produce the desired pharmacological effect. These photoresponsive therapies can also include carriers (nanomaterial or cellular drug delivery vehicles) and require light and a light source (**Figure 1.2**). Since PDT has already achieved FDA approval, it is important to consider the challenges this photoresponsive therapy faced to achieve approval as precedent for similar challenges photoactivatable therapeutics may encounter.

NIR responsive systems are amenable to the desired safety and accessibility for patient-controlled stimulation, provide means by which to both image and deliver therapeutics, and have achieved precedential approval with PDT. This Chapter will thus focus on DDSs which release an active therapeutic substance in response to light, while considering the precedent PDT has already established in the clinic (section 1.4 and section 1.3 respectively). The Chapter will then describe the components of photoactivatable DDSs in the context of biological relevance and the necessary steps to develop these therapies with the end-goal of patient trials (section 1.5).

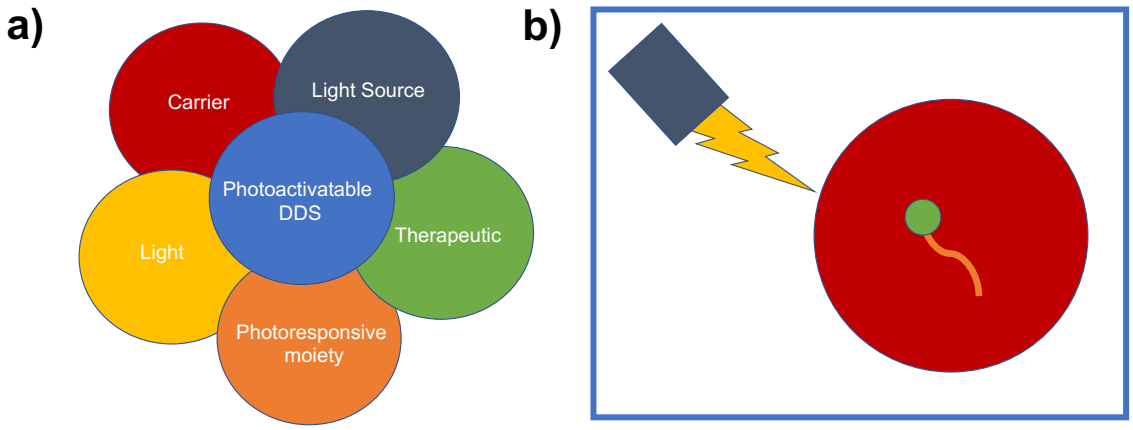

Figure 1.2 Designing Photoactivatable DDSs. a) The components of photoactivatable DDSs. **b)** A schematic illustrating the components of a photoactivatable DDS. The components follow the color coding from **a)**.

1.3 Current FDA Approved Photoresponsive Therapies and Devices

With the isolation of naturally photoresponsive chemicals in the early 1900's by Professor Herman von Tappeiner, light-responsive therapeutics were introduced into Western medicine and the first PDT tested for cancer.[15] After the work of Tappeiner, the PS haematoporphyrin and its derivatives (HPD) were discovered, developed, and finally tested in systematic human trials in 1978.[15] Dougherty and Gomer worked on the development of HPD from 1978 to the early 1990's, finally achieving approval of Photofrin in 1993 for the treatment of bladder cancer and in 1995 for esophageal cancer.[16, 17] Since then, multiple second-generation PSs have been clinically approved, with now even third-generation PSs that employ nanocarriers and ADCs under clinical development.[17] With more than 100 years of development, PDT and its associated approved irradiation sources light the stage for the clinical approval of photoactivatable DDSs.

1.3.1 Photosensitizers (PSs)

PSs are substances that interact with cellular substrates to produce ROS after exposure to light. These ROS, frequently singlet oxygen, induce cell death by multiple mechanisms including apoptosis, necrosis, and autophagy of cells as well as damaging surrounding vasculature.[18] Thus, PSs have been heavily developed for cancer applications due to their localized toxicity, but have also been applied in dermatological indications and age-related macular degeneration (AMD) (**Table 1-2**). PSs are commonly macrocyclic compounds which include porphyrins, chlorins, bacteriochlorins, phthalocyanines, naptholocyanines, corroles, etc.

Table 1-2 Clinical characteristics of FDA approved photosensitizers, including their clinical excitation wavelength (λ), quantum yield (Φ), extinction coefficient (ε) at the clinical wavelength, approved indications, and method of administration.

Photosensitizer	**Tradename**	**λ (nm)**	**Administration**	Φ_Δ	**ε (M^{-1} cm^{-1})**	**Approved Indications**
Hematoporphyrin	Photofrin	630	IV	0.25[19]	3,000	Esophageal cancer, endobronchial non-small cell lung cancer, High grade dysplasia Barrett's esophagus
Benzoporphyrin derivative monoacid ring A (BPDMA), Verteporfin	Visudyne	690	IV	0.82[19]	13,500	Age-related macular degeneration
5-aminolevulinic acid (ALA)	Levulan, Gleolan, Ameluz	635	Oral, topical gel, and solution	0.54[19]	5,000	Actinic keratoses, photoimaging glioma
Methyl aminolevulinate*	Metvixia	635[20]	Topical cream	NA	NA	Actinic keratoses
Hexyl amino levulinate	Cysview	380-450[20]	Solution	NA	NA	Photo diagnosis of bladder cancer
Riboflavin	Photrexa	365	Solution	0.54[21]	13,000[22]	Keratoconus and Corneal Ectasia

*Discontinued; Φ_Δ: quantum yield of singlet oxygen; IV: Intravenous; NA: Not Available

1.3.1.1 Quantifying Photosensitizer Efficacy and Light Dosimetry

A PS's efficacy depends on its sensitivity to light, the amount of light exposure, and its ability to efficiently convert light to the pharmacological singlet oxygen. While these factors are easily measured during *in vitro studies*, *in vivo* measurements are complicated by the need to account for light attenuation, geometry, and penetration depth. Although more complex equations are required to truly assess PS efficiency, the following simple equation takes into account the necessary variables:

$$PS\ efficiency = \#\ singlet\ oxygen\ produced \propto \#\ photons\ absorbed\ by\ the\ PS\ x\ \Phi\ of\ the\ PS$$

Quantum yield (Φ), an intrinsic property of PSs, is the ratio of singlet oxygen generated to the number of photons absorbed and reported as a number between zero (no singlet oxygen generated) and one (all absorbed photons produce singlet oxygen). This probability of producing singlet oxygen is commonly measured under perfect conditions of excess PS, light, and oxygen, meaning the only limiting step in the process is how effectively the energy absorbed is transferred into producing ROS.[23] Poor PSs with a low Φ, release the absorbed energy as fluorescence, phosphorescence, or through other forms of vibrational energy (**Figure 1.3**). A PS with a Φ of one, will conversely always transform the energy from absorbed photons into singlet oxygen. Thus, multiplying the number of photons absorbed by Φ produces the total quantity of singlet oxygen generated. Limitations of an optimized PS occur due to limited environmental oxygen, such as in hypoxic cancers, and when few photons penetrate tissue. It is important to note, Φ does not indicate the rate of release. Therefore, even high Φs may require an hour or longer of illumination to produce enough therapeutic to produce the desired effect. Such periods may be unfeasible in the clinic due to the photoactivatable DDS diffusing away from the light source as well as the potential inability to illuminate patients for extended periods of time, depending on the application.

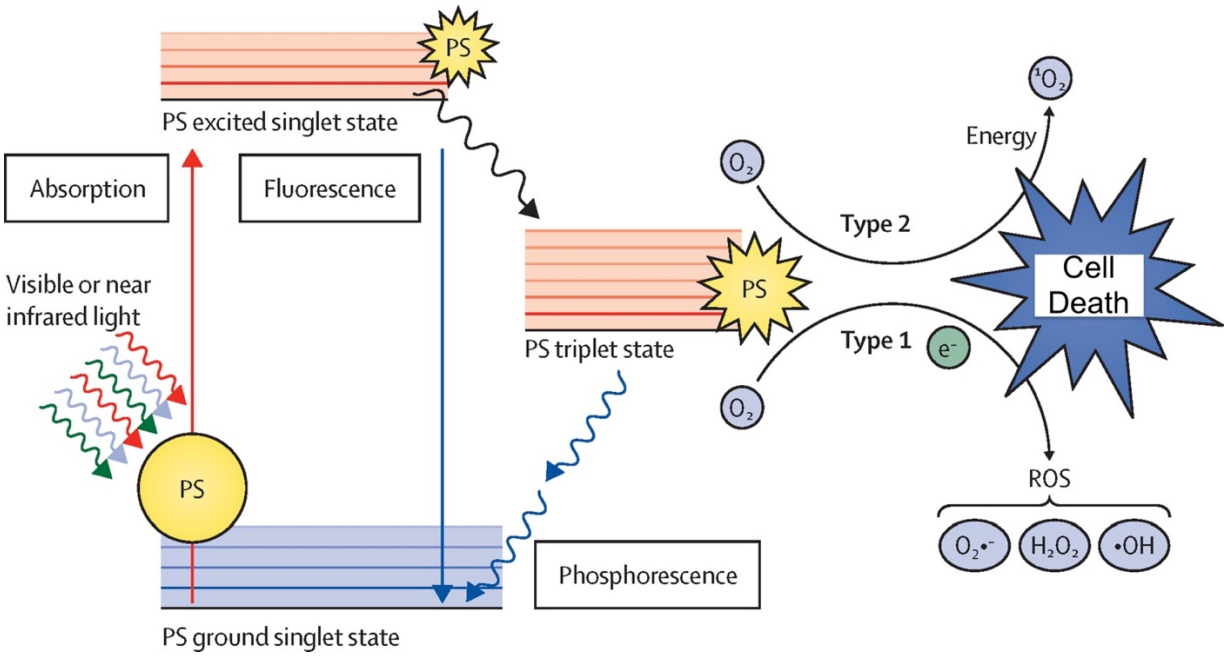

Figure 1.3 Jablonski Diagram illustrating light absorbed by PS (red) to excite electrons to the excited singlet state which can be converted to a triplet state by intersystem crossing (black). ROS can be generated by Type 1 and Type 2 mechanisms from the longer-lived triplet state. Energy can be lost by fluorescence or phosphorescence (blue arrows) decreasing the Φ. Adapted with permission.[24]

Multiple factors contribute to the number (#) of photons absorbed by the PS, including: the PS's extinction coefficient (ε) at the wavelength of treatment, the local dosage of light (J/cm^2), and the PS's concentration in the illuminated tissue.

A PS's ability to absorb photons at a specific wavelength of light, ε ($M^{-1}\ cm^{-1}$), is dependent on the solvent and concentration of PS.[25] Though the ε is easily measurable in solutions of water and ethanol, the environment of *in vivo* tissues can make quantifying the ε challenging.[26] **Figure 1.1b** demonstrates how the ε of hemoglobin and oxidized hemoglobin (left axis) as well as the ε of water, which is a $1x10^6$ magnitude lower (right axis), vary with wavelength. Within the optical window of tissue, the ε of hemoglobin ranges from 400 - 2,400 $M^{-1}\ cm^{-1}$.[27] The PS's ε should be sufficiently high to absorb as many photons as possible and outcompete the absorbance of hemoglobin and water, especially at NIR wavelengths.[28]

The local dosage of light the PS is exposed to within tissue is assessed by dosimetry.[28-31] Dosimetry evaluates the properties of the tissue (such as refractive index and architecture), the wavelength of light, geometry and intensity (mW/cm^2) of the light source, and the time of illumination to optimize the light penetrance and distribution through tissue. Tissue affects light penetrance by scattering, reflecting, refracting, and absorbing light. Scattering occurs at all visible wavelengths and is described by the transport scattering coefficient which is commonly found to be 1 - 2 orders of magnitude larger than the absorption coefficients of tissue.[28] However, the degree of scattering is very hard to accurately assess as it is highly dependent on the architecture of the tissue and the fluctuations in the tissue's refractive index.[32] Scattering leads to the dispersion of light and reduction in its intensity. Light is also reflected and refracted at the surface of tissue due to the refractive index mismatch at this boundary.[31] Light is then absorbed by water, hemoglobin, and pigments, such as melanin within tissue (**Figure 1.1**).[28] Wavelengths between 600 - 950 nm optimize penetrance to cm depth by minimizing absorption effects.[29]

The light device's geometry is also crucial to ensure the desired tissue is uniformly illuminated. To achieve optimal irradiation geometry, multiple delivery devices have been developed which include contact, non-contact, and interstitial (inserted into the tissue) optical fibers. These fibers can be applied individually, in a 3D array, by scanning mechanisms, and in light-diffusing mediums (**Figure 1.4**).[30, 31] Dosimetry is still limited in its ability to measure light distribution in human patients, while *in vitro* measurements do not truly mimic the complexity of tissue.[28]

The dosage (J/cm^2) of light the tissue is exposed to is measured by multiplying the intensity of the device by the total illumination time. For PSs, an optimal rate of illumination is required to ensure that the oxygen is being replenished at a similar rate in tissue.[28] The dosage can also be modulated by irradiating the target tissue for one continuous period of time, for staggered periods of times, or metronomically. Light sources with high power can cause tissue heating and eventual damage with prolonged periods of high intensity exposure. Metronomic treatments apply light at lower intensities for extended periods of time, which has been found to minimize tissue necrosis in PDT treatments.[28]

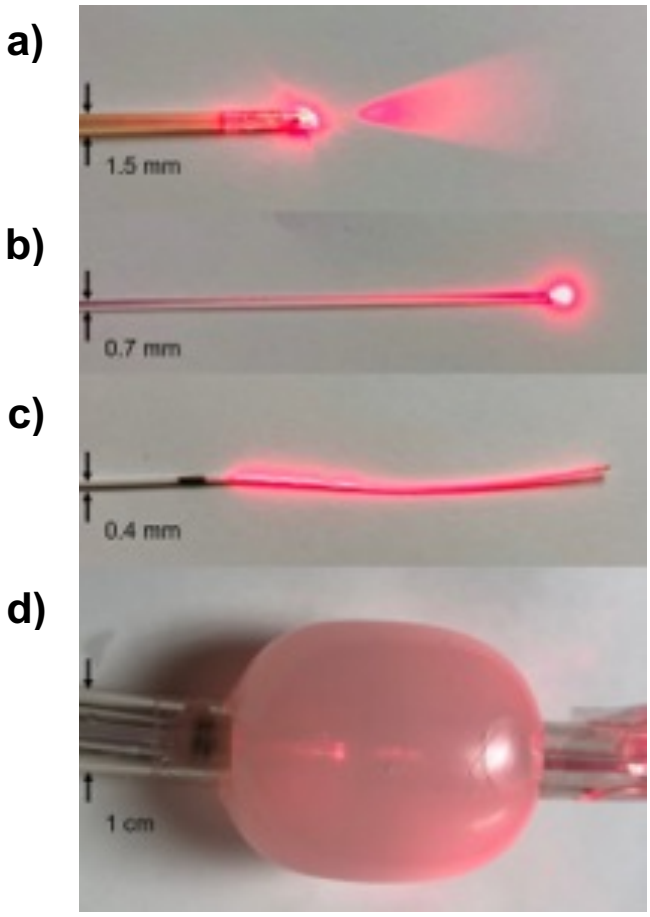

Figure 1.4 Examples of the diverse geometries of delivery devices for PDT. a) Microlens used for flat surfaces, **b)** spherical diffusor and **c)** cylindrical diffuser used in contact and interstitial applications, and **d)** balloon applicator scattering medium used for contact irradiation of interior tissue surfaces. Reprinted with permission.[31]

Finally, the PS's concentration in the irradiated tissue is measurable by PK methods *in vivo* and theranostic methods in the clinic. The concentration will correlate to the total amount of ROS produced and consequently the efficacy of the treatment. Thus, to achieve an optimal concentration it is crucial to understand how the PS distributes, the dosage to administer to the patient, and how much time after administration is required before irradiation. The concentration will vary between tissues in the body, between individual patients, and over time will undergo metabolism and clearance emphasizing the potential theranostics provide to PDT.[28]

Thus, optimal PSs should have a high Φ as well as a high ε at long wavelengths (especially for interstitial applications). Beyond photophysical considerations, optimal PSs also distribute well in the desired tissue, have minimal phototoxicity (lingering light sensitivity after treatment), and are patentable. Interestingly, the first developed PS, Photofrin, does not follow the prescribed guidelines closely.

1.3.1.2 FDA Approved Photosensitizers

Photofrin is known as the first PS developed and approved in 1995 for the treatment of esophageal cancer, which has since expanded to include treatment of lung cancer and early-stage cervical cancer. Due to its precedent in the PDT field as well as what are now considered sub-optimal properties, Photofrin is classified as a first-generation PS. Photofrin treatment occurs at 630 nm to achieve sufficient tissue penetration and efficacy in the clinic, even though its maximal absorbance peak occurs at 400 nm.[33] Photofrin treatment requires intravenous injection followed by illumination 48 h later with a laser connected to optical fibers or endoscopes.[12, 20] The Φ of Photofrin is a modest 0.25 while its ε is a subpar 3,000 cm^{-1} M^{-1}, which is within the range of hemoglobin's ε in the optical window of tissue. [14] Although, Photofrin was approved early on for the treatment of bladder cancer, over time adverse stenosis and other obstructive structures resulted from treatment which may have contributed to its disuse in that indication.[12] Limitations

of Photofrin include its weak absorption of NIR light, up to 90 days of phototoxicity, and solubility issues due to its hydrophobicity. Thus, Photofrin is limited to externally accessible tissues.[18]

Second generation PSs have been developed by discovering new photosensitizing macrocycles or modifying the core porphyrin structure to improve long wavelength sensitivity and Φs. In 1999, the PS 5-aminolevulinic acid (ALA) was approved for actinic keratoses and since has been also approved for acne, esophageal cancer, gastrointestinal cancer, and basal cell carcinoma, as well as imaging gliomas during brain surgery (Gleolan). Though not a macrocycle itself, ALA induces the cellular production of protoporphyrin IX, a derivative of porphyrin and highly photosensitive compound.[18] Although, ALA does not have an excessively high ε, its Φ is an efficient 0.54. ALA treatment requires topical or oral administration and laser or LED illumination for internal indications or skin cancers respectively. Derivatives of ALA have been developed and include methyl aminolevulinate (Metvixia) and hexyl 5-aminolevulinate (Cysview) which have been approved by the FDA for skin and bladder cancer respectively.[20] Metvixia was a topical cream with improved water solubility and efficacy which was used in the treatment of skin cancers. Metvixia was withdrawn in 2015 for undisclosed reasons (though not for safety concerns).[34]

Cysview and Gleolan are employed for PS fluorescence detection (PSFD) in bladder cancer and brain cancer respectively. PSFD improves established techniques to identify pre-invasive and early stage cancer by autofluorescence in the lungs, bladder, ovaries, skin, brain, and gastrointestinal tract. PSs act in general by selective uptake and retention in abnormal tissue which allows for imaging or treatment of this tissue. Both Gleolan and Cysview are fluorescently excited at their higher absorbance peaks in the short, 375 to 440 nm, wavelength range with low power devices (such as LEDs). PS-based diagnostic systems are currently being further developed into theranostic applications that would allow detection of abnormal tissue by harnessing the fluorescent and targeting properties of PSs that require low intensity devices and

then exciting PSs by high intensity lasers in the NIR range to treat the identified tissue.[35] Current applications of PSFD are limited to diagnosis and guided imaging for surgery.

Benzoporphyrin derivative monoacid ring A (BPMDA, commonly known as Verteporfin) has been approved for AMD. BPDMA acts by accumulating in abnormal blood vessels and can successfully damage these vessels when illuminated with long wavelength light.[12] BPDMA is administered intravenously followed by activation with an ophthalmoscope equipped with a 690 nm diode.[36] BPDMA has a very efficient Φ of 0.84 and an ε of 13,500 cm^{-1} M^{-1}. Further, Verteporfin induces minimal phototoxicity with complete systemic clearance of clinical doses after 2 days. Verteporfin PDT is now undergoing clinical investigation for cancer treatment after monoclonal antibody treatments surpassed BPMDA in the clinical treatment of AMD.[19]

Ultraviolet (UV) based PSs have also been approved in ophthalmologic indications with the approval of Riboflavin in 2016 for the treatment of keratoconus and ectasia. Topical application of a riboflavin solution to the eye is followed by ultraviolet A illumination to induce corneal crosslinking. ROS improve the stiffness of the cornea by creating crosslinked covalent connections between collagen molecules of the eye. Although, riboflavin has high Φ and ε, the need for UV illumination limits the treatment to superficial applications and low concentrations to avoid UV damage. Riboflavin itself is a natural vitamin and thus poses minimal toxicity and solubility concerns.[37]

Second generation PSs still produce adverse side effects, including phototoxicity, due to systemic administration, which have led to more targeted third generation PSs with improved solubility and clearance. By conjugating PSs to carrier biomolecules or targeting agents the specificity of treatment, safety, and efficacy can be improved. Though none of these systems have yet to be approved, they are under investigation with targeting tags, polymeric nanoparticles (NPs), polymeric micelles, nanostructured lipids, liposomes, and metallic NP carriers as methods of improving solubility, distribution, and minimizing toxicity.[18] Other porphyrin derivatives (such as

chlorins which are more responsive to long wavelength) and macrocycles (such as phthalocyanines) are being investigated for their use as PSs and have been approved by other regulatory administrations.

In general, further development of PSs faces many challenges that should be considered in the development of photoactivatable DDSs. The current FDA approved systems are limited to externally accessible regions of the body due to the minimal sensitivity of current PSs to long wavelength light. Second generation PSs that have high photosensitivity, such as Foscan (which has reached regulatory approval in Europe but was denied by the FDA), were discovered to be too potent and present high phototoxicity for multiple weeks. These more potent PSs also are commonly hydrophobic and face solubility issues.[12] In general, PSs are cytotoxic therapeutics and thus are limited to destructive applications (cancer, dermatologic and ophthalmic abnormal tissue). However, the clinical approval of these more toxic therapeutic systems with a limited range of applications, when compared to the photoactivatable DDSs described herein, provides precedent and promise for the eventual approval of photoactivatable DDSs.

1.3.2 Photosensitizer Light Sources

Devices for PDT include noncoherent light sources (e.g., conventional arc lamps, LEDs, and sunlight) and coherent light sources limited to lasers most commonly connected to fiber optics or endoscopy tubes. PDT light sources are currently used for surface illumination during skin treatment, intra-operative illumination using operating microscopes and endoscopes adapted with a light emitting source, or optical fibers coupled to a laser used intra-operatively and interstitially. Optical fibers are classified as non-contact, contact, and interstitial and are made from glasses and plastics which act to guide light through the fiber. Microlenses and diffusing tips are often added to optical fibers to modify the geometry of illumination (**Figure 1.4**). Optical fibers have been designed for bladder, anal cavity, cervix, and nasopharynx applications.[31] Light devices

must be approved as medical devices with specifications for the light dose (J/cm^2), wavelength of absorption (nm), and total time of exposure (min, s). FDA approved devices and doses are described by treatment and indication in **Table 1-3**.

Table 1-3 FDA Approved Light Sources, delivery devices, and light doses with PS, administration method, and indication

Photosensitizer (Tradename)	Admin-istration	Treatment Site & Indication	Light Source	λ (nm)	Light Dose (J/cm^2)	Time (min)	Delivery Device
Hematoporphyrin (Photofrin)[38]	IV	Oral Cavity and oropharynx *FOR* esophageal cancer, endobronchial non-small cell lung cancer,& high-grade dysplasia in Barrett's Esophagus	DIOMED solid-state laser diode *OR* Argon-pumped Rhodamine B-dye laser (Laserscope series 600 PDT dye molecule) *OR* Modulight ML7710	630	300 J/cm† (Esophageal) 200 J/cm† (Endobronchial) 130 J/cm† (Barrett's Esophagus) (200-400 mW/cm)	12 min 30 s 8 min 20 s 8–10 min 50 s	Microlens optical fiber 0.4 mm core for surface treatment Interstitial cylindrical Optiguide™ optical fiber diffuser (1 cm tip inserted 12-gauge angiocatch implantation) X-Cell Photodynamic Therapy Balloon with Fiber Optic Diffuser
Verteporfin (Visudyne)[39]	IV	Retina *FOR* Age related macular degeneration	Non-thermal diode laser: Lumenis Coherent Opal Photoactivator Zeiss Visulas 690s Biolitec Ceralas I Quantel Activis	689	50 (600 mW/ cm^2)	1 min 23 s	Fiber optic with a slit lamp and circular opening with ophthalmic magnification lens: Lumenis Coherent LaserLink adapter Zeiss Visulink PDT adapter Biolitec Ceralink Slit lamp adapter Quantel ZSL30 ACT, ZSL20 ACT, HSBMBQ ACT
ALA (Ameluz)[40]	Topical gel	Superficial (scalp, facial) *FOR* Actinic Keratoses	BF-Rhodo LED lamp	635	37	10 min	NA
ALA (Levulan)[41]	Topical solution	Superficial (scalp, facial) *FOR* Actinic Keratoses	BLU-U fluorescent lamp LumaCare Lamp	400-450	10	16 min 40 s	LumaCare Lamp has a variety of adjustable fiberoptic adapters
ALA (Gleolan)[42]	Oral	brain during surgery *FOR* imaging of grade III or IV glioma	LEDs with fluorescence guided imaging devices	375-440	40-80 mW/cm^2 *	NA	Standard Surgical operating microscope adapted with a blue light emitting sources
Methyl-ALA** (Metvixia)[43]	Topical Cream	Superficial (scalp, facial) *FOR* Actinic Keratoses	Aktilite CL128 LED Lamp	630	37	7-10 min	NA
Hexyl-ALA (Cysview)[44]	Intravesical solution	Bladder installation *FOR* diagnosis of bladder cancer	Karl Storz D-light C photodynamic diagnostic system using a Xenon lamp (Cermax Lamp)	360-450	NA	NA	cystoscope adapted with a blue light emitting source
Riboflavin (Photrexa)[45]	Topical Opthalmic Solution	Eyes *FOR* keratoconus and corneal ectasia	KXL system using a UVA laser	365	3 mW/cm^2	30 min	KXL system with circular delivery pattern

† measured per length of diffuser for the treatment of esophageal cancer

* No dosage due to imaging modality

** Discontinued

Non-coherent light sources are preferred for PDT as they are safer, easier to use, and less expensive.[36] Initially, filtered lamps were used, especially in applications requiring surface irradiation. Non-coherent lamp sources used for PDT include fluorescent, incandescent, metal halide, xenon arc, and sodium arc lamps. Excessive filtering is required to remove ultraviolet and infrared wavelengths which could cause thermal or genetic damage to the tissue.[31] Currently approved lamps for PDT include the BLU-U light illuminator in combination with ALA PDT for actinic keratosis and the LumaCare lamp for acne vulgaris. The BLU-U lamp is a fluorescent lamp which requires a dosage of 10 J/cm^2 (power output of 10 mW/cm^2) in the 402 - 432 nm region.[46, 47] The LumaCare lamp is a quartz halogen mixed lamp with a wavelength range of 400 - 800 nm and output power of 20 mW/cm^2 - 1000 mW/cm^2. The LumaCare's main strength is its adjustability in power and wavelength output which makes it amenable to a variety of PDT treatment protocols.[36]

LEDs have recently surpassed lamps due to their accessibility and compatibility with fiber optics, low cost, large application areas (treatments up to 150 mW/cm^2 over a 20 cm^2 area), arrangeable geometries, and variety of wavelengths (350 nm to 1100 nm).[46] Superficial applications using LEDs are considered FDA approved cosmetic procedures and are used in low level laser therapy.[9] Due to the generic clearance of LED light application, a multitude of light applicators exist and some have been approved in combination with ALA and methyl-ALA for actinic keratoses.[48, 49] Diagnostic systems such as Gleolan and Cysview also take advantage of cheap incoherent light sources, such as LEDs and lamps, as fluorescent excitation of PSs requires low power treatments.

Daylight is also gaining prominence as a cheaper light source for superficial PDT due to its high area of application, ability to achieve therapeutic activation, and decrease patient pain during treatment. With an approximate power of 2.5 mW/cm^2 in the 620 - 640 nm range, the sun does require longer periods of exposure (1.5 - 2 h) to achieve treatment and does include

exposure to UV-radiation.[30] Daylight PDT is being investigated with ALA and Metvixia in Europe. One very desirable aspect of the sun as a light source is that this "device" requires no FDA regulation.[50]

However, lasers (monochromatic, coherent light sources) are still the preferred light source for PDT due to their compatibility with optical fibers and production of high-power monochromatic light at the required wavelength. There are multiple kinds of lasers including dye lasers, diode lasers, and optical parametric oscillator lasers. Initially, the Laserscope PDT Dye Module, a potassium-titanyl-phosphate dye laser, was the most widely used laser for PDT treatment. It was then surpassed by the Diomed 630 PDT diode laser which was more portable, light weight, easier to use, and less expensive.[36] Since then the Modulight ML7710, a diode laser, has also been developed as a multichannel laser with laser outputs of 405 - 1064 nm and power output from 4.5 W to 70 W depending on the wavelength. Multiple diode lasers have been approved in combination with Verteporfin for retinal treatment of AMD. It is important to note that other lasers not specifically indicated for PDT are medically approved including excimer-based lasers for LASIK, home device lasers, the ND:YAG laser used for non-ablative dermatological purposes, and the Erbium-YAG lasers used for ablative dermatological purposes.[8, 51, 52]

1.4 Long-wavelength Photoactivated DDSs Under Development

To establish the current photoresponsive moieties for photoactivatable DDSs, the following section reviews photoremovable protecting groups (PPGs), photoswitches, and photogates (**Figure 1.5**). NIR photoresponsive moieties are crucial for any medical applications beyond dermatological indications as demonstrated by clinical PSs. Thus, the following review focuses on systems that are responsive to NIR wavelengths.

The first subsection describes PPGs, also known as photolabile, photoprotecting, photoactivable, photoreleasable, photocleavable, phototriggers, or photocaging groups. PPGs

are photoresponsive moieties (or scaffolds) that protect the therapeutic deliverable by inactivating it. Inactivation is commonly achieved by binding the therapeutic to a scaffold which cannot permeate into cells or by synthetically blocking a portion of the therapeutic that is crucial to its pharmacology. Upon irradiation by light the PPG irreversibly releases the therapeutic, most commonly by cleavage of the bond that binds the therapeutic to the PPG. The released therapeutic can then distribute into and effect the local tissue at the site of illumination.[53-55]

The second subsection describes NIR photoswitches under development that activate the therapeutic by undergoing reversable isomerization upon illumination. This photoisomerization includes double bond rotation, photo-oxidation, electrocyclization, and photo-crosslinking that can change conformation to improve therapeutic activity or induce drug release by hydrophilic/ hydrophobic transitions of nanocarriers. Photoswitches are being developed as molecular scaffolds as well as, more successfully, being integrated in liposome membranes, NPs, and other nanocarriers.[53, 56-59] Nanocarriers that employ photoswitches or PPGs as a photoresponsive gate ("photogate") for therapeutic release from the carrier are described in section 1.4.2 as well.

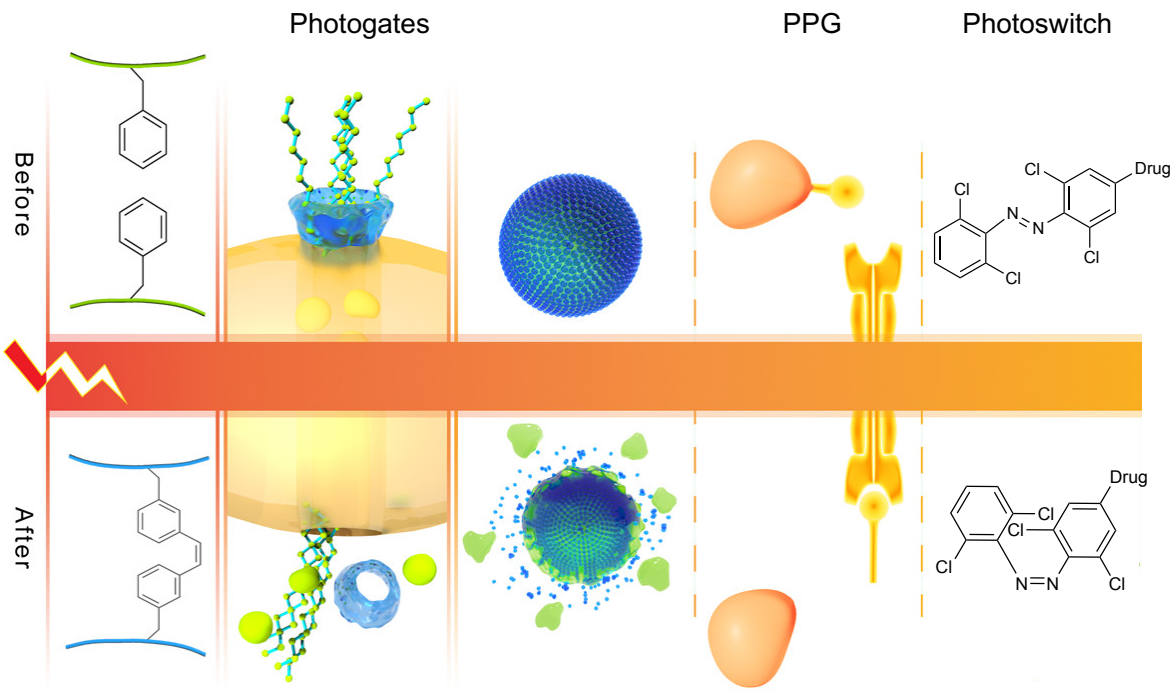

Figure 1.5 Photoactivatable DDSs as novel photoresponsive therapies. Adapted with permission.[59]

Both sections describe systems that are responsive to long wavelengths of light within the optical window of tissue (600 - 950 nm). Similar to ideal PSs, photoactivable DDSs require a high Φ of therapeutic release, which is achieved by removal of the scaffold for PPGs or isomerization of the photoswitch. Ideal photoactivatable therapeutics also require high ε at NIR wavelengths as these systems need to respond efficiently to minimal light penetration.[60] Prominent PPGs include boron-dipyrromethene (BODIPY), cyanine, cobalamin (Cbl), phthalocyanine (Pc), ruthenium (Ru), and amino-1,4-benzoquinones (AQ) while prominent photoisomerizers are azobenzenes (azo) and donor acceptor Stenhouse adducts (DASAs). Photogated nanomaterials under development with both systems include mesoporous nanoparticles (MSNs), micelles, hydrogels, red blood cells (RBCs), and other NPs. **Table 1-4** describes these prominent examples under pre-clinical development from both sections as well as the associated Φs and εs. Note, the Φ for PPGs is measured by calculating the released therapeutic per photons absorbed, while the Φ for photoswitches is calculated based on the desired isomerization product per photons absorbed. *In vivo* studies include only animal studies while *in vitro* studies comprise benchtop studies outside and in cells.

Table 1-4 The photophysical properties, stage of development, and potential indications of prominent photoactivatable DDSs organized by photoresponsive moiety.

Photo-responsive Moiety	Therapeutic Cargo	λ_{max} (nm)	ε_{max} (M^{-1} cm^{-1})	$\Phi^{a,b,c,d,e}$	Stage	Potential Indications
BODIPY	Dopamine[61]	643	63,000	0.0001[f]	In Vitro	Cardiac function, neuronal signaling
BODIPY	NO[62]	677	>40,000[f]	NR	In Vivo	Cardiovascular, neuronal signaling, inflammatory conditions, cancer
BODIPY	H_2S[63]	688	55,400	0.00036[a,g]	In Vitro	Cardiovascular, anti-inflammatory, diabetes
BODIPY	CO[64]	652	52,000	0.000014[a,g]	In Vivo	Cardiovascular; anti-inflammatory; anti-microbial; antineoplastic
Cyanine	NA, ICG[65, 66]	800-850	121,000	0.03-0.12[b,h]	FDA approved	Imaging of cardiac output, hepatic function, blood flow before during and after surgery; imaging lymph nodes in cervical and uterine tumors; ophthalmic angiography,
Cyanine	CO[67]	793	251,000	0.0003[a]	In Vivo	Cardiovascular; anti-inflammatory; anti-microbial; antineoplastic
Cyanine	Camptothecin[68]	720	N.R.	NR	In Vivo	Cancer
Cyanine	Duomarcyin[69]	750	70,000	NR	In Vivo	Cancer
Cyanine	Cisplatin[70]	790	45,000	NR	In Vitro	Cancer
Cbl	Colchicine[71]	780	NR	NR	In Vitro	Cancer
Cbl	Docetaxel[72]	645	250,000	NR	In Vivo	Cancer
Cbl	Dexamethasone[73]	645	250,000	NR	In Vivo	Cancer, Inflammatory diseases
Aluminum Pc	Photosens[74]	683	200,000	NR	Approved In Russia	Breast Cancer
SiPc	Combretastatin[75]	693	99,700	0.1[b,i]	In Vitro	Cancer
Ru (II)	Abiraterone[76]	535	9,850[c]	0.018[b]	In Vitro	Prostate Cancer
Ru (II)	NAMPT inhibitor[77]	535	609[j]	0.013[j]	In Vitro	Cancer
Ru (II)	Rigidin[77]	530	1,510	0.0038[e]	In Vivo	Cancer
1.4.2 Photoswitches and Photogates						
Azo	DENAQ[78]	~480	26,772[f]	NR	In Vivo	Age-Related Macular Degeneration; Retinitis Pigmentosa
trans-Azo	Trimethoprim[79]	365	18,111	0.18[a, g, k]	In Vitro	Anti-bacterial
Cis-Azo	Trimethoprim[79]	NR	1,282	0.02[a, g, k]	In Vitro	Anti-bacterial
Azo MSN	Doxorubicin[80]	~480	low	NR	In Vitro	Cancer
DASA micelle	Paclitaxel[81, 82]	553	~100,000[f]	NR	In Vitro	Cancer
Ru Hydrogel	TEM1 β-lactamase[83]	450	6,400	0.63	In Vitro	Protein Delivery
Cbl Hydrogels	None Tested[84]	660	127,500	0.074	In Vitro	Wound healing, Bone Defects, Protein Delivery
AQ NP	Paclitaxel[85]	550	NR	0.1[d]; <0.01[b]	In Vitro	Cancer
Cyanine Micelle	Camptothecin[86]	749	83,000[f]	NR	In Vivo	Theranostics for Cancer

NA not applicable; NR not reported; Φ were acquired in MeOH[a], aqueous media[b], DMSO[c], CH_2Cl_2[d], ACN[e]; [f]based on structurally related derivatives; [g]Irradiation was performed at 365 nm; [h]Φ of fluorescence; [i]Φ of singlet oxygen generation; [j]irradiated at 625 nm; [k]Φ of photoswitching

1.4.1 Long-wavelength Photolabile Protecting Groups (PPGs)

The first PPGs served to protect functional groups during synthesis in the 1960's.[87-89] The first biological applications of PPGs were *in vitro* tests releasing adenosine triphosphate and cyclic adenosine monophosphate.[90, 91] However, these groups were limited to *in vitro* applications due to their responsivity to only UV-light. Since then, many scaffolds have been structurally modified or discovered to respond to long wavelength light.

Boron-dipyrromethene (BODIPY) Scaffolds

BODIPY scaffolds are UV-responsive fluorescent dyes with high ε discovered in 1968. With pronounced stability in physiological conditions, inherent hydrophobicity, and subsequent cell permeability, these dyes originally gained biological prominence in uses for labelling proteins and DNA in cellular investigations.[92] Since their original discovery, modified *meso*-methyl BODIPYs have been developed with improved water solubility and photoresponsiveness to longer wavelengths of light (600 - 800 nm) by extending the π system and addition of polyethylene glycol (PEG) chains.[93]

Long wavelength BODIPY scaffolds have been developed for the delivery of dopamine[61], nitric oxide (NO),[62] carbon monoxide (CO),[64] and hydrogen sulfide (H_2S).[63] Many of these systems have been tested in cell lines, but only NO[62] and CO DDSs[64] have begun *in vivo* testing. *In vivo* results have demonstrated the safety of NO and CO systems and assessed the extent of therapeutic inactivation by BODIPY PPGs. BODIPY-NO have also been successfully developed for photoacoustic theranostic applications with detectable changes in their signal upon therapeutic release. Studies have successfully demonstrated localized treatment of xenografted mouse breast cancer by dual implantation of cancer into both mouse flanks and subsequent illumination of only 1 flank with the other flank acting as the "dark control". Applications of these BODIPY systems include cardiovascular diseases (dopamine, NO, CO, H_2S), neuronal signaling

(dopamine, NO), inflammatory conditions (NO, CO, H_2S), diabetes (H_2S), and cancer (NO, CO).[62, 94] Specifically, the gaseous molecules under investigation are established endogenous signaling molecules and thus have far reaching effects.[95] BODIPY scaffolds are also being modified for PDT.[19, 59]

Challenges facing BODIPY scaffolds include their low Φ, inherent hydrophobicity, and short wavelength responsivity of the core scaffold. Many synthetic modifications may be required to improve the Φ, potentially limiting structural flexibility to optimize multiple properties.[96, 97] Combinations with nanomaterials may improve the challenges associated with BODIPY's inherent cell permeability. However, the scaffold's low toxicity and strong fluorescence (with noted change in photoacoustic signal upon release of therapeutic) makes this a promising scaffold with theranostic potential.[58] Further, preliminary *in vivo* results demonstrate localized efficacy and minimal toxicity. Scientists moving forward with BODIPY photoactivatable DDSs should carefully consider the design to optimize the many strengths of BODIPY.

Cyanine Scaffolds

Like BODIPY dyes, cyanine scaffolds were first made in 1856 and have since become crucial fluorophores in chemistry and biology. Specifically, the heptamethine cyanine dyes have demonstrated long wavelength responsivity and minimal toxicity in the clinic. Indocyanine green (ICG) has been FDA-approved since 1959 for medical fluorescence imaging of ophthalmic angiography, cardiac output, hepatic function, liver blood flow, blood flow before, during, and after surgery, and imaging lymph nodes in cervical and uterine tumors.[98-100] Inherently, the cyanine scaffold is able to produce singlet oxygen in response to light which leads to the eventual photooxidative cleavage reaction and therapeutic release.[101] This multi-step reaction is a limiting factor for cyanine as the half-life of therapeutic release can take up to 20 - 30 min after illumination (tested at physiological pH, 30 J/cm^2 *in vitro*).[102]

Cyanine scaffolds have been developed as a source of ROS for PDT, and as a PPG for the therapeutic release of CO,[67] duocarmycin with the ADC panitumumab targeting agent,[69] cisplatin,[70] and camptothecin with a biotin targeting agent.[68] For PDT applications, cyanine PPGs had to be modified with a 2,2,6,6-tetramethylpiperidinyloxy ring to improve the singlet oxygen Φ from a sub-optimal 0.006 to a modest 0.20.[103] Again, *in vitro* and cellular testing have been mainstay testing methods of all these applications with CO, cyanine-camptothecin-biotin, and ADC-cyanine-duocarmycin systems additionally tested *in vivo*. Animal studies have demonstrated biocompatibility of the PPG therapeutics and successful enhanced targeting of systems with multiple layers of targeting. ADC-cyanine-duocarmycin and cyanine-camptothecin-biotin target cancer tumors externally by illumination and internally by a covalently bound targeting agent (in effect multiple layers of targeting, "multi-layered targeting") as demonstrated in metastatic breast cancer xenografted mice and in HeLa xenografted mice respectively.[67-69] Disease applications of the developed systems include the previously discussed applications of CO, as well as applications in cancer due to the highly cytotoxic nature of duocarmycin, camptothecin, and cisplatin. Duocarmycin is so cytotoxic that an additional targeting method with an ADC must be employed.[69]

For both multi-layered targeted systems, researchers imaged the time to achieve ideal biodistribution *in vivo*. Cyanine-camptothecin-biotin further displayed the biodistribution of inactivated and activated photoactivatable therapeutic due to its theranostic capabilities. By fluorescent imaging at 535 nm, which is only observed after therapeutic release, the cyanine PPG was observed to be activated in the liver and tumor even though only the tumor was exposed to 200 mW/cm^2 680 nm illumination. Further, control cyanine-camptothecin-alkyne was more extensively distributed throughout tissue for longer periods of time.[68] For treatment purposes, the ADC-cyanine-duocarmycin was further optimized in regard to the light dosage (time and power).

Efficacy of duocarmycin was assessed by both tumor size and survival rate from localized illumination for 2 min from an 800 mW/cm^2 laser.[69]

Multi-layered targeting of cyanines has extended beyond ADCs and biotin with the *in vitro* and *in vivo* development of the next-generation carrier-based theranostic cyanine-camptothecin. Cyanine-camptothecin was modified to create a self-assembling micelle that undergoes photolytic cleavage and therapeutic release only in hypoxic conditions. Excitingly, this micelle is responsive to both photoacoustic imaging and fluorescent imaging further enhancing the potential for theranostic applications. The micelle was also rendered pH-sensitive to improve therapeutic concentration in the acidic tumor environment (**Figure 1.6**). *In vivo* studies were completed by first imaging the biodistribution using photoacoustic imaging, and then releasing camptothecin from the cyanine micelles by NIR irradiation while monitoring the fluorescence shift of the system. Results validated the theranostic potential as well as the persistent localization of the cyanine therapeutic after 24 h.[86]

Although the ROS generated by cyanine PPGs are much more limited than Photofrin and other porphyrin-based PSs (due to the resulting cleavage and destruction of the cyanine after ROS release), it is important for PPG investigations with cyanine to differentiate between the clinical impact of ROS and the impact of the released therapeutic. Furthermore, like BODIPY scaffolds, cyanines are ideal fluorophores (as exemplified clinically by ICG) and thus face synthetic challenges to modify them into high Φ PPGs. These synthetic challenges have been addressed with more promising results as compared to BODIPY scaffolds due to the synthetic malleability of cyanine with multiple modification points, as demonstrated by the cisplatin scaffold and its 0.32 Φ. However, the success of the cisplatin scaffold's Φ may be potentially outweighed by the 5-fold decrease in ε. As previously discussed in section 1.3.1.1, therapeutic release depends heavily on the number of photons absorbed (which is significantly influenced by ε). Striking a balance between ensuring that the limited number of photons that penetrate tissue are

optimally absorbed and that the absorbed photons are successfully translated to therapeutic release is crucial.

Cyanine is a promising PPG as the scaffold has high inherent εs and there is extensive literary precedent beginning to overcome the previously discussed synthetic challenges.[69, 98] The major limitation of cyanine is its extremely low half-time of release (as previously noted 20 - 30 min *in vitro* with a dose of 30 J/cm^2), given the multi-step mechanism for therapeutic release.[102] *In vivo* testing may also require further analysis of the generated ROS species as well as distribution and clearance studies given the temporal sensitivity challenges facing therapeutic release. However, cyanine scaffolds may have minimal safety risks given the historical data of ICG. The novel pH sensitive self-assembling micelle seems to solve some of the previously presented issues of cyanine-based PPGs. This system provides multiple layers of targeting and a transition in structure and clearance properties upon encountering tumor tissue.[86] Although, this system provides potentially exciting applications for NIR theranostic PPG nanomaterials in the treatment of cancer, release rates and Φ still need to be improved to achieve high levels of therapeutic efficacy.

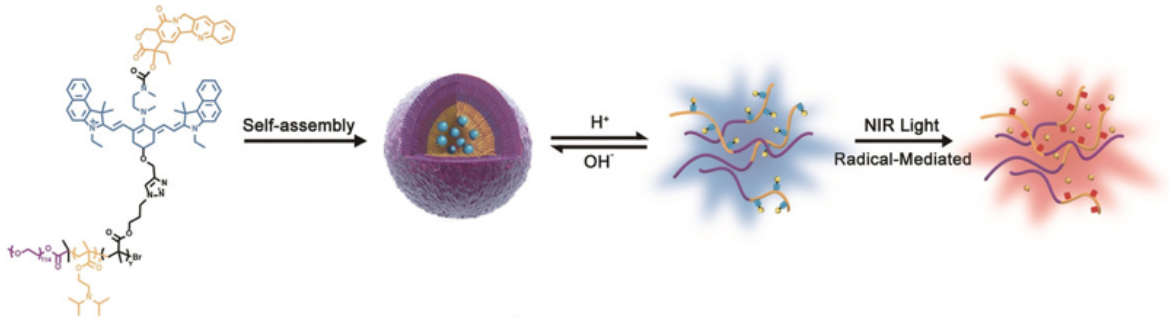

Figure 1.6 Self-assembling cyanine theranostic micelles can be imaged by photoacoustic imaging in the micellar form or by fluorescence-based imaging after pH driven reversible breakdown of the micelle. Reprinted with permission.[86]

Cobalamin (Cbl) Scaffolds

Cbl, more commonly known as vitamin B12, is an essential vitamin. The photoresponsivity of Cbl was initially discovered in the 1950's by observing cyanocobalamin degrade into hydroxocobalamin after being exposed to light during storage.[104] The axial bond appended to the cobalt core photocleaves after exposure to short wavelengths of light outside the optimal window of tissue (330 - 580 nm). However, by synthetically appending a fluorophore antenna to the ribose hydroxyl end of Cbl, the photoresponsive properties are extended to the wavelength of the antenna (645 nm in the case of cyanine5, Cy5).[105] This antenna also attributes potential theranostic applications to Cbl by allowing for fluorescent imaging of its biodistribution.[106]

Cbl scaffolds have been developed to deliver multiple cancer therapeutics, including colchicine,[71, 107] paclitaxel,[71] methotrexate,[71, 107] dexamethasone,[71, 107] and docetaxel.[72] Dexamethasone is also a treatment in inflammatory conditions, such as rheumatoid arthritis. Cbl scaffolds that take advantage of the endogenous uptake of Cbl and the overexpression of transcobalamin receptors on a variety of cancer types are under development. Researchers have employed a Cbl-antenna species to image distribution. Although an enhanced degree of uptake in tumor tissue was observed, the Cbl species was distributed throughout all tissue, including the brain. No therapeutic release was tested in these studies.[106]

Due to the low levels of uptake of orally ingested vitamin B12 and previously demonstrated systematic recognition of Cbl PPGs, novel methods of sheltering the Cbl scaffold have been developed to minimize dark activity.[106, 108] Colchicine, paclitaxel, methotrexate, docetaxel, and dexamethasone (Dex) have all been successfully loaded into and released from RBCs. Cbl and the covalently appended therapeutic are successfully retained within RBCs until illumination due to Cbl's membrane impermeable nature. Upon irradiation, the hydrophobic therapeutic can permeate through the cell membrane and affect the surrounding tissue (**Figure 1.7a**).[71-73] Another Cbl RBC system developed externally co-loads Cbl-therapeutic and a long wavelength

fluorophore antenna onto the surface of RBCs by synthetic lipid modifications (**Figure 1.7b**).[107] Although promising cellular data was observed in the externally loaded system, only the internally loaded docetaxel and Dex RBC systems have been tested to date in mice.[72, 73] *In vivo* studies have successfully validated localized release as intravenously administered internally loaded Cy5-Cbl-docetexal RBCs cause endothelial damage only to the irradiated mouse ear and no damage to the mouse's other non-irradiated ear.[72] Further, comparable therapeutic efficacy of Cy5-Cbl-Dex RBCs to standard of care Dex treatment has been observed in treatments of a collagen antibody induced arthritis mouse model.[73] Both *in vivo* findings demonstrate the potential of Cbl loaded RBCs to provide spatiotemporally controlled release.

The Cbl scaffold retains its natural vitamin structure and thus should be minimally toxic, is not cell permeable, and can retain the high ε of appended fluorophore antennas.[109] Furthermore, studies of photocleavage of biological Cbls have found that Co-C breaks with near unity Φ in 100 ps, however only about 25% of cargo does not recombine with the Cbl scaffold.[104] Challenges of this PPG arise due to inherent qualities of vitamin B12 persisting. The modified Cbl scaffold is still recognizable by transcobalamin II in the blood and the transcobalamin II-receptor on cell membranes leading to non-specific cell uptake. Recent biodistribution studies have demonstrated Cbl disseminates into sensitive tissues such as the brain, heart, and lungs which will need to be thoroughly studied to address potential toxicity concerns.[72, 106] Though synthetic modifications to block interaction with natural transport proteins of Cbl are available, the exposure of the weaker axial bond may lead to metabolic therapeutic release.[108] Thus, more complex delivery systems have been considered as intravenous and oral delivery methods pose challenges in the ability of the PPG to inactivate the therapeutic until illumination. Only 2.5 mg of vitamin B12 can be absorbed by the adult body per day, further limiting oral administration methods. These carriers, such as RBCs, can introduce another level of complexity in design and will require addressing extensive regulation (discussed in section 1.5.5). The largest challenge, however, may indeed be

the patentability of vitamin B12 as complex nuances surround patenting natural products. Still, patents can be attained for unique use, new materials produced from a natural product, or for the synthetic methods of producing the natural product.[110] Since, as previously described, the Cbl scaffold needs to be modified to achieve NIR photoresponsivity, these modified structures and their synthesis can potentially be easily patented. However, care should be taken when publishing information on any patentable products.[111]

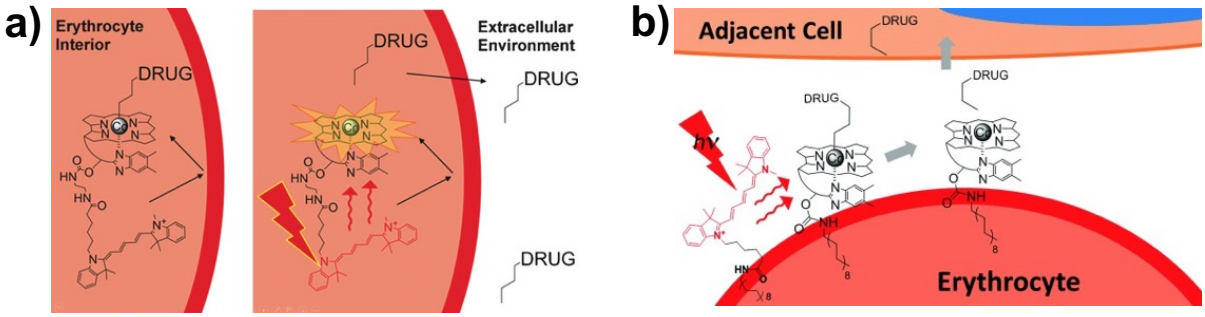

Figure 1.7 Schematics of Cbl RBC therapeutic DDSs. a) Cyanine-Cbl therapeutics sheltered within RBCs. **b)** Cbl therapeutics and long-wavelength antennas externally loaded on RBCs. Reprinted with Permission.[71, 107]

Phthalocyanine (Pc) Scaffolds

Pcs have been under development as PSs for PDT since the 1980s. With NIR wavelength responsiveness and a variety of core metals, these synthetic dyes demonstrate high Φs of ~0.4. Photosens, a complex mixture of aluminum Pc derivatives, has been approved in Russia for the treatment of skin, breast, gastrointestinal, and lung cancer demonstrating a high ε, high tumor accumulation, and fast clearance.[74, 75, 112, 113] Under hypoxic conditions, silicon Pcs (SiPcs) have been discovered to convert photon energy into the release of small molecules, as the Φ for singlet oxygen production decreases dramatically with limited O_2 in the environment. Applications for PPG SiPcs include cancer, myocardial ischemia, metabolic diseases, chronic heart and kidney diseases, and reproductive diseases in which hypoxia plays critical roles.[114] SiPcs have only been tested *in vitro* for small molecule release. However, as previously referenced, Pcs in general have been clinically tested and even approved in some regions. SiPcs, specifically, have been tested *in vitro, in vivo*, and through Phase I clinical trials as PDT PSs, with Pc 4 as a current prominent SiPc that has exhibited potential in breast, colon, and ovarian cancers.[113]

Modification of Pcs as PPGs shows promise due to the established clinical safety of Pcs, long wavelength responsivity, and potential for dual PDT/ small molecule cancer therapy. However, small molecules appended to the axial bond of Si were observed to decrease the Φ of singlet oxygen to an unsatisfactory 0.1 depending on the appended therapy's structure. This sensitivity limits the dual application to certain therapeutics and requires further synthetic investigation to optimize Φs of both therapeutic release and singlet oxygen production. It is important to note an electron donor (such as glutathione) is also required for the therapeutic release which may limit *in vivo* efficacy further depending on the hypoxic environment. Many Pc dyes originally demonstrated low water solubility but their biomedical development over the last 30 years has significantly tackled this issue by synthetically appending sulfonic acid groups.[113]

The dual-modality PS/ PPG of SiPcs provides a novel way of introducing PPGs to the clinic as PSs have minimal therapeutic effect when not illuminated and the Pc may also act to shelter the cytotoxic small molecule therapeutic from systematic cellular uptake. This ability was validated during *in vitro* therapeutic release and cytotoxicity tests on HeLa cells with minimal dark activity and toxicity observed.[75] NP-appended Pcs have already been explored to improve the photodegradation of Pcs, which could also be applied to dual PDT/ photoactivatable DDSs to further enhance sheltering of small molecules.[113] Further *in vitro* and *in vivo* testing is required to fully establish SiPcs for dual photoresponsive therapies.

Ruthenium (II) Scaffolds

Similar to Pcs, Ruthenium (Ru) scaffolds have been investigated for applications in PDT as well as PPGs for therapeutic release.[112] These compounds have been tested alone as cytotoxic therapeutics similar to cisplatin. Interestingly, NAMI-A and KP1019 (the Ru investigational products tested up through Phase II clinical trials) display a low degree of systemic toxicity with KP1019 producing a cytotoxic effect and NAMI-A producing anti-metastatic effects.[115] With very different mechanisms of action, the complexes demonstrate the variety of geometries, oxidation states, and consequently applications of Ru scaffolds. Octahedral Ru(II) complexes specifically have been found to undergo ligand dissociation in response to illumination by long wavelength light, although these complexes do require insertion of a cyclo-metalating ligand to shift photoresponsiveness toward the optimal window of tissue.[116] These complexes have been tested *in vitro* for the delivery of abiraterone, a P450 inhibitor used in metastatic prostate cancer, a nicotinamide phosphoribosyl transferase (NAMPT) inhibitor, and the cytotoxic natural product rigidin. *In vivo* studies of rigidin were conducted in xenografted human lung cancer tumors implanted on both flanks of nude mice. Illumination exhibited a localized effect on tumor growth as the non-irradiated tumor continued to grow. Inactive controls showed no effect on tumor,

however intravenous therapeutic doses of 2 mg/kg presented severe adverse effects including mouse death.[117]

Ru(II) scaffolds are promising PPGs as they are clinically established, have the potential to deliver up to 2 ligands per PPG, and have extensive synthetic malleability providing a variety of properties for optimal PPG production. Limitations arise from the required synthetic optimization per therapeutic cargo, as the cargo attached can significantly affect the rate of release due to changes in the Ru-Ligand bond strength and tuning of the metal to ligand charge transfer band. Thus, optimization of the remaining ligands is required to improve physiochemical states and Φs: for example, addition of a triphenylphosphine ligand improved Φ of a γ-aminobutyric acid therapy by seven-fold to 0.21.[118] These modifications are crucial as the inherent responsivity of the metal to ligand charge transfer band of octahedral Ru(II) lies between 400 - 500 nm. Ru complexes attached to rhodamine B antennas, similar to the previously discussed Cbl scaffolds, as well as terpyridine ligands, have achieved long wavelength light responsivity.[118-120] Further, the dual nature of Ru structures to act as potential PSs and PPGs with nearly equivalent Φ values (0.036 and 0.013 respectively) may be both beneficial and add further complexity to pharmacological testing.[77] Though Ru complexes have a precedent of low toxicity and clinical investigation as well as promising initial *in vivo* results, further synthetic exploration and optimization is required to produce a photoactivatable DDS with a sufficiently high Φ, NIR responsivity, and low toxicity.[121]

1.4.2 Long-wavelength Photoswitches and Photogates

Photoswitches are classically considered small molecules that undergo a reversible isomerization in response to light and have been predominantly developed in the field of optogenetics and photopharmacology to target enzymes, G-protein coupled receptors, the cytoskeleton, and ion channels, transports, and pumps with a variety of light dependent and tethering modalities. For therapeutic applications, photoswitches are most commonly synthetically

integrated with the structure of a targeting ligand for a specific biologic. The photoswitch then provides a light-dependent modification of the affinity of the ligand: i.e., by "flicking the switch" the drug can become therapeutically active. The majority of photoswitch development is still focusing on *in vitro* discovery and optimization and still relies on responsivity to short wavelengths (300 - 500 nm).[122] One of the most developed therapeutic photoswitches is the azobenzene DENAQ (responsive to 450 - 550 nm) that has demonstrated *in vivo* promise for treatment of AMD and retinitis pigmentosa.[78, 123] Therapeutic photoswitches that are responsive to red-shifted wavelengths will be focused on below.

A variety of photoswitches, PPGs, and photopolymerizable phospholipids have been developed to act as photoresponsive "gates" (photogates) for nanocarriers that release drugs from within the carrier upon irradiation. Photoswitches, as previously described, undergo an isomeric change that often shifts their conformation or polarity. By integrating photoswitches with carriers, the light triggered change can cause the release of therapeutic by shifts in polarity or removal of physical capping agents (**Figure 1.5**). Photochemically activated systems, such as PPG based nanomaterials and photopolymerizable phospholipids, often undergo crosslinking changes to induce nanocarrier breakdown. Carriers and their considerations as photoactivatable DDSs will be further discussed in section 1.5.5.

1.4.2.1 Photoswitches that Reversibly Isomerize

Azobenzenes (azo)

Since their discovery in 1937, azobenzenes are the most developed photoswitch as both a molecular and gated photoactivatable DDS.[124]. Azobenzenes have prevailed outside of photoresponsive investigations as artificial food dyes and the anti-bacterial Protonsil. Azobenzenes undergo trans to cis isomerization upon illumination and NIR responsive azobenzenes have been developed by appending ring substituents or by further modifying the

benzene rings.[125] Photoresponsive therapies include light activated anti-bacterial photoswitches (modified antibiotic trimethoprim) and nanomaterials (MSNs releasing doxorubicin and hydrogels releasing protein upon isomerized release of a capping agent, as well as hydrogels that undergo gelation in response to red light for biomedical applications) (**Figure 1.8**). All systems have been tested only *in vitro* thus far.[79, 80, 126, 127]

Although azobenzene scaffolds have been extensively researched, multiple challenges face these long wavelength photoswitches. The initial investigations with Protonsil, led to the discovery that azo dyes can be reduced in the human gut. Glutathione's high cellular concentrations can also lead to a similar reduction of the critical azo structure for therapeutic photoswitches. Thus, rigorous investigation of stability is required as it varies significantly with structure. Azo food dyes also demonstrate potential for clinical safety, however long-term exposure to azo food dye methyl yellow was found to induce cancer in rats and thus safety may be derivative specific and also require thorough investigation.[128] When considering photoswitches in general, and azobenzenes specifically, it is important to ensure that the "on" state of the photoswitch is sufficiently long lived to produce the desired effect (nanomaterial breakdown, cargo diffusion, or therapeutic activation). This is a challenge as the "off" state of the photoswitch should be more thermodynamically stable to ensure that the photoswitch remains inactive without light. Further, the low εs and Φs of azobenzenes in the long wavelength range requires extensive modification to produce optimal NIR responsive systems. These modifications have led to large molecules and highly polarized structures with photophysical properties that vary significantly with solvent. Although further investigations are underway, the current leading NIR materials are azonium salts which have extremely pH-dependent properties.[129] Nanomaterial applications may be modified to maintain the desired azobenzene properties, however therapeutic applications that require permeating cells may face insurmountable challenges.[125, 130, 131]

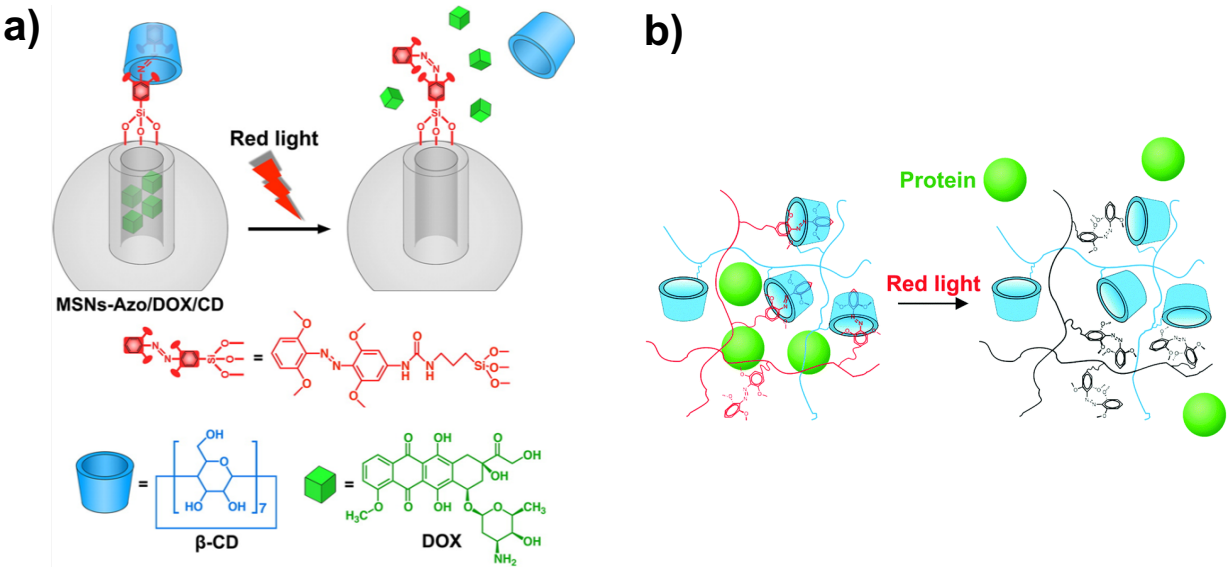

Figure 1.8 Azobenzene Photoswitch based photogated carriers. a) Azobenzene gated MSNs which release the β-CD nanocapping agent upon isomerization. **b)** Azobenzene gated hydrogels which breakdown upon release the β-CD nanocapping agent releasing protein therapeutics. Reprinted with Permission.[80, 126]

Donor-Acceptor Stenhouse Adducts

Donor-acceptor Stenhouse adducts (DASAs) undergo a cyclization and dramatic shift in polarity in response to light. These photoswitches are responsive up to 750 nm of light by appending cyclic substituents and aliphatic amines.[82, 132] DASAs have been developed as photogates for nanocarriers of paclitaxel,[81] as well as incorporated in photoresponsive nanoreactor systems.[133] These photogated carriers have only been tested *in vitro* (**Figure 1.9**).

DASAs are small molecules with minimal synthetic modifications that can dramatically shift photophysical properties. The range of photoresponsive wavelengths have been successfully modulated such that specific derivatives respond in a narrow wavelength range allowing for development of orthogonal DASA photogates. For example, orthogonal nanoreactors have been developed which permeabilize green-responsive DASA nanoreactors upon irradiation with green light and red-responsive DASA nanoreactors upon irradiation with red light, allowing for sequenced nanoreactor systems.[133] It was also noted that DASA micelles demonstrated minimal sensitivity to ambient light thus requiring few precautions for storage and administration.[81] However, sensitivity to polar solvents and spontaneous cyclization in the dark has been observed for certain derivatives. The extreme shift in physical properties of DASA upon isomerization make these photoswitches ideal photoresponsive gates for nanomaterials.[57] Further *in vivo* development will truly establish DASA photoswitches and photogated nanocarriers as prime candidates for clinical translation.

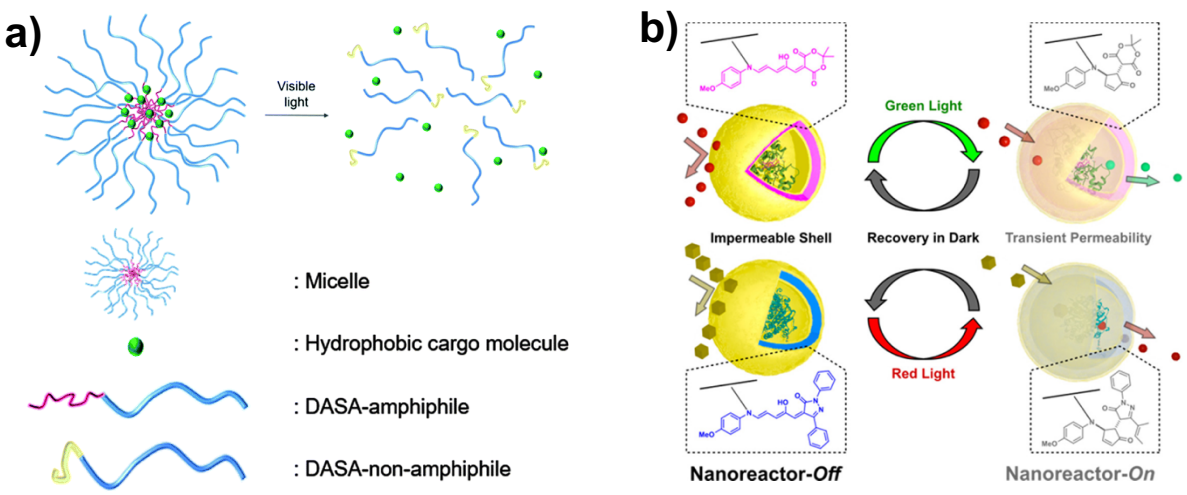

Figure 1.9 DASA Photoswitch based photogated carriers. a) Photoresponsive micelle that breaks down upon photoisomerization of DASA into its hydrophilic form **b)** Photoresponsive DASA polymersome which increases permeability to small molecules upon isomerization and subsequent shift in polarity. Adapted with Permission.[81, 133]

Synthetic Development of Prominent Reversible Photoswitches

Similar to azobenzenes, many other photoswitches have undergone lengthy synthetic development but still continue to face challenges of stability and achieving NIR responsiveness. Long wavelength response requires significant synthetic modification that may limit applications of therapeutic photoswitches due to large size and unfavorable properties for circulation and cell permeation. Further, NIR therapeutic photoswitches and gated nanomaterials have yet to be developed for the photoswitches discussed below. These structures may still be under early synthetic development and have many more challenges to overcome before translational applications.

Red-shifted spiropyran (up to a λ_{max} of 560 nm) photoswitches that form or cleave rings within their structure in response to light have been developed by introducing sulfo groups and extending the number of appended rings.[134, 135] Spiropyrans do not undergo significant conformational change in response to light, making nanomaterial applications more challenging. However, applications in UV responsive MSNs and self-assembled nanocarriers are under development, though face challenges based on spiropyran's environmental sensitivity.[54, 57]

Diarylethenes are another cyclizing photoswitch. NIR responsivity of the closed ring has been developed to 635 nm by extending the conjugation and triplet sensitization of the core structure.[136, 137] Diarylethenes are plagued by low water solubility, though the ring structure is thermally resistant responding solely to long wavelength light. Similar to spiropyrans, a minimal conformational change occurs requiring nanomaterial applications to take advantage of stacking properties. Though development of such nanomaterials is underway they have not yet successfully demonstrated cargo delivery.[54, 57]

Hemithioindigos (HTI) have also been under development for the last 100 years. Based on a photoswitchable E/Z transition, HTI have extended responsivity up to 545 nm while requiring addition of minimal substituents.[138] Though no species in the optical window of tissue have been

developed yet, HTI's show promise with the varied photophysical properties achievable by minimal modification. No applications in nanomaterials have yet been fully developed though lipidated HTI's have been synthesized.[57, 139]

Though under development for only half as long as many of the established photoswitches discussed above, hexaarylbiimidazoles (HABI) have shown promise with long wavelength responsivity to white light during which they undergo a homolytic cleavage.[140] However, due to their limited development, multiple challenges still face HABI photoswitches. HABI structures are quite large and composed of multiple rings making them very sterically constrained. Since the photolytic mechanism produces radicals, these radicals can in turn produce ROS. Conversely, certain derivatives have been discovered to be sensitive to oxygen which can oxidize photoresponsive C-N bonds easily. Long wavelength photoresponsive derivatives have also been found to be thermally sensitive.[57] HABI photoswitches have not yet been employed as DDSs but may be able to be sufficiently protected by nanomaterials while preserving and taking advantage of their photoresponsive properties.

1.4.2.2 PPG Photogates

Ruthenium (Ru)

Beyond photoswitch applications, MSNs have been used in coordination with Ru PPGs to entrap cargo. These 1.5 nm Ru moieties act as obstacles to therapeutic release. Upon irradiation (455 nm), the Ru scaffold no longer caps the MSN although it does remain conjugated to it.[141] Ru moieties have also been developed as photodegradable crosslinkers in hydrogels (**Figure 1.10a**). These hydrogel systems degrade extremely quickly in response to 520 nm irradiation (λ_{max}= 450 nm). Sample proteins have been successfully released from Ru crosslinked hydrogels which retain the Ru PPG.[83]

Having only been tested *in vitro*, further development is required to ensure release of therapeutic cargo from Ru photogated carriers. Although these systems are not currently responsive to light within the optimal window of tissue, the previous discussion on the synthetic opportunities for Ru PPGs can be applied to these already established nanomaterials.

Cobalamin (Cbl)

Cbl PPGs have recently been developed as gates for the destructive release of protein therapeutics from RBCs (**Figure 1.10b**). The natural RBC hemolytic peptide melittin (derived from bee venom) and a natural blocking segment that inhibits melittin activity attached to photoresponsive Cbl were associated to the surface of RBCs by lipidation to create a gate that inhibits hemolysis in the dark. In the light, the blocking segment is photocleaved and released allowing melittin hemolytic activity to resume. Long wavelength responsivity was re-introduced to the Cbl PPG via a cyanine antenna attached to the blocking segment and appended to Cbl by means of the photoresponsive bond (Cbl-Cy5-Blocking Segment).[142] *In vivo* studies successfully demonstrated the localized release of thrombin upon 561 nm irradiation of mouse ears. Due to its potency, only topical applications of thrombin for surgical purposes have been approved.[143]

Cbl based hydrogels have also been developed to improve hydrogel solidification under physiological conditions by introducing photoresponsivity to hydrogel gelation at NIR wavelengths. Ethyl Cbl scaffolds with a Cy5 antenna were found to produce alkyl radicals that could cross-link polymers with radical sensitive acrylates. Although the Φ of radical production was a sub-optimal 7%, the Cbl radical photoinitiators were able to polymerize up to 80% of certain polymers. Studies were limited to *in vitro* assays and thus require further *in vivo* assessment. Hydrogel solidification has applications in bone defects, wound healing, and protein delivery.[84]

Cbl gated RBCs and hydrogels have the potential to deliver biomacromolecule therapeutics by tackling the issues of quick clearance and systemic effects for potent biologics

like thrombin. Challenges associated with the current developed systems include potential toxicity issues raised by melittin and acrylate polymers. Although, melittin is under development as a biotoxin cancer therapeutic and acrylic polymers are under development as natural polymer hydrogels.[144, 145] The low Φ of Cbl photoinitiators and lack of *in vivo* studies on the NIR responsivity of the melittin system requires further optimization. Further synthetic development and *in vivo* studies will solidify these novel photoresponsive biologic DDSs.

Amino-1,4-benzoquinone (AQ)

Amino-1,4-benzoquinones (AQ) release therapeutic cargo upon aromatization in exposure to long wavelength light (up to 700 nm). Although this reaction is slowed by polar solvents, this PPG was discovered to maintain its therapeutic release efficiency when sheltered in hydrophobic NPs. AQ NPs have been tested *in vitro* releasing paclitaxel upon >590 nm irradiation (**Figure 1.10c**).[85]

AQ PPGs show promise with modest Φ and long wavelength photoresponsivity. It appears that their greatest challenge of environmental sensitivity has been overcome by using NPs. However, only *in vivo* testing will assure the continued promise of AQ NPs.

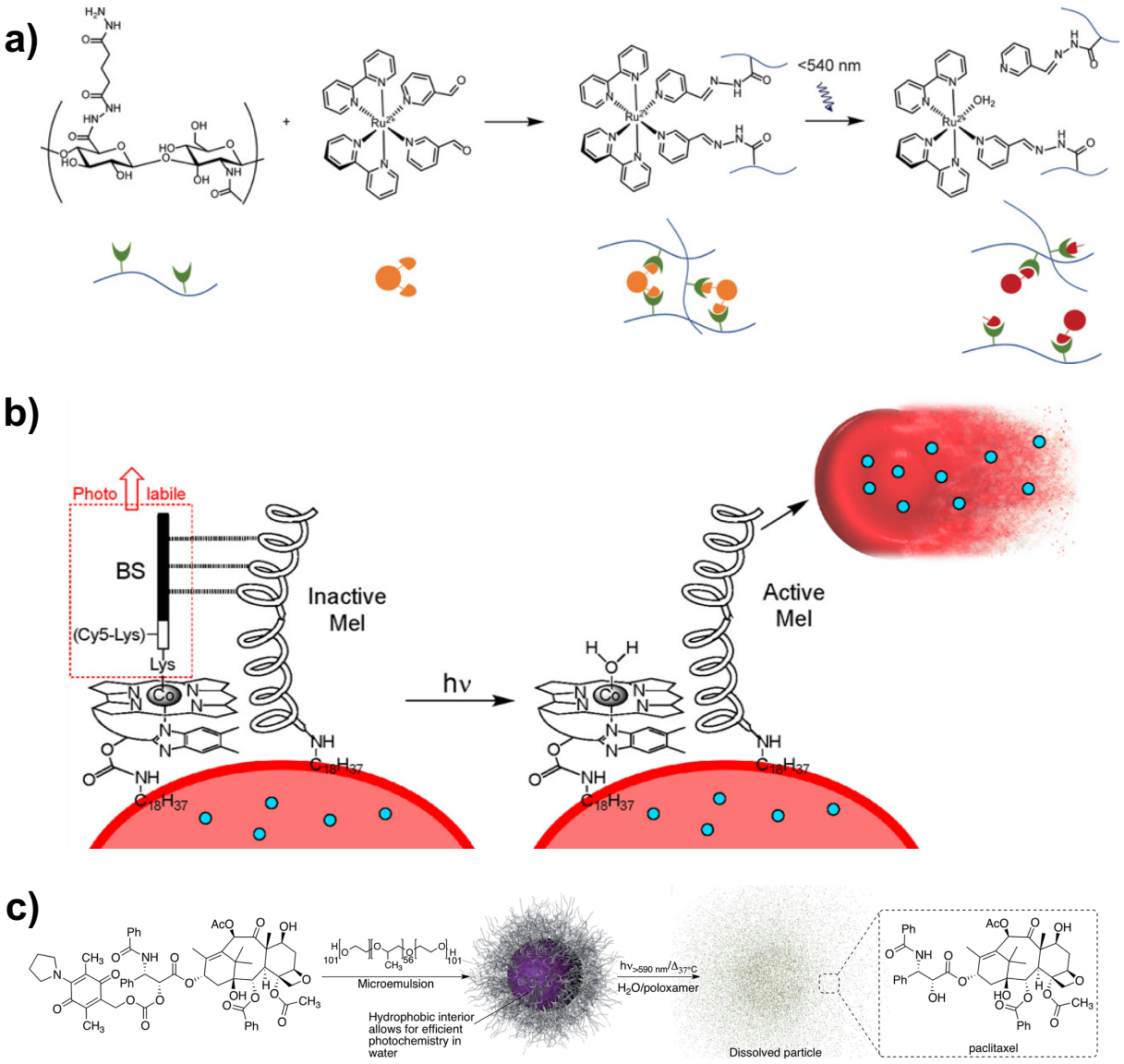

Figure 1.10 PPG based photogated carriers. a) Ru hydrogels that degrade upon exposure to green light for protein therapeutic delivery. **b)** RBC melittin-driven hemolysis triggered by photorelease of blocking segment releases peptide therapeutics from within RBCs. **c)** AQ NPs employ a hydrophobic core to shelter AQ photochemistry and allow for photoresponsive release of paclitaxel therapeutic. Reprinted with Permission.[83, 85, 142]

1.4.2.3 Photopolymerizable Phospholipids

Beyond PPG and photoswitch based photogates, photogates have also been built from photopolymerizable lipid moieties. These moieties undergo photocrosslinking which destabilizes the lipid bilayer, leading to the breakdown of the nanomaterial and release of therapeutic cargo (**Figure 1.11**). Though out of scope for this discussion, liposomes that take advantage of ROS sensitive phospholipids which undergo photooxidation and consequent photofragmentation can also release therapeutic cargo in combination with PSs. These dual PDT/ small molecule therapeutic systems currently in clinical trials as cancer treatments have built upon the previously discussed long-wavelength PSs to develop novel PDT/ therapy systems.[146-149] Such nanomaterials are reviewed more comprehensively elsewhere.[4, 150-152]

Under development for the last 30 years, 1,2- bis[10-(2′,4′-hexadienoyloxy)decanoyl]-*sn*-glycero-3-phosphocholine (bis-SorbPC) has been recently red shifted (up to 550 nm) by addition of a cyanine dye into the bilayer of these liposomes.[153] Though having undergone limited development since their first discovery and preliminary *in vitro* tests, bis-SorbPC provide promise in their red-shifted photoresponsivity. Persistent challenges include their hydrophobicity and further extending their photoresponsive range. However, nanomaterials provide extensive opportunities for synthetic and physical modification of properties.[154]

Finding more success 1,2 bis(tricosa-10,12-diynoyl)-*sn*-glycero-3-phosphocholine ($DC_{8,9}PC$) based liposomes have demonstrated *in vivo* efficacy against cancer. Although initial work demonstrated $DC_{8,9}PC$ photocrosslinking at 254 nm, encapsulation with PS Photochlor adjusted the photoresponsive range to 660 nm by means of an ROS-dependent destabilizing mechanism. *In vitro* studies have also included doxorubicin in liposomes responsive to 514 nm by means of ROS-dependent mechanisms.[148] Although $DC_{8,9}PC$ crosslinking does occur at shorter wavelengths, the ROS fragmentation supersedes crosslinking at longer wavelengths.[149]

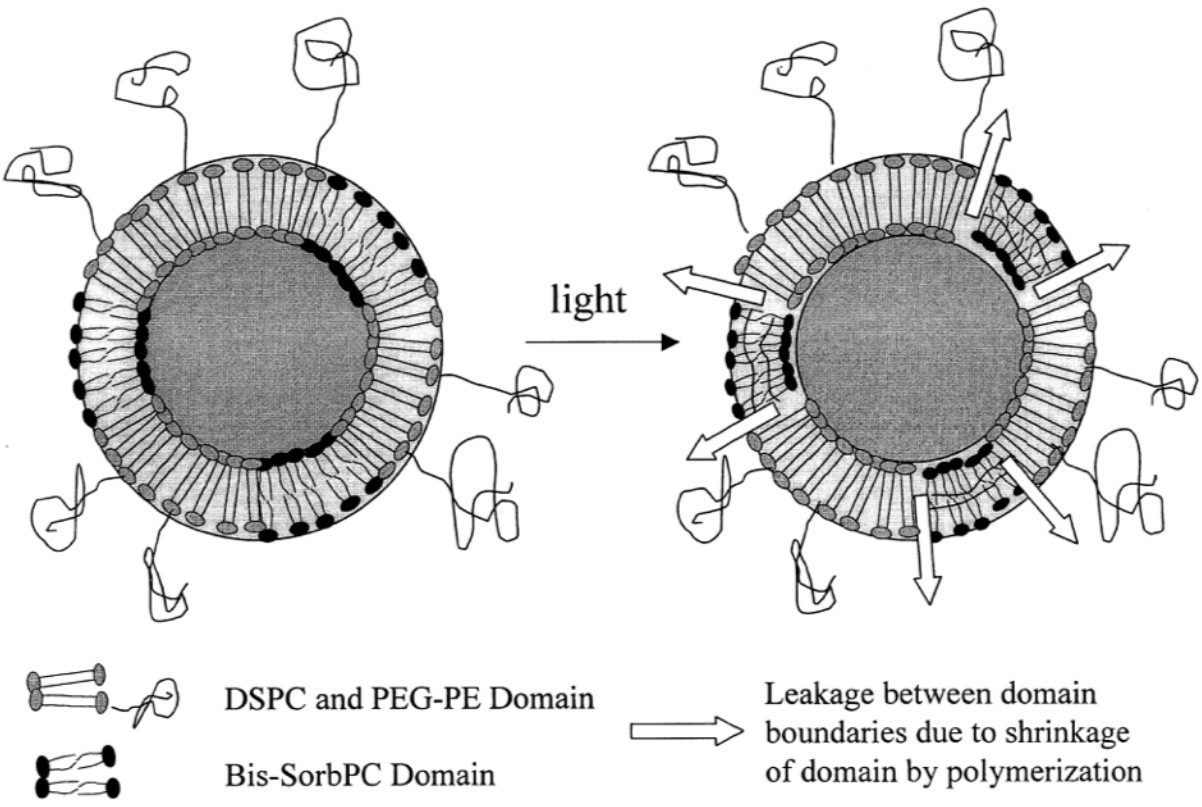

Figure 1.11 Bis-SorbPC photopolymerizes creating permeabilized gaps in the PEG-liposome membrane. Reprinted with Permission.[153]

1.5 Considerations of Photoactivatable DDS Development: Designing and Developing for Clinical Translation

With the foundation of currently developed long wavelength PPGs, photoswitches, and photogates (section 1.4) as well as the precedent of FDA approved light devices and photodynamic therapies (section 1.3), this section will provide crucial considerations in the design of photoactivatable therapeutics. Specifically, the design of its unique components (**Figure 1.2**) as well as a path towards the FDA Investigational New Drug (IND) application (**Figure 1.12**) – the first step in translating a novel therapeutic into clinical trials. When considering the design of novel photoactivatable therapeutics, it is important to note the precedent PDT has set. In general, approved PSs have confirmed that perfection is not required for clinical approval. Photofrin does have sub-standard (considering current standards) Φ, ε, and significant phototoxicity (up to three months), and yet is still relevant after 30 years in the clinic in Barrett's esophagus and endobronchial non-small cell lung cancer. These indications include non-resectable tissues that require targeted therapy, for which PDT poses less risks and more benefits than ionizing radiation.[155, 156] However, applications beyond accessible tissue (e.g., esophagus, bladder, pancreas) will require more ideal photophysical properties than even currently established PDT systems have been able to provide.[157] Many in the field have argued nanomaterial DDSs for such applications.[158]

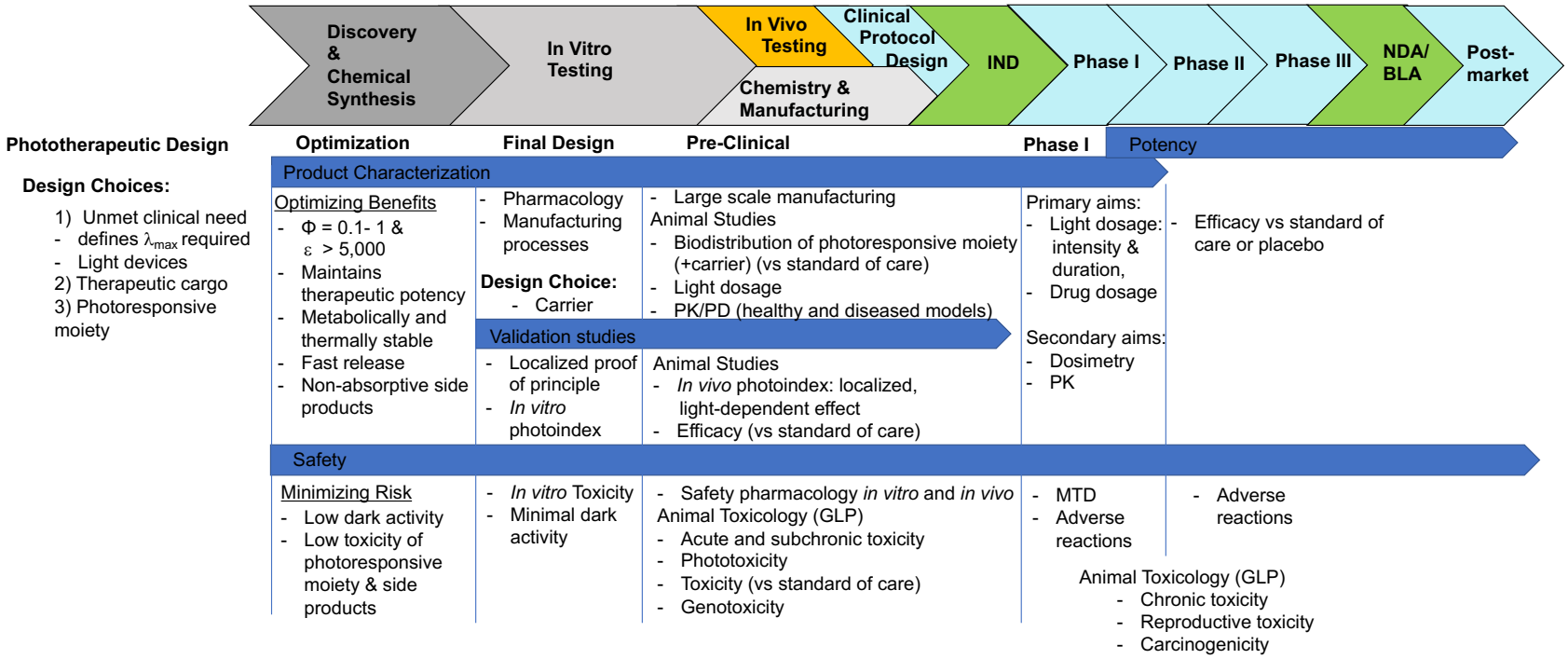

Figure 1.12 Path towards the FDA IND for pre-clinical photoactivatable DDS development.

The continued relevance of Photofrin, with its less-than-ideal photophysical properties, highlights the most crucial idea in successful clinical translation: unmet medical need.[159] Although the below discussion includes considerations of which therapeutics and treatments can be refined by photoactivatable systems (section 1.5.2), meeting an unmet medical need (potentially multiple needs) will determine the degree of benefit the photoactivable therapy provides, the standard of care it is compared to, and the overall success of translation. Development should always focus on the unmet medical need(s) the photoactivatable DDS can resolve which should guide the development process. This approach can enhance efficiency in each step, resolution of challenges early on, and with multiple applications the potential to pivot the technology if necessary. In his 2018 perspective on photoactivated chemotherapeutics (PACTs), Dr. Sylvestre Bonnet noted that "Focusing more on the disease will be of primary importance for developing PACTs in the future. Questions such as market size, current prognostics, availability of other treatments and unmet clinical needs will determine whether a PACT reaches the patients' beds or not."[159] In tandem with this ideology the below discussion on considerations of the key elements of photoactivable therapeutics will refer to the potential approaches for answering unmet medical needs throughout the design process (see sections 1.5.2 - 1.5.5).

The FDA evaluates novel technology developed towards an unmet medical need by analyzing the risks and benefits the technology brings to the current treatment for an indication. Thus, when the unmet medical need is high or in extreme need of even small benefits, the benefit of an additional month of survival may be sufficient for clinical approval (provided it outweighs the risks of the treatment, as previously observed in pancreatic adenocarcinoma).[160] Likewise, when limited therapies are available but the disease is serious and severe, toxic treatments such as cisplatin with higher risks are permitted. Thus, the discussions on the photoactivatable therapeutic's components will also present considerations in a risk/ benefit analysis including the unique toxicity risks introduced by each component. A selected unmet medical need will create

boundaries on what risks are permissible and what is considered a true benefit. The FDA's IND (section 1.5.1) requires 1) the manufacturing process and 2) the animal pharmacology and toxicology information broken into i. Pharmacology, ii. Toxicology, and iii. Pharmacokinetics studies which include Absorption, Distribution, Metabolism, and Excretion (ADME) studies.

1.5.1 Preparation of Therapeutics for an FDA IND Application

One of the first steps when embarking on therapeutic development and clinical translation is to be familiar with the regulatory agency requirements and processes (e.g., the FDA in the USA). The FDA oversees the majority of investigational studies taking place in humans in the USA to ensure safety of the investigational substance. Clinical testing is a multi-year process during which a continuous relationship with the FDA will need to be maintained, from before IND application to continued safety and efficacy regulation post-marketing approval (**Figure 1.12**). More extensive reviews and resources on the history of, interactions with, and approval processes of the FDA are available.[161] The following brief synopsis will focus on the FDA's requirements for therapeutics attempting to transition from pre-clinical studies to first in human trials.

The first milestone for therapeutic translation is opening of the IND, which conveys the sponsor's intent to begin clinical investigations in the USA which, for a typical development program, are often first in human Phase I trials. A Phase I trial aims to establish safe dosage levels and can also begin to assess PK in a small (typically 20 to 80 patients total), healthy patient population. Beyond regulatory forms, the IND is composed of 3 main sections: i. non-clinical pharmacology, PK, and toxicology, ii. chemistry, manufacturing, and controls (CMC) information, and iii. clinical documents for the Phase I trial including the clinical protocol, investigator's brochure, and any previous clinical findings relevant to the product.[162] It is important to note that 30 calendar days after the submission of an IND, the first in human trial can be initiated unless the FDA directly contacts the sponsor with further questions or to halt the trial. Thus, many of the

clinical components including the investigational brochure and clinical protocol need to be prepared, and for multi-site trials other sites should have been contacted to have already begun the lengthy process of contracts and institutional review board approval.

To support opening an IND, the main sources of information to consider even at the beginning of the drug development process are: 1) the CMC/ quality of the product and 2) the non-clinical information (**Figure 1.12**). The non-clinical information can be broken down further into i. Pharmacology, ii. PK, and iii. Toxicology studies and contain information from both *in vitro* (cellular studies) and *in vivo* studies (in animal models) that aim to establish the safety of the proposed product for use in first in human trials.

The quality section requires CMC information for the drug substance (the active pharmaceutical ingredient), the drug product (drug substance(s) plus any excipients), and the placebo formulation as well as any environmental impacts of manufacturing the therapeutic and any associated devices. Each component will require full characterization, a description of the manufacturing process which must be compliant with Good Manufacturing Practice (GMP) standards, a description and data for the analytical methods established to ensure the purity and consistent production of the substances, and assessments of stability.[162]

The non-clinical pharmacology section focuses on both safety and potential for efficacy by providing information about the intended (mechanism of action/ enzyme targets) and unintended pharmacological consequences (such as effects on cardiovascular tissue, respiratory tissue, nervous system, etc.) of a proposed product. In addition, when applicable, information from animal models of the indication/ disease of interest should also be included. The non-clinical PK section provides ADME information and potential drug-drug interaction information that can be used to guide minimum and maximum dose selection for the first-in-human Phase I studies. Important results of the non-clinical studies include the MTD, dose-response curves, as well as indicators of the NOEL and NOAEL and how these data support the safety of first in human

dosages as well as the proposed treatment protocol (multiple staggered doses versus a one-time treatment). Though efficacy results from animal models of the human disease may be included in the non-clinical portion they are not as rigorously critiqued by the FDA for Phase I trials. However, it is important for sponsors to validate their potential therapeutic efficacy to justify the financial costs to run a clinical trial, as well as to justify the risk-benefit analysis once clinical studies begin.

The toxicology studies support the safety of the therapeutic before the Phase I trial. Pivotal toxicology studies are required to be compliant with Good Laboratory Practice (GLP) standards and include acute (single-dose) and subacute (repeat-dose) tests usually in at least one rodent and one non-rodent animal model. Acute toxicity is the simplest to measure by assessing the LD_{50} (lethal dose to 50% of animals) and monitoring effects on animal health, food consumption, and clinical pathology, and are crucial to understand for regulatory approval. Sub-chronic toxicity measures the effects of repeated exposure on clinical signs, motor activity, food consumption, clinical pathology, and ophthalmology, and at termination how critical organs were affected by gross necropsy and histopathology. *In vitro* toxicity and efficacy are often measured by finding the LC_{50} (lethal concentration that suppresses cellular growth) and EC_{50} (effective concentration that produces the desired biological effect in 50% of the population). These terms commonly contribute to dose selection for *in vivo* studies.[163] Toxicology studies will often continue after the initiation of clinical trials with long-term (6 month and 2 year) toxicology and genotoxicity being completed in tandem with clinical investigation. Eventually chronic toxicity tests, effects on reproduction and the developing fetus, and toxicity related to the drugs mode of administration will be required for the new drug application (NDA).[162] Similarly, eventual *in vivo* efficacy studies will require animals to demonstrate the desired biological outcome (tumor reduction, survival rates, remission of inflammation, etc.).

During photoactivatable DDS design and development, it is crucial to consider how the eventual requirements of the IND (and NDA) can be integrated throughout the developmental

process (**Figure 1.12**). For example, by targeting cellular and animal studies toward an unmet clinical need, vital optimization toward the indication, as well as supportive results for the IND, will be attained more efficiently. With knowledge of the unmet clinical need and the current therapeutic landscape, even initial *in vitro* testing can be done on disease relevant cell models contributing to both *in vitro* characterization of the phototherapeutic as well as preliminary pharmacology tests. Furthermore, photoactivatable DDSs can be improved at the design stage, by ensuring tissue-penetrant long-wavelength responsivity as well as considering toxicity of the caging moiety and how easily the synthesis can be scaled up to manufacturing requirements. Since photoactivatable therapeutics seek to enhance the TI of many novel or existing therapeutics, demonstrating how the photoactivatable therapeutic compares to the therapeutic precursor or standard of care may be crucial validation required for approval. Though these early considerations may require more time to complete development, they will contribute significantly toward ensuring some of the main challenges facing photoactivatable therapeutics have been tackled in the pre-clinical stage.

1.5.2 Therapeutic Cargo: Drugs with Room for Improvement

Therapeutics modifiable for photoactivatable DDSs can include approved FDA drugs, therapeutics in clinical trials, or novel agents that require spatiotemporal control provided by photoresponsive systems. Photoactivatable therapeutics can improve on existing drugs by minimizing toxicity or enhancing efficacy through spatial or temporal control of delivery. Enhanced localized therapeutic delivery enables reduction in the therapeutic dose required and further diminishes toxicity. A more extensive analysis of the ways photoactivable therapeutics can modify the TI will be reviewed in section 1.5.6.2.

When adopting FDA approved or promising therapeutics in clinical trials for photoactivatable DDS, it is crucial to understand how the therapeutic is currently employed in the clinic and what the associated benefits and risks of the therapeutic are. By preserving the benefits

and minimizing the risks, an improved derivative of that therapy can be produced. On the other hand, when developing completely novel therapies that have not been approved, understanding the current market and therapies that are addressing the clinical need is important. This section will discuss current indications for photoactivatable therapeutics focused on minimizing toxicity and enhancing efficacy.

1.5.2.1 Minimizing Toxicity

Photoactivated chemotherapeutics (PACTs) for Cancer

Although PDT is an approved photoresponsive therapy for the treatment of superficial cancers, its further development faces challenges, due to a reliance on oxygen to generate ROS and limitations of the mechanism of ROS therapy. PACTs have been proposed as an alternative that can overcome these limitations.[157] Cancers often create a hypoxic environment which results in insufficient oxygen for PDT to be truly effective. Furthermore, ROS cytotoxic therapy requires high powered lasers to generate enough ROS to create cytotoxic levels of oxidative stress leading to multiple mechanisms by which oxidative stress induces cell death, including by necrosis, apoptosis, and autophagy.[58, 159] Metronomic illumination has evolved as a means of attempting to control the mechanistic pathway of cytotoxicity to diminish negative side effects and improve efficacy.[28] These negative side effects, include tissue necrosis and pain, have led patients to reject further PDT treatments and driven the rise of sunlight based therapy.[50]

PACT therapies are expected to minimize pain due to fast-acting cytotoxic mechanisms and avoid the challenges of PDT, such as hypoxia and the varied cytotoxic mechanisms, by eliminating the reliance on ROS. PACT can deliver highly cytotoxic compounds, such as cisplatin, auristatin, and duocarmycin in a highly localized manner. These cytotoxic compounds are FDA approved or in clinical trials and result in a powerful cytotoxic effect at low doses (e.g., IC_{50} of 20 - 50 pM for duocarmycin). Many of these therapies (e.g., duocarmycin and auristatin) already

require ADC targeting in the clinic to minimize systemic toxicity.[69] Undeniably, it is the inherent cytotoxicity of these therapies that introduces high risk to patients due to non-targeted cytotoxicity. Present severe side effects including severe chronic kidney disease, neurotoxicity, as well as neutropenia, risk of infections, and other common chemotherapeutic side effects.[164] Even with ADC targeting, concerning systemic toxicity still occurs.[165]

Novel photoactivatable therapeutics under development have the potential to target systemically present enzymes in a localized manner and combine PDT with PACT. For example, Ru based NAMPT (nicotinamide phosphoribosyl transferase) inhibitors which target NAMPT, an enzyme found within many tissues but upregulated in cancer, are under development. Systemic administration in rats of NAMPT inhibitors *without* photoactivatable caging led to severe adverse effects including blindness.[166] Thus, NAMPT inhibitors are a prime candidate for photoactivated release as long as activity can be significantly diminished in the dark. Currently only an 18-fold difference between dark and light activity has been attained by Ru PPGs.[77] Pc, Ru, and cisplatin derivatives are also under development for PDT. These scaffolds have been found to be synthetically amenable to dual therapeutic activation and can provide the additional benefit in the market of inducing cytotoxic effects via multiple mechanisms which may be necessary to eliminate extremely resilient cancers.[75, 159] Separate administration of chemotherapeutics (such as cisplatin and doxorubicin among others) and PDT in *in vivo* studies have already demonstrated improved tumor growth control and antitumor activity.[14] Further, combination therapies are also in pre-clinical development with nanomaterial carriers and ROS activated therapeutic release which can release both therapies at the site of treatment and enhance localization due to enhanced permeation and retention (EPR) effects of the tumor environment (discussed further in section 1.5.5).[59, 147, 158] Indeed, finding ways to counteract cancer's resiliency and ensure eradication of abnormal cell populations by multiple mechanism may improve treatment of extremely robust cancers.

Higher staged and metastasized cancers as well as tumors that recur often lead to lower prognostic success.[167] Cancers that still have extensive unmet clinical needs and thus may be ideal for PACT are non-resectable tumors, tumors where surgery dramatically lowers the quality of life, and rare diseases where current therapies do not sufficiently treat patients (**Table 1-5**).[157] As previously discussed, Photofrin is commonly applied to non-resectable tumors and is currently approved for non-resectable non-small cell lung cancer.[156] Further, surgery in many head, neck, and brain tumors drastically lowers the quality of life, which is why PDT therapies are investigated in these tumors and have been approved in Europe for these indications (e.g. Foscan and Laserphyrin).[20, 157] PACT and other novel chemotherapeutics can also begin to address the extensive treatment gap for rare cancers. Rare cancers accounted for 22% of all diagnosed cancers worldwide in 2017. These cancers face extremely poor prognosis due to limited treatment experience and limited treatment options.[168] As previously, discussed PACT can improve chemotherapeutic therapy predominantly by minimizing off-target toxicity as well as potentially improving efficacy from localized delivery.

Table 1-5 Available cancer therapies and situations in which they fail.

Available cancer therapies	Unmet clinical needs where cancer therapies can fail
Surgery	Non-resectable tumors
Chemotherapy	Dose-limiting side effects
Radiation therapy	Metastases
Photodynamic therapy	Hypoxia
Targeted therapy (e.g. ADC)	Resistances
Immunotherapy	

Improving the Safety of Endogenous Signaling Molecule Therapies

There are many natural potent signaling molecules that have been successfully harnessed or mimicked for therapeutics. However, due to their potency, these signaling molecules often have undesired side effects. Again, photoactivatable DDSs provide the means to locally deliver the potent signal and minimize off-target signaling and resulting adverse effects.

Dex is an anti-inflammatory treatment for rheumatoid arthritis, asthma, and other chronic auto-immune illnesses. By mimicking natural corticosteroids, Dex can inhibit immune responses. However, long-term usage, which is required for chronic diseases, leads to adverse effects including osteoporosis, weight gain, diabetes, and immunosuppression.[169] Chronic illnesses are also the most in need of patient-driven treatments to resolve symptom flare-ups as chronic pain and debilitating symptoms in these illnesses have led to chronic work disability and absenteeism.[170, 171] By localizing therapeutic release to the lungs or joints by means of simple handheld laser, patients may be able to resolve symptoms with minimal adverse effects. Slow-release nanomaterials for Dex treatment have been previously approved as hydrogels (Dextenza) and are currently under clinical development with RBC carriers (EryDex).[172, 173] Further development of these systems with photoactivated therapies could form drug depots which provide patient-controlled remission of symptoms during flare-ups while minimizing the systemic adverse effects that arise with chronic Dex usage.

Potent biologics, such as thrombin, vasopressin, and dopamine are also FDA approved but have limited application or require extensive oversight during administration due to the non-desired effects when injected systemically. Current treatments are either given topically (thrombin) or intravenously (vasopressin and dopamine) along with close monitoring of the patient's response. Both vasopressin and dopamine cause erratic effects on cardiac function during treatment. Thus, localizing the release of these potent therapies to the desired tissue may diminish the erratic effects on cardiac function.[61, 174] Thrombin and vasopressin proteins also have

fast clearance times and *in vivo* instability, which will require some form of carrier as demonstrated by the photoresponsive RBC and hydrogel systems.[83, 142, 175] Thus, photoactivatable DDSs could improve treatments by not only sheltering these therapeutics from their environment and inhibiting their activity until illumination, but also allowing for more rigorous measurement of delivery, especially if developed in theranostic systems.

Other photoactivatable therapeutics in development are the gaseous signaling molecules NO, CO, and H_2S. These endogenously generated molecules are crucial signaling agents and mediators that can provide antioxidative, anti-inflammatory, vasorelaxant, cytoprotective, and neurosignaling effects, which may provide benefits in cardiovascular, inflammatory, and neurological diseases. Although NO and H_2S are not as stable as CO, they have both had clinical success. H_2S therapies are currently in Phase 2 trials as an abdominal analgesic and NO is commonly used to treat infants with pulmonary hypertension and is in trials for myocardial infarction.[64, 176, 177] Photoactivatable BODIPY-H_2S has been developed and tested *in vitro*, while photoactivatable BODIPY-NO has been tested *in vivo*.[63] Further, BODIPY-NO has been developed as a theranostic which can be imaged with photoacoustic imaging for more precise therapeutic release.[62] CO is the most toxic gasotransmitter under development with potent toxic effects due to its high affinity for hemoglobin. However, clinical trials have successfully demonstrated minimal short-term toxicity at CO-hemoglobin levels of <18%.[178] CO therapies may face more challenges to achieve FDA approval due to the high potential risk. Beyond these regulatory challenges, CO treatments may face market resistance due to the molecule's history of being a "silent killer". Both aspects may thus require considerable evidence of large benefits. In general, further research and understanding on how all of these signaling molecules can achieve specialized, desired clinical results will be required before successful clinical translation of photoactivatable gasotransmitters.

1.5.2.2 Increasing Efficacy

Although most applications of photoactivatable DDSs seek to minimize toxicity, spatiotemporal control of therapeutic release can also impact efficacy by localizing the concentration of therapeutic. Efficacy based development of photoresponsive therapy is currently limited to anti-bacterial treatments. The efficacy of anti-bacterial therapies has recently diminished by the rise of antimicrobial resistance. Photoactivatable anti-microbials propose a new way of minimizing resistance by limiting the exposure and localizing the treatment: bacteria exposed to the anti-microbial do not have the potential for developing resistance to the drug in its inactive dark state, while upon illumination high concentrations of activated drug kill off bacteria.[79] Further developments are also occurring with PS-based antimicrobials. As previously proposed with dual active Ru, platinum, and Pc, these PSs could release both a therapeutic and ROS species to induce microbial death by multiple mechanisms decreasing the likelihood of resistance further.[24]

Other growing fields such as, optogenetics and photoactivatable systems for chemical biology research, may eventually lead to novel classes of targeted photoactivatable therapies which will also improve localized efficacy. The growth of gene therapy as well could benefit from localized delivery, potentially improving transfection efficiency in the desired tissue.[179] Further, the continued development of light devices and research in dosimetry may improve the understanding of light penetration leading to more specialized and localized therapies requiring high localized concentrations for efficacy. This would allow for specialized therapeutic proteins (such as vascular endothelial growth factor, VEGF), specialized protein targeting and gene activation (for pain treatment among other indications), and temporal delivery of these systems by orthogonal delivery systems (described further in 1.5.5).[122, 180]

1.5.3 The Photoresponsive Moiety: The Foundation for Optimizing Benefit and Minimizing Risk

The photoresponsive moiety (photoswitch, photogate, or PPG) is the foundation of the entire light responsive system. Thus, selecting the proper moiety is critical to the development process. A risk/ benefit analysis provides opportunities to further develop photoresponsive systems into photoresponsive therapeutics based on medical need. Although challenges exist in accounting for every potential variable that contributes to the ideal drug, the following proposals are suggested to improve the chances of success.

When selecting a photoresponsive moiety, it is important to balance the risks and benefits as the photoresponsive moiety can significantly affect both the safety and efficacy of selected cargo by means of spatial and temporal control. **Table 1-6** summarizes the PPG/ photoswitch systems presented in section 1.4 and their pros and cons as photoactivatable therapeutic delivery systems.

Table 1-6 Pros and Cons of the Photoresponsive Moieties introduced in Section 1.4.

Photoresponsive Moiety	Pros	Cons	Stage of Development
BODIPY	Optimal window of tissue Safe Theranostic applications	Strong Fluorophore properties Hydrophobic	In vivo
Cyanine	Optimal window of tissue Safe Hydrophilic Fast release Theranostic applications	Fluorophore properties Generates ROS	ICG FDA approved In vivo
CbI	Optimal window of tissue Safe Natural Vitamin Scaffold Hydrophilic	Non-specific distribution Limited absorbance	In vivo
Pc	Optimal window of tissue Dual PDT and PPG	Limited to PPG activity in hypoxic environments	Russia approved for PDT In vitro
Ru	Potential safety Multiple drugs per PPG Nanomaterial development	Not in optimal window of tissue Properties are therapeutic dependent	Clinical trials as cytotoxic drugs Synthetic development
Azo	Optimal window of tissue Nanomaterial development	Potential toxicity Sub-optimal kinetics	Synthetic development
DASA	Optimal window of tissue	Unstable	Synthetic development
AQ	Optimal window of tissue	Requires nanomaterials	In vitro NPs

1.5.3.1 Benefit Analysis: Photophysical Properties, Synthesis, and Kinetics

Photophysical properties λ_{max}, Φ, ε: effects on the depth of tissue penetration

Although shorter wavelength photoresponsive moieties are numerous, PDT sets the precedent that their development and translation may be limited to very superficial dermatological applications (such as actinic keratoses), ophthalmology, and imaging applications (**Table 1-2**). Because of limited penetration (<1 cm), short wavelength responsive therapies have limited applications even in dermatological cancers.[14, 50] Thus, long wavelength photoresponsive moieties within the optical window of tissue are required to optimize the potential unmet clinical needs the photoactivatable therapeutic can address.

However, current PDT systems, even within the optimal window of tissue, have been limited to more superficial indications that can still be accessed by means of optical fibers without requiring surgery (**Table 1-2**). This limitation may be in part due to the risk posed by surgical

insertion of light sources as compared to the risks of other systemic therapeutics. Even the best PDT systems currently approved have sub-optimal Φ and ε, biodistribution, and require costly high-powered laser sources, further limiting penetrance and potential applications. For treatment of non-accessible organs, photoactivatable systems will require high Φ, ε, and may need to incorporate nanomaterials to improve delivery quantities by means of EPR and other passive modifications of biodistribution as proposed for PDT (further discussed in section 1.5.5).[158] As previously mentioned, many scaffolds have been extensively modified to impact and improve the Φ depending on the photoresponsive moiety as reviewed in the cited publications.[69, 121, 181, 182] Both synthetic expertise and knowledge of past synthetic development will be crucial to accelerate the development process. Potentially developing 2 - 3 photoresponsive moieties in tandem as potential scaffolds may improve efficiency depending on resources and expertise available.

It is important to note the balance required between Φ and ε. Photoresponsive moieties that have extremely high ε tend to be better fluorophores than therapeutic delivery systems. Though, these fluorescent properties are important for imaging and theranostic applications, if the goal of the system is to release therapeutic the energetic loss by fluorescence will need to balance with mechanisms of energetic transformation for cargo release. This challenge is present in both PSs and PPGs: PSs undergo an electron transfer to produce ROS and PPGs undergo photoinduced electron transfer reactions for therapeutic release.[183] Thus, unintended release of energy as fluorescence poses a challenge to efficiency in both systems. Furthermore, balancing the Φ and ε is even more important in PPGs that release inherently cytotoxic therapeutics as too sensitive systems will produce cellular damage during administration similar to PSs which have demonstrated undesirable phototoxicity. For example, Foscan (Φ = 0.35 and ε = 23,000 M^{-1} cm^{-1}) did not receive approval in the US although it was approved in Europe, potentially due to high phototoxicity side effects including burns at the site of administration.[12, 19] Thus, when developing cytotoxic photoactivatable therapeutics, activation by incident light may pose another toxicity

challenge and may require lower Φ and ε values. Similarly, drug depots may require lower Φ and ε to ensure limited release from ambient light supporting long-term inertness until illumination. The ideal photoresponsive moiety faces a complexity of variables, both known and unknown as questions remain about the degree of light penetration and how it relates to phototoxicity. For simplicity, aiming for a high Φ balanced with a high ε responsive to long wavelength light will help tackle variables such as penetration through a variety of skin types and tissues expanding the potential applications of the photoresponsive moiety.

Synthetic Modification of Therapeutic Potency and the Resulting Photoproducts

Another consideration in photoactivatable design is the synthetic modifications required to append the therapeutic to the PPG. By appending the PPG to the therapeutic by a crucial site for therapeutic efficacy, PPGs can inactivate the therapeutic. Only when the therapeutic is released upon illumination is the site revealed and activity regained.[55] However, these synthetic modifications may diminish the efficacy of the therapeutic or the Φ of the PPG depending on the lability of the covalent attachment between the two. Photoswitch systems face greater challenges in therapeutic modification as a minor conformational change in response to light is required to significantly improve therapeutic efficacy. In general, photogated carriers may be optimal for synthetically sensitive cargo, although carriers do require further optimization (discussed further in section 1.5.5).

When selecting a photoresponsive moiety, it is also important to consider the photoproducts. Once illuminated and the therapeutic is released, the resulting scaffold should ideally no longer absorb light to optimize the photons available for PPGs still carrying their cargo. With the previously mentioned challenges facing light tissue penetration, this understated consideration may be crucial in deeper tissue therapies. The therapeutic photoproduct should also regain its therapeutic efficacy upon release. Interestingly, photoproduct considerations are

less crucial for photoswitch development as the conformationally modified photoswitch does not commonly produce multiple photoproducts. Instead, in theory, the photoswitch returns to its inactive state by exposure to a different wavelength of light. Further, when the photoswitch returns to its “off state”, illumination should re-isomerize the therapeutic to its active state improving therapeutic activity.

ADME

The photoresponsive kinetics and general ADME properties of the photoresponsive moiety will contribute significantly to therapeutic efficacy. First, localized efficacy can only be achieved if the kinetics of cargo release and delivery outcompete rates of diffusion away from the site of illumination. Theoretically, the kinetics of absorption and electronic excitation are nearly instantaneous as determined by the Franck-Condon principle. However, absorption is limited by the tissue penetrance of light and the moiety’s ability to absorb photons (ε). Once absorption does occur however, the major limiting step for a successful PPG is the release of the cargo (Φ). It is crucial that this rate is kept sufficiently fast to outcompete the rate of diffusion away from the target tissue.[181, 184] Due to these kinetic concerns, as well as the general slow rate of photolysis from cyanine, the ADC Panitumumab was introduced to the cyanine-duocarmycin photoactivatable therapeutic to improve the kinetics of diffusion and accumulation.[102] As previously discussed, the control of spatial and temporal delivery is the main therapeutic advantage of using photoresponsive moieties and thus the kinetics of cargo release need to be sufficient to maintain these benefits *in vivo*. For photoswitch and photogate systems the kinetics maintain similar constraints. A therapeutic photoswitch needs to isomerize into and maintain the active form for enough time that the “on state” can achieve its therapeutic effect. Photoswitches that insufficiently maintain the active form and cannot achieve efficacy may require constant illumination. Similarly,

photogates need to open and therapeutic cargo diffuse into the illuminated tissue before diffusion of the nanomaterial away from the site of treatment.

Therapeutic potency can be further limited by ADME as demonstrated by the sub-optimal biodistribution of some PSs.[12, 158] The bioavailability of the photoresponsive therapy is initially dictated by its administration, absorption, and solubility. While many PDT systems are delivered intravenously, a few are orally available (**Table 1-2**). Although intravenous administration ensures a high bioavailability, oral treatments still provide many benefits that could improve safety and feasibility of treatment. Orally available treatments require diminished cost of treatment and allow for ease of dosing outside the clinic (crucial for when ideal biodistribution is achieved after extended periods of time as demonstrated by Photofrin).[12, 185] Oral treatments would also further support patient-controlled treatment and delivery.

Photoresponsive moieties need to also be water soluble to diffuse well in the bloodstream and ensure distribution to the treatment site. For orally administered treatments physiochemical properties (such as pH, molecular weight, and polarity) are further constrained to ensure optimal absorption through the gastrointestinal tract.[186] Although, there have been approved and tested hydrophobic PDT systems (such as Verteporfin and Tookad) that took advantage of liposomal or other nanomaterial preparations to improve their water solubility, these more complex designs introduce their own absorption-based challenges (discussed in section 1.5.5).[12] Similar to these nanomaterial preparations, the photoresponsive moiety may help improve poorly soluble therapeutic cargo. The photoresponsive moiety circulates and shelters the therapy until illumination and therapeutic release, at which point the more hydrophobic cargo permeates into the laser-targeted tissue. Extensively hydrophilic properties of the photoresponsive moiety may also minimize PPG uptake by tissue which may help minimize inadvertent activation outside the laser-targeted tissue. Again, the desired physiochemical properties of the photoactivatable therapeutic are extremely complex and not completely understood. The fact that the

photoactivatable therapeutic is a composition of two unique molecules enhances this complexity. In general, however, the system should be water soluble to ensure ideal bioavailability and ideally provide multiple methods of administration before illumination.

The photoresponsive moiety's stability, or ability to resist metabolism and clearance, will affect how long the optimal bioavailability persists. Inherently, PPGs balance the bond strength required to bind cargo and the inherent bond weakness required for photolability to absorbed NIR energy. To optimize photoactivatable benefits, therapeutic release should not happen until illumination. Thus, the photolabile bond must resist enzymatic and filtering processes in the blood and in organs such as the liver and kidney. Interestingly, isomerizable photoswitches do not have the same concerns regarding photolabile bonds. However, their structures often do have desaturated bonds that can be reduced or weak ring structures that are crucial to switching.[57] Thus, *in vitro* testing of stability throughout the moiety optimization process is crucial for all photoresponsive systems. Finally, the rate of clearance or excretion from the body needs to be slower than the time required for sufficient uptake, ideal distribution, activation, and therapeutic release, but not so slow that phototoxicity persists (discussed further in the risk analysis).

1.5.3.2 Risk Analysis: Dark Activity and Toxicity

Dark Activity

Photoactivatable therapies rely on diminishing the activity of the drug until illumination for therapeutic improvement. Consequently, the therapeutic activity without illumination (referred to as "dark activity") needs to be minimal. Dark activity can be a result of therapeutic release from metabolism (in the blood, the liver, kidney, or other tissues), activation by ambient light (as demonstrated by PDT phototoxicity), or persistent therapeutic efficacy while appended to the photoresponsive moiety. The photoindex quantifies dark activity by comparing efficacy without illumination ("dark") to the efficacy with illumination (light). Tested photoswitches have only

attained 8-fold improvement between dark and light while PPGs have achieved 2-fold to almost 4,000-fold improvement in cellular studies.[69, 79, 117] The concept of photoindex and examples of its calculation are further explored and elaborated on in section 1.5.6.

Low levels of dark activity do not indicate therapeutic failure as photoactivatable DDSs can act to enhance effects of less potent therapies by localizing therapeutic release. Such therapies may cause minimal toxicity at lower concentrations in the dark. Thus, the risk imposed by dark activity will be significantly defined by the therapeutic cargo selected (section 1.5.2). However, in general, a minimized dark activity minimizes off-target effects and preserves the available photoresponsive cargo, optimizing localized release of therapeutic at the site of illumination.

Toxicity of the Photoresponsive Moiety and Photoproducts

As noted previously, the FDA's highest priority is safety. Therefore, establishing the toxicity of the photoresponsive agent and photoproducts throughout pre-clinical studies is essential for development. This exploration commonly includes off-target pharmacology of the photoactivatable system which could be introduced earlier in development. For example, off-target cellular studies alongside validation cellular studies may begin to indicate potential non-desired pharmacological targets and inadvertent metabolism which could be expected *in vivo* and later in patients. Previous clinical tests of scaffolds may also indicate their potential safety in other novel derivations and applications. For example, although heavy metal NIR-responsive PPGs exist, they are more likely to exhibit serious toxicity and were thus predominantly excluded from the reviewed photoresponsive moieties in section 1.4.[184] However, heavy metal species are not always toxic and can induce a therapeutic effect by multiple mechanisms of action, as demonstrated by NAMI-A and KP1019. Both Ru therapeutics display a low degree of systemic toxicity but with varying mechanisms of action: KP1019 produces a cytotoxic effect and NAMI-A

produces anti-metastatic effects.[115] Thus, thorough pre-clinical investigation (including off-target cellular studies and preliminary assessments of toxicity before GLP studies) may begin to account for unexpected effects of novel derivatives of tested scaffolds, begin to provide preliminary assessments of toxicity of the scaffold, as well as any synthetic modifications that remain on the photoproducts. Certainly, *in vivo* and patient trials will truly assess the safety of the system as demonstrated by the extensive toxicity assessments in GLP *in vivo* studies and Phase I trials.

ADME's Impact on Toxicity

The risks associated with using toxic photoresponsive agents or even toxic therapeutic cargo will be influenced by excretion and distribution into vulnerable tissue. For example, one of the risks of Photofrin usage is the month of phototoxicity due to its slow clearance. Patients must avoid direct sunlight and bright indoor lighting to minimize the risk of burns and other superficial lesions. Similarly, Photofrin's distribution and buildup in collagen and smooth muscle layers has led to stenosis and other obstructive structures upon illumination. These adverse effects and the development of better therapies have led investigations of Photofrin treatment for bladder cancer to be discontinued.[12] Thus, second and third generation PSs have begun to be address Photofrin's sub-optimal biodistribution, excretion, and inherent phototoxicity. Similar concerns should be investigated and addressed during photoactivatable therapy development.

Unlike PDT, many PPG and photoswitch systems can modify their therapeutic to be non-cytotoxic and potentially avoid ADME toxicity concerns, however, the majority are still being developed with cytotoxic cargo as reviewed above (**Table 1-4**) and discussed in section 1.5.2. Thus, more rigorous optimization of ADME properties may be required for the successful development of inherently toxic therapeutics. For example, ADC-cyanine-duocarmycin was developed to optimize the localization of the duocarmycin therapeutic in the tumor. Specifically, the ADC improves the PK of the photoactivatable therapeutic at the tumor site as a means of

countering cyanine's slow photocleavage rates.[102] Toxic photoresponsive moieties, on the other hand, should ideally be avoided but can also be sheltered within photogated carriers. For example, Ru based photogated carriers ensure that Ru is retained within the hydrogel to diminish its potential toxic effects.[83] In general, thorough GLP studies of *in vivo* toxicity are required to convince the FDA of the safety of novel photoactivatable therapeutics regardless of cargo and scaffold, while preliminary pre-clinical studies can help to assess initial toxicity and select between multiple photoresponsive moiety candidates.

1.5.3.3 Feasibility Considerations: Ease of Synthesis, Patentability, and Theranostic Potential

Beyond the risks and benefits of photoactivatable therapeutics, feasibility of these complex novel systems should be contemplated early in the selection and design of photoresponsive moieties to ensure success of achieving marketing status. These considerations include: 1) can the photoactivatable therapeutic be easily synthesized (in high quantities), 2) is the photoactivatable therapeutic stable during storage and administration, 3) can the system be patented, and 4) is there potential for theranostic measurements.

The ease of synthesis of the photoresponsive moiety and photoactivable therapeutic will make development more efficient in both the pre-clinical and clinical stages. Pre-clinically, an easier synthesis will allow for more attempts at optimization and minimize the time waiting on compound for *in vitro* and *in vivo* tests. Eventually, a simpler synthesis can be more easily scaled up to provide enough therapeutic for hundreds of patients in clinical trials. The more challenging the synthesis, the more challenging it will be to iterate and test the photoactivatable system through optimization and pre-clinical development, and eventually the more costly it will be for patients to purchase. The cost of the therapy, depending on what competitive drugs are available and the benefit of the photoactivated system, will affect its usage and continued relevance in the

market. Thus, the synthetic methods used to attain the final product should be compared to other therapeutics available for the targeted indication.

Along those lines, general instability and inadvertent photoresponsivity of photoactivable therapeutics can also make their development and clinical adoption more challenging. During synthesis, special dark facilities and training may be required to produce photoactivatable therapeutics which can slow development and potentially increase the likelihood of error or inadvertent activation of product. To assess the likelihood of inadvertent activation as well as intrinsic instability, initial optimization studies can measure background hydrolysis rates similar to assays conducted for optimization of ADC-cyanine-duocarmycin leads.[69] Although the ADC studies were performed under 37 ºC to assess potential physiological stability, performing similar studies under cold storage temperatures or under normally lit settings would indicate general stability of storage and photoresponsivity for manufacturing and administration. Fluorescence or liquid chromatography mass spectrometry can measure background photolysis, hydrolysis, or degradation. Once a potential administration method is selected, performing similar measurements of background hydrolysis during *in vivo* administration would assess the likelihood of background photolysis in similar clinical applications. Especially during administration, requiring medical personnel to prepare syringes or administer therapeutic in dark or low light conditions can increase the likelihood of error. Thus, speaking to clinicians and drug manufacturing organizations about these potential obstacles may help further scope feasibility. Unlike PDT, PPGs release therapeutic only once after photoactivation. Thus, thoroughly understanding limitations of synthetic production, inherent stability, and clinical administration are crucial for feasible translation. Once again, having the highest possible Φ and ε can increase the risk of activation during administration in well-lit clinics diminishing the benefits of the photoactivatable DDSs and increasing the potential of phototoxicity depending on the therapeutic.

Patenting the photoactivatable therapeutic is also crucial for feasible translation and successful marketing. Beginning conversations with patenting teams early in the design process can help ensure a patent will be attained and even potentially sway selection of photoresponsive moiety based on patentability. In industry, many potential drugs from high throughput screens are often discarded due to potentially weak patent protection. For academic research, patent exploration will also help support cognizance of prior art and how the research team furthers prior art by publications throughout the development of the system. Such knowledge will help support both research ventures, as well as, ensure the technology is not disqualified from patenting by no longer meeting the novelty and non-obviousness requirements.[111] Although, somewhat beyond the scope of this introduction, a review of current patents as well as patents that reposition drugs for novel indications may be useful in further learning the landscape of an unmet clinical need and gaining a better grasp of how novel photoactivatable therapeutics can meet requirements for successful patenting.[187]

Finally, theranostic applications of photoactivatable therapeutics may not only expand the application and benefits the system provides to a variety of unmet medical needs, but also can help support validation assays by clearly demonstrating spatial and temporal control. Intrinsic theranostic capabilities (such as those of BODIPY and cyanine PPGs) require the side products to continue to absorb light and the scaffold to have inherent fluorescent properties. However, counter to the previous concerns of how these properties diminish photoactivatable efficacy, theranostics harness these attributes as a means to monitor distribution and release, which may accelerate addressing concerns of efficacy for novel photoactivatable therapeutics.

1.5.4 Light and Light Devices

As reviewed in section 1.3, PDT therapies have been applied to multiple indications. In tandem with these developments a variety of light sources and fiber optic devices have also been made and approved. Although, the FDA approved PSs require some form of easy external access to illuminate the tissue, there are many more PDT systems that have been tested or are currently being tested in the clinic in parenchymal tissue alongside novel light sources and delivery devices. When addressing unmet clinical need(s) with a photoactivatable therapeutic it is important to consider the light devices available and limitations of these devices, as the current devices available and their cost will contribute significantly to the feasibility of the therapeutic. This section will therefore provide a more generic discussion on the clinical precedent of devices and their applications as well as the importance of dosage and dosimetry when considering the role of light and selection of a light source in photoactivatable therapeutics.

1.5.4.1 Selecting a Device Based on Indication

When selecting a device for photoactivatable treatment it is important to consider the precedent set by previous PDT devices including the intensity of treatment that may be required, the necessity of fiber optics based on the indication, and the costs associated with certain devices (**Table 1-7**).[31] Laser devices with optical fibers that are loosely inserted or interstitially incised into tissue are ideal for internal applications to the gastrointestinal tract, bladder, lung, prostate, head, and neck as they provide high intensity, coherent light efficiently. Conversely, lamps are the preferred application for superficial indications such as AMD, breast cancer, skin malignancies, actinic keratoses, and other applications as they can provide high intensity, incoherent light that can be used for multiple wavelength treatments by filters.[36] LEDs provide a cheaper alternative to both lasers and lamps and have been applied to both internal and superficial applications as they efficiently transmit light in fiber optics, can be modified into desired geometries, and do not

require filtering. However, LEDs cannot achieve intensities of lasers as they inefficiently convert electrical energy to light often resulting in inadvertent heating.[28] The continued development of LEDs with improvements in their intensity and maximizing compatibility with fiber optics may further minimize the current financial costs of treatment associated with lasers.

Novel applications of PDT that have not yet achieved approval but have been heavily investigated include the brain, liver metastases, liver bile ducts, and pancreatic cancer.[12, 36] PDT has been tested in high grade glioma treatment to ensure removal of any residual cancerous cells that can spread throughout the brain and regrow. In previous clinical trials, the PS was administered to the patient before surgery. Then, after tumor resection, the surgical cavity was coated with intralipid for uniform light delivery and illuminated with a fiber optically delivered high-intensity laser.[158] PDT has also reached the bile ducts for the treatment of hilar cholangiocarcinoma and other unresectable gastroenterological diseases by endoscopic illumination.[188] In pancreatic and liver cancers, multiple diffuser fibers are applied interstitially to the respective organ.[158, 189] The challenges with these indications for PDT has been the minimal concrete evidence of improved response based on PDT treatment. Further trials, novel PACTs, and developments in dosimetry may support conclusive evidence for treatment of these parenchymal cancers.

Table 1-7 Pros and Cons of FDA Approved Light Sources for PDT

Light Source	Pros	Cons
Laser	Capable of high doses Monochromatic Highly compatible with fiber optics	Expensive Can be large Requires high maintenance
LED	Small, adaptable, configurable geometry Low cost Endoscopic and interstitial applications	Thermal effects Low power Broad spectral width Incoherent light
Lamp	Low cost Ease of transitioning between multiple wavelengths Can achieve high power	Often less efficient with fiber optics Broad spectral width Incoherent light Requires filtering

1.5.4.2 Dosimetry: Optimizing Dosage, Geometry, and Timing

As previously discussed, the dosage and dosimetry of light is highly dependent on the intensity, duration, and geometry of light exposure and the distribution of the photoresponsive agent. These crucial variables led to the failure of motivating lutetium as Phase I dosimetry analysis of prostate cancer treatment was found to be substantially heterogeneous both between patients and individually in the patients themselves.[12] Thus, beginning dosimetry studies and understanding potential efficacious dosages as well as optical properties of the target organs in pre-clinical *in vivo* studies may help reveal such challenges before clinical trials. Initial results can be further validated in Phase I clinical trials measuring dosimetry and PK (**Figure 1.12**).

The range of intensities under consideration will be limited by the device itself as referenced in section 1.5.4.1 with lasers providing up to 8 W, LEDs up to hundreds of mW, and lamps up to tens of W.[28, 31] The total dosage of light, which correlates to the total therapeutic released, is calculated by multiplying the intensity of exposure by the duration of the exposure. For PDT, intensities of 1-5 W are required at longer wavelengths of light for successful treatment in tens of minutes.[28] Similarly scoping the required intensity for photoactivatable therapeutics is important to minimize potential photothermal toxicity effects as well as develop feasible treatment times. Photothermal toxicity is governed by the Planck-Einstein relationship and occurs when the rate of energy delivery to tissue from irradiation exceeds the rate of energy dissipation. Although longer wavelength light is, in general, less likely to induce phototoxicity as it is lower energy, if the intensity of irradiation is too high ablative effects can still occur.[32] Further guidance is offered by the American National Standards Institute in the form of maximum permissible exposure.[190] Ensuring that such photothermal toxicity does not result from required light doses during toxicology studies will be important for ensuring safety and required in the FDA IND.

The other components of dosage, the duration and sequence of irradiation, needs to also be optimized to ensure therapeutic efficacy and minimize chance of photothermal toxicity. Most

photoresponsive therapies aim for the highest intensity in the shortest duration to optimize local therapeutic concentrations and ensure efficacy. However, novel sequences of illumination have recently developed in PDT such as metronomic irradiation. Metronomic illumination employs a lower rate of light delivery as well as a lower dose of PS for a longer period of time to shift a PS's mechanisms of cytotoxicity from necrosis to apoptosis as the rate of energy delivery is lowered.[28] Although, such mechanistic changes are not expected in photoactivatable therapeutics, they are beneficial to understand when considering combinatorial treatments with PDT. Further, the illumination duration and sequence of photoactivatable therapeutics may significantly affect the kinetics of release as well as the kinetics of diffusion to the therapeutic site. For photoswitches especially, the sequence of light delivery may be crucial. Multiple scenarios of irradiation were recently proposed for photoswitches with different properties including illumination before injection, illumination at the site for short periods of time, and a sequence of illumination to turn on and off photoswitches.[191] As previously mentioned, photoswitches that quickly return to their "off state" may also require extended periods of illumination. These scenarios begin to provide an understanding of the potential opportunities of photoactivatable therapeutics as well as the complexities of irradiation to make these opportunities feasible. Understanding the ideal illumination sequence and duration of dosing will require expertise in dosimetry and can benefit from theranostic measurements.

Dosimetry studies can also elucidate the geometry of illumination to determine the ideal spatial boundaries. Indeed, the field of dosimetry seeks to optimize the distribution of light dose to ensure efficacious and homogeneous treatment in the desired tissue for both the indication generally but also specifically per patient, presenting another way to achieve personalized medicine. In 1986, a method for "light therapy planning" was developed based on modeling data, data on the optical properties of the target tissue, the patient's specific treatment requirements, and *in vitro* testing to generate the optimum irradiation parameters.[30] Although, dosimetry is still

undergoing *in vitro*, *in vivo*, and clinical trial development, the multitude of fiber optics available with both non-contact, contact, and interstitial applications do require planning especially when moving into completely interstitial tissues such as the pancreas and liver (**Figure 1.4**).[31] For interstitial applications sequential illumination of multiple areas, as well as, simultaneous illumination using multiple diffusing fibers have been employed clinically to irradiate a greater expanse of tissue and deeper tissue volumes.[28] Since photoactivatable therapeutics rely on spatial control for their efficacy ensuring that the light reaches the desired treatment area in a uniform manner is paramount to achieving this control and consistent efficacy between patients. For this reason, theranostics may also be crucial to furthering the development of both dosimetry and photoactivatable therapeutics as these substances provide a method of monitoring the therapeutic release based on illumination.

Beyond the considerations of dosage, another consideration is when to begin illumination which relies on the administered dose of the photoactivatable therapeutic and its bioavailability in the targeted tissue. As previously mentioned in section 1.5.3, Photofrin requires 48 h of circulation before ideal concentrations for treatment are attained at the target tissue.[12] Similarly, ADC-cyanine-duocarmycin demonstrated ideal biodistribution in *in vivo* cancer tissue after 3 - 4 days post-dosing. Such studies ensured an optimal localized dose before illumination. Undeniably, temporal control is one of the unique benefits of photoresponsive therapies and may require extensive investigation especially when paired with other targeting methods (such as ADCs). Investigation should be conducted during pre-clinical development to take full advantage of this benefit of photoresponsive therapeutics and maximize the localized delivery promised by photoresponsive therapy (**Figure 1.12**).[69]

1.5.5 Carriers: Modifying Stability and Distribution

In section 1.4, photogated systems made from hydrogels, RBCs, NPs, and liposomes were introduced. This section will further elaborate on these carriers, beyond photogated applications, and consider the benefits a carrier can provide photoactivatable therapeutics. The discussion will be limited to more generic classes of DDSs presented in 1.4 as the field of nanomaterials is quite expansive and under great development (**Figure 1.13**). DDSs that respond to other stimuli will also be briefly mentioned in relation to developing multi-responsive systems. Many carriers have required camouflaging to improve their biocompatibility, which has been clinically achieved by PEGylation. Although RBC membranes and other innovative camouflaging techniques have demonstrated pre-clinical success in diminishing recognition and clearance of foreign nanomaterials, these techniques have not yet been translated into the clinic and thus are considered beyond the scope of this introduction.[192, 193] Many expansive reviews have been written to discuss the diverse and growing field of carriers, which are recommended to assist in selecting the ideal carrier for the photoactivatable therapeutic and the indication to be addressed.[10, 194, 195]

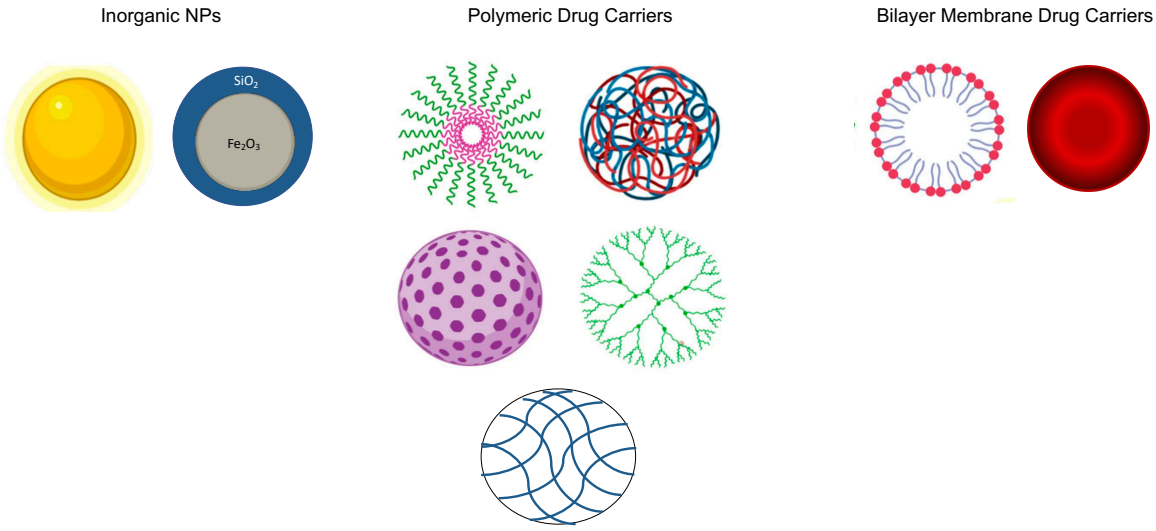

Figure 1.13 Reviewed potential carriers for photoactivatable therapeutics that have achieved clinical success. Inorganic NPs include gold NPs and superparamagnetic iron oxide NPs. Polymeric drug carriers include micelles, polymeric NPs, mesoporous NPs, dendrimers and hydrogels. Bilayer membrane drug carriers include liposomes and RBCs. Adapted with permission.[196]

1.5.5.1 An Introduction to Carriers in the Clinic and their Potential Indications

Inorganic Nanoparticles (NPs)

Although inorganic NPs, in general, display higher cytotoxicity and less biocompatibility than other nanomaterials there have been successful applications of these NPs that harness their mechanisms of clearance or are modified to improve biocompatibility by cellular masking. Many inorganic NP systems are covered in the next few paragraphs as well as their clinical applications. The unique distribution and imaging properties of these systems can be harnessed for applications in pre-clinical validation, theranostics, as well as targeting therapeutics to specific tissues as will be discussed in section 1.5.5.2.

Although gold NPs were first discovered in the 1850's, they have only recently achieved clinical translation as a photothermal method to ablate cancer tumors with the clinical studies of AuroLase. AuroLase is undergoing testing for the thermal ablation of metastatic lung tumors. The PEGylated gold-silica nanoshell displays NIR photoresponsivity which it converts into photothermal energy.[194] Gold NPs have also been tested pre-clinically as radiation dose enhancers and chemotherapeutic carriers.[197] Although having achieved limited clinical success in these other therapeutic techniques, gold NPs demonstrate a multi-functionality that may be useful for certain indications and photoactivatable DDSs.

Superparamagnetic iron oxide NPs (SPIONs) have had more success with clinical translation as they have been applied in both therapeutic and imaging applications (predominantly magnetic resonance imaging - MRI). Iron NPs, such as Faraheme, take advantage of clearance mechanisms to act as a slow-release system for iron supplementation in anemic patients, while Feridex and Resovist are used in MRI liver imaging and GastroMARK is a contrast agent for darkening of bowel loops.[198] Pre-clinically, SPIONs have also been tested as magnetically guided NPs, as another means of thermal ablation excited by an alternating electric field, and as a means of drug delivery to the pancreas of type I diabetes patients due to enhanced accumulation.

Electromagnetically excited photothermal effects of SPIONs are also under development in early clinical trials with Hafnium oxide NPs (NBTXR3) for squamous cell carcinoma and NanoTherm which has been approved in Europe for brain cancer.[194] It is important to note, however, that in 2008, 2012, and 2009 the FDA-approved MRI contrast enhancers Feridex, GastroMARK, and European approved Resovist respectively were withdrawn due to a lack of users. Feridex, which cannot be injected as a fast bolus due to adverse effects, may have been unable to compete with Resovist (injectable as a fast bolus).[198] The reasons for the withdrawal of Resovist and GastroMARK were not clarified.[199] However, the continued withdrawal of the majority of clinically approved SPIONs may require further investigation before selecting this carrier above others.

Silica NPs and MSNs are under investigation as photogated systems, although no clinically approved MSNs yet exist. MSNs contain nanopores on their surface that can be used to encapsulate hydrophobic drugs or biomacromolecules as previously presented in section 1.4.[4] However, observed cytotoxicity has led to applying previously discussed cell membranes as well as PEGylation to their surface to enhance biocompatibility. Antibodies have also been applied to MSN surfaces for active targeting.[194] Using MSNs for photogated applications may be ideal for this unique NP as therapeutics can easily diffuse out of the MSN interior. However, MSNs may also be useful in developing multi-responsive DDSs (discussed in 1.5.5.2).

Potential Indications

Inorganic NPs have demonstrated a variety of safety and success in the clinic. However, inorganic NPs pose unique opportunities as carriers that should be noted when considering unmet clinical needs. Both gold and iron oxide NPs have demonstrated photothermal and imaging properties in the clinic. These unique inherent qualities may be beneficial for multi-responsive systems as well as in the development of theranostic applications. SPIONs can additionally add another layer of drug targeting by means of magnetic guidance. Although SPIONs are commonly

metabolized into iron, they have successfully been used to treat chronic kidney disease, myocardial infarction, and other cardiovascular diseases.[198] Although, SPIONs and gold NPs provide unique opportunities for photoactivatable therapeutics they are limited systems in their current development. The surface of gold NPs cannot be easily modified and they are often produced as mixtures, while as previously mentioned approved SPIONs have been unexpectedly withdrawn from clinic.[199] Before undertaking the complexity of bringing a multi-layered novel DDS to clinic, ensuring that the benefits will outweigh the risks is paramount with inorganic NPs.

Intravenous Polymeric Carriers

Polymeric NPs and Polymer-Drug Conjugates

Polymeric NPs and polymer-drug conjugates have been cited to make up 30% of all FDA approved nanomedicines from 1995 to 2016. This widespread approval is partially due to the high synthetic versatility and ease of modifications of these NPs.[200] These NPs are commonly prepared as nanocapsules or nanospheres that are composed of poly(glycolic acid), poly(lactic acid), poly(lactic-co-glycolic acid), and other synthetic polymers as well as natural polymers, including chitosan, gelatin, collagen, dextran, etc. Polymeric NPs are one of the most common carriers due to their biocompatibility as well as drug release tunability which is adjusted by manipulating the lactide to glycolide ratio and molecular weight. Further, each of the compositional synthetic and natural polymers, as well as their modifications, attribute unique properties to the carrier and can affect the circulation and distribution of many different therapeutics. Notably, PEG external modifications can significantly improve biocompatibility and circulation half-life. Thus, many polymer-biologic conjugates are clinically approved including adenosine deaminase enzyme, granulocyte-stimulating factor, interferon beta-1a, and antihemophilic factor for the treatment of combined immunodeficiency, febrile neutropenia, multiple sclerosis, and hemophilia, respectively. Both natural and synthetic polymers have also found success as delivery vehicles for cancer

including albumin-paclitaxel among other albumin conjugates, and a polymerized leuprolide acetate.[194] Polymeric NPs and conjugates are ideal for improving biocompatibility and circulation time and may be useful in sheltering photoactivatable therapeutics.

Polymeric Micelles

Resembling monolayer vesicles, polymeric micelles are composed of amphiphilic copolymers. The core is commonly hydrophobic with a hydrophilic outer shell. However, inverted micelles also exist. Clinical applications of micelles have been limited due to their non-specific drug release, instability, and synthesis as mixtures, but micelles have been successful in solubilizing poorly soluble drugs and have gained traction for stimuli-responsive and targeted therapies including PDT.[194] Although no micelle therapeutics have been approved by the FDA, micelles carrying paclitaxel and docetaxel are approved in South Korea. Other trials underway include improving the safety profiles of chemotherapeutics such as cisplatin and doxorubicin.[201] Silicon phthalocyanine PC4 is also undergoing development in PEG-polycaprolactone micelles.[12] The micellar mixture Cremophore EL has been more widely accepted and has been clinically employed for the original hydrophilic form of PDT Tookad, as well as Redaporfin, currently under clinical trials.[12] However, the biological effects of Cremophore EL are not completely understood and may be a potential source of adverse events.[202] Micelle based DDSs are ideal for systems where the therapeutic can escape the micelle on its own. As demonstrated with photogated micelles, photoactivatable therapeutics that take advantage of polarity differences or require improved solubility may seek success in micelles.

Dendrimers

Dendrimers are highly branched polymeric macromolecules which incorporate therapeutics by encapsulation in void spaces or covalent bonding. Dendrimers have achieved minimal clinical success due to challenges of therapeutic release as well as complex synthesis and resulting issues with mass production.[194] A limited number of clinical tests with dendrimers have been completed with the most prominent treatment being OP-101. OP-101 is a N-acetyl cysteine covalently coupled to a dendrimer that has been found to localize to neuroinflamed regions of the brain for the treatment of X-linked adrenoleukodystrophy.[203] OP-101 has completed Phase I tests and there is now an active Phase II study in COVID-19 patients.[204] The feasibility of mass-producing photoactivatable dendrimers should be considered before selecting this carrier. Further, since products are commonly a mixture of branched species, the FDA may require more extensive safety analysis.

Potential Indications

Of the discussed polymeric carriers only polymeric NPs and polymer-drug conjugates have achieved FDA approval by improving the circulation, drug delivery, and clearance of biomacromolecules and cytotoxic therapeutics.[194] NPs gather in the vasculature of tumors due to the EPR effect, which causes smaller nanomaterials to accumulate in the leaky tumor vasculature.[32] This passive targeting initially catapulted NPs into the clinic as potential chemotherapeutic DDSs with improved PK in cancer tissue. Since then, NPs conjugated with antibodies or coated with targeting ligands have been developed and tested in the clinic as a means of active targeting and further improving biodistribution and PK.[205] NPs can be extensively modified and have been conjugated successfully with a multitude of drugs and peptides. Thus, NPs are employed for indications ranging from rare diseases to cancer and have thus far been bound to albumin or polymer particles. Many polymeric NPs still face challenges with fast

clearance which may have contributed to the greater success of liposomes (discussed below).[206, 207] However, NPs still offer an opportunity to manipulate the PK for therapeutic targeting and delivery, while avoiding challenges in therapeutic release that other carriers may face. Although many micelles have been clinically tested none have yet to receive FDA approval due to the instability previously mentioned. Similarly, dendrimers face challenges with their complex synthesis and variability.

Hydrogels

Hydrogels are hydrophilic or amphiphilic polymers that swell upon absorbing water, have high loading capacities, enhanced stability, and mimic tissue in water content and malleability. The FDA has approved over 30 injectable hydrogels products and there are over 400 clinical trials involving hydrogel materials. Hydrogels are available as topical applications, coils, or bulk materials. Examples include topical application to burn wounds, coils in the treatment of aneurisms, and bulk materials for tissue augmentation or regeneration. Hydrogels are commonly composed of natural polypeptides and saccharides or synthetic polymer chains. In general, there are more FDA approved naturally derived hydrogels than synthetic hydrogels, likely due to differences in biocompatibility. Although, the current clinical landscape is more thoroughly reviewed elsewhere some prime examples of successful hydrogels include: dermal fillers in facial correction aesthetics with delivery of lidocaine, subcutaneous hormonal therapy for testosterone dependent prostate cancer that relies on an implantable diffusion controlled reservoir, spinal applications as scaffolds for bone growth, advanced heart failure treatments, treatments for urinary disorders, and PEG-based hydrogels for image-guided soft tissue alignment.[208] Hydrogels are ideal delivery vehicles for proteins and other fragile biological cargo.[83, 209] Challenges hydrogels face include sufficiently low viscosity for injection, rate of drug delivery, costly synthesis,

and regulatory approval due to their classification as devices.[208] Photoactivatable therapeutics that require localized delivery may benefit from hydrogel carriers.

Potential Indications

PEGylated NPs and hydrogels are a prime choice for protein therapeutic delivery. Many stimuli-responsive protein DDSs are under development to enhance both the PK/ PD of proteins and enable spatiotemporal delivery. These systems have been tested with vasopressin, VEGF, and insulin for applications in cardiovascular indications and in diabetes. Undeniably, diabetes affects a widespread and growing population of patients that require continuous insulin injections. Development of stimulated, such as light or glucose-responsive, long-term insulin reservoirs may begin to address the unmet and growing medical need of insulin administration.[175] Although, many systems are in early stages of development, the expansive clinical approval of both hydrogels and PEGylated NPs may be a positive indicator for photoactivatable protein therapeutics.

Since there are many clinically approved hydrogels, further harnessing the already existing applications of hydrogels for improving therapeutic delivery with spatiotemporal control may be a promising method to translate photoactivatable therapies into the clinic. For example, the process of tissue regeneration is extremely complex and may be suited for temporally controlled, orthogonally delivered photoactivatable therapies. Further, hydrogels can be topically applied to joints and injected into subdermal tissue which may improve dermatological therapies by allowing for patient-controlled therapeutic delivery.

Red Blood Cells (RBCs)

Although RBC therapeutics, outside of transfusions, have not yet gained FDA approval, they have been successfully tested up to Phase III clinical trials by multiple companies for the delivery of Dex 21-phosphate, asparaginase, thymidine phosphorylase, and RTX-134. Specifically, Dex 21-phosphate is a pro-drug that undergoes dephosphorylation by RBC enzymes, which then allows the parent drug Dex to escape the RBC over a period of a month. This slow-release system has been tested in multiple indications including irritable bowel disease, Crohn's disease, cystic fibrosis, chronic obstructive pulmonary disorder, and ulcerative colitis, but has found significant success in ataxia telangiectasia. RBCs have also been employed as bioreactors for enzyme replacement therapy. Specifically, RBCs have successfully delivered thymidine phosphorylase for the rare mitochondrial neurogastrointestinal encephalomyopathy and phenylalanine ammonia lyase (PAL) for the treatment of phenylketonuria. Initial treatments with PAL in a PEGylated form resulted in adverse reactions and anaphylaxis, which were overcome by RBC delivery and sheltering of the enzyme. RBCs that can express PAL are now undergoing Phase I clinical trials.[210] Surface loaded RBC therapeutics have also been under development for an extended amount of time but have yet to reach clinical trials.[211, 212]

RBCs have many desirable characteristics as carriers. They have an extremely high loading capacity (RBCs have a volume of 85 - 91 mm^3), they are easily obtained from patients with minimal negative impact, and transfusion of blood is a clinically established protocol.[213] Internally loaded RBCs that meet transfusion standards have been prepared by using the EryDex System and have gained FDA approval.[210, 214] RBCs are ideal for targeting the reticuloendothelial system (RES) which clears damaged RBCs or any tissues that are heavily vascularized. RBCs are also ideal carriers as long-term drug depots, demonstrated by the slow-release therapeutics under development.

Potential Indications

Since RBCs circulate in the blood stream and thus have been proposed to reach the central nervous system during a stroke or traumatic brain injury, penumbra of the myocardial infarction zone post ischemia, alveolar and airway compartments in pulmonary hypertension or acute lung injury, and other locations of vessel damage such as post-surgery as blood pools in these locations.[192] Other ideal applications of RBCs are in blood related diseases, such as chronic anemia, sickle cell, blood-derived cancers, or cardiovascular diseases as these are most accessible to RBC carriers. Applications that already require common transfusions, including sickle cell anemia and beta-thalassemia, can overcome the feasibility challenges of asking patients to receive therapeutics via transfusion. RBCs are regularly captured and cleared by means of the RES, thus any therapeutic targets in this space may be ideal. Indications in these organs may include enzyme deficiencies, hepatic tumors, parasitic diseases, iron overload in thalassemic patients, and toxic agents.[213] Dex RBCs and cytokine IL-1B with ceftriaxone in RBCs, reduced glutathione with antiretroviral drugs combined into RBCs, and RBCs modified with an insulin derived peptide are currently under *in vivo* development for rheumatoid arthritis, AIDS treatment, and Type I diabetes respectively.[212]

Slow release RBC therapeutics are also under development that take advantage of passive diffusion, such as Dex 21-phosphate RBCs, and include antineoplastics, antiparasitics, vitamins, steroids, antibiotics, and cardiovascular drugs.[213] While Dex 21-phosphate RBCs have improved outcomes in cystic fibrosis patients, bioreactor RBCs with L-asparaginase have also been tested in Phase I and II clinical trials for metabolic deprivation of acute lymphoblastic leukemia and pancreatic adenocarcinoma patients with minimal adverse effects.[212] RBC bioreactors are commonly applied as replacement therapies for enzyme deficiencies, which can gather in the RES, circulate in the blood stream, or release enzymes upon hemolysis.[213] RBC carriers thus have a wide range of applications but may be best for therapies that act as

bioreactors in the blood, can affect blood clotting, require delivery to the endothelium, improve efficacy by long-term circulation and slow release, or affect the immune system.[192]

Liposomes

Liposomes are bilayer phospholipid carriers made up of native phosphatidylethanolamine, phosphatidylserine, phosphatidylcholine, phosphatidylglycerol lipids, and cholesterol which acts as a stabilizer. The type of lipids used, ratio of lipids, surface modifications, and cholesterol content affects the size, lamellarity, and surface properties of liposomes and allows for tuning the targeting ability and drug release rates. Liposomes can deliver both hydrophilic and hydrophobic drugs carried in the aqueous core and lipid bilayer respectively. However, loading of therapeutics into liposomes can be challenging. Newly developed methods improve loading, including ammonium sulfate gradients that cause weak base drugs to precipitate within the core of the liposome. Liposomes are quickly cleared due to plasma proteins opsonization and resulting recognition and clearance by the liver and spleen. However, PEGylation of liposomes has dramatically increased their circulation times. Further, the extent of PEGylation allows for tuning the circulatory half-life.[194]

Liposomes have been extremely successful in reaching the clinic and attaining FDA approval due to their ability to carry hydrophobic therapeutics and shelter cytotoxic drugs. Liposomes have found the most success with cytotoxic therapies by diminishing toxicity to improve the TI.[215] Thus, the majority of clinical liposomes are cancer treatments as well as treatments for infectious diseases, with a few liposomes achieving approval as analgesics. Doxil was the first liposome (carrying Doxorubicin) to achieve FDA approval in 1995. Since then, AmBisome (carrying Amphotericin B), DaunoXome (liposomal daunorubicin), DepoCyt (liposomal cytarabine/ Ara-C), Mariqibo (liposomal vincristine sulfate), Onivyde (carrying irinotecan), Onpattro (siRNA therapy for polyneuropathy), and Vyxeos (liposomal combination of

daunorubicin and cytarabine) among others have all achieved FDA approval.[150, 200, 215, 216] Liposomal systems have been also employed as carriers of hydrophilic PDT therapeutic Visudyne for AMD and tested with zinc Pc clinically before being abandoned.[12] Examples of liposome systems still under development include Arikace (encapsulated Amikacin), and actively targeted MM-302, MBP-426, and SGT53 therapy for the targeted delivery of Oxaliplatin. ThermoDox is one of the first thermosensitive liposomes to reach Phase III trials for cancer treatment.[194] ThermoDox's initial clinical success sets a precedent for photoactivatable liposomes. Further, the general improvement to safety liposomes provide may be useful for multi-layered improvements of safety in conjunction with photoactivatable therapeutics. Liposomes may also be a means of sheltering photoactivatable therapeutics from dark activation and be a means of combinatorial therapeutic release as demonstrated by Vyxeos.

Potential Indications

Similar to PEGylated NPs, liposomes can improve the circulation, drug delivery, and clearance of biomacromolecules and cytotoxic therapeutics.[194] Liposomes also collect near tumors due to the EPR effect.[32] Although, this may improve therapeutic delivery to tumors surrounded by vasculature it may have minimal effect on hypoxic tumors. Thus, liposomes may be ideal for PACT applications as demonstrated by the multitude of cancer liposomal therapies currently approved. Other applications include enhancing the safety of antifungals and antibiotics.

Beyond re-purposing suboptimal therapeutics, novel applications of liposomes include improving the distribution of PSs, localizing release of PDT by means of ROS sensitive unsaturated phospholipids incorporated within liposomes, and combination treatments of PDT and immunotherapy. Similarly, liposomes can improve the biodistribution of photoactivatable therapeutics, target release in a multi-layered manner (especially with cyanine PPGs that produce ROS as well) and be developed for combination treatments. Liposomes are also undergoing

research for CRISPR delivery by combining liposomes with gold NPs for targeted gene therapy. The gold NPs induce photothermal effects which subsequently cause breakdown of the liposome and release of internal contents.[150] Photoactivatable therapeutics may be another means by which gene therapies could be locally targeted from within liposomes.

1.5.5.2 Considering Carriers for Photoactivatable Therapeutics

With the precedent of stimuli responsive carriers, including micellar and liposomal PDT and thermally responsive liposomes and inorganic NPs now in clinical trials, carriers offer immense potential to support the translation of photoactivatable DDSs. Carriers can shelter photoactivatable therapeutics from dark activation, modify their ADME, as well as provide other novel benefits discussed in 1.5.5.3. Carriers may be the perfect solution to avoid dark activation as liposomal carriers have already proven to improve the PK and PD of cytotoxic systems and hydrophobic photoresponsive moieties (as demonstrated with PDT hydrophobic systems).[12, 215] Carriers, however, can not only shelter the photoactivatable system, but also improve its circulation and clearance half-lives and localization by providing an additional layer of tunability with surfaces that can be PEGylated to improve circulation and to which targeting agents can be appended to.[32, 192] Carriers can also deliver high quantities of therapeutic.[10] These considerations will be discussed in greater depth below.

Both photogated DDSs as well as PPGs and photoswitches encapsulated within non-stimuli responsive carriers exist. Because photogated DDSs have not yet achieved clinical approval and face similar challenges as their foundational carrier, the discussion below will focus on carriers that photoactivatable therapeutics can be encapsulated within that have achieved clinical approval. These considerations can then be expanded to the photogated systems which still require further optimization and *in vivo* testing.[217]

ADME

Absorption/ Administration

Most carriers, including liposomes, micelles, polymeric NPs and internally loaded RBCs, are injected intravenously as these carriers inefficiently permeate across the gastrointestinal wall during oral delivery.[186] Hydrogels, on the other hand, are usually injected into the targeted tissue, but require the appropriate viscosity for successful injection.[208] Other DDSs can also be directly injected, but are expected to be quickly cleared.[186] Thus, intravenous injection remains the mainstay of all systems (except for hydrogels). The administration method should be considered in the benefits and risks analysis of selecting a carrier. As previously discussed, orally available therapeutics improve opportunities for personalized medicine and decrease costs among other benefits.[185]

Distribution and Targeting

Passive and active targeting dictates carrier distribution. In general, most carriers are retained within the vascular space, clearance organs, and tumors due to their inability to pass between endothelial pores of other tissue. Specifically, carrier sizes over 200 nm concentrate in the liver, sizes over 400 nm in the spleen, while those less than 10 nm are cleared by the kidney. Polymeric micelles of sizes 50 - 100 nm and liposomes of sizes 100 - 200 nm are considered ideal for maximal blood concentrations and minimal RES clearance.[186, 201, 218] Tumors often have enhanced permeability due to immature chaotically branched vasculature which causes the EPR effect and passively targets liposomes and NPs to this tissue. Thus, the manipulation of nanomaterial size is crucial to manipulate biodistribution via passive targeting.

However, distribution is dependent on more than just size. For micelles, liposomes, and NPs the distribution also depends on morphology, composition, and mechanical properties. NPs, including MSNs and gold NPs, that are rod shaped rather than spherical stay in circulation for

longer periods of time. Similarly, NPs covered in hydrogels to improve flexibility circulated for longer periods of time while “hard” NPs concentrate in macrophages, endothelia, and tumors.[186] It is important to note, the majority of carriers are produced as mixtures and these properties (including size) vary within that mixture.[201] This variability is partially why the FDA is so resistant against mixtures, as uncertainty surrounds whether the mixture can produce consistent, reproducible safety and efficacy.

The accumulation of nanomaterials by passive targeting can improve the PK of therapeutic release as the high quantity of concentrated drug within the nanomaterial passively accumulates in the target location. Active targeting by a light source can then further improve the PK as a large burst of therapeutic is released during localized illumination. Layering other active targeting agents, such as antibodies, peptides, and small molecules, on these DDSs can further improve distribution within tissue.[10, 186] Although maximizing the coating density of the targeting agent is generally ideal, caveats include how the density affects extravasation through the endothelium and how widely the target is expressed throughout tissue. A phenomenon known as the “binding site barrier” affects uniform diffusion of high affinity ADCs through targeted tissue and can be overcome by optimal dosing and lowering antibody affinity.[219] Other nuances of targeting agents include the potential of immunogenicity as full antibodies are known to generate an immune response. Employing antibody fragments instead can minimize the immune response and immune mediated clearance.[186] There are many more caveats to active targeting agents not covered in this paragraph that should be considered when developing these multi-layered targeted DDSs.[219]

RBCs and hydrogels pose more limited means of targeting distribution. Unless focusing on clearance organs, RBCs are retained within the vasculature for extended circulatory periods. However, this systemic distribution may be ideal for reaching tissues and organs that are less accessible during cardiovascular events as previously described.[220] Hydrogels, on the other hand,

are targeted during administration, but as the hydrogel is cleared any attached therapeutics will also be systemically cleared.

Metabolism and Therapeutic Release

One of the main advantages of a carrier is their ability to shelter the photoactivatable therapeutic until activation by light. The main concern, however, is to ensure the photoreleased therapeutic can still exit the carrier and affect the targeted site. Thus, it is important to consider and design means of therapeutic escape with appropriate kinetics of release from the carrier to the targeted tissue.[200, 217] For example, Doxil has enhanced tumor accumulation, but doxorubicin release from the liposomes is less than ideal and diminishes the potential efficacy.[218] Out of the discussed classes of photoresponsive moieties, PPG's may face the least therapeutic release issues as they can modify therapeutic polarity to anchor therapeutics within the carrier, as demonstrated by internally loaded Cbl RBCs.[72] Photoswitches, on the other hand, may need to rely on cellular uptake and breakdown of carriers. This approach would still be feasible if the photoswitch is minimally active in its "off state" and would consequently have a minimal effect on non-target cells that uptake the photoswitch.

Liposomes and micelles release therapeutic by drug leakage over time or carrier breakdown during RES clearance. Further, micelles require a specific concentration to maintain their assembly, otherwise they entirely disassemble or undergo changes in size and morphology at lower concentrations.[201] The PK of therapeutic within these carriers is therefore affected by multiple states: free therapeutic in the plasma and therapeutic still within carriers. Current liposomal therapeutics take advantage of the breakdown of liposomes as well as endocytosis into cells to generate a unique drug specific release profile.[150 4, 194] This release profile is dependent on many factors including the stability of the lipid bilayer and the encapsulated therapeutic. Photoactivatable therapeutics carried via liposomes will need to ensure that the drug release

profile from metabolism and breakdown of the liposome does not inhibit the targeting potential of the photoresponsive therapy. For this reason, photogated systems that induce the breakdown of liposomes by affecting the hydrophilic and hydrophobic balance may be beneficial.[4]

NPs, on the other hand, must either interstitially release drug or be internalized by cellular phagocytosis or pinocytosis to induce pharmacological effects.[218] Although there are many complexities to NP uptake, including what organelles (such as lysosomes) the NP encounters, surface modifications (such as folate acid) can improve cellular uptake to tumor cells.[221] Similar to liposomes and micelles, photogated systems that release therapeutic from NP carriers upon illumination may minimize the necessity for cellular uptake.

While cellular uptake of liposomes and polymeric NPs is based on passive and active targeting, RBC targeting will require careful PK consideration to ensure therapeutic quickly reaches the targeted tissue before not only diffusing away, but also being carried away by circulation. Although more resolution is required, initial *in vivo* tests have demonstrated localized therapeutic release at the target tissue after illumination.[72]

Excretion/ Clearance

Not only can carriers protect photoactivatable therapeutics from dark activation, but they can also protect biological macromolecules from early clearance.[175] The majority of carriers, including liposomes and NPs, are cleared by the liver and spleen. Other components of the RES can also support clearance including bone marrow and lungs. Opsonization of carriers by serum proteins can help enhance recognition by these tissues. For this reason, PEGylation and other surface modifications can help carriers be “stealthier” as confirmed with liposomal carriers.[186] Initially, liposomes were found to localize extensively to the spleen and liver due to their extremely fast clearance. However, PEGylation helped diminish the clearance rates of liposomes.[194] Similarly, PEGylating the surface of NPs increased these nanomaterials’ circulation time.

However, PEGylation has been noted to induce an immune reaction after chronic injections and to affect carrier stability, cellular uptake, and drug release. Thus, PEGylation must be optimized in both molecular weight and amount used.[218]

Previously mentioned carrier properties, including size and shape, influence their distribution as well as their clearance. Neutral to cationic surface charges improve circulation and minimize clearance for NPs and liposomes respectively.[194, 215] However, extended circulation is not always beneficial for photoactivatable therapeutics. Depending on the therapeutic cargo, long term circulation of a highly photoresponsive cytotoxic phototherapeutic may induce phototoxicity similar to the PSs Photofrin and Tookad.[12, 212] Fortunately, the degree of PEGylation can be tuned to modify the rate of clearance.[194, 215] Different clearance rates may need to be tested in animal models to assess the ideal treatment efficacy.

As previously discussed, inorganic NPs can be minimally biocompatible and thus very quickly cleared, which PEGylation can counter to a degree.[194] However, clearance rates can vary based on the patient's RES activity. Thus, personalized treatment taking into account patient RES activity (e.g. increased monocytes) when determining therapeutic dose may further enhance treatments.[218]

Toxicity

Whenever incorporating a new component to any therapeutic system, ensuring safety is paramount. As mentioned throughout the considerations above, many nanomaterials have demonstrated safety concerns. Inorganic NPs most prominently have demonstrated the potential for inherent toxicity due to their composition of heavy metals. Antibody targeting techniques as well as PEGylation have demonstrated potential concerns for immunogenicity.[218] Similarly, liposomes composed of synthetic lipids with high cationic charges have also demonstrated risk of immune toxicity as well as general toxic effects on cells.[150] Thus, predominantly, natural lipids and

polymers have been preferred and approved for polymeric NPs and hydrogels due to potential biocompatibility and safety.[208] In general, carriers are cleared by the RES in high quantities, which could pose a risk for liver and spleen toxicity due to high concentrations. Further, as previously noted when selecting a therapeutic (section 1.5.2), the therapeutic carried by the photoactivatable DDS will modify the risk posed by these inherent clearance mechanisms.

Feasibility Considerations: Manufacturing, Storage, and FDA Approval

Synthetic Nanomaterials

During early development, synthetic materials (including liposomes, micelles, hydrogels, and polymeric NPs) faced challenges with synthesis and therapeutic preparation. However, advancements in synthetic processes, loading processes, and growth of FDA approved carriers have improved ease of synthesis and the compatibility of carriers with a variety of drugs.[194] Although hydrogels have wide-spread clinical applications and approval, manufacturing and storage of hydrogels still remains very costly as they face challenges with sterilization due to their high water content.[208] Liposomes and micelles also face challenges with long-term storage stability as both are known to leak as their membranes permeabilize over time.[150] Cryoprotectants, such as dextrose, sucrose, and trehalose, have been incorporated into the storage solutions as stabilizers.[150] However, these stabilizers provide another product that requires manufacturing, optimization, and safety testing.

Although liposomes, polymeric NPs, and hydrogels have achieved FDA approval with multiple therapeutics, micelles have yet to achieve regulatory approval. In general, the FDA maintains strict regulation over the pharmaceutically active species and excipients, which need to be thoroughly characterized and uniformly produced to ensure reproducible safety. Synthetic nanomaterials have faced challenges in uniformizing carrier production and thus have required more extensive regulatory testing. Translating carriers therefore requires sufficient data to confirm

that although properties of individual batches may vary, products are in general the same and will produce the same *in vivo* effect. Micelles still face further challenges due to their varied properties and inherent instability both *ex vivo* and within physiological environments, making consistent results more challenging to achieve. Conversely, inorganic NPs can be more easily prepared. However, long-term circulation of metal-containing NPs is considered a high risk of potential toxicity.[195] Thus, clearance of these systems needs to occur within a reasonable time frame for FDA approval. **Table 1-8** provides an overview of the preclinical considerations specific to NPs, but these considerations can be expanded to all synthetic nanomaterials.

The regulatory classification of carriers can also affect their development requirements and delay clinical translation. Carriers are commonly considered new medicinal products, even if they incorporate existing drugs, as was the case for Doxil, Abraxane, and Vyxeos.[201] Thus, introducing a carrier requires the same degree of development as any other novel therapeutic, regardless of the therapeutic cargo. Uniquely, hydrogels are considered devices as they do not achieve an effect by chemical action. Thus, hydrogels that carry therapeutics have been termed combination products which typically require 7 - 10 years of negotiations and compliance testing before approval.[208] Thoroughly understanding the limitations and scope of development required for introducing a carrier to a photoactivatable therapeutic will help weigh benefits and risks including high costs from synthesis and development that can limit adoption.

Table 1-8 Preclinical Considerations of Translating NPs. Reprinted with permission.[195]

Category	Issue	Considerations
Synthesis and Physicochemical Characterization	Structure, morphology, and formulation	Solubility, size and size distribution, morphology, structural arrangement, spatial distribution, density, geometric features, composition (organic vs. inorganic), shape (nanoemulsions, nanocrystal colloid dispersions, or liposomes), surface charge, and drug combination (drug-device, drug-biologic, drug-device-biologic)
	Stability	Short- and long-term stability in various environments such as in serum, under different pH, temperature, and salt concentrations
	cGMP synthesis	Residual solvents, processing variables, impurities, and excipients
	Scale-up process	Critical steps in the scale-up and manufacturing process for NP products
	Tools	Standard characterization tools of NP properties such as NMR, MS, DLS, SEC, CE, SEM, TEM, AFM, DSC, and XRD
Safety and Toxicity	Size-specific effects on activity	1) Will NPs gain access to tissues and cells that normally would be bypassed by larger particles? 2) Once NPs enter tissues, how long do they remain there? 3) How are they cleared from blood, tissues, and body? 4) If NPs enter cells, what effects do they have on cellular and tissue functions (transient and/or permanent)? 5) Do different cell types exhibit different effects?
	Route-specificity	1) Inhalation: local respiratory toxicity and bioavailability 2) Subcutaneous: sensitization 3) Dermal: bioavailability, follicular retention, local lymph nodes, and phototoxicity 4) IV: hemocompatibility, sterility, different tissue distribution and half-life of API (with targeted delivery and liposomes) 5) Oral: bioavailability 6) Ocular: intravitreal retention
	ADME	1) **A**bsorption: how readily can the NP cross biological barriers (e.g., skin, cell membranes, and BBB)? 2) **D**istribution: how easy is it for the NP to travel to other locations, and what organs do the NPs tend to target? 3) **M**etabolism: does the nanomaterial get degraded into further constituents? 4) **E**xcretion: do the particles get excreted or do they accumulate in various tissues? This ADME framework provides a structure that can be used to address the potential biological effects of nanomaterials. 5) What are the differences in the ADME profile for NPs versus larger particles of the same drug? 6) Are current methods used for measuring drug levels in blood and tissues adequate for assessing levels of NPs? 7) How accurate are mass balance studies, especially if levels of drug administered are very low; i.e. can 100% of the amount of drug administered be accounted for? 8) If NPs concentrate in a particular tissue, how will clearance be assessed accurately? 9) Can NPs be successfully labeled for ADME studies?
	Blood tests	CBC, electrolytes, hemolysis, platelet aggregation, coagulation time, complement activation, and leukocyte proliferation
	Toxicity	1) Developmental and reproductive toxicity 2) (Sub)chronic toxicology 3) Immunotoxicity 4) Neurotoxicity 5) Genotoxicity 6) Respiratory toxicity 7) Carcinogenicity 8) Histopathology
Environmental	Toxicity and elimination	1) Can NPs be released into the environment following human or animal use? 2) What methodologies would identify the nature, and quantify the extent of NP release into the environment? 3) What might be the environmental impact on other species (animals, fish, plants, or microorganisms)?
Future Testing	Safety evaluation	1) What is the role of new technologies to help identify potential toxicities? 2) What is the role of modeling (in predicting exposure, safety concerns, and design of personalized therapies)?

Red Blood Cells (RBCs)

Internally loaded RBCs are currently being tested by autologous administration in patients using the ERYcaps and Red Cell Loader devices. These autologously administered RBCs have exhibited a 24 h survival of at least 75% of loaded RBCs in patients, a half-life of ~28 days which is comparable to non-modified RBCs, and an encapsulation rate of ~30%.[222] In general, RBCs have to be transfused pretty quickly upon preparation due to the quick rise in storage lesions, unless targeting the RES.[212, 220] The complex process of loading RBCs and the exacerbation of storage lesions pose challenges to adopting stored RBCs as a treatment method. Internally loading therapeutics into RBCs also can face challenges as certain therapeutics have been found to make RBCs undergo eryptosis.[220]

Fortunately, RBCs are easily accessed from patients with minimal negative impact.[212] However, the unique, complex loading process that requires blood collection, loading, and transfusion will be expensive which may slow widespread adoption.[212] These modified RBCs also need to be thoroughly characterized throughout the development process further increasing costs. The final manufacturing process should change RBC *in vitro* properties (including membrane plasticity, mean cell volume, percent cell recovery, percent hemoglobin content, etc.) by less than 20%.[213, 222] *In vivo* tests of transfusion can be conducted on mice, cattle, pigs, dogs, sheep, goats, and monkeys.[213] However, by ensuring comparable qualities of internally loaded RBCs to transfused RBCs, the regulatory testing required can be minimized. For example, FDA regulation has allowed the ERYcaps system to classify their internally loaded RBCs as comparable to transfusable RBCs.[212]

RBCs are regulated by the Center for Biologics Evaluation and Research and blood banks are considered “manufacturers” of drugs as they process RBCs for transfusions.[192] Adoption of the ERYcaps or other loading systems into hospital blood banks may help expedite application of loaded RBCs into the clinic, as FDA regulations for manufacturers of RBC species are already

met by blood banks. However, costs associated with maintaining the sterility of the loading environment and process, required immediacy of the loading and administration process, and additional costs of the loading devices may be inhibitory to the feasible application of loaded RBC therapeutics.

1.5.5.3 Novel Benefits of Carrier-Based Photoactivatable DDSs

Photoactivatable therapeutics are poised to provide a novel method of therapeutic delivery and personalized medicine. Specifically, long-term circulation of therapeutics may provide a photoresponsive therapeutic depot that could be released by NIR handheld patient-owned devices.[8] RBCs and liposomes provide the potential for long-term circulation and accessibility at superficial tissue for treatment of dermatological and joint-based problems. Hydrogels also provide a means for long-term slow release with bursts of light-directed release. As has been demonstrated with facial applications of hydrogels, hydrogels can take 1 - 2 years to be completely absorbed.[208] Applications of such long-term hydrogels may include light-directed analgesics for post-surgical or spinal applications. Longer circulating carriers are also being developed with enzyme cargo to act as bioreactors, such as RBCs carrying L-asparignase.[222] In general, carrier-based bioreactors are ideal for acting within the blood. Although potentially facing clearance issues, photogated DASA polymersomes are also under development as photogated bioreactors that can be turned on and off.[133] The unique combination of photoresponsive therapy with drug or bioreactor depots can be an innovative solution to chronic unmet clinical needs and support patient-directed treatment.

As mentioned previously, multiple layers of targeting may be required to maximize the TI, especially of cytotoxic therapeutics as each targeting method incorporates its own limitations. For example, the development of ThermoDox which both passively targets the tumor by EPR and actively targets the tumor by directed heat application has achieved a 25-fold increase in

doxorubicin delivery to tumors. Inorganic NPs also passively target different tissues, such as SPIONs which localize to the pancreas during the onset of type 1 diabetes and are thus under investigation for imaging and diagnosis applications.[199] Thus, carriers can enhance targeting by contributing their inherent passive targeting to photoactivatable therapeutics which rely on light-activated targeting.

Similarly, carriers that are both photoactivatable as well as have other methods of active targeting, such as heat as previously established by ThermoDox or magnetism by incorporation of SPIONs, may further tune targeting and therapeutic release. Magnetic targeting by incorporating SPIONs into liposomes or carbon particles has also reached clinical testing for cancer applications.[217, 223] Other stimuli-responsive systems under pre-clinical development include pH, electrical, and ultrasound as presented in **Table 1-1**.[4, 10, 175] Specifically, photoactivatable cyanine pH-responsive micelles have demonstrated promising enhanced localization *in vivo*.[86] Although, it may be some time before multi-stimuli responsive carriers are ready for development and translation, the potential enhancements they could provide to the TI may be worth the wait.

Magnetically targeted systems have the additional benefit of theranostic drug delivery as SPIONS can be detected by MRI.[217] Providing theranostic capabilities may accelerate translation with strong proof of concept results as well as develop another opportunity for personalized medicine. Theranostic systems currently under pre-clinical development that could take advantage of multi-stimuli systems and photoresponsive moieties include photoacoustic imaging, surface enhanced Raman scattering, optical coherence tomography, luminescence imaging, and Cerenkov radiation techniques.[209] Other more clinically accepted imaging techniques include fluorescent imaging, computed tomography, MRI, and positron emission tomography.[209, 224]

As previously discussed, carriers provide a means of delivering not only high quantities of therapeutic, but also delivering multiple therapeutics and potentially multiple therapeutics by

orthogonal wavelengths. As more photoresponsive moieties are developed, therapeutic delivery may become so finely tunable that specific therapeutics could be delivered from carriers by activation with unique wavelengths. Vyxeos liposomes have already demonstrated the potential for combinatorial therapeutic delivery.[150] Orthogonally responsive Cbl photoactivatable therapeutics and DASA photogated carriers are also under development.[105, 133] Delivering multiple drugs orthogonally (dependent on the wavelength of excitation) may be useful for diseases which already require combinatorial treatments, including cancer and cardiovascular diseases, among others.

1.5.6 The Photoactivatable Therapeutic: Developing New Treatments and Improving Existing Therapeutics

As referenced throughout this Chapter, photoactivatable therapeutics provide an opportunity for active targeting of therapeutic delivery with improved spatial and temporal control. Since photon absorption can lead to both therapeutic release and fluorescence, photoactivatable therapeutics can also improve personalized medicine by monitoring therapeutic delivery location and dosage with theranostic applications. Further, photoactivatable therapeutics encased in long-term drug depots create opportunities for patient-controlled therapeutic release. Due to the multitude of applications and potential unmet needs photoactivatable therapeutics can address, section 1.5.6.1 will describe the path that has been developed thus far to successfully translate photoactivatable therapeutics and what steps remain. Section 1.5.6.2 will then clearly define the multitude of benefits and applications of photoactivatable therapeutics.

1.5.6.1 Illuminating the Path to Clinical Trials for Photoactivatable Therapeutics: Current Progress and Future Steps

Many photoactivatable therapeutics have progressed into *in vivo* studies. However, as compared to other established fields of therapeutic development, the number of *in vivo* studies underway are still limited. As photoactivatable DDSs begin to prepare to transition into the clinic, the approach needs to transition from development of novel photoresponsive moieties toward assessing and optimizing a photoactivatable therapeutic's ability to address the unmet clinical need.[157] This section aims to provide a path by which researchers have begun to prepare photoactivatable therapies for clinical trials and targeting unmet clinical needs (**Figure 1.12**).

Stage 1: *In vitro* Characterization and Optimization

Photophysical Properties and Stability

As introduced in section 1.3.1 and further emphasized in 1.5.3, ideal photophysical properties (Φ, λ_{max}, and ε) are crucial for the success of photoactivatable therapeutics. Specifically, these properties support enhancing therapeutic release in response to potentially limited light penetration. Many groups have approached optimization of these properties by high throughput or rational design methods.[182] Photoresponsive moieties that have been thoroughly investigated and optimized provide structure-function understanding to accelerate adaptation of photoresponsive moieties to novel therapeutic cargo. Taking advantage of such precedent may then accelerate clinical translation.

Notably, cyanine PPGs have been thoroughly investigated as photoresponsive moieties and successfully optimized for efficient and fast photorelease.[69, 98] Lead ADC-cyanine-duocarmycins were initially modified from a first-generation scaffold to adjust the sensitivity of the photoresponsive linker in the dark and to improve the photoresponsive wavelength. Synthetic changes were assessed by measuring efficiency of therapeutic release in the light and dark.[69]

Rational design approaches resulted in to two lead compounds for *in vivo* testing. Similarly, rational design techniques were employed to merge CO-releasing flavanol to a heptamethine cyanine photoresponsive moiety and to improve solubility.[67] Precedent with cyanines may have made both approaches easier and more efficient.[98]

BODIPY groups have been similarly investigated and derivatized for both PDT and PPG applications. BODIPY based photoactivatable CO releasing molecules (photoCORMs) have been successfully developed by means of computational screening followed by structure-activity relationships of BODIPY with a carboxy substituent for CO release. Optimization included shifting toward long wavelength responsivity and improving photophysical properties. Additionally, an inactive control was developed to understand the mechanism of release, as well as to provide a control for further studies.[64] This development process may have also relied on the precedent of BODIPY scaffolds for rational design development.[19, 92, 93, 182]

By relying on established synthetic methods (such as high throughput testing, rational design, and computational methods), as well as literary precedent, improved photophysical properties and solubility may be efficiently achieved. Quick, efficient tests for photophysical properties such as kinetics, Φ, and dark activation will also help minimize unintended dark activity and improve long-term stability.[69] Further, development of an inactive control during optimization can improve mechanistic understanding as well as accelerate pre-clinical characterization.

Irradiation Dose

Oftentimes, studies of Φ and other photophysical properties will result in *in vitro* assessment of the required irradiation dose for photorelease. Of course, *in vitro* assessments will not truly mimic *in vivo* conditions. However, assays have been developed to begin to mimic *in vivo* conditions to determine ideal ranges of illumination dosage.

In vitro development of ADC-cyanine-duocarmycin conjugates included testing a variety of irradiation doses in cellular efficacy assays (**Figure 1.14**). This assay ensures that under ideal *in vitro* conditions a sufficient irradiation and therapeutic dose (100 pM for duocarmycin-ADCs) achieves efficacy.[69] Undeniably, if ideal therapeutic efficacy is not achieved at irradiation doses and therapeutic concentrations under *in vitro* conditions, then surely *in vivo* efficacy will be further minimized due to limitations of light penetrance.

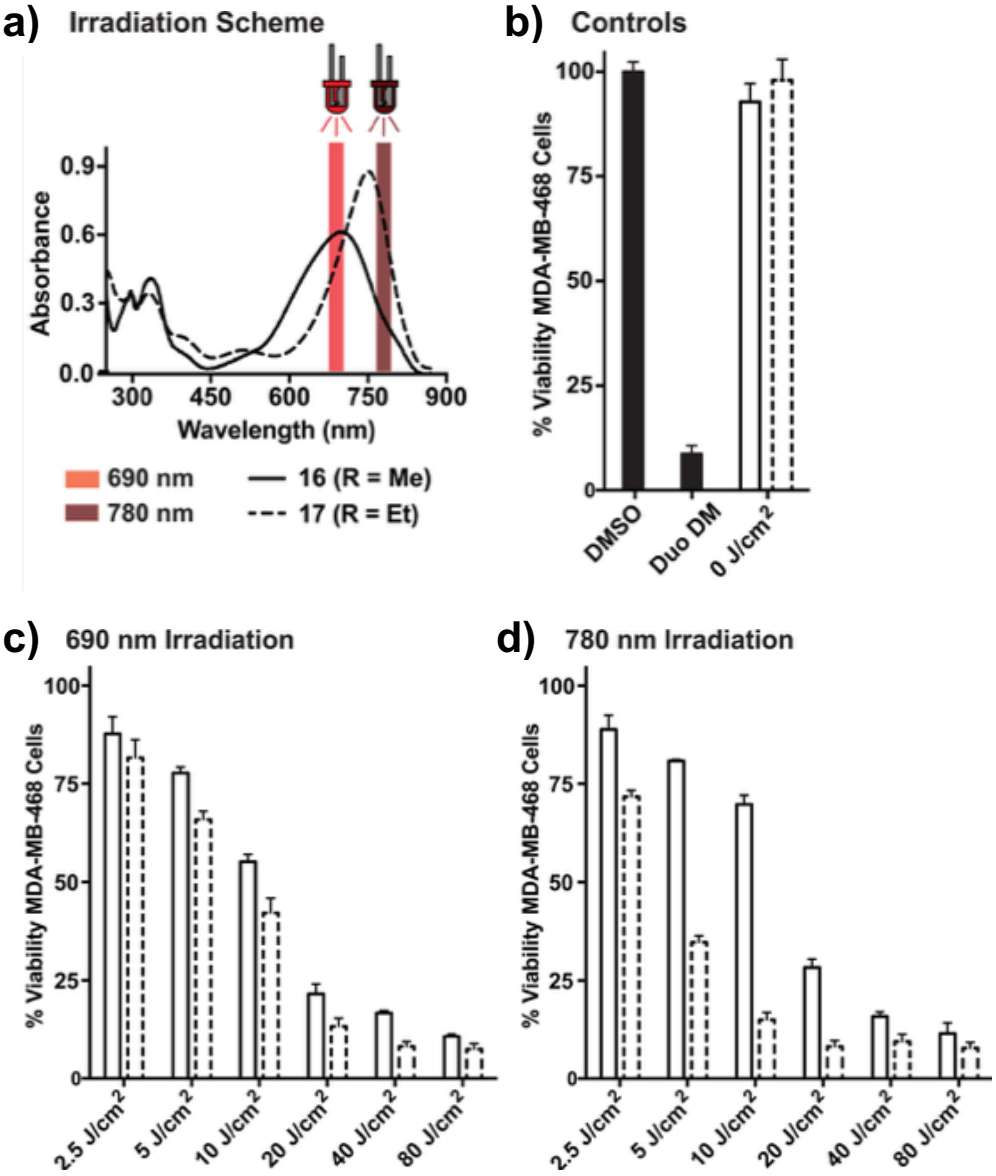

Figure 1.14 ***In vitro*** **optimization of irradiation dose. a)** Absorbance spectra of the two lead compounds (**16**, **17**) and the two tested irradiation wavelengths (690, 780 nm). **b)** Cell viability under control conditions (vehicle, free duocarmycin, and lead compounds in the dark). **c)** and **d)** Viability of cells exposed to 100 pM of each lead compound and a range of light doses at the two irradiation wavelengths. Reprinted with permission.[69]

In vitro assays can also be conducted that account for light scattering and absorption that occurs through tissue. The development of Cy5-Cbl-Dex RBCs included testing of both Cy5-Cbl-Dex in solution as well as from within RBCs with Fitzpatrick tissue phantoms (**Figure 1.15**). Fitzpatrick tissue phantoms mimic the light absorption and scattering properties of tissue by passing light through solutions of mixed lysed RBCs lipids, hemoglobin, and varying amounts of melanin to mimic a variety of skin types (pale-dark, types I-VI).[84] Cy5-Cbl-Dex was successfully photolyzed through all tissue phantoms with a minimal lamp power of 1 mW/cm^2 for 3 min.[73] Such efficient photoresponsivity is promising for *in vivo* studies as these studies expectedly will require higher light doses for treatment.

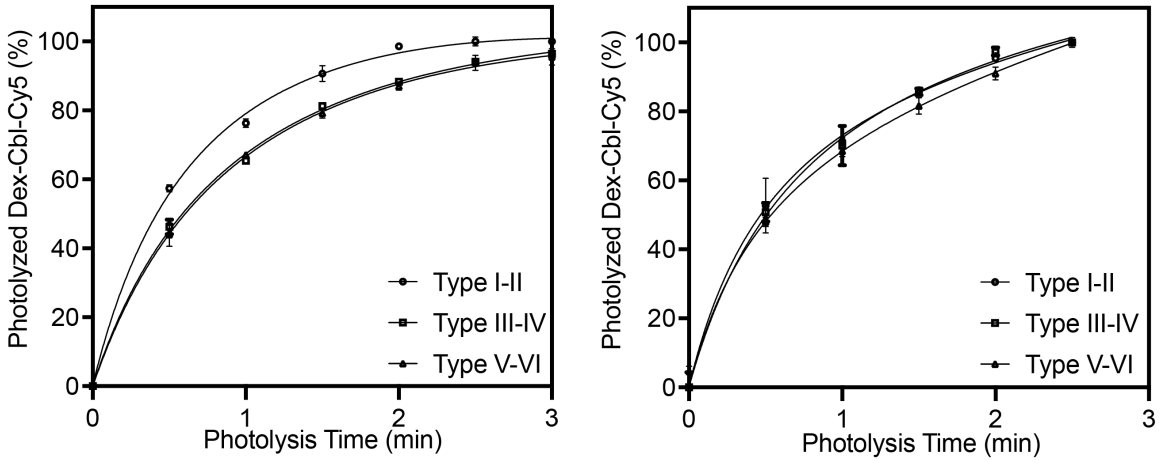

Figure 1.15 Photolysis of Cy5-Cbl-Dex in a PBS solution (left) or from within RBCs (right). Complete photolysis occurs within 3 min of 1 mW/cm^2 illumination through all Fitzpatrick types.[73]

In vitro assays provide the opportunity to assess light doses for further *in vivo* studies. Similar to how PK studies contribute to selecting Phase I doses, so too can *in vitro* assessments optimize ideal doses of both therapeutic and light for *in vivo* experiments. Often, animal disease models can be costly, time consuming, and logistically challenging, especially with photoresponsive species as animal facilities commonly employ extremely bright lights to regulate animal sleep cycles. Thus, quick *in vitro* assays such as cellular efficacy tests and Fitzpatrick series of photorelease can help provide minimum light doses required for *in vivo* studies.

Toxicity and Efficacy

In general, toxicity and efficacy studies are required for both *in vitro* and *in vivo* tests and will often be included in the pharmacology and safety sections of the IND. However, not only does the photoactivatable DDS need to be tested for toxicity, but also the photoproducts should be individually tested for toxicity. The development of the previously discussed cyanine photoCORMs included cellular assays to measure toxicity of the CO photoproduct as well as the cyanine photoproducts towards a hepatoblastoma cell line.[67] Photoproducts were tested by illuminating the cyanine photoCORM alone and adding the resulting mixture to hepatoblastoma cells. Presumably, CO is not concentrated in the illuminated mixture as it can transition into a gaseous state, thus addition of the resulting mixture only tests the remaining photoproducts. Promisingly, the photoproducts demonstrated no toxicity up to 200 mM, while the irradiated photoCORM in the presence of cells exhibited cytotoxic effects from concentrations of 100 mM.[67] Although, the presence of CO did improve the intended cytotoxicity by 2-fold, the high concentration required may be unfeasible under physiological conditions, especially with the inherent risk high doses of CO pose to patients.

Ideally, toxicity studies should also be conducted on normal cells that surround the desired target cell population. Studies of cyanine-camptothecin-biotin tested the PACT's cytotoxic effect

on both cervical cancer cells and normal liver cells *in vitro* (**Figure 1.16**). Minimal cytotoxicity was observed on both cell lines without irradiation. Nonetheless, illuminated camptothecin was cytotoxic to both normal and cancer cells, as is expected of generically cytotoxic therapies. Further, the uptake of the PPG by both cell lines was measured using flow cytometry. Although uptake did increase as exposure time increased, the rate of endocytosis was slower for normal cells than cancer cells, potentially due to the biotin targeting agent. However, the targeted uptake (reaching a 6-fold difference after 30 min of exposure) and minimal dark activation does establish promise for *in vivo* studies.[68] Of course, *in vitro* cellular studies have extended exposure to therapeutic, which does not always occur physiologically due to additional kinetic rates of extravasating from and into circulation.

a)

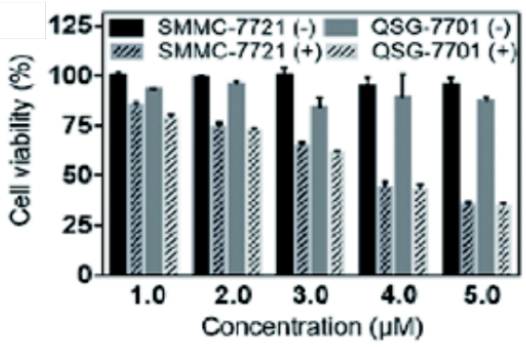

b)

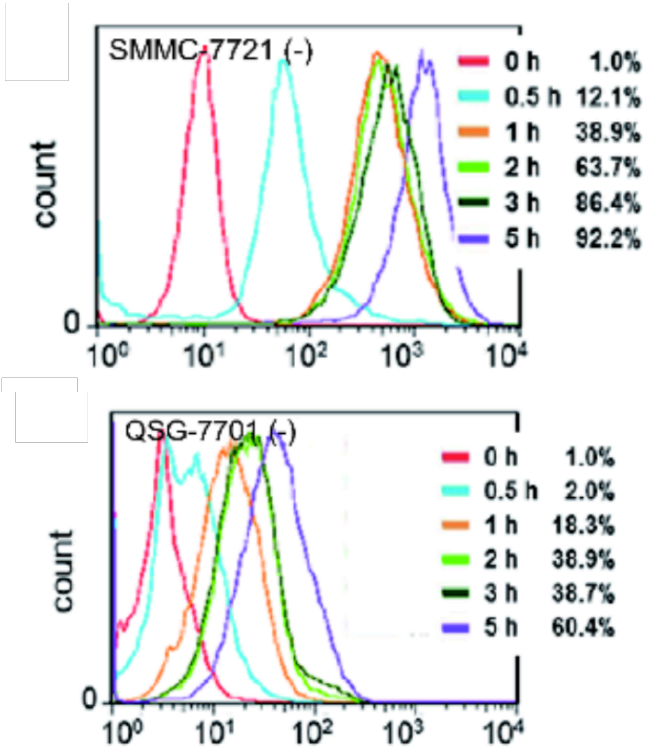

Figure 1.16 Cytotoxicity of cyanine-camptothecin-biotin PACT to cancer (SMMC-7721) and healthy (QSG-7701) cells. a) Cell viability of a range of cyanine-camptothecin-biotin doses (mM) with (+) and without (-) 20 mW/cm^2 680 nm illumination. **b)** Flow cytometry quantification of cellular endocytosis over time. Cancer cells (left) show increased rates of PACT uptake than normal cells (right). Reprinted with permission.[68]

Another way to ensure that the photoproducts and the photoresponsive moiety have a minimal toxic effect is by measuring the toxicity and efficacy of the active photoactivatable therapeutic as compared to an inactive scaffold control. Cy5-Cbl-Dex RBCs were tested for both efficacy and toxicity towards target primary fibroblast-like synoviocyte (FLS) cells and compared to the inactive control Cy5-Cbl-H_2O RBCs. FLS cells are one of the most important mediators of inflammation in inflammatory arthritis.[225] FLSs demonstrate clear localization of glucocorticoid receptor α (GRα; a crucial inflammatory mediator within FLS and other cells and a pharmacological target of Dex) to the nucleus. Treatment with inactive control Cy5-Cbl-H_2O RBCs had comparable localization effects to no treatment controls, while treatment with Cy5-Cbl-Dex RBCs localized GRα comparably to conventional Dex treatment (**Figure 1.17a**). Further, Cy5-Cbl-Dex RBCs displayed similar toxicity as conventional Dex to FLS and Dex-sensitive Sup-B15 B cells. Specifically, Dex is minimally cytotoxic to FLS cells but is notably cytotoxic to Sup-B15 cells, properties successfully reproduced with the photoactivatable DDS. Control Cy5-Cbl-H_2O RBCs had no significant effect on GRα localization or cell viability of FLS or Dex-sensitive B cells (**Figure 1.17b**).[73]

The described assays and applications demonstrate the significance of the *in vitro* validation of the photoactivatable system. PhotoCORM testing not only confirmed the safety of the photoresponsive moiety, but also highlighted the concerns of high therapeutic doses for efficacy. Assessments of uptake *in vitro* also began to indicate potential dark activity as well as targeting efficiency. Comparison to standard of care and inactive controls helps quantify the risks and benefits of a photoactivatable DDS. Further assessments on normal cell lines may provide an improved understanding of the safety pharmacology and set expectations for toxicology studies.

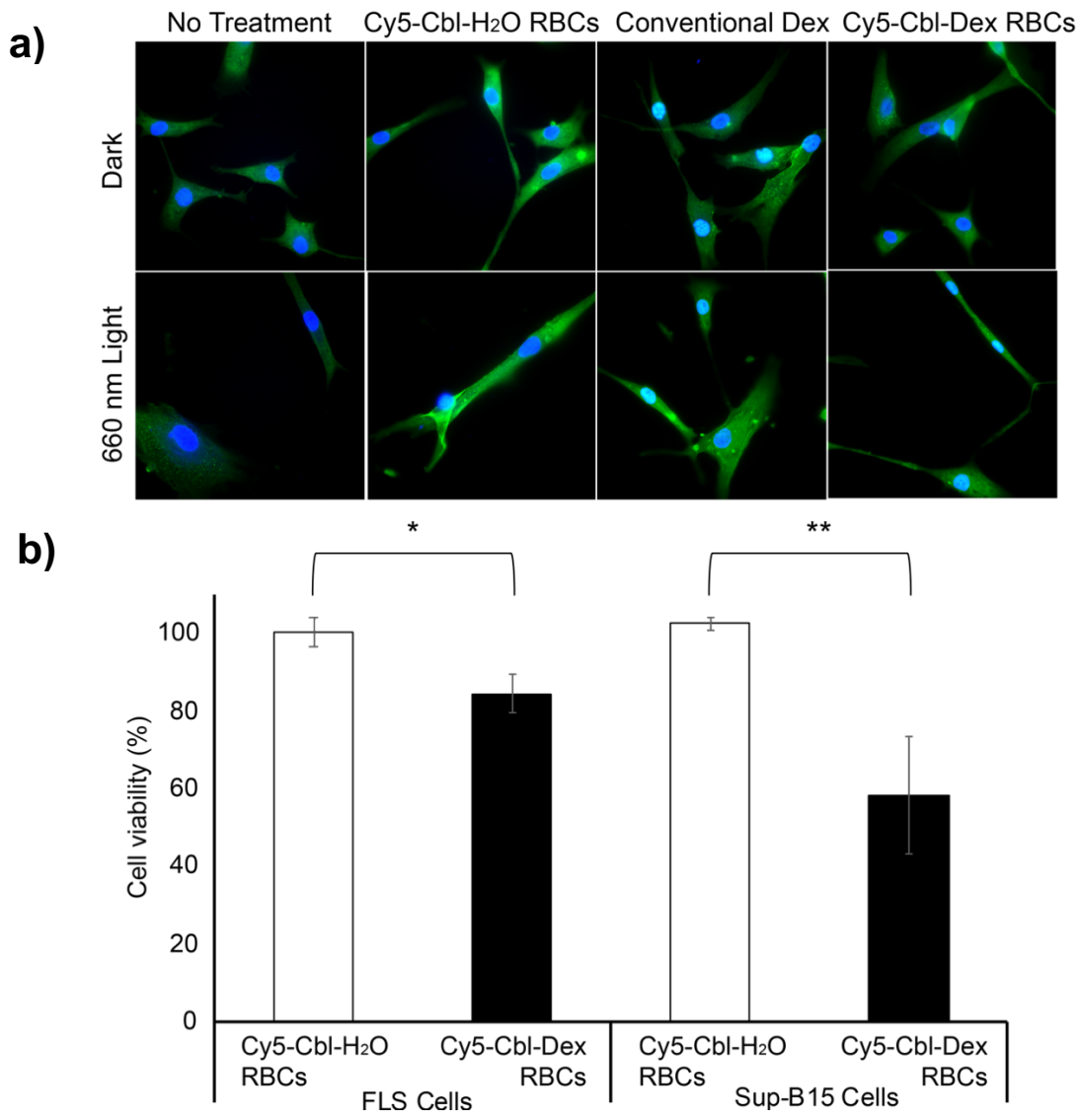

Figure 1.17 Assessing safety of photoresponsive moiety and photoproducts with inactive controls. a) Immunocytochemical analysis of GRα localization in FLS cells. Inactive control Cy5-Cbl-H_2O RBCs localize GRα comparably to no treatment. Only illuminated Cy5-Cbl-Dex RBCs localize GRα comparably to positive control Dex. **b)** Illuminated Cy5-Cbl-H_2O RBCs have no toxic effect on inflammatory FLS cells or Dex-sensitive Sup-B15 B cells. Cy5-Cbl-Dex RBCs are minimally toxic effect to FLS cells and potently toxic to Sup-B15 cells. (*P < 0.05; **P < 0.01)[73]

In vitro Photoindex

In vitro efficacy studies can also rigorously assess the photoindex of a photoactivatable therapeutic. The photoindex quantifies the ratio of dark activity to light activity and assesses the metabolic sensitivity of PPGs. For true comparison of light and dark efficacies it is important to use comparable light doses and therapeutic concentrations to the clinical standard of care. As previously mentioned, the photoswitch antibacterial Azo-Trimethoprim achieves a 7-fold photoindex.[79] In general, photoswitches face challenges inactivating therapeutics and are thus more likely to encounter dark activity.

More expansive studies of photoindex were completed with the Ru-Rigidin complex introduced in section 1.4. The complete complex, rigidin positive control, inactive scaffold control, and standard of care were tested in both 2D and 3D spheroid lung cancer models under normoxia and hypoxia. Inclusion of hypoxic models further mimicked potential physiological conditions of the target tumors. Further, a non-cancer cell line was included as an additional control. Positive, scaffold, and standard of care controls achieve photoindices between 0 and 2, while Ru-Rigidin attains photoindices from 4 to 29 in different 2D cell lines. Normoxic conditions improve photoindices up to 2.5-fold as compared to hypoxic conditions, potentially due to the mechanism of therapeutic release from Ru. 3D spheroids demonstrate more minimal photoindices of 1.6 to 6.1.[117] Due to the novelty of photoactivatable DDSs the required photoindex value for clinical translation is not yet known and as demonstrated varies significantly with cell line. Significantly, ADC-cyanine-duocarmycin successfully reaches photoindices of 580 in target cell lines to more than 3,900 in non-targeted cell lines.[69]

Although many qualitative demonstrations of differences between light and dark activity have been performed, ideally this difference is tested in a quantitative fashion indicating a photoindex. The photoindex also should be assessed in the larger context of standard of care and not only tested on target cells. If the standard of care demonstrates comparable efficacy as the

dark activity of the photoactivatable therapeutic, the photoactivatable therapeutic may be expected to present similar systemic benefits and risks as the standard of care. However, if dark activity occurs at concentrations below the standard of care, the results could serve as *in vitro* validation of the potential for more targeted delivery as opposed to the standard of care. Photoindex also relates to the TI as the greater the difference between dark efficacy and light efficacy the more likely the photoactivatable therapeutic can minimize toxicity of cytotoxic therapeutics by localizing therapeutic effect. Of course, the ratio is a simplification as *in vitro* studies are not limited by concentrations tested, thus both 5 pM to 30 pM and 50 mM to 300 mM will have a resulting photoindex of 6. In some ways, this value may be an oversimplification of the required efficacy and the surrounding context, however demonstrating a difference between light and dark activity is crucial to photoactivatable DDSs. Due to the field's nascency, rigorous photoindex tests are not yet widespread but may be crucial proof of principle data for INDs in the future.

Stage 2: *In vivo* Characterization and Validation

Proof of Principle: "Localized" light dependent release, a qualitative in vivo photoindex

An *in vivo* photoindex can be attained by rigorous PK/PD studies. However, before completing such intensive studies, many researchers have performed more qualitative proof of principle validation with distal sites analyzed for comparison of "localized" therapeutic effect. These distal comparisons have included vascular effects measured in mice ears as well as xenografted tumors on both mouse flanks.

Cbl loaded RBCs successfully localize release in irradiated ears as compared to the mouse's non-irradiated "dark" ear. Docetaxel from Cbl-Docetaxel RBCs is successfully locally released upon illumination causing endothelial damage, which is not observed in the "dark" ear.[72] Photogated Cbl RBCs have also employed this model to demonstrate the localized effect of potent

thrombin (**Figure 1.18**). Fibrinogen is only observed in the light activated ear as compared to the dark control.[142] Of course, the two ears of a mouse are distal to each other, and thrombin effects could potentially be observed throughout the entire irradiated ear or further in the vasculature rather than only at the site of illumination. For such vasculature therapeutics, PK measures of blood concentrations may further quantify the photoindex. BODIPY based photoCORMs have employed such PK measures to assess the modest photoindex of 1.4 for CO levels in the blood.[226] However, successful photoactivated release was observed, further validating the system's light-dependent effect.

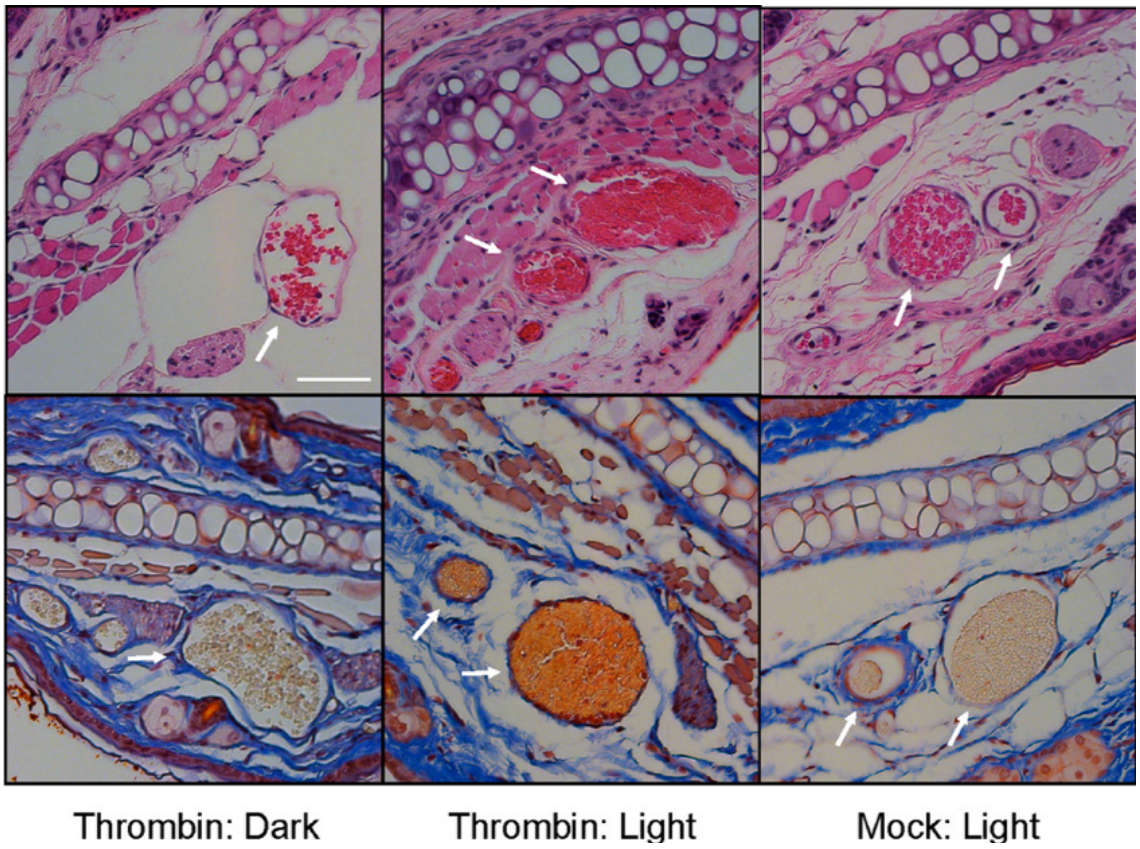

Figure 1.18 Localized *in vivo* effect of photogated Cbl thrombin RBCs. Mouse RBCs externally loaded with the photogating Cbl-blocking segment and melittin system and internally loaded with thrombin were injected intravenously into mice. Immediately after injection, the ear was illuminated with a 561 nm laser. The left column shows the non-illuminated ear, the center column the illuminated ear, and the right column shows the ear of a mouse that received buffer loaded RBCs. Hematoxylin and eosin staining on top shows congestion of illuminated vasculature (center), while bottom images stained with Martius Scarlet Blue dye (which labels collagen blue, RBCs yellow, and fibrin red) show fibrin formation in illuminated ear. Scale bar represents 50 μm. Reprinted with permission.[142]

Distally xenografted tumors on mouse flanks have also served as controls for localized measures of efficacy in cancer models. For example, Ru-Rigidin treatment requires both illumination and the photoactivatable therapeutic to produce a therapeutic effect. Irradiation alone, the scaffold alone with and without light, and the photoactivatable therapeutic without light all had minimal effects on tumor growth. Only the illuminated flank with active photoactivatable treatment furnishes efficacy.[117] The “dark” flank is then a control for excess released rigidin that may be circulating in the vasculature or dark activated rigidin. The model also provides more efficient use of animals, including more controls in the number of animals used. By employing a similar model, photoactivated release of therapeutic from BODIPY-NO theranostics was imaged (**Figure 1.19**). Enhanced therapeutic release is observed in the illuminated tumor. This enhanced therapeutic release is sufficient to suppress tumor growth while dark and vehicle control treatments have minimal effect.[62]

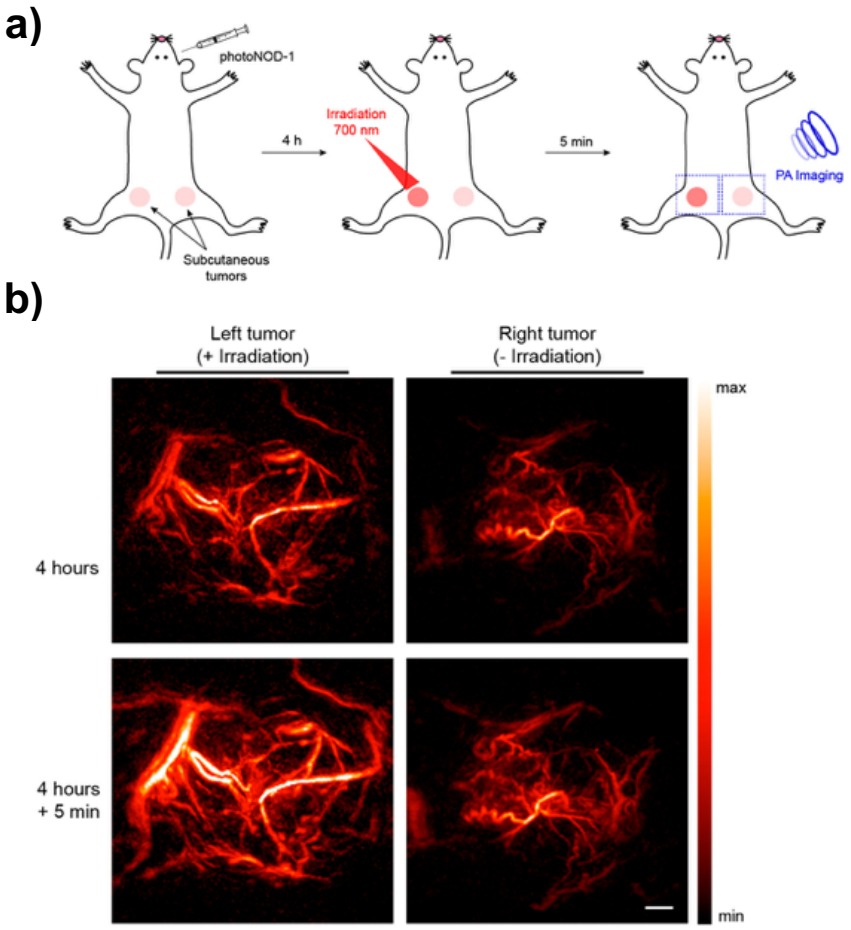

Figure 1.19 Photoactivated therapeutic release observed in irradiated tumors by photoacoustic imaging of theranostic BODIPY-NO (photoNOD-1). a) Scheme of photoNOD-1 injection and irradiation after 4 h of circulation for 5 min. Photoacoustic imaging occurred before and after irradiation. **b)** Photoacoustic images of light tumor and dark tumor before (top) and after irradiation (bottom). Higher intensity areas after irradiation signify therapeutic release. Reprinted with permission. Reprinted with permission.[62]

Preliminary proof of principle studies have been crucial in establishing photoactivatable therapeutics as feasible DDSs and challenging concerns of limited light penetrance. However, for successful translation of therapeutics to the clinic more extensive PK/PD studies that truly begin to assess an *in vivo* photoindex will be required, especially for the IND application.

Biodistribution: Enhancing Temporal Control

Biodistribution studies serve two crucial roles in photoactivatable therapeutic development, due to the inherent ability to temporally control therapeutic release. First, biodistribution studies begin to establish the PK of therapeutic treatment which is vital for measuring the photoindex as well as providing indications of safety and potential phototoxicity (as cytotoxic therapeutics that are not cleared in a reasonable amount of time pose a higher risk of phototoxicity). Second, biodistribution studies serve to provide optimal parameters for when therapeutic activation and release should occur. For *in vivo* studies, experiments should characterize the ideal time of treatment to optimize chances of achieving the therapeutic potential. Depending on the DDS, timing of treatment may vary depending on when the therapeutic sufficiently localizes. Photoactivatable therapeutics have yet to cure cancer in mice, thus many protocols focus on releasing as much therapeutic as possible initially and continuing illumination treatments for multiple days following initial treatment. Such multi-day studies are possible as long wavelength light commonly causes few adverse effects but may pose a feasibility risk for translation into clinic.

Biodistribution studies can provide an indication of which tissues are of concern for toxicology studies. For instance, biodistribution studies of a fluorescent Cbl derivative discovered extensive distribution of Cbl throughout the body, including into the brain. In addition, a high concentration of Cbl accumulating in the tumor within 3 h was noted. Although a therapeutic was not appended to Cbl, this study did validate enhanced tumor uptake of Cbl with the caveat of Cbl

distributing throughout major tissues. Since endogenous Cbl is observed in the liver, kidneys, and lungs as well as to some degree in the heart and brain these tissues should be closely monitored especially with cytotoxic therapeutics.[106] Investigators have also quantified the concentration of CO after illumination of cyanine photoCORM in vulnerable tissues such as the blood and heart.[67] Such knowledge provides researchers with forewarning of potential toxicity risks while also making the most efficient use of animal studies.

As previously discussed, carriers and additional targeting moieties on photoactivable therapeutics can affect biodistribution. A proof-of-concept study of the potential of targeting agents compared the biodistribution of biotin targeted cyanine-camptothecin-biotin to control cyanine-camptothecin-alkyne. The alkyne is imaged throughout tissue for a full 6 h, while the biotin targeted PPG concentrates within 3 h in the liver and tumor (**Figure 1.20**). Further, theranostic images of illuminated cyanine-camptothecin at 820 nm show liver metabolism of the PPG emphasizing a need for further toxicology and safety studies.[68] Next generation cyanine-camptothecin micelles also distribute into the liver and tumor, but after 12 - 24 h PPG fluorescence are only observed in the tumor. Since the cyanine micelles rely on accumulating in tissue with an acidic pH it appears that this accumulation begins after 6 h and concentrates after 12 h.[86] Both cyanine systems demonstrate the need for liver safety investigations. Further the power of theranostic measures highlights how preliminary biodistribution studies can assess both ideal localization of photoactivatable therapeutic and potential dark activation by metabolism. The comparison of biotin targeting to the control alkyne also highlights how multi-layer targeting can further improve safety.

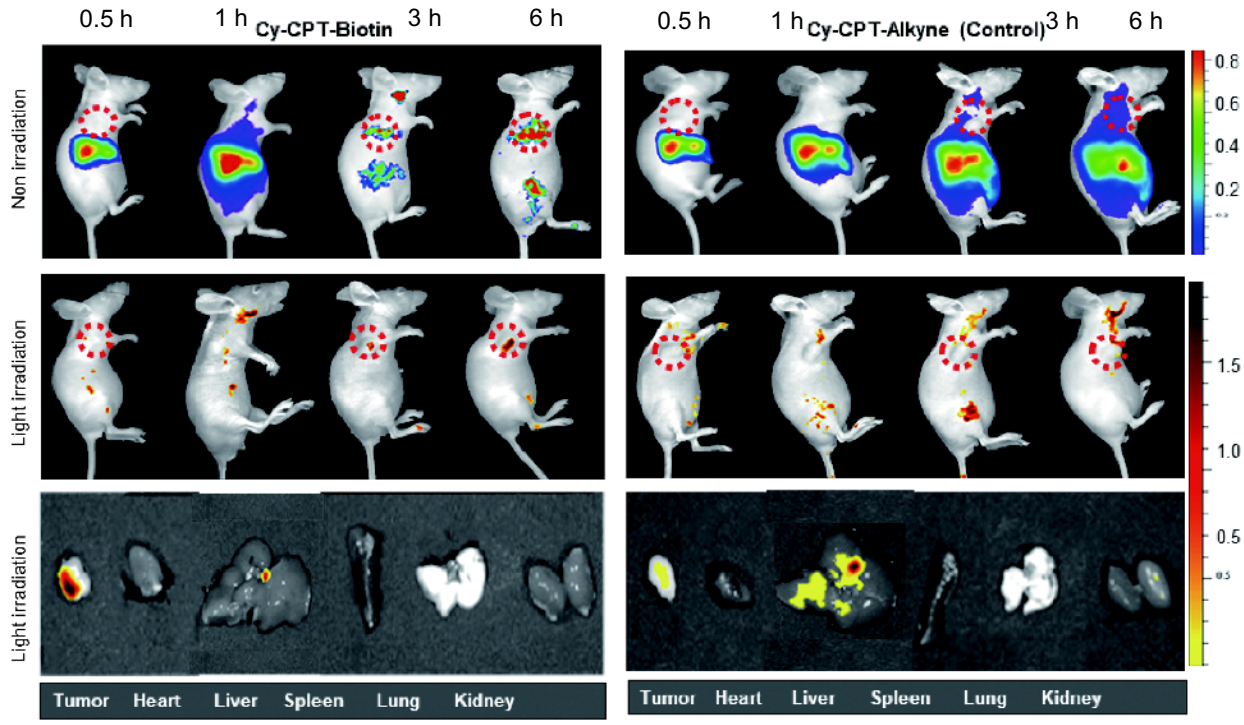

Figure 1.20 Improved biodistribution and PK of targeted cyanine-camptothecin-biotin (Cy-CPT-Biotin, left) as compared to control alkyne (Cy-CPT-Alkyne, right). Fluorescent signal at 820 nm of inactivated cyanine (top) accumulates in the tumor over 6h due to biotin targeting as compared to alkyne control (red circle represents tumor site in top and middle images). Fluorescent signal at 535 nm of activated cyanine shows localized therapeutic release at the irradiated tumor (680 nm, 200 mW/cm^2) and potential dark activation in the liver (middle and bottom). Internal organs show enhanced liver metabolism of non-targeted Cy-CPT-Alkyne 24 h post injection and illumination (bottom). Reprinted with permission.[68]

Similarly, biodistribution of ADC-cyanine-duocarmycin was assessed before tests of therapeutic efficacy. ADC-cyanine-duocarmycin concentrates in the tumor over 3 - 4 days.[69] This discovery played a key role in developing an ideal *in vivo* treatment plan during which light exposure was implemented 4 days after dosing. Although waiting a significant amount of time between dosing and treatment may be sub-optimal due to risk of phototoxicity, if systemic concentrations of inactivated drug cause minimal toxicity and a sufficiently localized concentration for effective dosing is achieved during the wait period, these benefits may outweigh the risks. As mentioned, Photofrin is still used in the clinic even though patients have to wait 48 h between dosing and treatment.[12]

Biodistribution studies can also indicate the need for a carrier, as photoactivatable therapeutics that have short circulation times and non-selectively diffuse into all tissue diminish bioavailability and increase the risk of dark activation. For example, non-photoactivatable Cbl≡Cy5 was imaged systemically distributing throughout tissue 5 min after injection (**Figure 1.21**).[106] Addition of an RBC carrier and internalization of Cbl≡Cy5 within RBCs ensures localized exposure of the Cbl≡Cy5 to the vasculature for up to 1.5 h. This localization was further validated by comparing to control externally labeled mouse RBCs with lipidated cyanine fluorophore 1,1-dioctadecyl-3,3,3,3-tetra-methylindodicarbocyanine (DiD).[72] Since the highest therapeutic dose needs to be released locally for photoactivated efficacy, current studies of vascular-localized photoactivatable therapeutics illuminate soon after intravenous injection as vascular based therapies achieve the highest potential concentration in the desired tissue (i.e. vasculature) during this time.

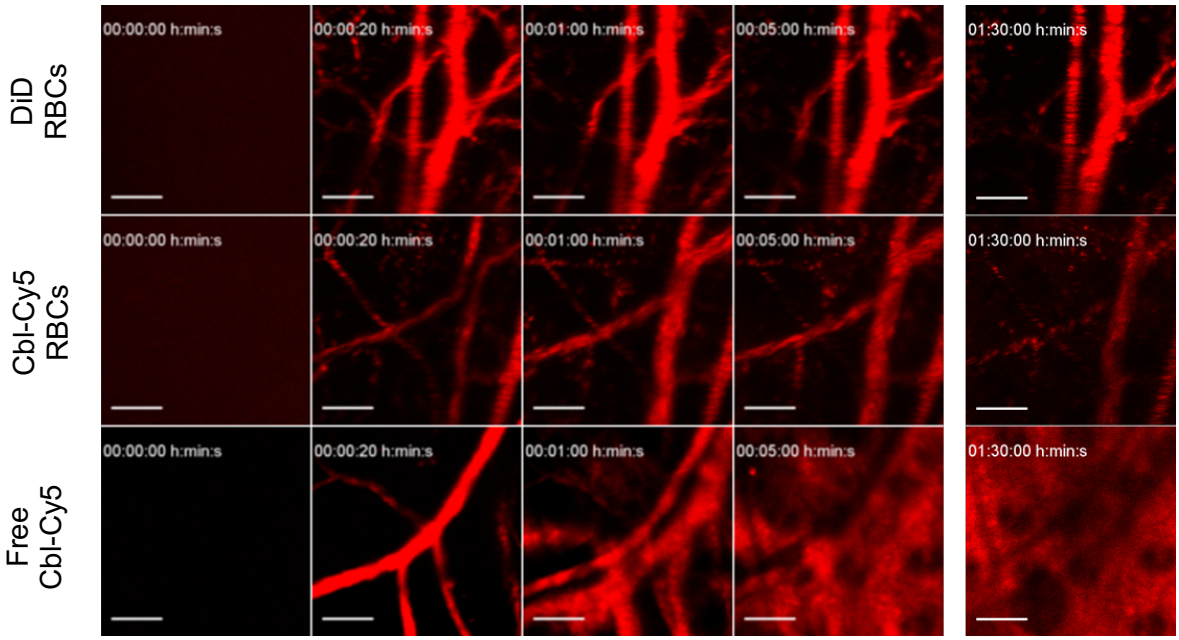

Figure 1.21 RBC carrier-based modification of Cyanine-Cbl-Docetaxel (Cy5-Cbl-DTX) biodistribution. Control externally loaded DiD mouse RBCs are localized to the vasculature for 1.5 h (top). Cy5-Cbl-DTX mouse RBCs also remain localized to the vasculature for 1.5 h (middle). Free Cy5-Cbl-DTX permeates throughout tissue within 5 min and persists through 1.5 h (bottom). Reprinted with permission.[72]

Thus, investigating biodistribution early in development can help optimize photoactivatable DDS in multiple ways: 1) results can provide researchers with indications of which tissues are at risk of dark activity/ toxicity effects and need to be examined and validated for further translation of the photoactivatable therapeutic; 2) studies support optimizing *in vivo* efficacy by providing the time required to achieve an ideally localized distribution; 3) studies can indicate whether a carrier or targeting agent may be necessary to improve localization/ minimize systemic exposure. Comparing biodistribution of the photoactivatable therapeutic to the parent drug or standard of care may help elucidate other potential risks and benefits of the photoresponsive DDS. Theranostic photoresponsive moieties are also extremely beneficial for biodistribution studies as they can easily image both the inactivated and activated therapeutic. Since many photoresponsive moieties generate a fluorescent signal, such signals can potentially be imaged during *in vivo* biodistribution studies. As noted previously, therapeutics are often dependent on the pharmacological processing of the body, but photoactivatable therapeutics can inactivate therapeutic to allow for optimal biodistribution before delivery to the site of disease.

Achieving Complete Remission: Optimizing Efficacy Studies

At this point, few photoactivatable therapeutics have achieved complete remission of disease in animal models. Thus, optimizing the parameters of treatment to ensure optimal localized efficacy is a necessity. Cbl-Dex RBCs and ADC-cyanine-duocarmycin have achieved success in animal models by thorough optimization and by including standard of care controls. Additional testing can be performed to ensure that the ideal dose is achieved including using doses compared to standard of care dosing or established dosing in that model and optimizing the irradiation dose treatment.

After investigating the biodistribution of ADC-cyanine-duocarmycin for ideal treatment time, the *in vivo* treatment plan was further optimized by ensuring the irradiation (800 nm, 80

J/cm^2 for 2 min) led to extensive photobleaching which is assumed to indicate complete activation. Although, photobleaching may correlate to the degree of therapeutic activation, dosimetry provides a better understanding of the degree of light penetrance and subsequent degree of activation. Further optimization of the ADC-cyanine-duocarmycin DDS included testing the efficacy of multiple photoactivatable therapeutic doses, including 10, 30, and 100 μg. The highest and most effective dose of 100 μg included both light and dark conditions (**Figure 1.22**). The results from the range of doses provide insight into the PK and true photoindex of ADC-cyanine-duocarmycin as 10 μg has no therapeutic effect even with illumination due to potential clearance or insufficiently localized concentrations. Illuminated 30 μg treatment achieves similar efficacy to 100 μg treatments in the dark. Further, biodistribution imaging during treatment shows that 30 and 100 μg treatments localize to the tumor after 4 days and are fully photobleached after illumination. At both doses, the ADC was observed to re-localize in the tumor supporting multiple day irradiation treatments. However, high concentrations of photoactivatable therapeutic are imaged throughout tissue at the 100 μg dose, which may be sufficient to achieve efficacy even in the dark due to metabolic activation.[69] For future animal studies with more aggressive irradiation or multiple injection treatments, ideal dosing may lie between 30 and 100 μg to achieve the optimal photoindex.

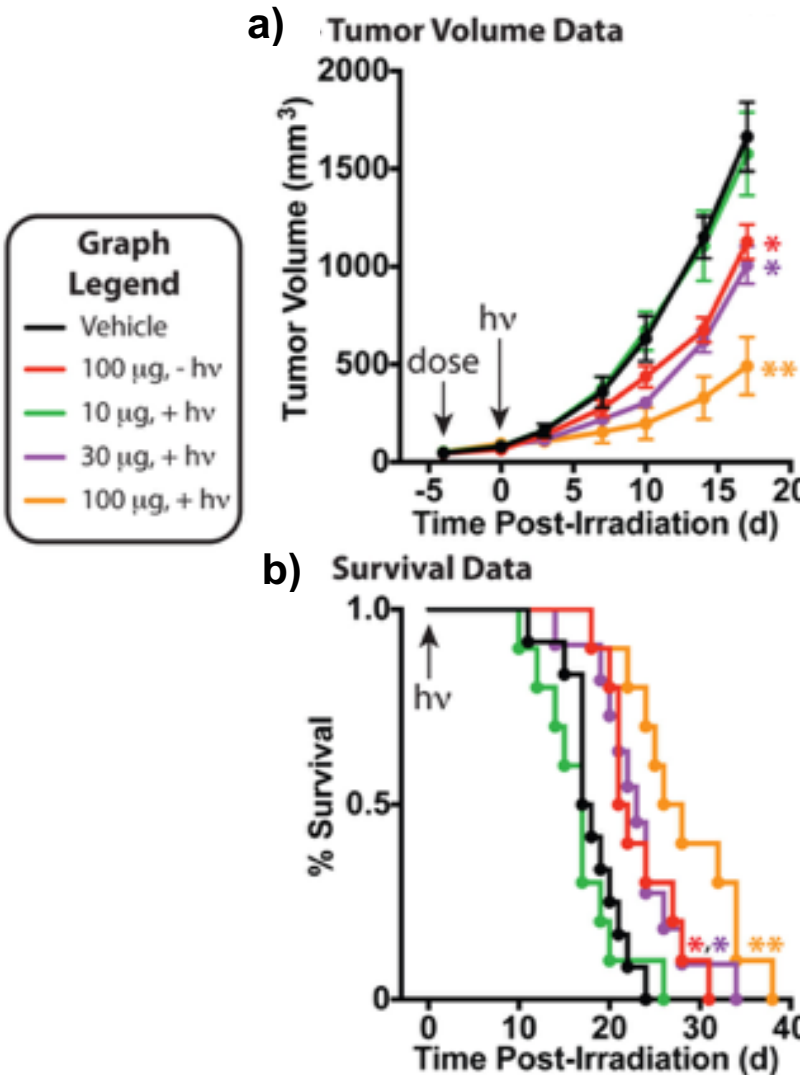

Figure 1.22 *In vivo* dose response efficacy of photoactivated ADC-Cyanine-Duocarmycin in breast cancer xenografts. a) Tumor growth as a function of days. Mice were treated with and without illumination and with 10, 30, and 100 μg doses as shown in the graph legend. 100 μg does produce efficacy in the dark, but illuminated treatment diminishes tumor growth by 3-fold in 20 days (d). **b)** Survival of treated and untreated mice. Irradiated 100 μg treatment improves mouse survival by 2-fold, while 10 μg treatment has no efficacious effect. (*$P < 0.05$, **$P < 0.01$). Reprinted with permission.[72]

Cbl-Dex RBC treatments in the acute collagen antibody induced arthritis mouse model also ensured an optimal *in vivo* testing plan.[73] Since biodistribution studies confirmed that the highest potential concentrations of the photoactivatable DDS are achieved upon initial injection, efficacy studies illuminated inflamed mouse paws immediately after injection. Further, *in vitro* irradiation studies confirmed complete therapeutic release after 1 mW irradiation for 3 min. Consequently, 3 mW irradiation for 5 min was proposed to sufficiently penetrate through the thin tissues of mouse paws. The previously optimized highest dose of photoactivatable therapeutic was loaded into mouse RBCs and the highest intravenous injectable dose of loaded mouse RBCs was injected into mice. Uniquely, these were the first reviewed *in vivo* studies to employ a standard of care control. Excitingly, the anti-inflammatory efficacy of Cbl-Dex RBCs is comparable to standard intraperitoneal Dex (**Figure 1.23**). Further, the initial dose of photoactivatable DDS is more effective than the initial dose of intraperitoneal standard. To further validate the phototherapeutic effect, future studies need to elucidate the localized effect by comparing illuminated mouse paws to control inflamed dark paws and to “dark” mice treated with the photoactivatable DDS but not illuminated. However, the initial results demonstrate the promise of photoactivatable DDSs to achieve the same effect as standard of care.[73]

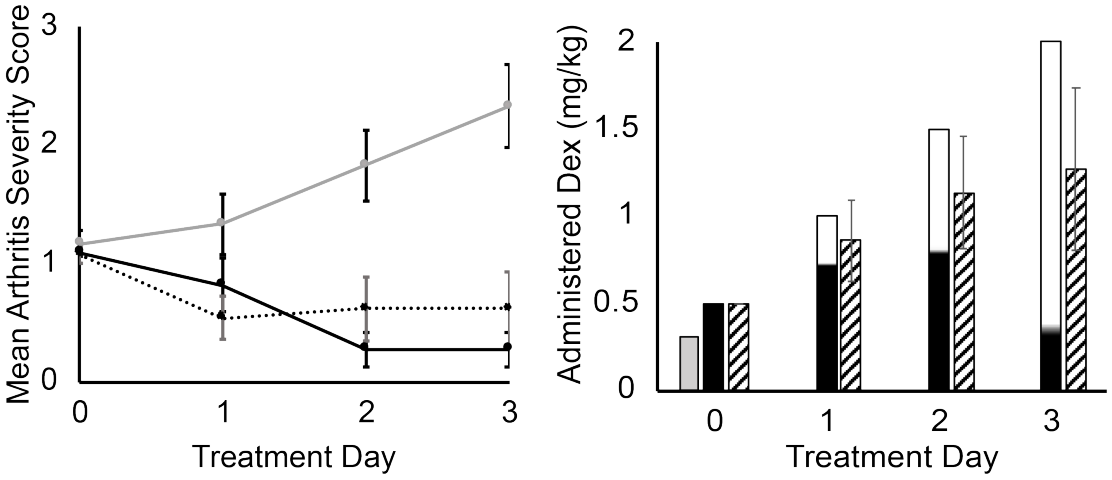

Figure 1.23 *In vivo* efficacy of Cy5-Cbl-Dex RBCs as compared to standard of care intraperitoneal Dex (IP Dex). Mice were treated with Cy5-Cbl-Dex RBCs (dotted line, n = 13) and IP Dex (solid line, n = 11) until remission of arthritis as measured by the mean arthritis severity score (left). After 1 day of treatment only Dex RBCs demonstrated significant improvement from inactive control Cy5-Cbl-H_2O RBCs treated mice (gray line, n = 12). (P = 0.01) The average amount of Dex (mg/kg) administered to IP Dex mice (hatched) and total Dex to Dex RBC mice (gray) per treatment day to achieve comparable remission shows IP Dex mice required daily dosing (of 0.5 mg/kg Dex) to achieve remission (right). Shaded bars represent the ratio of mice (out of 11 mice) that required more IP Dex and the cumulative dose administered to those mice. After 3 days of dosing, 78% more IP Dex was administered to achieve remission than Dex loaded in RBCs (P < 0.0001).[73]

ADC-cyanine-duocarmycin employed biodistribution investigations before and during efficacy studies to ensure therapeutic could still be released. Similarly, the ideal Cbl-Dex RBC biodistribution was validated and treatment was compared to a standard of care control. These initial *in vivo* studies demonstrate the power of dark controls, standard of care controls, and dose-response testing to truly begin to quantify the *in vivo* photoindex and demonstrate the potential benefits of photoactivatable DDSs. Since animal studies can be quite costly and time-consuming, ensuring that all potential data is collected, including collecting tissues for initial toxicology studies, can support development and further optimization of the treatment system before costly GLP studies. Thorough pre-clinical investigations can support IND application by indicating whether multiple injections may be required to achieve efficacy as the FDA will then further emphasize sub-chronic toxicology tests. In the end, an optimized treatment protocol will not only ensure ideal efficacy, but also provide guidance on the required toxicology tests remaining.

Remaining Steps: PK/PD and GLP Toxicology studies

Although not commonly published in literature, once efficacy and an ideal photoindex are achieved *in vivo*, researchers may begin establishing companies surrounding their technology and searching for investor capital to support rigorous PK/ PD and GLP toxicology studies. Mindful investigation in earlier pre-clinical work will support such studies with established chemistry and manufacturing, as well as ranges of therapeutic and illumination dosing for toxicology studies and eventual first in human trials. Further, early investigations can indicate potential pharmacology concerns and what tissues may be most at-risk to the therapeutic's pharmacological effects based on biodistribution studies. Investigating patent potential early on can also help ease this transition. When the PK/PD and GLP tests are underway may also be an appropriate time to begin pre-IND discussions with the FDA to support the transition to the clinic.

1.5.6.2 The Spatiotemporal Benefits of Photoactivatable Therapeutics

Spatiotemporal control provided by photoactivatable therapeutics can improve the TI in a multitude of ways. As always, the acceptable efficacy, toxicity, risks, and benefits of photoactivatable therapeutics need to be compared against the current standard of care for the unmet clinical need. Although there may be subacute toxicity, the assessment should consider whether the photoactivatable therapeutic improves characteristics of the therapeutic cargo or provides greater benefit than the standard of care. This assessment will commonly include the strength of spatiotemporal control and can be validated with the TI acting as a guide. In the following discussion, the spatiotemporal benefits of photoactivatable therapeutics will be framed within the concept of TI.

Modifying TI

Diminishing Toxicity/ Increasing the MTD

With the persistence of clinical need in cancer and the cytotoxic nature of therapeutics, many targeted methods of drug delivery have been developed, including PACTs and PDT. PACTs seek to improve the TI by increasing the MTD of toxic therapies and diminishing systemic side effects via spatial control provided by light and lasers.[157] PPGs, photoswitches, and photogates can diminish toxicity by means of inactivating or sheltering therapeutics until targeted laser activation at the site of disease. Thus, highly cytotoxic species such as doxorubicin, duocarmycin, rigidin, docetaxel, and camptothecin have reached *in vivo* studies for targeted therapeutic delivery. Indeed, most therapeutics under development in **Table 1-4** are cytotoxic therapeutics for the treatment of cancer. As previously discussed, the clinical success of both ThermoDox, NanoTherm, AuroLase, and PDT establish a regulatory precedent for externally stimulated DDSs in the treatment of cancer and validate the potential to minimize toxicity by deactivating cytotoxic activity until external stimulation.

Beyond cancer, the photogated Cbl, melittin RBC system highlights the potential of photoactivatable therapeutics to minimize severe adverse effects by means of external stimulation and the resulting release of thrombin in a localized manner (**Figure 1.18**).[142] Thrombin's extreme potency can lead to undesired clotting if administered systemically. Consequently, thrombin is only clinically approved for topical applications. Although toxicity studies are still underway, the photogated melittin system highlights the potential of photoactivatable therapeutics to improve safety by diminishing toxicity for both cancer and non-cancer indications.

Increasing Efficacy

Photoactivatable therapeutics can also salvage sub-optimal therapeutics by spatially enhancing the local concentration of drug and thus improving efficacy. For example, NO is known to have a plethora of roles in the body and potential in treatment of a variety of indications.[227] NO itself is not excessively dangerous or toxic and has recently been employed as an at-home inhaled therapy for COVID-19.[228] Due to the plethora of its roles within the body and on disease, targeted NO delivery systems have been developed for cancer therapy.[229] Specifically, BODIPY based photoactivatable NO donors (photoNODs) have successfully achieved an localized photoactivated on illuminated subcutaneous flank tumors in Balb/c mice. Suppression of tumor growth only occurs in illuminated tumors and has no effect in control dark flank tumors in the same animal. This result not only provides further validation of NO's ability to suppress tumor growth, but also the photoactivatable therapeutic's ability to improve desired efficacy by localizing therapeutic release and improving local concentrations. Future implications may include salvaging therapeutics that do not successfully progress through clinical trials due to insufficient efficacy caused by insufficient local drug concentrations.

Both Improving Efficacy and Diminishing Toxicity

Therapeutics that are both insufficiently effective and highly toxic can also be salvaged by photoactivatable therapeutics because light-activated DDSs can potentially improve efficacy of treatment to the extent that lower doses of therapeutic are needed which in turn diminishes systemic toxic effects. The most compelling example of this control is the development of BODIPY and cyanine based photoCORMs. Similar to NO, CO has prolific roles throughout the body and has been implied in the treatment of inflammation, cardiovascular disease, organ transplantation and preservation, as well as cancer.[178] However, CO binds 220 times more potently to hemoglobin than oxygen which has resulted in fatal consequences in the past.[230] Photoactivatable therapeutics can both minimize the off-target toxic binding to hemoglobin and potentially provide localized therapeutic effects similar to photoNODs. Early *in vivo* investigations have demonstrated biocompatibility and irradiation-dependent release of CO.[64]

Other Benefits: Personalized Medicine and Temporal Control of Multi-Targeted DDSs

Beyond improving the TI by salvaging cytotoxic and insufficiently effective therapeutics, the unique inherent properties of photoactivatable therapeutics provide potential for other novel applications. These applications include the development of personalized medical treatments in the form of theranostics and drug depots for patient-controlled at-home photoresponsive therapy and enhancement of multi-targeted DDSs due to the temporal control photoactivatable therapeutics provide. These applications have successfully been tested *in vivo*. However, other unique benefits of photoactivatable therapeutics have undergone *in vitro* testing, such as SiPcs that are dual PDT and photoactivatable therapeutic treatments. The potential for photoactivatable therapeutics is only now being illuminated as imaging devices, light devices, and photoresponsive moieties develop in tandem.

Personalized Medicine: Theranostics

As previously discussed, energy absorbed from photons can be converted to therapeutic release or fluorescence. Although fluorescence of photoactivatable therapeutics does decrease the Φ of therapeutic release, many research teams have taken advantage of this inherent dual modality to both image therapeutic distribution and measure therapeutic release as theranostics. The current theranostics under development include the BODIPY photoNOD and the cyanine-camptothecin therapeutics.[62, 68, 86] Although, fluorophores conjugated to Cbl have demonstrated potential theranostic capabilities, the imaging process has not yet been separated from therapeutic release.[105, 106] Ideally theranostic imaging is independent of therapeutic release allowing for a cycle of detection, therapeutic delivery, and monitoring personalized to each patient.[231]

BODIPY photoNOD is successfully imaged with photoacoustic imaging, activated with NIR light, and then imaged at another unique wavelength of photoacoustic imaging for ratiometric monitoring of therapeutic release.[62] Monitoring shows 65-88% therapeutic release *in vivo* upon irradiation. Similarly, cyanine-camptothecin micelles, the next-generation of theranostic cyanine-camptothecin (**Figure 1.16**), have been developed that can detect the micellar state with photoacoustic imaging and the disrupted micellar state at 810 nm.[86] Subsequent therapeutic release is triggered with 670 nm and the resulting photoproduct is detectable at 530 nm. *In vivo* studies demonstrate successful therapeutic release at the site of irradiation measurable by fluorescence imaging and photoacoustic imaging.

Both theranostic systems have demonstrated the ability to detect therapeutic distribution, excite therapeutic release, and subsequently quantify the degree of release. In general, these systems are limited by their need for photoacoustic imaging which has yet to reach the clinic. Thus, the cyanine micelles may demonstrate a greater potential for accelerated translation given their fluorescence detection. Both systems however demonstrate the power theranostics may

provide both for proof of principle validation of targeted delivery and development of this unique form of personalized medicine.

Personalized Medicine: Drug Depots

As previously discussed, RBCs have been tested as both slow-release systems and bioreactor systems with extended circulation. In general, RBCs can circulate for up to 180 days which makes them an optimal carrier as a long-term circulating drug depot. Internally loaded L-asparaginase and Dex 21-phosphate RBCs have been found to circulate for ~25 days in patients.[222] Although internally loaded RBCs display a reduced half-life compared to native RBCs, they experience a loss similar to transfused RBCs which only circulate for 50-60 days.[232] It is not surprising that internally loaded RBCs do not circulate for as long as their non-permeabilized counterparts. The therapeutic loading process requires RBCs undergo a hypotonic dialysis which causes membrane disruption and loss of some internal contents, which may lead to a more accelerated clearance as compared to native RBCs. However, internally loaded RBCs can still provide a notable increase in circulation time for therapeutic cargo, as exemplified by Cbl DDSs.[72]

Cbl-Dex internally loaded RBCs are under development to both minimize the toxicity of Dex, as well as provide (eventually patient-controlled) localized therapeutic release. Dex has negative side effects from chronic usage, including bone-thinning, weight gain, diabetes, and immunosuppression.[233] Cbl-Dex RBCs will allow for patient-based therapeutic symptom treatment for morning pain and flare-ups while minimizing the toxicity of Dex. This system takes advantage of the long-term circulation of internally loaded Cbl-Dex RBCs which can be released in response to low-power long-wavelength light in the hands and feet by patient-controlled lasers. Though still in early development, Cbl-Dex RBCs have successfully induced arthritic remission in a mouse model.[73] These promising preliminary results, as well as the established Erytech loading system

and the successful 1-month circulation studies of EryDel RBCs in clinical trials establishes the near-future potential of photoactivatable drug depot therapeutics.[222]

Temporal Targeting of Multi-targeted DDSs

Photoactivatable therapeutics can also improve efficacy, and thus the TI, by means of temporal control. The potential of this control has been most clearly demonstrated by DDSs that employ multiple means of targeting including ADC-cyanine-duocarmycin and pH-responsive cyanine-camptothecin micelles.[69, 86] The scientists introduced the clinically available ADC targeting agent Panitumumab (which targets EGFR on cancer cells) and the pH-sensitivity to the acidic tumor environment respectively, to enhance the localization benefits of photoactivatable therapeutics. Both groups then completed biodistribution studies to optimize the ideal time for therapeutic release. The ADC duocarmycin demonstrated an optimal distribution after 3 - 4 days while the cyanine micelles demonstrated a localized presence in the tumor environment after 24 h.[69, 86]

The biodistribution results highlight that clearance of excess DDS has occurred and the resulting localization is potentially due to the enhanced targeting provided by ADC and pH-sensitivity respectively. This potential was further confirmed as previously discussed by targeted cyanine-camptothecin-biotin, the precursor of the cyanine-camptothecin micelles (**Figure 1.20**).[68] With these ideal treatment times, the ADC system successfully demonstrated a suppression of tumor growth and almost doubling of survival rates.[69] The temporal control provided by the photoactivatable DDS further enhanced the potential efficacy of the targeted system by allowing for dosing upon optimal distribution.

1.6 Outlook for the Future of Photoactivated Drug Delivery Systems

Photoactivatable therapeutics provide a completely novel way of salvaging and delivering drugs. Altogether the spatial and temporal control of phototherapeutics can improve the TI of the therapeutic cargo by multiple strategies: by modifying the systemic exposure, by minimizing the dose of therapeutic required, and by enhancing the local concentration. Further, the inherent properties of photoactivatable therapeutics can be enhanced to improve personalized medicine by theranostic and drug depot applications. However, with the multitude of benefits that photoactivatable DDSs present, there are still quite a few challenges systems need to overcome:

1) Although the depth of light penetration varies dependent on tissue, in general, ensuring optimal photophysical properties of photoresponsive moieties will support penetration into deeper tissue indications. Fortunately, many light devices for these spaces have already been developed (section 1.3).
2) Current photoresponsive moieties under development may be insufficiently optimized for clinical translation (section 1.4). Though no precedent yet exists for the photophysical properties of an ideal theranostic or even photoresponsive therapy, photoresponsive moieties that have low Φ due to high fluorescence may be modified for theranostic applications. Other photoresponsive moieties will have to achieve the minimum Φ and εs of at least 0.1 and 5,000 respectively that Photofrin has set.[19]
3) Though briefly mentioned, generating a reliable and easy synthetic route for mass production of the photoactivatable DDS will be crucial for clinical translation. Many clinical holds arise from concerns or changes to the chemistry and manufacturing. To ensure efficient translation, regulated synthesis and quality control of these complex therapies will be of utmost importance.
4) High spatiotemporally controlled efficacy *in vivo* with minimal dark activity has yet to be demonstrated. As this principle is the crux of photoactivatable therapeutic's benefits,

thorough validation will be crucial. Once the initial approved system proves efficacy with minimal dark activity, the photoactivatable therapeutic field may see a boon of confidence and rise of capital to support translation.

5) Photoactivatable therapeutic need to be designed as simply as possible. Every complexity added to the DDS will require optimization and may cause nuanced problems that require further troubleshooting and a variety of expertise. For example, adding a carrier may further complicate synthesis and regulatory translation.[221] Thus, minimizing the complexity of the DDS is ideal, as validated by Tookad's accelerated development once a lipidated carrier was no longer required.[12] However, early generations of photoactivatable DDSs may require carriers to overcome limitations of dark activation until more ideal photoresponsive moieties are developed.
6) Careful planning should go into animal studies. As discussed throughout 1.5.6 a plethora of information can be obtained from even preliminary animal tests. Using animal models that begin to validate spatiotemporal control (such as double tumor models or comparing illuminated to dark tissue) may provide crucial justification of the phototherapeutic benefits. These animal studies can also indicate risks of potential dark activation, toxicity, feasibility of administration method, as well as insufficient therapeutic effect. Including proper controls such as standard of care treatments can also help further the crucial proof of principle data required to continue the growth of photoactivatable therapeutics.
7) Externally controlled DDSs are often called "smart" drugs, originally named thusly because these DDS can be controlled to only react in the desired diseased tissue. However, although these DDS may in themselves be "smart", they also require extensive expertise (**Figure 1.2**) and planning (**Figure 1.12**) to develop successfully. Embarking on developing these exciting and novel systems should be taken with great care and thought. Having in mind an unmet clinical need and potentially multiple therapeutic cargoes and

photoresponsive moieties that can meet the need will tremendously help guide and accelerate the journey. Further, understanding the scope of the current standard of care's risk and benefits will provide boundaries and goals for the photoactivatable therapeutic's risks and benefits.

Only 30 years have passed since the first photoresponsive therapy, Photofrin, was approved.[12] Since then, the field of PDT has observed both successes and failures. It would be naïve to think that photoactivatable therapeutics will not face similar struggles. However, the foundation of PDT and established light devices help support the translation of photoactivatable therapeutics. The many photoresponsive moieties responsive to long wavelength light, literary background on the synthesis and photochemical mechanisms, and success of *in vivo* validation of localized effect and therapeutic efficacy provides hope for many therapeutics approaching clinic. The personalized medicine applications of photoactivated drug depots and theranostics may still be far-off, but we can now begin to see the light at the end of this tunnel.

REFERENCES

1. Vogenberg, F. R.; Barash, C. I.; Pursel, M., Personalized Medicine: Part 1: Evolution and Development into Theranostics. *P & T* **2010,** *35* (10), 560-576.

2. Lee, Y. T.; Tan, Y. J.; Oon, C. E., Molecular targeted therapy: Treating cancer with specificity. *European Journal of Pharmacology* **2018,** *834*, 188-196.

3. Keefe, D. M. K.; Bateman, E. H., Potential Successes and Challenges of Targeted Cancer Therapies. *JNCI Monographs* **2019,** *2019* (53).

4. Linsley, C. S.; Wu, B. M., Recent advances in light-responsive on-demand drug-delivery systems. *Ther Deliv* **2017,** *8* (2), 89-107.

5. Muller, P. Y.; Milton, M. N., The determination and interpretation of the therapeutic index in drug development. *Nature Reviews Drug Discovery* **2012,** *11* (10), 751-761.

6. Baird, T. J.; Caruso, M. J.; Gauvin, D. V.; Dalton, J. A., NOEL and NOAEL: A retrospective analysis of mention in a sample of recently conducted safety pharmacology studies. *Journal of Pharmacological and Toxicological Methods* **2019,** *99*, 106597.

7. Park, Y.-C.; Cho, M.-H., A New Way in Deciding NOAEL Based on the Findings from GLP-Toxicity Test. *Toxicological Research* **2011,** *27* (3), 133-135.

8. Juhász, M. L. W.; Levin, M. K.; Marmur, E. S., A review of available laser and intense light source home devices: A dermatologist's perspective. *Journal of Cosmetic Dermatology* **2017,** *16* (4), 438-443.

9. Sorbellini, E.; Rucco, M.; Rinaldi, F., Photodynamic and photobiological effects of light-emitting diode (LED) therapy in dermatological disease: an update. *Lasers in Medical Science* **2018,** *33* (7), 1431-1439.

10. Gu, M.; Wang, X.; Toh, T. B.; Chow, E. K.-H., Applications of stimuli-responsive nanoscale drug delivery systems in translational research. *Drug Discovery Today* **2018,** *23* (5), 1043-1052.

11. Swenson, C. E.; Haemmerich, D.; Maul, D. H.; Knox, B.; Ehrhart, N.; Reed, R. A., Increased Duration of Heating Boosts Local Drug Deposition during Radiofrequency Ablation in Combination with Thermally Sensitive Liposomes (ThermoDox) in a Porcine Model. *PLOS ONE* **2015,** *10* (10), e0139752.

12. Hamblin, M. R., Photodynamic Therapy for Cancer: What's Past is Prologue. *Photochemistry and Photobiology* **2020,** *96* (3), 506-516.

13. Kobayashi, H.; Ogawa, M.; Alford, R.; Choyke, P. L.; Urano, Y., New Strategies for Fluorescent Probe Design in Medical Diagnostic Imaging. *Chemical Reviews* **2010,** *110* (5), 2620-2640.

14. Agostinis, P.; Berg, K.; Cengel, K. A.; Foster, T. H.; Girotti, A. W.; Gollnick, S. O.; Hahn, S. M.; Hamblin, M. R.; Juzeniene, A.; Kessel, D.; Korbelik, M.; Moan, J.; Mroz, P.; Nowis, D.; Piette, J.; Wilson, B. C.; Golab, J., Photodynamic therapy of cancer: An update. *CA: A Cancer Journal for Clinicians* **2011,** *61* (4), 250-281.

15. Daniell, M. D.; Hill, J. S., A history of photodynamic therapy. *Aust N Z J Surg* **1991,** *61* (5), 340-8.

16. Kessel, D., Photodynamic Therapy: A Brief History. *J Clin Med* **2019,** *8* (10).

17. Baskaran, R.; Lee, J.; Yang, S. G., Clinical development of photodynamic agents and therapeutic applications. *Biomater Res* **2018,** *22*, 25.

18. Chilakamarthi, U.; Giribabu, L., Photodynamic Therapy: Past, Present and Future. *The Chemical Record* **2017,** *17* (8), 775-802.

19. Kamkaew, A.; Lim, S. H.; Lee, H. B.; Kiew, L. V.; Chung, L. Y.; Burgess, K., BODIPY dyes in photodynamic therapy. *Chemical Society Reviews* **2013,** *42* (1), 77-88.

20. Shi, H.; Sadler, P. J., How promising is phototherapy for cancer? *British Journal of Cancer* **2020,** *123* (6), 871-873.

21. Baier, J.; Maisch, T.; Maier, M.; Engel, E.; Landthaler, M.; Bäumler, W., Singlet oxygen generation by UVA light exposure of endogenous photosensitizers. *Biophys J* **2006,** *91* (4), 1452-1459.

22. Finch, A. J.; Benson, J. M.; Donnelly, P. E.; Torzilli, P. A., Light Absorptive Properties of Articular Cartilage, ECM Molecules, Synovial Fluid, and Photoinitiators as Potential Barriers to Light-Initiated Polymer Scaffolding Procedures. *Cartilage* **2019,** *10* (1), 82-93.

23. Liu, T.; Zhang, X.; Zhang, H.; Zhao, H.; Zhang, Z.; Tian, Y., Method for monitoring singlet oxygen quantum yield in real time by time resolved spectroscopy measurement. *Opt. Express* **2020,** *28* (18), 25757-25766.

24. Wainwright, M.; Maisch, T.; Nonell, S.; Plaetzer, K.; Almeida, A.; Tegos, G. P.; Hamblin, M. R., Photoantimicrobials—are we afraid of the light? *The Lancet Infectious Diseases* **2017,** *17* (2), e49-e55.

25. Ellis-Davies, G. C. R., Caged compounds: photorelease technology for control of cellular chemistry and physiology. *Nat Methods* **2007,** *4* (8), 619-628.

26. Glass, S.; Rüdiger, T.; Griebel, J.; Abel, B.; Schulze, A., Uptake and release of photosensitizers in a hydrogel for applications in photodynamic therapy: the impact of structural parameters on intrapolymer transport dynamics. *RSC Advances* **2018,** *8* (72), 41624-41632.

27. Zhao, Y.; Qiu, L.; Sun, Y.; Huang, C.; Li, T., Optimal hemoglobin extinction coefficient data set for near-infrared spectroscopy. *Biomed Opt Express* **2017,** *8* (11), 5151-5159.

28. Wilson, B. C.; Patterson, M. S., The physics, biophysics and technology of photodynamic therapy. *Physics in Medicine and Biology* **2008,** *53* (9), R61-R109.

29. Star, W. M., Light dosimetry in vivo. *Physics in Medicine and Biology* **1997,** *42* (5), 763-787.

30. Wilson, B. C.; Patterson, M. S., The physics of photodynamic therapy. *Physics in Medicine and Biology* **1986,** *31* (4), 327-360.

31. Kim, M. M.; Darafsheh, A., Light Sources and Dosimetry Techniques for Photodynamic Therapy. *Photochemistry and Photobiology* **2020,** *96* (2), 280-294.

32. Rwei, A. Y.; Wang, W.; Kohane, D. S., Photoresponsive nanoparticles for drug delivery. *Nano Today* **2015,** *10* (4), 451-467.

33. Pye, H.; Stamati, I.; Yahioglu, G.; Butt, M.; Deonarain, M., Antibody-Directed Phototherapy (ADP). *Antibodies* **2013,** *2*, 270-305.

34. GmbH, B. B. Ameluz NDA Cross Discipline Team Leader Review. U.S. Food and Drug Administration. https://www.accessdata.fda.gov/drugsatfda_docs/nda/2016/208081Orig1s000StatR.pdf (accessed June 16 2021).

35. Josefsen, L. B.; Boyle, R. W., Unique diagnostic and therapeutic roles of porphyrins and phthalocyanines in photodynamic therapy, imaging and theranostics. *Theranostics* **2012,** *2* (9), 916-966.

36. Huang, Z., A Review of Progress in Clinical Photodynamic Therapy. *Technology in Cancer Research & Treatment* **2005,** *4* (3), 283-293.

37. Raiskup, F.; Spoerl, E., Corneal Crosslinking with Riboflavin and Ultraviolet A. I. Principles. *The Ocular Surface* **2013,** *11* (2), 65-74.

38. SCANDIPHARM, A. Photofrin [Labelling]. Drugs@FDA Database. U.S. Food and Drug Administration. https://www.accessdata.fda.gov/drugsatfda_docs/label/2003/20451s012_photofrin_lbl.pdf (accessed June 16 2021).

39. LUXEMBOURG, V. Visudyne [Labelling]. Drugs@FDA Database. U.S. Food and Drug Administration. https://www.accessdata.fda.gov/drugsatfda_docs/label/2000/21119lbl.pdf (accessed June 16 2021).

40. BIOFRONTERA Ameluz [Labelling]. Drugs@FDA Database. U.S. Food and Drug Administration. https://www.accessdata.fda.gov/drugsatfda_docs/label/2016/208081s000lbl.pdf (accessed June 16 2021).

41. DUSA Levulan [Labelling]. Drugs@FDA Database. U.S. Food and Drug Administration. https://www.accessdata.fda.gov/drugsatfda_docs/label/1999/20965lbl.pdf (accessed June 16 2021).

42. NXDC Gleolan [Labelling]. Drugs@FDA Database. U.S. Food and Drug Administration. https://www.accessdata.fda.gov/drugsatfda_docs/label/2017/208630s000lbl.pdf (accessed June 16 2021).

43. LP, G. L. Metvixia [Labelling]. Drugs@FDA Database. U.S. Food and Drug Administration. https://www.accessdata.fda.gov/drugsatfda_docs/label/2012/021415s004lbl.pdf (accessed June 16 2021).

44. ASA, P. Cysview [Labelling]. Drugs@FDA Database. U.S. Food and Drug Administration. https://www.accessdata.fda.gov/drugsatfda_docs/label/2010/022555s000lbl.pdf (accessed June 16 2021).

45. GLAUKOS Phototrexa [Labelling]. Drugs@FDA Database. U.S. Food and Drug Administration. https://www.accessdata.fda.gov/drugsatfda_docs/label/2016/203324s000lbl.pdf (accessed June 16 2021).

46. Brancaleon, L.; Moseley, H., Laser and Non-laser Light Sources for Photodynamic Therapy. *Lasers in Medical Science* **2002,** *17* (3), 173-186.

47. DUSA PHARMACEUTICALS, I. BLU-U BLUE LIGHT PHOTODYNAMIC THERAPY ILLUMINATOR [Labelling]. Premarket Approval. U.S. Food and Drug Administration. https://www.accessdata.fda.gov/cdrh_docs/pdf/P990019C.pdf (accessed June 16 2021).

48. Masuda, H.; Kimura, M.; Nishioka, A.; Kato, H.; Morita, A., Dual wavelength 5-aminolevulinic acid photodynamic therapy using a novel flexible light-emitting diode unit. *Journal of Dermatological Science* **2019,** *93* (2), 109-115.

49. Eric, M. K.; Kai, Z.; Matt, W.; Ryan, T. L.; Alejandro, O.; Bryan, Q. S., High-power light-emitting diode array design and assembly for practical photodynamic therapy research. *Journal of Biomedical Optics* **2020,** *25* (6), 1-13.

50. Morton, C. A.; Braathen, L. R., Daylight Photodynamic Therapy for Actinic Keratoses. *American Journal of Clinical Dermatology* **2018,** *19* (5), 647-656.

51. Trivedi, M. K.; Yang, F. C.; Cho, B. K., A review of laser and light therapy in melasma. *Int J Womens Dermatol* **2017,** *3* (1), 11-20.

52. Gold, M. H.; Goldberg, D. J.; Nestor, M. S., Current treatments of acne: Medications, lights, lasers, and a novel 650-μs 1064-nm Nd: YAG laser. *Journal of Cosmetic Dermatology* **2017,** *16* (3), 303-318.

53. Li, Y.; Zhang, Y.; Wang, W., Phototriggered targeting of nanocarriers for drug delivery. *Nano Research* **2018,** *11* (10), 5424-5438.

54. Ahmed, I.; Fruk, L., The power of light: photosensitive tools for chemical biology. *Molecular BioSystems* **2013,** *9* (4), 565-570.

55. Silva, J. M.; Silva, E.; Reis, R. L., Light-triggered release of photocaged therapeutics - Where are we now? *Journal of Controlled Release* **2019,** *298*, 154-176.

56. Wang, G.; Zhang, J., Photoresponsive molecular switches for biotechnology. *Journal of Photochemistry and Photobiology C: Photochemistry Reviews* **2012,** *13* (4), 299-309.

57. Jia, S.; Fong, W.-K.; Graham, B.; Boyd, B. J., Photoswitchable Molecules in Long-Wavelength Light-Responsive Drug Delivery: From Molecular Design to Applications. *Chemistry of Materials* **2018,** *30* (9), 2873-2887.

58. Dcona, M. M.; Mitra, K.; Hartman, M. C. T., Photocontrolled activation of small molecule cancer therapeutics. *RSC Medicinal Chemistry* **2020,** *11* (9), 982-1002.

59. Karimi, M.; Sahandi Zangabad, P.; Baghaee-Ravari, S.; Ghazadeh, M.; Mirshekari, H.; Hamblin, M. R., Smart Nanostructures for Cargo Delivery: Uncaging and Activating by Light. *Journal of the American Chemical Society* **2017,** *139* (13), 4584-4610.

60. Olejniczak, J.; Carling, C.-J.; Almutairi, A., Photocontrolled release using one-photon absorption of visible or NIR light. *Journal of Controlled Release* **2015,** *219*, 18-30.

61. Sitkowska, K.; Hoes, M. F.; Lerch, M. M.; Lameijer, L. N.; van der Meer, P.; Szymański, W.; Feringa, B. L., Red-light-sensitive BODIPY photoprotecting groups for amines and their biological application in controlling heart rhythm. *Chemical Communications* **2020,** *56* (41), 5480-5483.

62. Zhou, E. Y.; Knox, H. J.; Reinhardt, C. J.; Partipilo, G.; Nilges, M. J.; Chan, J., Near-Infrared Photoactivatable Nitric Oxide Donors with Integrated Photoacoustic Monitoring. *Journal of the American Chemical Society* **2018,** *140* (37), 11686-11697.

63. Štacko, P.; Muchová, L.; Vítek, L.; Klán, P., Visible to NIR Light Photoactivation of Hydrogen Sulfide for Biological Targeting. *Organic Letters* **2018,** *20* (16), 4907-4911.

64. Palao, E.; Slanina, T.; Muchova, L.; Solomek, T.; Vitek, L.; Klan, P., Transition-Metal-Free CO-Releasing BODIPY Derivatives Activatable by Visible to NIR Light as Promising Bioactive Molecules. *J Am Chem Soc* **2016,** *138* (1), 126-33.

65. Gibbs, S. L., Near infrared fluorescence for image-guided surgery. *Quant Imaging Med Surg* **2012,** *2* (3), 177-187.

66. Hong, N. Y.; Kim, H. R.; Lee, H. M.; Sohn, D. K.; Kim, K. G., Fluorescent property of indocyanine green (ICG) rubber ring using LED and laser light sources. *Biomed Opt Express* **2016,** *7* (5), 1637-1644.

67. Štacková, L.; Russo, M.; Muchová, L.; Orel, V.; Vítek, L.; Štacko, P.; Klán, P., Cyanine-Flavonol Hybrids for Near-Infrared Light-Activated Delivery of Carbon Monoxide. *Chemistry – A European Journal* **2020,** *26* (58), 13184-13190.

68. Guo, Z.; Ma, Y.; Liu, Y.; Yan, C.; Shi, P.; Tian, H.; Zhu, W.-H., Photocaged prodrug under NIR light-triggering with dual-channel fluorescence: in vivo real-time tracking for precise drug delivery. *Science China Chemistry* **2018,** *61* (10), 1293-1300.

69. Nani, R. R.; Gorka, A. P.; Nagaya, T.; Yamamoto, T.; Ivanic, J.; Kobayashi, H.; Schnermann, M. J., In Vivo Activation of Duocarmycin–Antibody Conjugates by Near-Infrared Light. *ACS Central Science* **2017,** *3* (4), 329-337.

70. Mitra, K.; Lyons, C. E.; Hartman, M. C. T., A Platinum(II) Complex of Heptamethine Cyanine for Photoenhanced Cytotoxicity and Cellular Imaging in Near-IR Light. *Angewandte Chemie International Edition* **2018,** *57* (32), 10263-10267.

71. Hughes, R. M.; Marvin, C. M.; Rodgers, Z. L.; Ding, S.; Oien, N. P.; Smith, W. J.; Lawrence, D. S., Phototriggered Secretion of Membrane Compartmentalized Bioactive Agents. *Angewandte Chemie International Edition* **2016,** *55* (52), 16080-16083.

72. Marvin, C. M.; Ding, S.; White, R. E.; Orlova, N.; Wang, Q.; Zywot, E. M.; Vickerman, B. M.; Harr, L.; Tarrant, T. K.; Dayton, P. A.; Lawrence, D. S., On Command Drug Delivery via Cell-Conveyed Phototherapeutics. *Small* **2019,** *15* (37), 1901442.

73. Zywot, E. M.; Orlova, N.; Ding, S.; Rampersad, R. R.; Rabjohns, E. M.; Wickenheisser, V. A.; Wang, Q.; Welfare, J. G.; Haar, L.; Eudy, A. M.; Tarrant, T. K.; Lawrence, D. S., Light Directed Therapeutic Delivery to Arthritic Joints. *Science Advances* **2021**.

74. Li, X.; Zheng, B.-D.; Peng, X.-H.; Li, S.-Z.; Ying, J.-W.; Zhao, Y.; Huang, J.-D.; Yoon, J., Phthalocyanines as medicinal photosensitizers: Developments in the last five years. *Coordination Chemistry Reviews* **2019,** *379*, 147-160.

75. Anderson, E. D.; Gorka, A. P.; Schnermann, M. J., Near-infrared uncaging or photosensitizing dictated by oxygen tension. *Nature Communications* **2016,** *7* (1), 13378.

76. Li, A.; Yadav, R.; White, J. K.; Herroon, M. K.; Callahan, B. P.; Podgorski, I.; Turro, C.; Scott, E. E.; Kodanko, J. J., Illuminating cytochrome P450 binding: Ru(ii)-caged inhibitors of CYP17A1. *Chemical Communications* **2017,** *53* (26), 3673-3676.

77. Lameijer, L. N.; Ernst, D.; Hopkins, S. L.; Meijer, M. S.; Askes, S. H. C.; Le Dévédec, S. E.; Bonnet, S., A Red-Light-Activated Ruthenium-Caged NAMPT Inhibitor Remains Phototoxic in Hypoxic Cancer Cells. *Angew Chem Int Ed Engl* **2017,** *56* (38), 11549-11553.

78. Tochitsky, I.; Polosukhina, A.; Degtyar, Vadim E.; Gallerani, N.; Smith, Caleb M.; Friedman, A.; Van Gelder, Russell N.; Trauner, D.; Kaufer, D.; Kramer, Richard H., Restoring Visual Function to Blind Mice with a Photoswitch that Exploits Electrophysiological Remodeling of Retinal Ganglion Cells. *Neuron* **2014,** *81* (4), 800-813.

79. Wegener, M.; Hansen, M. J.; Driessen, A. J. M.; Szymanski, W.; Feringa, B. L., Photocontrol of Antibacterial Activity: Shifting from UV to Red Light Activation. *Journal of the American Chemical Society* **2017,** *139* (49), 17979-17986.

80. Wang, D.; Wu, S., Red-Light-Responsive Supramolecular Valves for Photocontrolled Drug Release from Mesoporous Nanoparticles. *Langmuir* **2016,** *32* (2), 632-636.

81. Poelma, S. O.; Oh, S. S.; Helmy, S.; Knight, A. S.; Burnett, G. L.; Soh, H. T.; Hawker, C. J.; Read de Alaniz, J., Controlled drug release to cancer cells from modular one-photon visible light-responsive micellar system. *Chemical Communications* **2016,** *52* (69), 10525-10528.

82. Helmy, S.; Leibfarth, F. A.; Oh, S.; Poelma, J. E.; Hawker, C. J.; Read de Alaniz, J., Photoswitching Using Visible Light: A New Class of Organic Photochromic Molecules. *Journal of the American Chemical Society* **2014,** *136* (23), 8169-8172.

83. Rapp, T. L.; Highley, C. B.; Manor, B. C.; Burdick, J. A.; Dmochowski, I. J., Ruthenium-Crosslinked Hydrogels with Rapid, Visible-Light Degradation. *Chemistry – A European Journal* **2018,** *24* (10), 2328-2333.

84. Rodgers, Z. L.; Hughes, R. M.; Doherty, L. M.; Shell, J. R.; Molesky, B. P.; Brugh, A. M.; Forbes, M. D. E.; Moran, A. M.; Lawrence, D. S., B12-Mediated, Long Wavelength Photopolymerization of Hydrogels. *Journal of the American Chemical Society* **2015,** *137* (9), 3372-3378.

85. Carling, C.-J.; Olejniczak, J.; Foucault-Collet, A.; Collet, G.; Viger, M. L.; Nguyen Huu, V. A.; Duggan, B. M.; Almutairi, A., Efficient red light photo-uncaging of active molecules in water upon assembly into nanoparticles. *Chemical Science* **2016,** *7* (3), 2392-2398.

86. Zhang, Y.; Yan, C.; Zheng, Q.; Jia, Q.; Wang, Z.; Shi, P.; Guo, Z., Harnessing Hypoxia-Dependent Cyanine Photocages for In Vivo Precision Drug Release. *Angewandte Chemie International Edition* **2021,** *60* (17), 9553-9561.

87. Barltrop, J. A.; Schofield, P., Photosensitive Protecting Groups. *Tetrahedron Letters* **1962,** *3* (16), 697-699.

88. Barton, D. H. R.; Beckwith, A. L. J.; Goosen, A., 28. Photochemical transformations. Part XVI. A novel synthesis of lactones. *Journal of the Chemical Society (Resumed)* **1965,** (0), 181-190.

89. Patchornik, A.; Amit, B.; Woodward, R. B., Photosensitive protecting groups. *Journal of the American Chemical Society* **1970,** *92* (21), 6333-6335.

90. Engels, J.; Schlaeger, E. J., Synthesis, structure, and reactivity of adenosine cyclic 3',5'-phosphate-benzyltriesters. *Journal of Medicinal Chemistry* **1977,** *20* (7), 907-911.

91. Kaplan, J. H.; Forbush, B.; Hoffman, J. F., Rapid photolytic release of adenosine 5'-triphosphate from a protected analog: utilization by the sodium:potassium pump of human red blood cell ghosts. *Biochemistry* **1978,** *17* (10), 1929-1935.

92. Loudet, A.; Burgess, K., BODIPY Dyes and Their Derivatives: Syntheses and Spectroscopic Properties. *Chemical Reviews* **2007,** *107* (11), 4891-4932.

93. Peterson, J. A.; Wijesooriya, C.; Gehrmann, E. J.; Mahoney, K. M.; Goswami, P. P.; Albright, T. R.; Syed, A.; Dutton, A. S.; Smith, E. A.; Winter, A. H., Family of BODIPY Photocages Cleaved by Single Photons of Visible/Near-Infrared Light. *Journal of the American Chemical Society* **2018,** *140* (23), 7343-7346.

94. Bełtowski, J.; Wójcicka, G.; Jamroz-Wiśniewska, A., Hydrogen sulfide in the regulation of insulin secretion and insulin sensitivity: Implications for the pathogenesis and treatment of diabetes mellitus. *Biochemical Pharmacology* **2018,** *149*, 60-76.

95. Kashfi, K., The role of hydrogen sulfide in health and disease. *Biochemical Pharmacology* **2018,** *149*, 1-4.

96. Shrestha, P.; Dissanayake, K. C.; Gehrmann, E. J.; Wijesooriya, C. S.; Mukhopadhyay, A.; Smith, E. A.; Winter, A. H., Efficient Far-Red/Near-IR Absorbing BODIPY Photocages by Blocking Unproductive Conical Intersections. *Journal of the American Chemical Society* **2020,** *142* (36), 15505-15512.

97. Slanina, T.; Shrestha, P.; Palao, E.; Kand, D.; Peterson, J. A.; Dutton, A. S.; Rubinstein, N.; Weinstain, R.; Winter, A. H.; Klán, P., In Search of the Perfect Photocage: Structure–Reactivity Relationships in meso-Methyl BODIPY Photoremovable Protecting Groups. *Journal of the American Chemical Society* **2017,** *139* (42), 15168-15175.

98. Štacková, L.; Štacko, P.; Klán, P., Approach to a Substituted Heptamethine Cyanine Chain by the Ring Opening of Zincke Salts. *Journal of the American Chemical Society* **2019,** *141* (17), 7155-7162.

99. AKORN IC-Green [Labelling]. Drugs@FDA Database. U.S. Food and Drug Administration. https://www.accessdata.fda.gov/drugsatfda_docs/label/2015/011525s027lbl.pdf (accessed June 16 2021).

100. TECH, N. Spy Agent Green Kit [Labelling]. Drugs@FDA Database. U.S. Food and Drug Administration. https://www.accessdata.fda.gov/drugsatfda_docs/label/2018/211580s000lbl.pdf (accessed June 16 2021).

101. Gorka, A. P.; Schnermann, M. J., Harnessing cyanine photooxidation: from slowing photobleaching to near-IR uncaging. *Current Opinion in Chemical Biology* **2016,** *33*, 117-125.

102. Luciano, M. P.; Nourian, S.; Gorka, A. P.; Nani, R. R.; Nagaya, T.; Kobayashi, H.; Schnermann, M. J., Chapter Eleven - A near-infrared light-mediated cleavable linker strategy using the heptamethine cyanine chromophore. In *Methods in Enzymology*, Chenoweth, D. M., Ed. Academic Press: 2020; Vol. 641, pp 245-275.

103. Jiao, L.; Song, F.; Cui, J.; Peng, X., A near-infrared heptamethine aminocyanine dye with a long-lived excited triplet state for photodynamic therapy. *Chemical Communications* **2018,** *54* (66), 9198-9201.

104. Jones, A. R., The photochemistry and photobiology of vitamin B12. *Photochemical & Photobiological Sciences* **2017,** *16* (6), 820-834.

105. Shell, T. A.; Lawrence, D. S., Vitamin B12: A Tunable, Long Wavelength, Light-Responsive Platform for Launching Therapeutic Agents. *Accounts of Chemical Research* **2015,** *48* (11), 2866-2874.

106. Gendron, L. N.; Zites, D. C.; LaRochelle, E. P. M.; Gunn, J. R.; Pogue, B. W.; Shell, T. A.; Shell, J. R., Tumor targeting vitamin B12 derivatives for X-ray induced treatment of pancreatic adenocarcinoma. *Photodiagnosis and Photodynamic Therapy* **2020,** *30*, 101637.

107. Smith, W. J.; Oien, N. P.; Hughes, R. M.; Marvin, C. M.; Rodgers, Z. L.; Lee, J.; Lawrence, D. S., Cell-Mediated Assembly of Phototherapeutics. *Angewandte Chemie International Edition* **2014,** *53* (41), 10945-10948.

108. Clardy, S. M.; Allis, D. G.; Fairchild, T. J.; Doyle, R. P., Vitamin B12 in drug delivery: breaking through the barriers to a B12 bioconjugate pharmaceutical. *Expert Opinion on Drug Delivery* **2011,** *8* (1), 127-140.

109. Adams, J. F., Biological Half-life of Vitamin B12 in Plasma. *Nature* **1963,** *198* (4876), 200-200.

110. Tallmadge, E. H., PATENTING NATURAL PRODUCTS AFTER MYRIAD. *Harvard J. of Law & Tech.* **2017,** *30* (2), 569-598.

111. Roin, B. N., Unpatentable Drugs and the Standards of Patentability. *Texas Law Review* **2009,** *87*.

112. Abrahamse, H.; Hamblin, Michael R., New photosensitizers for photodynamic therapy. *Biochemical Journal* **2016,** *473* (4), 347-364.

113. Lo, P.-C.; Rodríguez-Morgade, M. S.; Pandey, R. K.; Ng, D. K. P.; Torres, T.; Dumoulin, F., The unique features and promises of phthalocyanines as advanced photosensitisers for photodynamic therapy of cancer. *Chemical Society Reviews* **2020,** *49* (4), 1041-1056.

114. Chen, P.-S.; Chiu, W.-T.; Hsu, P.-L.; Lin, S.-C.; Peng, I. C.; Wang, C.-Y.; Tsai, S.-J., Pathophysiological implications of hypoxia in human diseases. *Journal of Biomedical Science* **2020,** *27* (1), 63.

115. Alessio, E.; Messori, L., NAMI-A and KP1019/1339, Two Iconic Ruthenium Anticancer Drug Candidates Face-to-Face: A Case Story in Medicinal Inorganic Chemistry. *Molecules* **2019,** *24* (10), 1995.

116. Mari, C.; Pierroz, V.; Ferrari, S.; Gasser, G., Combination of Ru(ii) complexes and light: new frontiers in cancer therapy. *Chemical Science* **2015,** *6* (5), 2660-2686.

117. van Rixel, V. H. S.; Ramu, V.; Auyeung, A. B.; Beztsinna, N.; Leger, D. Y.; Lameijer, L. N.; Hilt, S. T.; Le Dévédec, S. E.; Yildiz, T.; Betancourt, T.; Gildner, M. B.; Hudnall, T. W.; Sol, V.; Liagre, B.; Kornienko, A.; Bonnet, S., Photo-Uncaging of a Microtubule-Targeted Rigidin Analogue in Hypoxic Cancer Cells and in a Xenograft Mouse Model. *Journal of the American Chemical Society* **2019,** *141* (46), 18444-18454.

118. Zayat, L.; Filevich, O.; Baraldo, L. M.; Etchenique, R., Ruthenium polypyridyl phototriggers: from beginnings to perspectives. *Philosophical Transactions of the Royal Society A: Mathematical, Physical and Engineering Sciences* **2013,** *371* (1995), 20120330.

119. Loftus, L. M.; Rack, J. J.; Turro, C., Photoinduced ligand dissociation follows reverse energy gap law: nitrile photodissociation from low energy 3MLCT excited states. *Chemical Communications* **2020,** *56* (29), 4070-4073.

120. Loftus, L. M.; Al-Afyouni, K. F.; Turro, C., New RuII Scaffold for Photoinduced Ligand Release with Red Light in the Photodynamic Therapy (PDT) Window. *Chemistry – A European Journal* **2018,** *24* (45), 11550-11553.

121. Havrylyuk, D.; Stevens, K.; Parkin, S.; Glazer, E. C., Toward Optimal Ru(II) Photocages: Balancing Photochemistry, Stability, and Biocompatibility Through Fine Tuning of Steric, Electronic, and Physiochemical Features. *Inorganic Chemistry* **2020,** *59* (2), 1006-1013.

122. Hüll, K.; Morstein, J.; Trauner, D., In Vivo Photopharmacology. *Chemical Reviews* **2018,** *118* (21), 10710-10747.

123. Nikonov, S.; Dolgova, N.; Tochitsky, I.; Van Gelder, R. N.; Kramer, R.; Aguirre, G. D.; Beltran, W. A., Azobenzene-based DENAQ photoswitch confers light sensitivity to degenerated but not to healthy canine retina. *Investigative Ophthalmology & Visual Science* **2016,** *57* (12), 602-602.

124. Hartley, G. S., The Cis-form of Azobenzene. *Nature* **1937,** *140* (3537), 281-281.

125. Dong, M.; Babalhavaeji, A.; Samanta, S.; Beharry, A. A.; Woolley, G. A., Red-Shifting Azobenzene Photoswitches for in Vivo Use. *Accounts of Chemical Research* **2015,** *48* (10), 2662-2670.

126. Wang, D.; Wagner, M.; Butt, H.-J.; Wu, S., Supramolecular hydrogels constructed by red-light-responsive host–guest interactions for photo-controlled protein release in deep tissue. *Soft Matter* **2015,** *11* (38), 7656-7662.

127. Accardo, J. V.; McClure, E. R.; Mosquera, M. A.; Kalow, J. A., Using Visible Light to Tune Boronic Acid–Ester Equilibria. *Journal of the American Chemical Society* **2020,** *142* (47), 19969-19979.

128. Robles, H., Dimethylaminoazobenzene. In *Encyclopedia of Toxicology (Third Edition)*, Wexler, P., Ed. Academic Press: Oxford, 2014; pp 158-159.

129. Dong, M.; Babalhavaeji, A.; Collins, C. V.; Jarrah, K.; Sadovski, O.; Dai, Q.; Woolley, G. A., Near-Infrared Photoswitching of Azobenzenes under Physiological Conditions. *Journal of the American Chemical Society* **2017,** *139* (38), 13483-13486.

130. Konrad, D. B.; Savasci, G.; Allmendinger, L.; Trauner, D.; Ochsenfeld, C.; Ali, A. M., Computational Design and Synthesis of a Deeply Red-Shifted and Bistable Azobenzene. *Journal of the American Chemical Society* **2020,** *142* (14), 6538-6547.

131. Zhu, M.; Zhou, H., Azobenzene-based small molecular photoswitches for protein modulation. *Organic & Biomolecular Chemistry* **2018,** *16* (44), 8434-8445.

132. Hemmer, J. R.; Poelma, S. O.; Treat, N.; Page, Z. A.; Dolinski, N. D.; Diaz, Y. J.; Tomlinson, W.; Clark, K. D.; Hooper, J. P.; Hawker, C.; Read de Alaniz, J., Tunable Visible and Near Infrared Photoswitches. *Journal of the American Chemical Society* **2016,** *138* (42), 13960-13966.

133. Rifaie-Graham, O.; Ulrich, S.; Galensowske, N. F. B.; Balog, S.; Chami, M.; Rentsch, D.; Hemmer, J. R.; Read de Alaniz, J.; Boesel, L. F.; Bruns, N., Wavelength-Selective Light-Responsive DASA-Functionalized Polymersome Nanoreactors. *Journal of the American Chemical Society* **2018,** *140* (25), 8027-8036.

134. Gao, H.; Guo, T.; Chen, Y.; Kong, Y.; Peng, Z., Reversible negative photochromic sulfo-substituted spiropyrans. *Journal of Molecular Structure* **2016,** *1123*, 426.

135. Bekere, L.; Larina, N.; Lokshin, V.; Ellern, A.; Sigalov, M.; Khodorkovsky, V., A new class of spirocyclic photochromes reacting with light of both UV and visible ranges. *New Journal of Chemistry* **2016,** *40* (8), 6554-6558.

136. Tosic, O.; Altenhöner, K.; Mattay, J., Photochromic dithienylethenes with extended π-systems. *Photochemical & Photobiological Sciences* **2010,** *9* (2), 128-130.

137. Fredrich, S.; Göstl, R.; Herder, M.; Grubert, L.; Hecht, S., Switching Diarylethenes Reliably in Both Directions with Visible Light. *Angewandte Chemie International Edition* **2016,** *55* (3), 1208-1212.

138. Maerz, B.; Wiedbrauk, S.; Oesterling, S.; Samoylova, E.; Nenov, A.; Mayer, P.; de Vivie-Riedle, R.; Zinth, W.; Dube, H., Making Fast Photoswitches Faster—Using Hammett Analysis to Understand the Limit of Donor–Acceptor Approaches for Faster Hemithioindigo Photoswitches. *Chemistry – A European Journal* **2014,** *20* (43), 13984-13992.

139. Eggers, K.; Fyles, T. M.; Montoya-Pelaez, P. J., Synthesis and Characterization of Photoswitchable Lipids Containing Hemithioindigo Chromophores. *The Journal of Organic Chemistry* **2001,** *66* (9), 2966-2977.

140. Yamaguchi, T.; Kobayashi, Y.; Abe, J., Fast Negative Photochromism of 1,1′-Binaphthyl-Bridged Phenoxyl–Imidazolyl Radical Complex. *Journal of the American Chemical Society* **2016,** *138* (3), 906-913.

141. Knežević, N. Ž.; Trewyn, B. G.; Lin, V. S. Y., Functionalized mesoporous silica nanoparticle-based visible light responsive controlled release delivery system. *Chemical Communications* **2011,** *47* (10), 2817-2819.

142. Vickerman, B. M.; O'Banion, C. P.; Tan, X.; Lawrence, D. S., Light-Controlled Release of Therapeutic Proteins from Red Blood Cells. *ACS Central Science* **2021,** *7* (1), 93-103.

143. King Pharmaceuticals, I. Thrombin-JMI [Labelling]. U.S. Food and Drug Administration. https://www.fda.gov/media/80429/download (accessed June 16 2021).

144. Rady, I.; Siddiqui, I. A.; Rady, M.; Mukhtar, H., Melittin, a major peptide component of bee venom, and its conjugates in cancer therapy. *Cancer Letters* **2017,** *402*, 16-31.

145. Chiulan, I.; Heggset, E. B.; Voicu, Ş. I.; Chinga-Carrasco, G., Photopolymerization of Bio-Based Polymers in a Biomedical Engineering Perspective. *Biomacromolecules* **2021,** *22* (5), 1795-1814.

146. Tian, Y.; Zheng, J.; Tang, X.; Ren, Q.; Wang, Y.; Yang, W., Near-Infrared Light-Responsive Nanogels with Diselenide-Cross-Linkers for On-Demand Degradation and Triggered Drug Release. *Particle & Particle Systems Characterization* **2015,** *32* (5), 547-551.

147. Luo, D.; Li, N.; Carter, K. A.; Lin, C.; Geng, J.; Shao, S.; Huang, W.-C.; Qin, Y.; Atilla-Gokcumen, G. E.; Lovell, J. F., Rapid Light-Triggered Drug Release in Liposomes Containing Small Amounts of Unsaturated and Porphyrin–Phospholipids. *Small* **2016,** *12* (22), 3039-3047.

148. Yavlovich, A.; Singh, A.; Blumenthal, R.; Puri, A., A novel class of photo-triggerable liposomes containing DPPC:DC8,9PC as vehicles for delivery of doxorubcin to cells. *Biochimica et Biophysica Acta (BBA) - Biomembranes* **2011,** *1808* (1), 117-126.

149. Sine, J.; Urban, C.; Thayer, D.; Charron, H.; Valim, N.; Tata, D. B.; Schiff, R.; Blumenthal, R.; Joshi, A.; Puri, A., Photo activation of HPPH encapsulated in "Pocket" liposomes triggers multiple drug release and tumor cell killing in mouse breast cancer xenografts. *Int J Nanomedicine* **2014,** *10*, 125-145.

150. Chen, W.; Goldys, E. M.; Deng, W., Light-induced liposomes for cancer therapeutics. *Progress in Lipid Research* **2020,** *79*, 101052.

151. Leung, S. J.; Romanowski, M., Light-activated content release from liposomes. *Theranostics* **2012,** *2* (10), 1020-1036.

152. Fomina, N.; Sankaranarayanan, J.; Almutairi, A., Photochemical mechanisms of light-triggered release from nanocarriers. *Advanced Drug Delivery Reviews* **2012,** *64* (11), 1005-1020.

153. Mueller, A.; Bondurant, B.; O'Brien, D. F., Visible-Light-Stimulated Destabilization of PEG-Liposomes. *Macromolecules* **2000,** *33* (13), 4799-4804.

154. Miller, C. R.; Clapp, P. J.; O'Brien, D. F., Visible light-induced destabilization of endocytosed liposomes. *FEBS Letters* **2000,** *467* (1), 52-56.

155. Penjweini, R.; Kim, M. M.; Ong, Y. H.; Zhu, T. C., 1O2 determined from the measured PDT dose and 3O2 predicts long-term response to Photofrin-mediated PDT. *Physics in Medicine & Biology* **2020,** *65* (3), 03LT01.

156. Kniese, C. M.; Musani, A. I., Bronchoscopic treatment of inoperable nonsmall cell lung cancer. *European Respiratory Review* **2020,** *29* (158), 200035.

157. Bonnet, S., Why develop photoactivated chemotherapy? *Dalton Transactions* **2018,** *47* (31), 10330-10343.

158. Alsaab, H. O.; Alghamdi, M. S.; Alotaibi, A. S.; Alzhrani, R.; Alwuthaynani, F.; Althobaiti, Y. S.; Almalki, A. H.; Sau, S.; Iyer, A. K., Progress in Clinical Trials of Photodynamic Therapy for Solid Tumors and the Role of Nanomedicine. *Cancers* **2020,** *12* (10), 2793.

159. Bonnet, S., Why develop photoactivated chemotherapy? *Dalton Trans* **2018,** *47* (31), 10330-10343.

160. Lambert, A.; Schwarz, L.; Borbath, I.; Henry, A.; Van Laethem, J.-L.; Malka, D.; Ducreux, M.; Conroy, T., An update on treatment options for pancreatic adenocarcinoma. *Ther Adv Med Oncol* **2019,** *11*, 1758835919875568-1758835919875568.

161. Thind, M.; Kowey, P. R., The Role of the Food and Drug Administration in Drug Development: On the Subject of Proarrhythmia Risk. *J Innov Card Rhythm Manag* **2020,** *11* (1), 3958-3967.

162. Administration, U. S. F. a. D. IND Applications for Clinical Investigations: Regulatory and Administrative Components. U.S. Food and Drug Administration. https://www.fda.gov/drugs/investigational-new-drug-ind-application/ind-applications-clinical-investigations-regulatory-and-administrative-components (accessed June 16 2021).

163. Program, N. T. Guidance Document on Using In Vitro Data to Estimate In Vivo Starting Doses for Acute Toxicity. https://ntp.niehs.nih.gov/iccvam/docs/acutetox_docs/guidance0801/iv_guide.pdf (accessed June 16 2021).

164. Imran, M.; Ayub, W.; Butler, I. S.; Zia ur, R., Photoactivated platinum-based anticancer drugs. *Coordination Chemistry Reviews* **2018,** *376*, 405-429.

165. Wolska-Washer, A.; Robak, T., Safety and Tolerability of Antibody-Drug Conjugates in Cancer. *Drug Safety* **2019,** *42* (2), 295-314.

166. Zabka, T. S.; Singh, J.; Dhawan, P.; Liederer, B. M.; Oeh, J.; Kauss, M. A.; Xiao, Y.; Zak, M.; Lin, T.; McCray, B.; La, N.; Nguyen, T.; Beyer, J.; Farman, C.; Uppal, H.; Dragovich, P. S.; O'Brien, T.; Sampath, D.; Misner, D. L., Retinal Toxicity, in vivo and in vitro, Associated with Inhibition of Nicotinamide Phosphoribosyltransferase. *Toxicological Sciences* **2014,** *144* (1), 163-172.

167. Wang, J. J.; Lei, K. F.; Han, F., Tumor microenvironment: Recent advances in various cancer treatments. *European review for medical and pharmacological sciences* **2018,** *22*, 3855-3864.

168. Pillai, R. K.; Jayasree, K., Rare cancers: Challenges & issues. *Indian J Med Res* **2017,** *145* (1), 17-27.

169. Bullock, J.; Rizvi, S. A. A.; Saleh, A. M.; Ahmed, S. S.; Do, D. P.; Ansari, R. A.; Ahmed, J., Rheumatoid Arthritis: A Brief Overview of the Treatment. *Medical Principles and Practice* **2018,** *27* (6), 501-507.

170. Sokka, T.; Kautiainen, H.; Pincus, T.; Verstappen, S. M. M.; Aggarwal, A.; Alten, R.; Andersone, D.; Badsha, H.; Baecklund, E.; Belmonte, M.; Craig-Müller, J.; da Mota, L. M. H.; Dimic, A.; Fathi, N. A.; Ferraccioli, G.; Fukuda, W.; Géher, P.; Gogus, F.; Hajjaj-Hassouni, N.; Hamoud, H.; Haugeberg, G.; Henrohn, D.; Horslev-Petersen, K.; Ionescu, R.; Karateew, D.; Kuuse, R.; Laurindo, I. M. M.; Lazovskis, J.; Luukkainen, R.; Mofti, A.; Murphy, E.; Nakajima, A.; Oyoo, O.; Pandya, S. C.; Pohl, C.; Predeteanu, D.; Rexhepi, M.; Rexhepi, S.; Sharma, B.; Shono, E.; Sibilia, J.; Sierakowski, S.; Skopouli, F. N.; Stropuviene, S.; Toloza, S.; Valter, I.; Woolf, A.; Yamanaka, H.; the, Q.-R. A. s. g., Work disability remains a major problem in rheumatoid arthritis in the 2000s: data from 32 countries in the QUEST-RA Study. *Arthritis Research & Therapy* **2010,** *12* (2), R42.

171. Taponen, S.; Uitti, J.; Karvala, K.; Luukkonen, R.; Lehtimäki, L., Asthma diagnosed in late adulthood is linked to work disability and poor employment status. *Respiratory Medicine* **2019,** *147*, 76-78.

172. Castro, M.; Rossi, L.; Papadatou, B.; Bracci, F.; Knafelz, D.; Ambrosini, M. I.; Calce, A.; Serafini, S.; Isacchi, G.; D'Orio, F.; Mambrini, G.; Magnani, M., Long-term Treatment With Autologous Red Blood Cells Loaded With Dexamethasone 21–Phosphate in Pediatric Patients Affected by Steroid-dependent Crohn Disease. *Journal of Pediatric Gastroenterology and Nutrition* **2007,** *44* (4).

173. Ocular Therapeutix, I. Dextenza [Labelling]. Drugs@FDA Database. U.S. Food and Drug Administration. https://www.accessdata.fda.gov/drugsatfda_docs/label/2019/208742s001lbl.pdf (accessed June 16 2021).

174. De Backer, D.; Biston, P.; Devriendt, J.; Madl, C.; Chochrad, D.; Aldecoa, C.; Brasseur, A.; Defrance, P.; Gottignies, P.; Vincent, J.-L., Comparison of Dopamine and Norepinephrine in the Treatment of Shock. *New England Journal of Medicine* **2010,** *362* (9), 779-789.

175. Lu, Y.; Sun, W.; Gu, Z., Stimuli-responsive nanomaterials for therapeutic protein delivery. *Journal of Controlled Release* **2014,** *194*, 1-19.

176. Wallace, J. L.; Wang, R., Hydrogen sulfide-based therapeutics: exploiting a unique but ubiquitous gasotransmitter. *Nature Reviews Drug Discovery* **2015,** *14* (5), 329-345.

177. Lundberg, J. O.; Weitzberg, E.; Gladwin, M. T., The nitrate–nitrite–nitric oxide pathway in physiology and therapeutics. *Nature Reviews Drug Discovery* **2008,** *7* (2), 156-167.

178. Motterlini, R.; Otterbein, L. E., The therapeutic potential of carbon monoxide. *Nature Reviews Drug Discovery* **2010,** *9* (9), 728-743.

179. Hardee, C. L.; Arévalo-Soliz, L. M.; Hornstein, B. D.; Zechiedrich, L., Advances in Non-Viral DNA Vectors for Gene Therapy. *Genes* **2017,** *8* (2), 65.

180. Giacca, M.; Zacchigna, S., VEGF gene therapy: therapeutic angiogenesis in the clinic and beyond. *Gene Therapy* **2012,** *19* (6), 622-629.

181. Klán, P.; Šolomek, T.; Bochet, C. G.; Blanc, A.; Givens, R.; Rubina, M.; Popik, V.; Kostikov, A.; Wirz, J., Photoremovable Protecting Groups in Chemistry and Biology: Reaction Mechanisms and Efficacy. *Chemical Reviews* **2013,** *113* (1), 119-191.

182. Weinstain, R.; Slanina, T.; Kand, D.; Klán, P., Visible-to-NIR-Light Activated Release: From Small Molecules to Nanomaterials. *Chemical reviews* **2020,** *120* (24), 13135-13272.

183. Falvey, D. E.; Sundararajan, C., Photoremovable protecting groups based on electron transfer chemistry. *Photochemical & Photobiological Sciences* **2004,** *3* (9), 831-838.

184. Alabugin, A., Near-IR Photochemistry for Biology: Exploiting the Optical Window of Tissue. *Photochemistry and Photobiology* **2019,** *95* (3), 722-732.

185. Cyriac, J. M.; James, E., Switch over from intravenous to oral therapy: A concise overview. *J Pharmacol Pharmacother* **2014,** *5* (2), 83-87.

186. Glassman, P. M.; Muzykantov, V. R., Pharmacokinetic and Pharmacodynamic Properties of Drug Delivery Systems. *Journal of Pharmacology and Experimental Therapeutics* **2019,** *370* (3), 570.

187. Mucke, H. A. M., Drug Repositioning in the Mirror of Patenting: Surveying and Mining Uncharted Territory. *Frontiers in Pharmacology* **2017,** *8* (927).

188. Park, D. H.; Lee, S. S.; Park, S. E.; Lee, J. L.; Choi, J. H.; Choi, H. J.; Jang, J. W.; Kim, H. J.; Eum, J. B.; Seo, D.-W.; Lee, S. K.; Kim, M.-H.; Lee, J. B., Randomised phase II trial of photodynamic therapy plus oral fluoropyrimidine, S-1, versus photodynamic therapy alone for unresectable hilar cholangiocarcinoma. *European Journal of Cancer* **2014,** *50* (7), 1259-1268.

189. Bown, S. G.; Rogowska, A. Z.; Whitelaw, D. E.; Lees, W. R.; Lovat, L. B.; Ripley, P.; Jones, L.; Wyld, P.; Gillams, A.; Hatfield, A. W. R., Photodynamic therapy for cancer of the pancreas. *Gut* **2002,** *50* (4), 549-557.

190. America, L. I. o. American National Standard for Safe Use of Lasers. https://eliceirilab.org/sites/default/files/2017-04/American%20National%20Standard%20for%20Safe%20Use%20of%20Lasers.pdf (accessed June 16 2021).

191. Welleman, I. M.; Hoorens, M. W. H.; Feringa, B. L.; Boersma, H. H.; Szymański, W., Photoresponsive molecular tools for emerging applications of light in medicine. *Chemical Science* **2020,** *11* (43), 11672-11691.

192. Villa, C. H.; Anselmo, A. C.; Mitragotri, S.; Muzykantov, V., Red blood cells: Supercarriers for drugs, biologicals, and nanoparticles and inspiration for advanced delivery systems. *Advanced Drug Delivery Reviews* **2016,** *106*, 88-103.

193. Gutiérrez Millán, C.; Bravo, D. G.; Lanao, J. M., New erythrocyte-related delivery systems for biomedical applications. *Journal of Drug Delivery Science and Technology* **2017,** *42*, 38-48.

194. Hassan, S.; Prakash, G.; Bal Ozturk, A.; Saghazadeh, S.; Farhan Sohail, M.; Seo, J.; Remzi Dokmeci, M.; Zhang, Y. S.; Khademhosseini, A., Evolution and clinical translation of drug delivery nanomaterials. *Nano Today* **2017,** *15*, 91-106.

195. Choi, H. S.; Frangioni, J. V., Nanoparticles for biomedical imaging: fundamentals of clinical translation. *Mol Imaging* **2010,** *9* (6), 291-310.

196. Shafiq, M.; Anjum, S.; Hano, C.; Anjum, I.; Abbasi, B. H., An Overview of the Applications of Nanomaterials and Nanodevices in the Food Industry. *Foods* **2020,** *9* (2).

197. Yang, C.; Bromma, K.; Di Ciano-Oliveira, C.; Zafarana, G.; van Prooijen, M.; Chithrani, D. B., Gold nanoparticle mediated combined cancer therapy. *Cancer Nanotechnology* **2018,** *9* (1), 4.

198. Wáng, Y. X. J.; Idée, J.-M., A comprehensive literatures update of clinical researches of superparamagnetic resonance iron oxide nanoparticles for magnetic resonance imaging. *Quant Imaging Med Surg* **2017,** *7* (1), 88-122.

199. Anselmo, A. C.; Mitragotri, S., A Review of Clinical Translation of Inorganic Nanoparticles. *AAPS J* **2015,** *17* (5), 1041-1054.

200. Sanadgol, N.; Wackerlig, J., Developments of Smart Drug-Delivery Systems Based on Magnetic Molecularly Imprinted Polymers for Targeted Cancer Therapy: A Short Review. *Pharmaceutics* **2020,** *12* (9).

201. Hwang, D.; Ramsey, J. D.; Kabanov, A. V., Polymeric micelles for the delivery of poorly soluble drugs: From nanoformulation to clinical approval. *Advanced Drug Delivery Reviews* **2020,** *156*, 80-118.

202. Gelderblom, H.; Verweij, J.; Nooter, K.; Sparreboom, A., Cremophor EL: the drawbacks and advantages of vehicle selection for drug formulation. *European Journal of Cancer* **2001,** *37* (13), 1590-1598.

203. Kannan, S., OP-101: A novel therapy for treatment of childhood cerebral adrenoleukodystrophy. *Journal of Genetic Syndromes & Gene Therapy* **2017,** *08* (03).

204. Orpheris, I. A Study to Evaluate OP-101 (Dendrimer N-acetyl-cysteine) in Severe Coronavirus Disease 2019 (COVID-19) Patients (PRANA). ClinicalTrials.gov. NIH U.S. National Library of Medicine. https://clinicaltrials.gov/ct2/show/NCT04458298?term=OP-101&draw=2&rank=3 (accessed June 16 2021).

205. Cheng, C. J.; Tietjen, G. T.; Saucier-Sawyer, J. K.; Saltzman, W. M., A holistic approach to targeting disease with polymeric nanoparticles. *Nature Reviews Drug Discovery* **2015,** *14* (4), 239-247.

206. Anselmo, A. C.; Mitragotri, S., Nanoparticles in the clinic. *Bioeng Transl Med* **2016,** *1* (1), 10-29.

207. Anselmo, A. C.; Mitragotri, S., Nanoparticles in the clinic: An update. *Bioeng Transl Med* **2019,** *4* (3), e10143.

208. Mandal, A.; Clegg, J. R.; Anselmo, A. C.; Mitragotri, S., Hydrogels in the clinic. *Bioeng Transl Med* **2020,** *5* (2), e10158-e10158.

209. Ai, X.; Mu, J.; Xing, B., Recent Advances of Light-Mediated Theranostics. *Theranostics* **2016,** *6* (13), 2439-2457.

210. Rossi, L.; Pierigè, F.; Aliano, M. P.; Magnani, M., Ongoing Developments and Clinical Progress in Drug-Loaded Red Blood Cell Technologies. *BioDrugs* **2020,** *34* (3), 265-272.

211. Magnani, M., Engineered red blood cells as therapeutic agents. *American Journal of Hematology* **2017,** *92* (10), 979-980.

212. Tzounakas, V. L.; Karadimas, D. G.; Papassideri, I. S.; Seghatchian, J.; Antonelou, M. H., Erythrocyte-based drug delivery in Transfusion Medicine: Wandering questions seeking answers. *Transfusion and Apheresis Science* **2017,** *56* (4), 626-634.

213. Gothoskar, A. V., Resealed Erythrocytes: A Review. *Pharmaceutical Technology* **2004**, 140-158.

214. Mambrini, G.; Mandolini, M.; Rossi, L.; Pierigè, F.; Capogrossi, G.; Salvati, P.; Serafini, S.; Benatti, L.; Magnani, M., Ex vivo encapsulation of dexamethasone sodium phosphate into human autologous erythrocytes using fully automated biomedical equipment. *International Journal of Pharmaceutics* **2017,** *517* (1), 175-184.

215. Bulbake, U.; Doppalapudi, S.; Kommineni, N.; Khan, W., Liposomal Formulations in Clinical Use: An Updated Review. *Pharmaceutics* **2017,** *9* (2), 12.

216. PHARMS, C. Vyxeos [Labelling]. Drugs@FDA Database. U.S. Food and Drug Administration. https://www.accessdata.fda.gov/drugsatfda_docs/label/2017/209401s000lbl.pdf (accessed June 16 2021).

217. Puri, A., Phototriggerable liposomes: current research and future perspectives. *Pharmaceutics* **2013,** *6* (1), 1-25.

218. Ernsting, M. J.; Murakami, M.; Roy, A.; Li, S.-D., Factors controlling the pharmacokinetics, biodistribution and intratumoral penetration of nanoparticles. *Journal of Controlled Release* **2013,** *172* (3), 782-794.

219. Glassman, P. M.; Abuqayyas, L.; Balthasar, J. P., Assessments of antibody biodistribution. *The Journal of Clinical Pharmacology* **2015,** *55* (S3), S29-S38.

220. Ding, S.; O'Banion, C. P.; Welfare, J. G.; Lawrence, D. S., Cellular Cyborgs: On the Precipice of a Drug Delivery Revolution. *Cell Chemical Biology* **2018,** *25* (6), 648-658.

221. Zhou, B.; Guo, Z.; Lin, Z.; Jiang, B.-P.; Shen, X.-C., Stimuli-Responsive Nanomaterials for Smart Tumor-Specific Phototherapeutics. *ChemMedChem* **2021,** *16* (6), 919-931.

222. Bourgeaux, V.; Lanao, J. M.; Bax, B. E.; Godfrin, Y., Drug-loaded erythrocytes: on the road toward marketing approval. *Drug Des Devel Ther* **2016,** *10*, 665-76.

223. Mura, S.; Nicolas, J.; Couvreur, P., Stimuli-responsive nanocarriers for drug delivery. *Nature Materials* **2013,** *12* (11), 991-1003.

224. Son, J.; Yi, G.; Yoo, J.; Park, C.; Koo, H.; Choi, H. S., Light-responsive nanomedicine for biophotonic imaging and targeted therapy. *Advanced Drug Delivery Reviews* **2019,** *138*, 133-147.

225. Bottini, N.; Firestein, G. S., Duality of fibroblast-like synoviocytes in RA: passive responders and imprinted aggressors. *Nature Reviews Rheumatology* **2013,** *9* (1), 24-33.

226. Palao, E.; Slanina, T.; Muchová, L.; Šolomek, T.; Vítek, L.; Klán, P., Transition-Metal-Free CO-Releasing BODIPY Derivatives Activatable by Visible to NIR Light as Promising Bioactive Molecules. *Journal of the American Chemical Society* **2016,** *138* (1), 126-133.

227. Ichinose, F.; Roberts, J. D.; Zapol, W. M., Inhaled Nitric Oxide. *Circulation* **2004,** *109* (25), 3106-3111.

228. Alvarez, R. A.; Berra, L.; Gladwin, M. T., Home Nitric Oxide Therapy for COVID-19. *Am J Respir Crit Care Med* **2020,** *202* (1), 16-20.

229. Hickok, J. R.; Thomas, D. D., Nitric oxide and cancer therapy: the emperor has NO clothes. *Curr Pharm Des* **2010,** *16* (4), 381-391.

230. Ling, K.; Men, F.; Wang, W.-C.; Zhou, Y.-Q.; Zhang, H.-W.; Ye, D.-W., Carbon Monoxide and Its Controlled Release: Therapeutic Application, Detection, and Development of Carbon Monoxide Releasing Molecules (CORMs). *Journal of Medicinal Chemistry* **2018,** *61* (7), 2611-2635.

231. Rai, P.; Mallidi, S.; Zheng, X.; Rahmanzadeh, R.; Mir, Y.; Elrington, S.; Khurshid, A.; Hasan, T., Development and applications of photo-triggered theranostic agents. *Advanced Drug Delivery Reviews* **2010,** *62* (11), 1094-1124.

232. Liumbruno, G.; Bennardello, F.; Lattanzio, A.; Piccoli, P.; Rossetti, G., Recommendations for the transfusion of red blood cells. *Blood Transfus* **2009,** *7* (1), 49-64.

233. Bullock, J.; Rizvi, S. A. A.; Saleh, A. M.; Ahmed, S. S.; Do, D. P.; Ansari, R. A.; Ahmed, J., Rheumatoid Arthritis: A Brief Overview of the Treatment. *Med Princ Pract* **2018,** *27* (6), 501-507.

CHAPTER 2: PHOTOACTIVATED CHEMOTHERAPEUTIC COBALAMIN-DOCETAXEL RED BLOOD CELLS LOCALLY RELEASE DRUG ON COMMAND

Reproduced with permission from Marvin, C. M.; Ding, S.; White, R. E.; Orlova, N.; Wang, Q.; Zywot, E. M.; Vickerman, B. M.; Harr, L.; Tarrant, T. K.; Dayton, P. A.; Lawrence, D. S., On Command Drug Delivery via Cell-Conveyed Phototherapeutics. *Small* **2019,** *15* (37), e1901442.

The work in this Chapter was a collaboration between the authors Christina M. Marvin, Song Ding, Rachel E. White, Natalia Orlova, Qunzhao Wang, Emilia M. Zywot, Brianna M. Vickerman, Lauren Harr, Teresa K. Tarrant, Paul A. Dayton, and David S. Lawrence. The first author of this publication, Christina M. Marvin, wrote the paper and contributed the most scientific ideas and experimental effort. Emilia M. Zywot, the author of this dissertation, was trained during the described studies and contributed experimental efforts involving red blood cell loading, cell culture assays, flow cytometry, and histology studies.

2.1 Introduction to Photoactivated Chemotherapeutics

Photoactivated chemotherapeutics (PACTs) seek to diminish the inherent off-target systemic toxicity of chemotherapeutic treatments.[1-4] PACTs are one of many drug delivery systems (DDSs) that rely on an external stimulant, specifically light illumination, to localize therapeutic release.[5-8] Other targeted DDSs in the clinic include liposomes, such as Doxil and ThermoDox, photothermal therapies AuroLase and NanoTherm, and many antibody drug conjugates (ADCs), such as trastuzumab and bevacizumab among others.[4, 9, 10] These systems rely on passive and/or active targeting to diminish off-target toxicity and enhance efficacy by localization including: passive targeting of nanomaterials due to the enhanced permeation and retention effect, active targeting by external stimulation (light or an alternating magnetic field) to induce a photothermal effect, and active targeting by inducing strong binding interactions to receptors and other biomarkers on the surface of cancer cells. Yet, these systems are limited by challenges with therapeutic release or uptake, drug payloads, and longer exposure times with

high intensity stimuli that cause inadvertent damage to treated tissue.[7, 11-13] Still, ThermoDox improves upon the limited therapeutic release from Doxil by providing a means of externally triggering liposomal degradation resulting in targeted therapeutic release which can be controlled by intensity, location, and time. Such clinically tested solutions establish the precedent for externally controlled DDSs enhancing therapeutic delivery as compared to passively targeted systems. Similar to AuroLase, PACTs rely on light as an external stimulant that triggers therapeutic release. PACTs may provide another solution to Doxil's and ADC's therapeutic release issues, while avoiding limitations of photothermal therapeutics and heat-dependent DDSs.[2, 14, 15] Herein, we assess the localized light-activated therapeutic release from red blood cell (RBC) carriers to support the continued development of PACTs and other photoactivated therapeutic DDSs.

We have successfully modified vitamin B12 (also known as cobalamin, Cbl) into a tunable PACT scaffold by shifting its inherent light-responsive properties (330 - 575 nm), which trigger photolysis of its axial cobalt bond, into the optical window of tissue (600 - 900 nm). Specifically, synthetically appended red and far-red fluorophores on the 5' hydroxyl of Cbl's ribose act as an antenna to shift the photoresponsive wavelengths of Cbl.[16] Many therapeutics have also been appended successfully via the photoresponsive axial cobalt bond.[17, 18] This study, specifically, focuses on development of the clinically-approved taxane docetaxel. Docetaxel is an antimitotic used in the treatment of a variety of solid tumors, including breast, gastric, prostate, and non-small cell lung cancers. However, taxanes produce a variety of short- and long-term adverse effects in more than 30% of patients.[19-21]

RBC carriers should limit the biodistribution and improve the circulation half-life of photoresponsive fluorophore-Cbl-Docetaxel, which further minimizes off-target toxicity and improves localized efficacy. The Cbl scaffolds are successfully loaded into RBCs by means of a dialysis loading procedure.[22-24] Dialysis-loaded RBCs have successfully been tested within the

clinic and demonstrated the ability to carry large therapeutic payloads and maintain biocompatibility up to ~25 days of circulation, making them flexible carriers for many indications.[24-27] Further, RBCs shelter the Cbl PACT as Cbl cannot escape the cell due to its inherent membrane impermeability. Thus, therapeutics covalently conjugated to Cbl are retained within the RBC until illumination in the optical window of tissue. Fluorophore-Cbl-Docetaxel RBCs provide a method of combining externally light-triggered therapy of AuroLase with the sheltering properties of ThermoDox ideally enhancing their beneficial properties that have achieved positive clinical results thus far.

2.2 Construction of Cobalamin-Docetaxel RBCs

A cyanine5 (Cy5) fluorophore antenna (responsive to 645 nm) and docetaxel (TAX) were appended to the Cbl derivative **1** to yield photoresponsive Cy5-Cbl-TAX (**2**) (**Figure 2.1**).[28] Briefly, the three-step synthesis requires condensation of N-Deboc TAX with the axial carboxylate of **1**, deprotection of the ribose Fmoc group, and condensation of the resulting deprotected amine with activated N-hydroxysuccinimide Cy5.[18] The inactive derivative Cy5-Cbl-H_2O (**3**), with no appended therapeutic, and non-photocleavable fluorescent analog Cbl≡Cy5 (**4**) were synthesized as in vitro and in vivo study controls (see section 2.7.1).[29, 30]

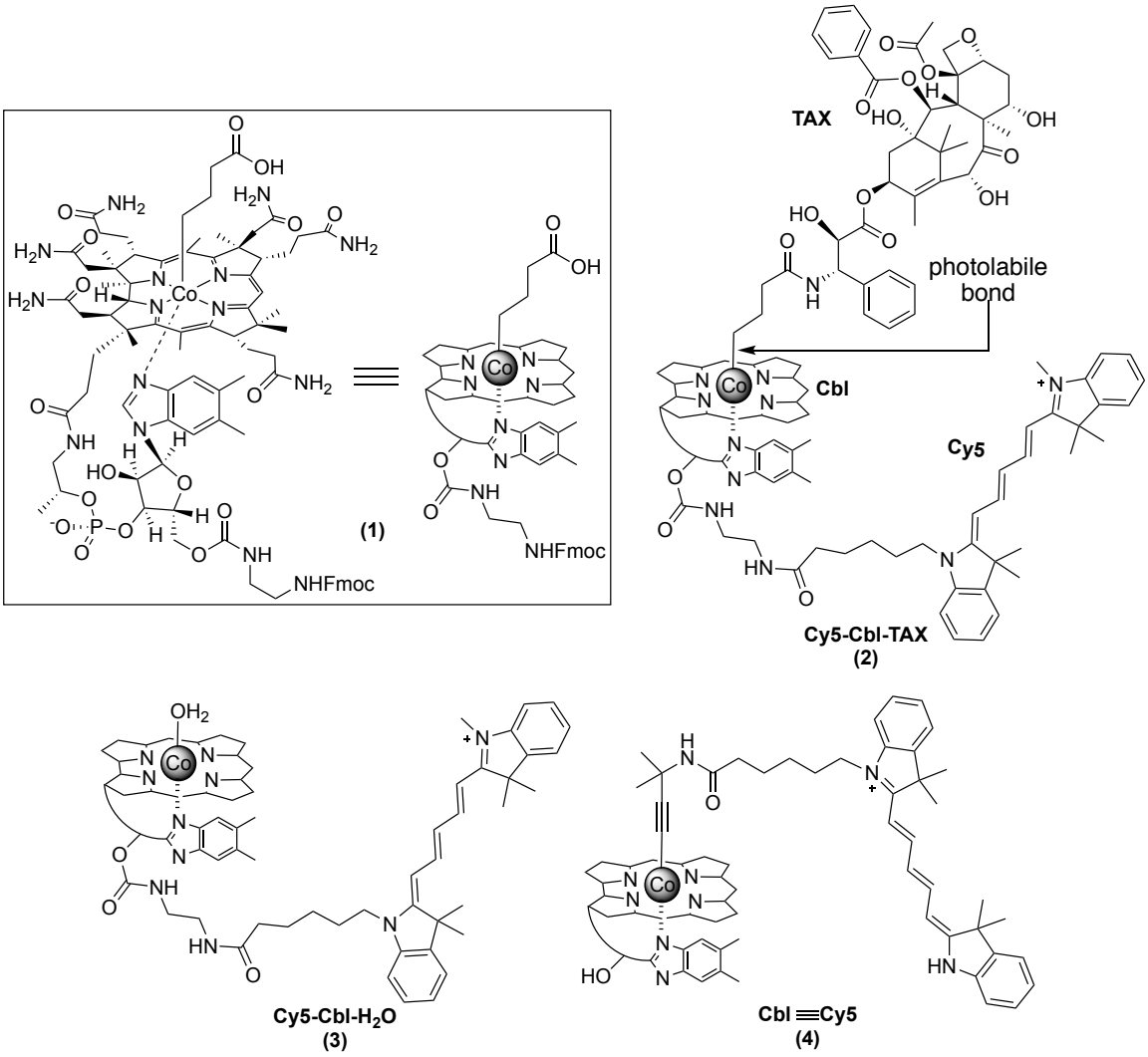

Figure 2.1 Structures of Cbl therapeutic and controls. Compound **1** (inset) shows the full Cbl structure modified with a carboxylate off the axial cobalt bond and Fmoc protection of the ethylamine linker off the ribose 5'-OH. The equivalent abbreviated structure is shown on the right. Compound **2** is the resulting PACT Cy5-Cbl-TAX synthesized from **1**. The photolabile axial bond is highlighted. The inactive derivative **3** is both a photoproduct of photolysis of **2** and acts as a non-therapeutic control. The non-photolytic analog **4** contains a Co≡C triple bond that is photostable and therefore allows Cy5 to be employed as a fluorescent tracker without inducing photolysis.

Therapeutic RBCs loaded with **2** or control RBCs loaded with **3** were prepared by hypotonic dialysis in PBS containing 6 x 10^{-3} M glucose, within which RBCs swell due to osmotic pressure and a pore(s) forms in the membrane. Cbl species can then freely diffuse into RBCs. After dialysis, the loaded RBCs are returned to an isotonic environment, which causes the pore(s) to reseal and traps the Cbl conjugates within. The hydrophobic drug can now only escape the RBCs when photolytic cleavage of the axial cobalt bond occurs upon excitation of the Cy5 antenna with 645 nm light (**Figure 2.2**).

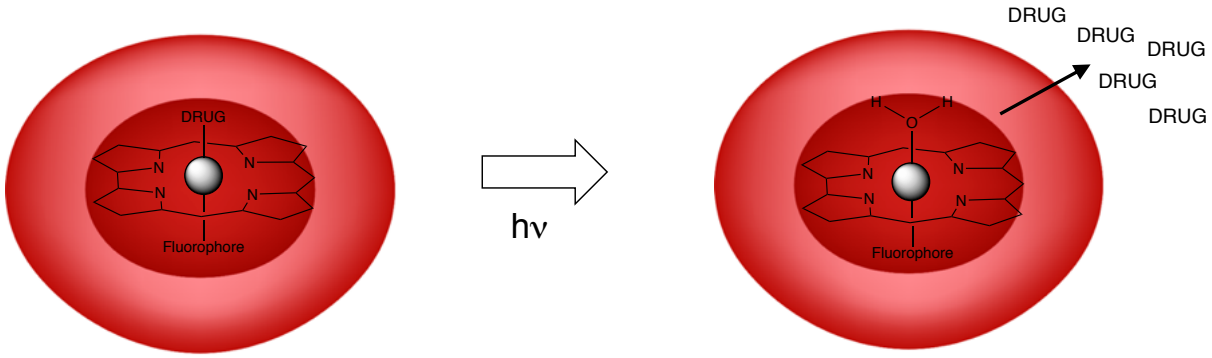

Figure 2.2 Chemotherapeutic release from Fluorophore-Cbl-Drug RBCs. Drug cannot escape from RBCs internally loaded with Cbl conjugates until illumination. Upon illumination, the photolabile axial bond cleaves releasing hydrophobic drug, which can permeate across the cell membrane and diffuse in the localized tissue.

2.3 Characterization of Cy5-Cbl-TAX Mouse Red Blood Cells *in vitro*

Widefield microscopy images of loaded mouse RBCs (mRBCs) indicate successful loading of Cy5-Cbl conjugates and conservation of the mRBC morphology as compared with native (isolated but unmodified) control mRBCs and vehicle-loaded mRBCs (mRBCs that undergo the loading process exposed to PBS rather than a Cbl species) (**Figure 2.3a**). Externally loaded 1,1-dioctadecyl-3,3,3,3-tetra-methylindodicarbocyanine (DiD) mRBCs verify Cy5 fluorescence, when appended to Cbl, is unaffected by the loading procedure and can be used for tracking loaded mRBCs. Further, confocal microscopy images taken through z-space can characterize the unique biconcave edges and spherical center planes of RBCs and identify distribution (external or internal) of fluorescent species. Confocal images of **2** mRBCs confirm internal loading within mRBCs as **2** distributes throughout the risen biconcave edges of the edge planes and throughout the spherical center plane (**Figure 2.3b**). Efficiency of loading was assessed by cell recovery and by hemocytometer counting of loaded mRBCs followed by ethanol extraction to determine the encapsulated concentration of **2** and **3**. 53 ± 6% of **2** mRBCs are recovered from the loading process and contain 39 ± 4 μM **2**, while 63 ± 4% of **3** mRBCs are recovered and contain 32 ± 2 μM **3** (**Figure 2.4**) (see section 2.7.2).

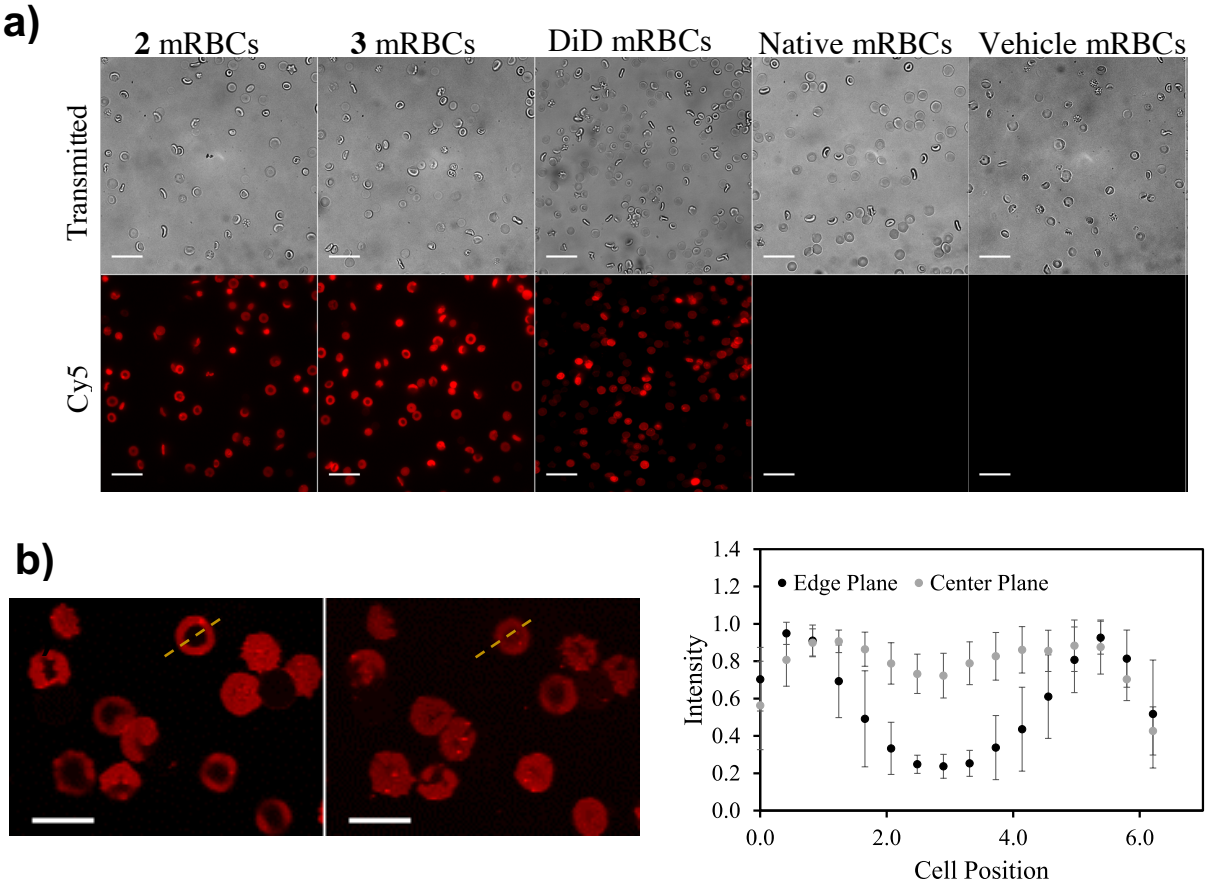

Figure 2.3 Microscopy characterization of mRBCs. a) Transmitted (top) and fluorescent (bottom) widefield images of internally loaded Cy5-Cbl-TAX (**2**) and Cy5-Cbl-H_2O (**3**) mRBCs, externally loaded (DiD), native mRBCs, and vehicle loaded mRBCs. Scale bar = 20 μm. **b)** Two confocal images (left) in different z-planes of **2** mRBCs demonstrate different fluorescent distributions of internally loaded **2** due to the mRBC biconcave shape. Quantitative analysis of 15 representative cells (right) across straight-line regions as exemplified in sample mRBC images of the edge (left image) and center plane (right image) confirm the biconcave distribution of **2** fluorescence indicating internal loading. Scale bar = 6 μm.

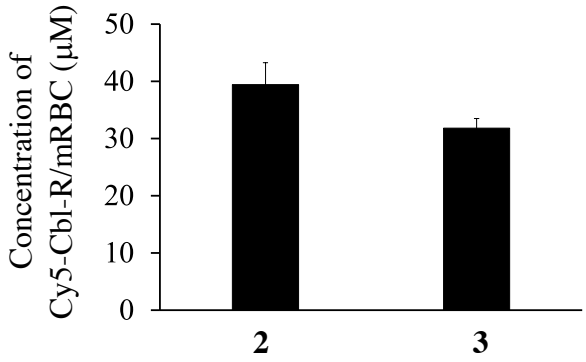

Figure 2.4 Concentration of 2 and 3 loaded into mRBCs. Concentration per mRBC was determined by hemocytometry counting of loaded mRBCs followed by ethanol extraction of Cy5-Cbl conjugates and calculation of concentration with UV-Visible spectroscopy absorbance of Cy5 at 645 nm. **2** mRBCs contain 39 ± 4 μM **2**, while **3** mRBCs contain 32 ± 2 μM **3**.

mRBCs loaded with **2** and **3** were further characterized with flow cytometry. Resulting overlaid histograms of in-focus singlets display the uniform loading of internal **2** and **3** mRBCs (**Figure 2.5a**). A linear region of interest was analyzed at an intensity of 1 x 10^4 fluorescent units to quantify the percentage of cells successfully loaded. 99.4% and 99.7% of **2** and **3** mRBCs are loaded respectively. Notably, only 49.3% of DiD mRBCs fall within the loaded gate, which signifies a more heterogenous external loading. Analysis of cell morphology using flow cytometry side scattering (an indicator of granularity of the cell interior) versus fluorescent intensity demonstrates DiD mRBCs have comparable SSC variability to native mRBCs (**Figure 2.5b**).[31] Conversely, internally loaded **2**, **3**, and vehicle mRBCs have comparable SSC variability, but increased heterogeneity when compared to the DiD and native controls. This heterogeneity suggests a less consistent internal composition which could result from the change in the internal environment of RBCs during the hypotonic dialysis process. Since 90% of an RBC's internal composition is hemoglobin and there is an observed loss of this protein during dialysis, variable loss of hemoglobin from individual cells may result in the observed SSC heterogeneity.[32, 33] Changes of the membrane shape upon pore resealing may also factor into this observed heterogeneity.[34] The flow cytometry findings further support successful internal loading of Cbl species into RBCs and validate a uniform loading of **2** and **3** into mRBCs, although the loading process may result in heterogeneous changes in the internal composition of native RBC species.

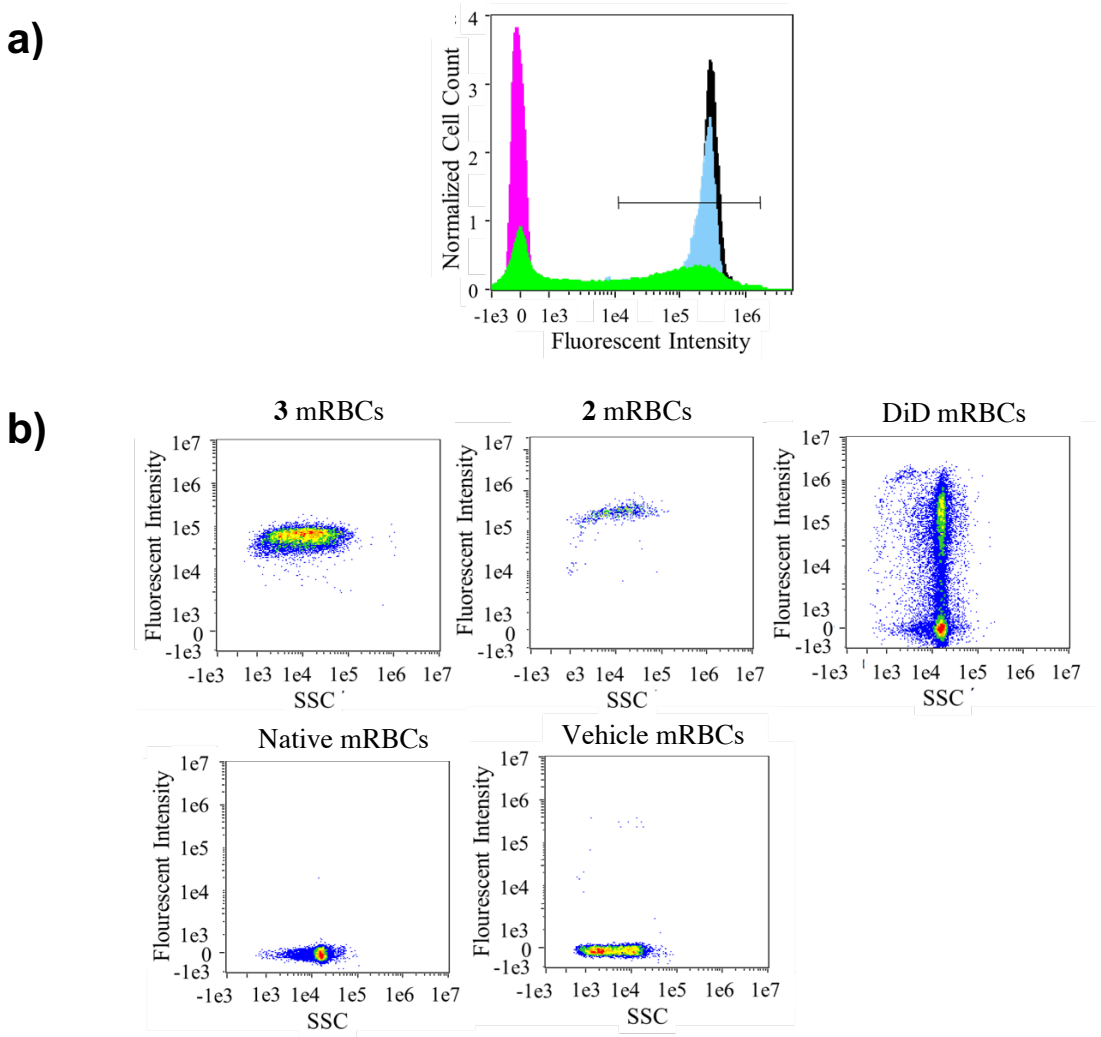

Figure 2.5 Flow cytometry characterization of mRBCs. a) Overlaid fluorescent histograms of native (magenta), externally loaded DiD (green), and internally loaded **2** (black) and **3** (blue) mRBCs. The linear region of interest beginning at 1 x 10^4 fluorescent intensity signifies loaded RBCs. 99.4% and 99.7% of **2** and **3** mRBCs are loaded respectively. Only 49.3% of DiD mRBCs fall within the loaded gate. **b)** Side scatter (SSC) versus fluorescent intensity dot plots of internally loaded **2**, **3**, and vehicle mRBCs compared to control native and externally loaded DiD mRBCs. Internally loaded mRBCs display higher variability in SSC values, while DiD mRBCs are comparable to native mRBCs in SSC complexity.

2.3.1 *In vitro* Assessment of Cbl-Tax RBC Stability and Photolysis

Due to the noted internal heterogeneity, the stability of loaded mRBCs was assessed to ensure mRBCs retain fluorescent conjugates during *in vivo* studies. Loaded mRBCs shelter Cbl species for at least 5 h *in vitro*, the length of time required for *in vivo* studies. Over 24 h at 4 °C *in vitro*, loaded mRBCs containing **2** are less stable than control native mRBCs as both visually assessed with widefield microscopy and quantified by measuring the amount of hemoglobin detected in the supernatant (indicative of hemolysis) and the amount of mRBC pellet remaining (**Figure 2.6a**,**c**). This inherent *in vitro* instability is enhanced in mRBCs as compared to human RBCs (hRBCs) as previously reported and experimentally validated (**Figure 2.6b**,**c**).[35, 36] The fragility of loaded mRBCs supports immediate injection upon preparation for *in vivo* studies. Conversely, both native and loaded hRBCs demonstrate significant *in vitro* and *in vivo* stability as compared to mRBCs, even after undergoing the internal loading process, which has also been exhibited in clinical trials of internally loaded hRBCs.[25, 26]

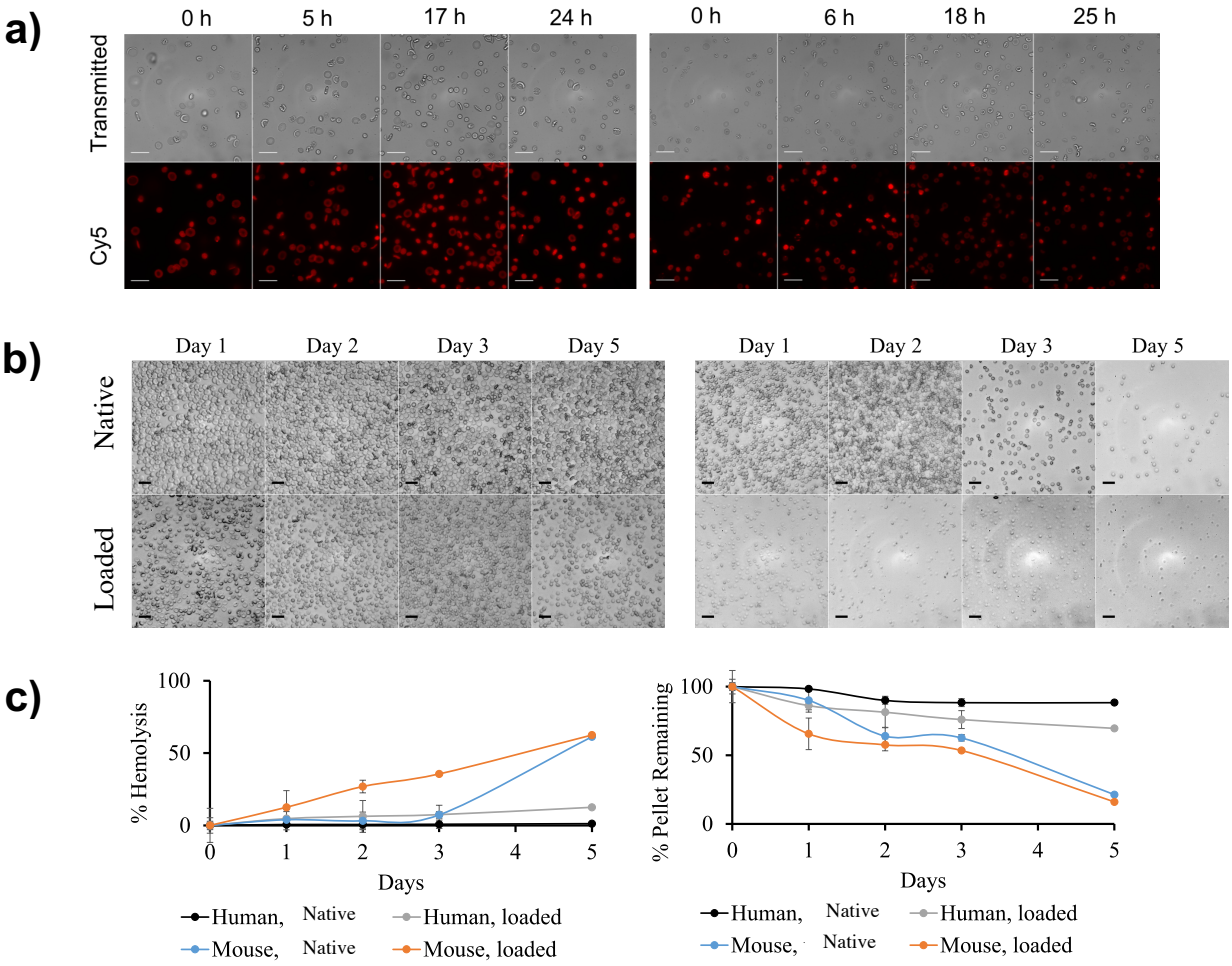

Figure 2.6 Stability assessments of internally loaded RBCs. a) Widefield analysis of **2** loaded hRBCs (left) and mRBCs (right) stability of loaded RBCs assessed by transmitted (top) and Cy5 channels (bottom) after incubating for 0, 6, 18, and 25 h in L-15 at 4 °C. Scale bar represents 20 μm. **b)** Widefield analysis of **2** loaded and native hRBCs (left) and mRBCs (right) after incubating for 1, 2, 3, and 5 days in DMEM media with 1X GlutaMAX and 1% FBS at 4 °C. Scale bar represents 20 μm. **c)** Quantified % hemolysis over time (left) of RBCs represented in b) measured by isolating hemoglobin from the supernatant and comparing to a 100% hemolysis control. Estimated quantity of 100 μL mRBC pellet remaining over time (right) validates enhanced hemolysis of mRBCs as compared to hRBCs.

Upon successful generation and characterization of Cbl loaded mRBCs in preparation for *in vivo* studies, it was important to ensure photolysis and escape of TAX from loaded RBCs. Photolysis of **2**, as well as **2** contained within hRBCs, was measured. After 30 min of 646 nm 800 mJ irradiation, free **2** in a solution of PBS is fully photolyzed. This result confirms that Cy5 serves as an antenna and extends the natural photoresponsivity of Cbl into the optical window of tissue (see section 2.7.3). Similarly, photolysis of hRBCs containing **2** results in release of 98% of loaded TAX into the supernatant (**Figure 2.7**). In addition, no detectable levels of TAX are found in the supernatant of hRBC pellets incubated in the dark (data not shown). Given the noted instability of mRBCs, photolysis of **2** from within mRBCs and illumination of inactive control **3** within mRBCs was validated to have no effect on mRBC stability. Minimal Cy5 fluorescence is observed in the supernatant of dark and illuminated mRBCs loaded with **2** or **3**, confirming intracellular retention of the non-cell permeable Cy5-Cbl (**Figure 2.8a**). Further, less than 25% of hemoglobin is released from both groups regardless of incubation in the light or dark (**Figure 2.8b**). Thus, although mRBCs are inherently less stable, illumination at 660 nm for 10 min, as well as activation of **2** or **3**, and photocleavage of TAX from **2** has a negligible effect on mRBC hemolysis as confirmed by quantification of both Cbl and hemoglobin release.

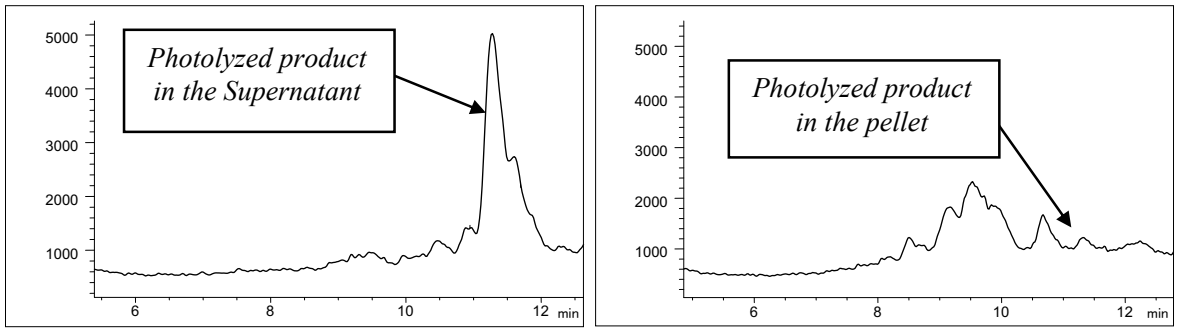

Figure 2.7 Photolysis of Cy5-CbI-TAX loaded hRBCs. hRBCs in human platelet rich plasma were photolyzed at 646 ± 10 nm using an Oriel Xe flash lamp (800 mJ, 62 Hz) and appropriate bandpass filters. Analysis by LC-MS revealed that the overwhelming majority (98 ± 1%) of the photolyzed TAX product was present in the supernatant (left) and not the pellet (right).

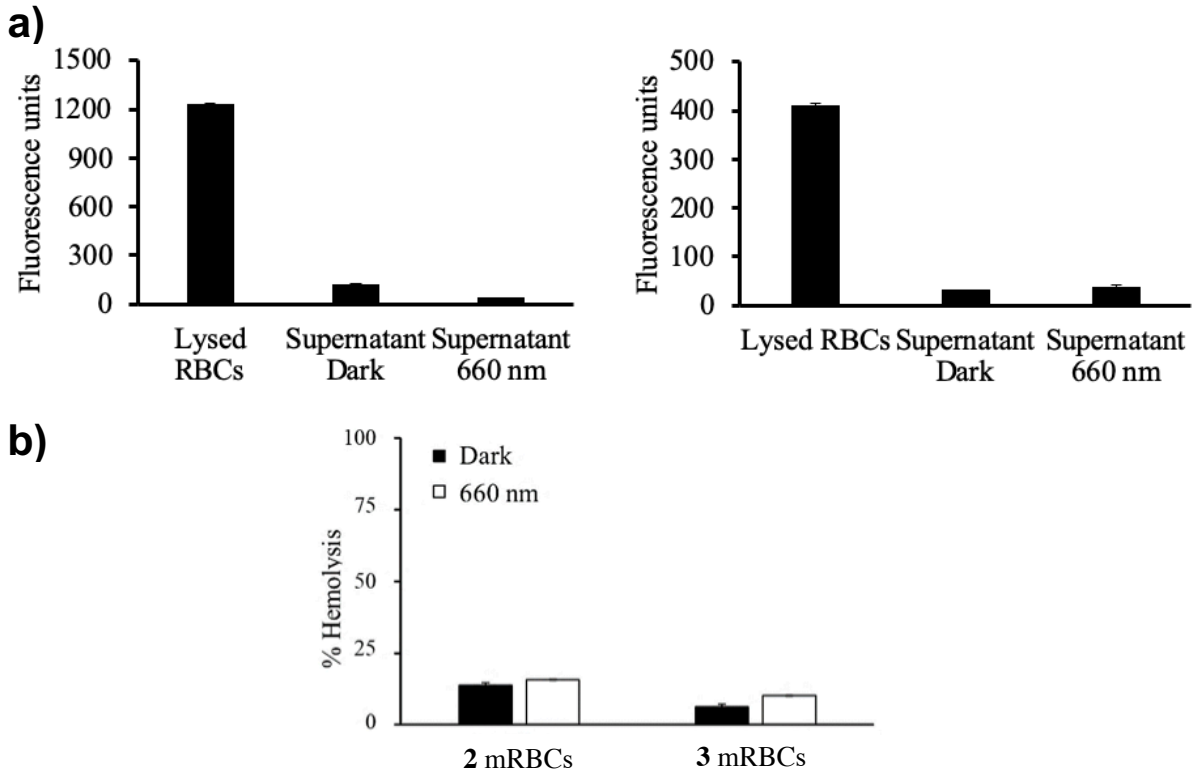

Figure 2.8 Stability of photolyzed mRBCs. a) Fluorescence from Cy5 conjugated to the Cbl species was measured from **2** mRBCs (left) and **3** mRBCs (right). Supernatants from treatment with 660 nm LED illumination for 10 min or incubated mRBCs in the dark is compared to control lysed mRBCs. **b)** % hemolysis as quantified by absorbance of hemoglobin was measured for all treatment groups of **2** and **3** containing mRBCs. Less than 25% hemoglobin is released under all conditions.

2.3.2 Cellular Assays of Cy5-Cbl-TAX Efficacy

To validate the pharmacological activity of TAX is preserved upon photoactivation and release from Cy5-Cbl hRBCs, photoreleased TAX cytotoxicity and mechanism of action were tested in HeLa cells. In general, taxanes, including docetaxel, are cytotoxic by suppressing microtubule dynamics and blocking mitosis in cancer cells.[21] TAX released from illuminated hRBCs containing **2** also affects microtubule dynamics of HeLa cells by polymerizing microtubules similarly to free TAX, while **2** hRBCs incubated in the dark and no treatment controls have a minimal effect on microtubule polymerization (**Figure 2.9a**). Similarly, illuminated **2** hRBCs affect HeLa cell viability equivalently to 1 μM TAX (**Figure 2.9b**). Thus, appending TAX to the photoactivable Cy5-Cbl scaffold does not eliminate TAX's inherent pharmacological impacts. In general, *in vitro* tests confirm Cy5-Cbl-TAX RBC stability, successful photolytic release of TAX, and preserved therapeutic effect of TAX in preparation for *in vivo* tests of localized TAX release and effect.

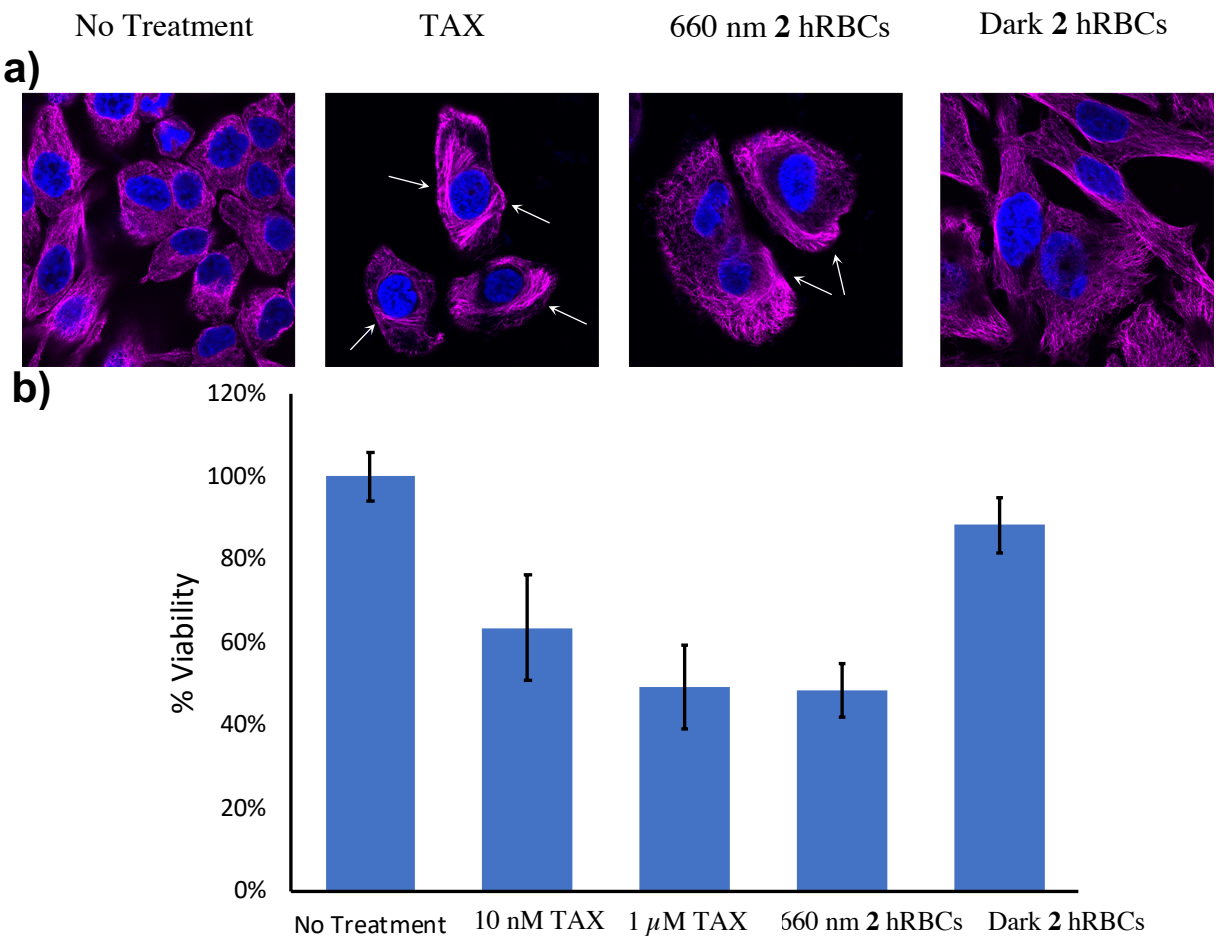

Figure 2.9 TAX photoreleased from Cy5-Cbl hRBCs has a similar effect on HeLa cells to conventional TAX. a) HeLa cells exposed to media (no treatment), docetaxel (TAX), and hRBCs containing **2** with or without 660-nm illumination for 30 min were fixed and stained for α-Tubulin (magenta) and nuclei with Hoechst 33342 (blue). TAX and illuminated mRBCs containing **2** polymerize microtubules (arrows). **b)** Viability of HeLa cells following treatment with TAX (10 nM or 1 μM), hRBCs loaded with **2** exposed to 660 nm LED light for 30 min or kept in the dark. Treatment with 1 μM TAX or 660 nm-exposed **2** hRBCs results in the same loss in cell viability.

2.4 Biodistribution of Cy5-Cbl-TAX mRBCs *in vivo*

Biodistribution of Cy5-Cbl-TAX mRBCs was assessed by intravital imaging vasculature of Cbl-treated healthy FVB mouse ears (**Figure 2.10a**). Non-photoresponsive control Cbl≡Cy5 served to control for effects of photocleavage of the axial cobalt bond, while DiD mRBCs served as a circulatory control as previously reported.[37] Mice were intravenously injected with the modified mRBC species and Cy5 was subsequently imaged in the lasered ear for 90 min (633 nm, 30% power, 0.5 mm diameter imaged every 5 s). The mouse's other ear was not exposed to laser illumination and, in general, environmental light was kept as dim as possible during injection and imaging. Freely injected **4** rapidly diffuses into surrounding tissue within 5 min, while externally loaded DiD and internally loaded **4** mRBCs are retained within the vasculature throughout the experimental time course (90 min) (**Figure 2.10b**). Quantification of fluorescence over 90 min from the treatment groups reveals fluorescent signal from freely injected **4** is no longer detectable after 20 min (**Figure 2.10c**). Conversely, DiD mRBCs and **4** mRBCs maintain 69 ± 2% and 53 ± 5% of their fluorescence respectively. Although, internally loaded **4** mRBCs are initially rapidly cleared, potentially due to incurred damage from the dialysis procedure, they retain comparable circulation fluorescence to DiD mRBCs after 40 min throughout the remaining imaging period. These preliminary biodistribution results underscore the benefit RBCs provide to shelter and modify the pharmacokinetics of Cbl PACTs.

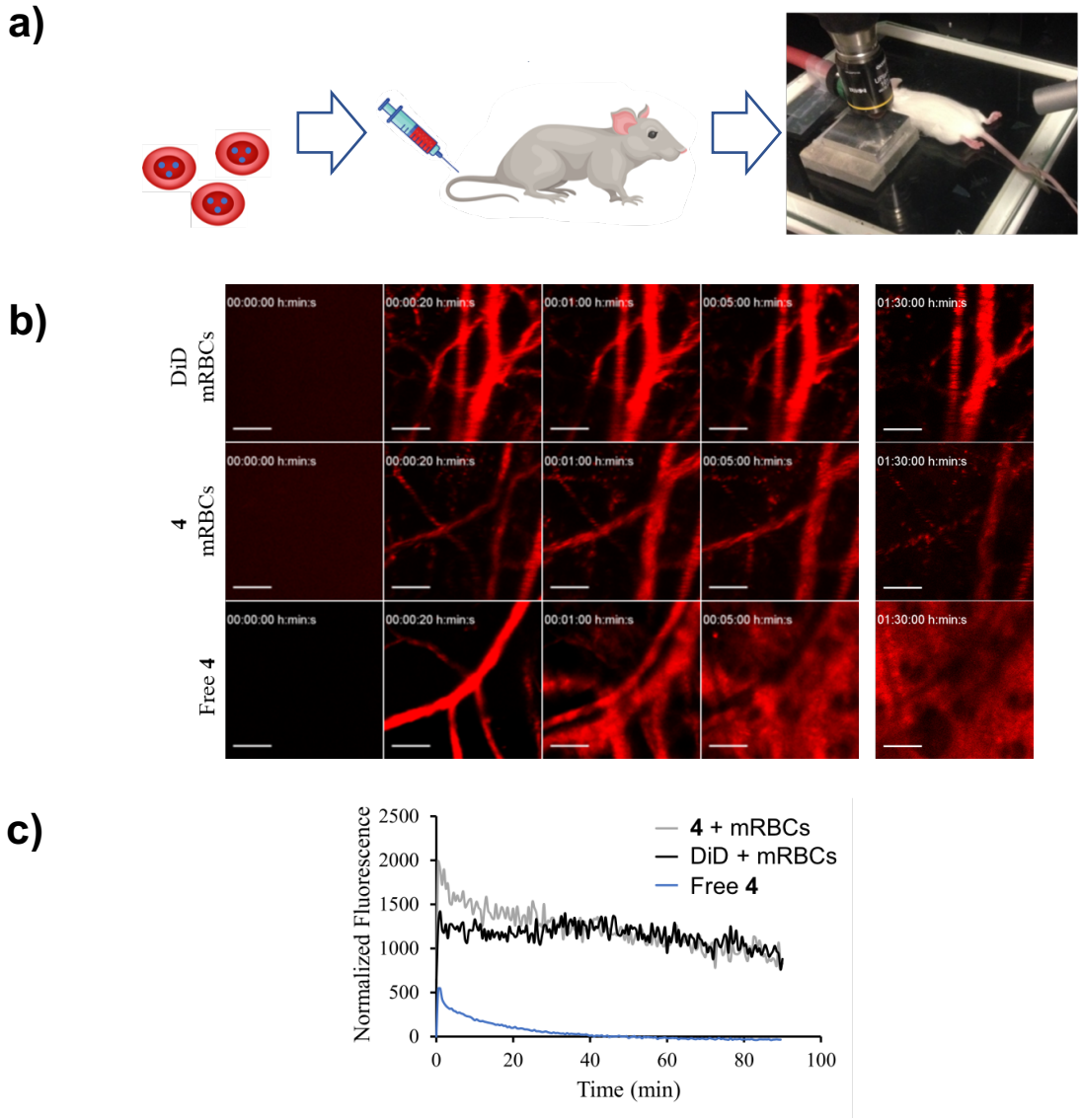

Figure 2.10 Biodistribution of Cy5-CbI-TAX mRBCs. a) Intravital imaging of free **4**, internally loaded mRBCs containing **4**, or externally loaded DiD mRBCs was performed. Treatments were intravenously injected into anesthetized mice followed by intravital imaging at 10X using a 633 nm laser. **b)** Intravital images for the first 0, 0.2, 1, 5 min and an offset image at 90 min of treatments. Scale bar represents 100 μm. **c)** Quantification of the fluorescence intensity of treatments for 90 min. The initial DiD fluorescence remains in circulation with a slope of –6, while intensity of **4** mRBCs drops with an initial slope of –21.

2.5 Localized *in vivo* Effect of Cy5-Cbl-TAX mRBCs

Having validated that 1) TAX is successfully photolyzed from RBCs *in vitro*, 2) the pharmacological effect of photocleaved TAX is preserved *in vitro*, and 3) the biodistribution of **4** mRBCs is predominantly constrained to the vasculature for 90 min, we prepared for *in vivo* evaluation of localized TAX release. Since TAX is a potent cytotoxic agent, it produces adverse cytotoxic effects on endothelial cells that line blood vessels, even at subclinical concentrations.[38-41] After intravenous administration, taxanes commonly associate with serum proteins in circulation due to their extremely lipophilicity, but do not interact with RBCs.[42, 43] Since RBCs do not naturally support free taxane circulation, sheltering taxanes within RBCs could help prevent inadvertent cytotoxicity to the endothelial wall. To test for a localized effect of TAX after photoactivation, we inverted this idea by releasing TAX to purposely identify localized cytotoxic damage to the endothelial wall. 100 µL of mRBCs (~8 x 10^7mRBCs) loaded with **2** were injected intravenously into mice. TAX was then photoactivated with the intravital imaging 633 nm laser, which both activated and was used to visualize the photoresponsive Cy5-Cbl species. After 90 min, significant extravasation of Cy5 fluorescence is observed signifying release of the Cy5-Cbl scaffold (**Figure 2.11a**). Since extravasation was not previously observed with DiD mRBCs or **4** mRBCs this property is potentially unique to the TAX therapeutic. While TAX release did not produce significant hemolysis *in vitro* as previously described, physiological cytotoxic damage to the endothelial wall by TAX may lead to a coagulation cascade that causes the more fragile internally loaded mRBCs to rupture as the vessel congests and RBCs, among other circulating species, pack.[44] Such events are observed during microangiopathic hemolytic anemias and as a result of venoms and drugs, including taxol.[45-47]

To confirm the suspicion of a cardiovascular damage and clotting, mice were euthanized, and ear tissue collected and fixed. Hematoxylin and eosin (H&E) staining of illuminated ears of mice treated with **2** mRBCs revealed congestion of the vasculature consistent with TAX-driven

endothelial damage (**Figure 2.11b**). The non-illuminated (dark) control ear from the same mouse shows spacing between the circulating RBCs themselves and between the RBCs and the vessel wall indicative of normal vascular circulation (**Figure 2.11c**). Similar spacing to the dark control ear is observed in the stained ears of untreated mice, while extensive cytotoxic effects are achieved by topically applying free TAX (20 μM) to a mouse ear (**Figure 2.12a,b**). To address concerns of photoactivation contributing to cardiovascular damage, **3** loaded mRBCs were also tested. Cy5-Cbl from **3** mRBCs does not significantly extravasate during activation and imaging as opposed to **2** mRBCs. However, a slight disturbance in the microvasculature is noted potentially due to generation of reactive oxygen species (ROS) during Cy5 photoactivation (**Figure 2.12c**).[48] Correspondingly, the illuminated ear does contain less space between the endothelium and RBCs, however the degree of distension of the endothelial wall is more limited than the vasculature of illuminated **2** mRBCs (**Figure 2.12d**). Thus, TAX release does create a potent localized effect of cytotoxic endothelial damage as compared to the dark ear, untreated mouse ears, and **3** mRBCs. The extent of this localization is further quantified as TAX carried within transfused mRBCs that produce this effect sums up to 1 μg, while the maximum tolerated dose of TAX is 15 mg/kg in mice, and typical doses in mouse treatments are between 5 to 10 mg/kg (75 to 250 μg) injected intravenously.[49] Therefore, the adverse cardiovascular effect is achieved at treatments much lower than the maximum tolerated dose of TAX due to the localized release at the site of the ear.

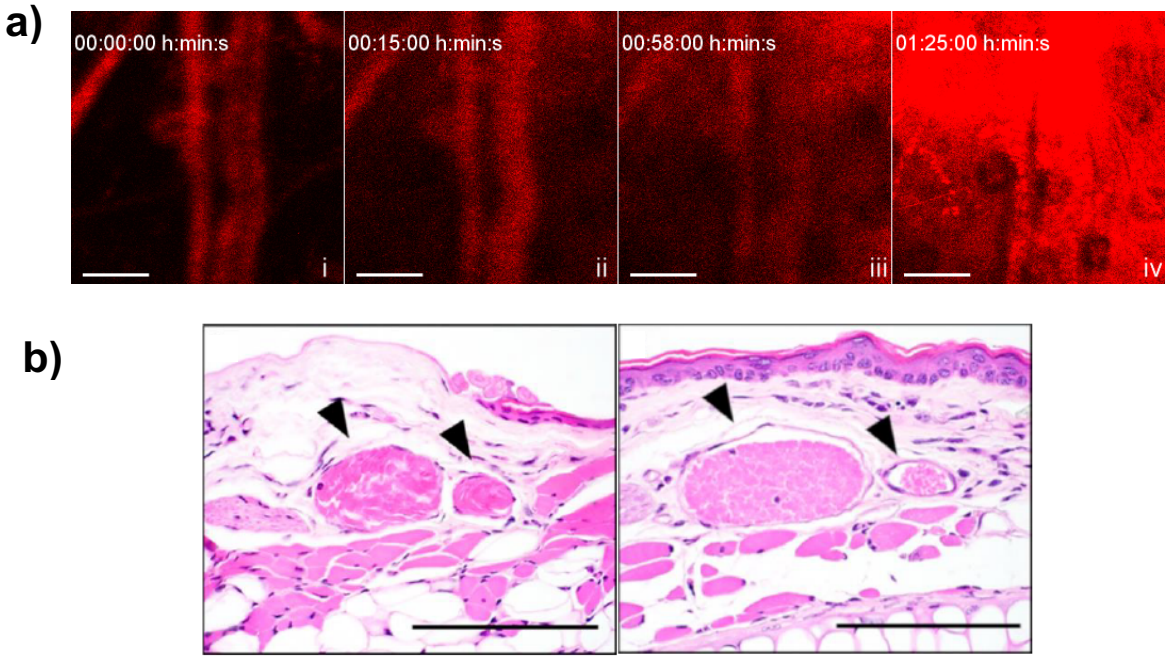

Figure 2.11 Localized TAX damage to the endothelial wall upon photoactivation. a) Intravital imaging of photoactivated **2** mRBCs led to extravasation of the Cy5 fluorescence over 90 min in healthy mouse ears. Representative images include 0, 15, 58, and 85 min with a scale bar of 100 μm. **b)** H&E staining of the photoactivated ear reveals a cardiovascular event due to minimal spacing between RBCs and distension of the endothelial wall (arrows, left). Control non-lasered ear has natural, generous spacing between RBCs and the endothelial wall (arrows, right). Scale bar represents 100 μm.

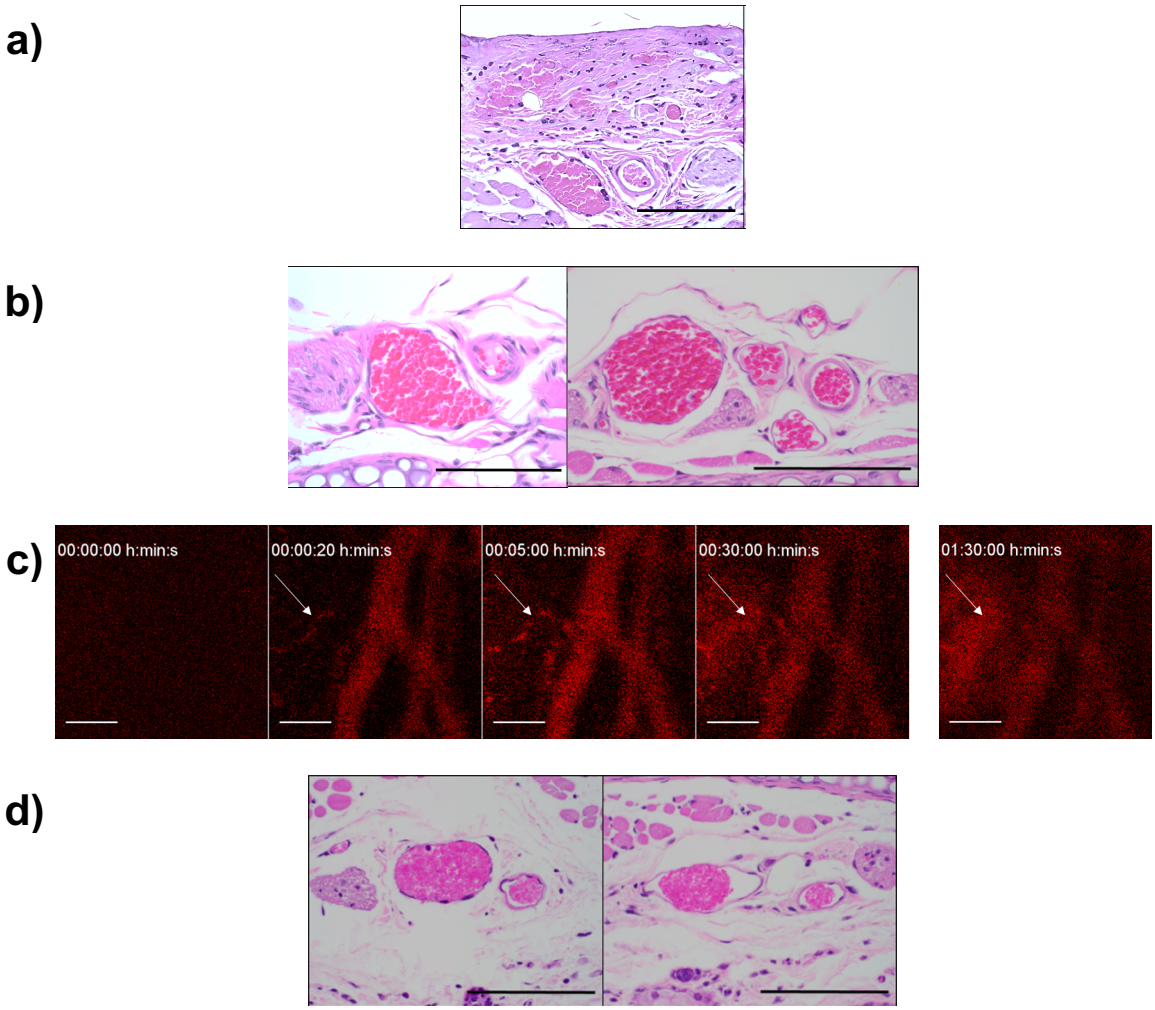

Figure 2.12 Additional controls of localized TAX release and resulting damage. Scale bar of all images represent 100 μm. **a)** H&E staining of topically applied free TAX (20 μM) to healthy mouse ears validates the extensive cytotoxic damage of TAX. **b)** Untreated left and right mouse ears display similar spacing between RBCs and the endothelial wall as the dark ear of the **2** treated mouse. **c)** Intravital imaging over 90 min (including 0, 0.2, 5, 30, and 90 min) of photoactivated release from **3** mRBCs *in vivo*. Arrows highlight the fluorescence leak potentially due to ROS-driven extravasation. **d)** H&E staining of **3** mRBC treated mouse including photoactivated ear (left) and dark ear (right). Photoactivated ear demonstrates a degree of distension, but not to the extent of **3** mRBC treated ears.

The localized effect of TAX was also analyzed in the tumor vasculature of an SVR angiosarcoma in immunodeficient Nu/Nu mice.[50] Changes in the microvasculature surrounding the tumor were imaged using acoustic angiography with microbubble contrast agents (**Figure 2.13a**).[51, 52] TAX was photoreleased from **2** mRBCs by illumination with a 100 mW, 655 nm laser for 5 min. Imaging with acoustic angiography was done before injection for baseline, and at 0, 25, and 45 min post-injection. Images of tumor vasculature after treating with **2** mRBC with and without 655 nm illumination, **3** mRBC with 655 nm illumination, and vehicle mRBCs with 655 nm illumination were collected (**Figure 2.13b,c**). The intensity of the images corresponds to the localization of the microbubble contrast agents. Qualitatively, treatment with illuminated **3** mRBCs caused extravasation of the microbubble contrast agent into the tumor (**Figure 2.13b**). Images were quantified by the ratio of the summated microbubble coverage within the tumor to the summated total 3D tumor volume (**Figure 2.14**). Quantification validated initial qualitative observations, finding near doubling of the area microbubbles covered after treatment with illuminated **3** mRBCs. By contrast, control dark **2** mRBCs, illuminated **3** mRBCs, and illuminated vehicle-loaded mRBCs do not exhibit a significant persistent enhancement of microbubble coverage over time. These findings validate previous intravital imaging results, as TAX damage to the vessel endothelium results in extravasation of microbubbles into the tumor. Further, since controls do not exhibit comparable extravasation, both mRBCs containing **3** and illumination are required to achieve the localized damage and resulting microbubble extravasation.

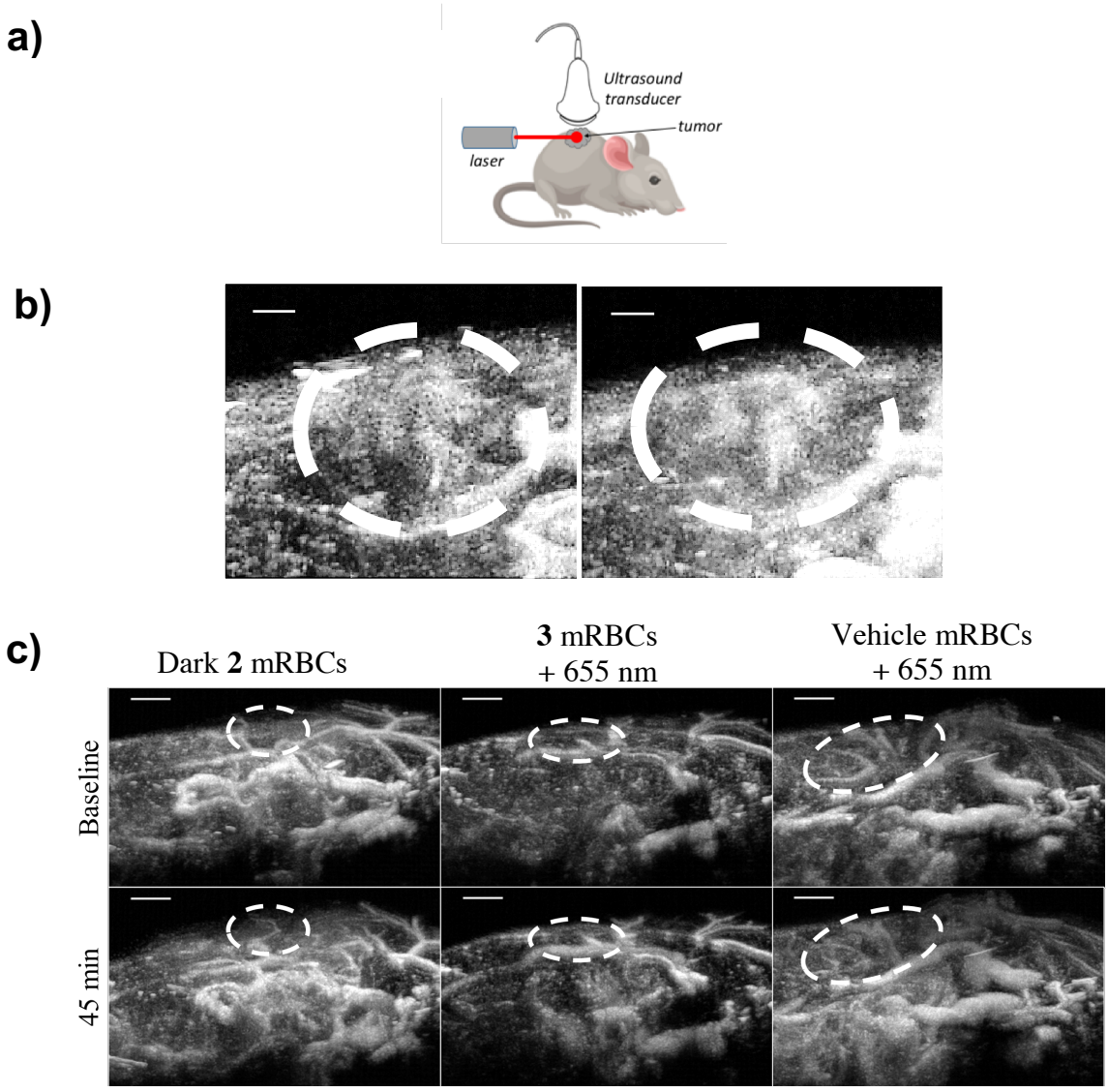

Figure 2.13 Localized TAX effect in SVR-tumor-bearing, female Nu/Nu mice. a) Ultrasound acoustic angiography imaging setup. Laser illumination (100 mW, 655 nm) for 5 min at the tumor site ensured localized stimulation of treatment mRBCs. Scale bar represents 1 mm. **b)** Ultrasound images of illuminated (655 nm, 100 mW, 5 min) **2** mRBCs within the tumor shows a qualitative increase in microbubble coverage from baseline (left) to 45 min (right). **c)** Ultrasound images of control dark **2** mRBCs (n = 7), illuminated **3** mRBCs (n = 4), and vehicle mRBCs (n = 4) at baseline (top) and after 45 min (bottom). Scale bar represents 2.5 mm.

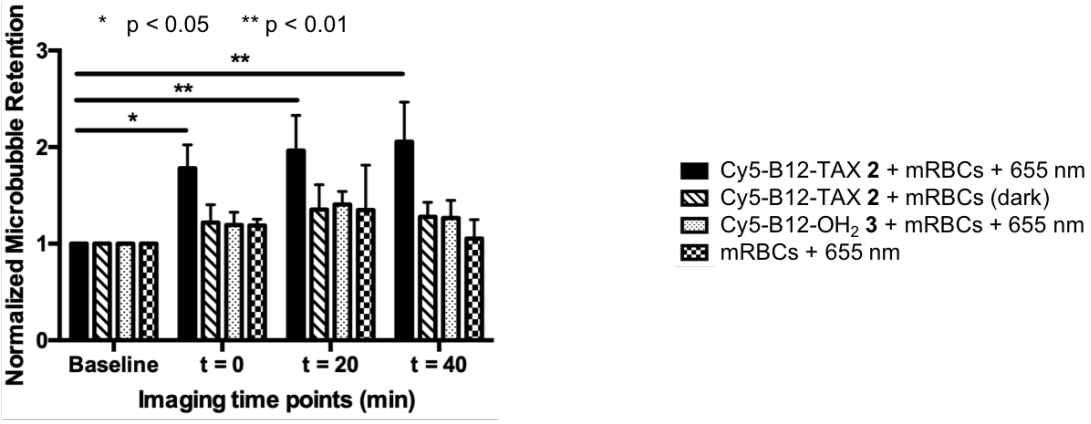

Figure 2.14 Quantification of localized TAX release as measured by microbubble coverage. The normalized microbubble retention was calculated as a ratio of summative microbubble coverage in the tumor to the summative 3D tumor size. These calculated values over time were then normalized to the baseline. Microbubble retention is significantly enhanced and persists over time in illuminated **2** mRBCs as compared to the controls: dark **2** mRBCs, illuminated **3** mRBCs, and illuminated vehicle-loaded mRBCs.

2.6 Conclusion

Although many taxane carrier systems are under development and incorporate RBC membranes commonly for improved biocompatibility and circulation (e.g. nanoparticles coated with RBC membranes), no localized RBC delivery system of taxanes yet exist.[53-58] The closest example, is paclitaxel loaded into RBCs, however no therapeutic release trigger is available in this system.[59] Thus, we have generated the first taxane PACT delivery system which employs a photoresponsive Cbl scaffold and RBC carriers. The RBC carriers preserve the pharmacologic effects of the TAX chemotherapeutic, carry high quantities of drug (>30 μM/ mRBC), improve biodistribution of Cbl, and shelter TAX until photoactivation. Further, we have successfully demonstrated the localized photoactivation, release, and expected pharmacological effect of TAX in response to long-wavelength illumination in two *in vivo* mouse models by two unique imaging methodologies.

RBC-based PACTs offer a biocompatible means of sheltering and localizing high quantities of therapeutic delivery to diminish off-target toxicity effects of potent chemotherapeutics. Stimulation with an external light device and response to wavelengths within the optimal window of tissue provides both spatial and temporal control over drug release at greater *in vivo* tissue depths. The inherent fluorescent properties of Cy5-Cbl PACTs also allow for imaging of distribution supporting the potential of theranostic applications. This initial validation of Cy5-Cbl-TAX RBCs further supports the benefits and clinical potential of both PACTs and RBC carriers.

2.7 Supporting Information, Figures, and Methods

Materials

All chemical reagents were purchased from Sigma-Aldrich or Thermo Fisher Scientific and were used as received. Human RBCs were purchased from ZenBio. Mice were purchased from Jackson Laboratories.

2.7.1 Synthesis of Cbl Conjugates

Synthesis of Cy5-Cbl-TAX (**Scheme 2-1**)

Precursors N-Deboc docetaxel and FmocAM2-Cbl-AC4 were synthesized according to the previously procedures reported.[18, 60] To prepare conjugate Cy5-Cbl-TAX, FmocAM2-Cbl-AC4 (100 mg, 58 μmol), 1-[bis(dimethylamino)methylene]-1H-1,2,3-triazolo[4,5-b]pyridinium 3-oxid hexafluorophosphate (HATU) (22 mg, 55 μmol) and N,N-*diisopropylethylamine (*DIPEA) (40 μL, 232 μmol) were reacted in 4 mL anhydrous dimethylformamide (DMF) for 2 h at room temperature in the dark. DMF (2 mL) containing N-Deboc TAX (41 mg, 58 μmol) was added and the reaction was incubated at room temperature for another 5 h. To remove the Fmoc protecting group, piperidine (286 μL, 290 μmol) was added into the reaction mixture and mixed at room temperature for additional 30 min. The reaction mixture was precipitated with anhydrous ethyl ether (6 x 40 mL) to remove piperidine. The crude sample was collected via centrifugation, mixed with Cy5-NHS ester (30 mg, 52 μmol) and DIPEA (40 μL, 232 μmol) in DMF (2 mL) and allowed to react overnight in the dark. The reaction mixture was precipitated by diethyl ether (3 x 40 mL), filtered and dried under vacuum for 2 h. The product was purified via reverse phase chromatography (30 g, RP-C18, Biotage) using a binary solvent system (A: water with 0.1% v/v TFA, B: MeOH with 0.1% v/v TFA) with a gradient change from 50% B to 70% B over 12 column volumes (Figure **2.15**). Lyophilization yielded the product as a blue solid (60 mg, 41%). ^{1}H NMR (400 MHz, DMSO-d6, δ): 8.33 (t, J = 13.1 Hz, 2H), 8.17 (d, J = 8.7 Hz, 1H), 8.00 – 7.80 (m, 3H), 7.77 – 7.58 (m, 7H),

7.57 – 7.06 (m, 17H), 7.05 – 6.76 (m, 5H), 6.71 – 6.45 (m, 3H), 6.32 – 6.23 (m, 4H), 5.80 (t, J = 8.9 Hz, 1H), 5.72 – 3.81 (m, 34H), 3.74 – 3.46 (m, 6H), 3.45 – 2.57 (m, 9 H), 2.40 – 1.96 (m, 28H), 1.96 – 1.44 (m, 24H), 1.44 – 0.75 (m, 29H), 0.55 (br.s, 2H), 0.32 (br.s, 2H), 0.04 (br.s, 2H), -0.27 (br.s, 2H); HRMS (ESI) m/z: $[M+H]^{2+}$ calculated for C139H181N18O29PCo, 1328.6194; found 1328.5982.

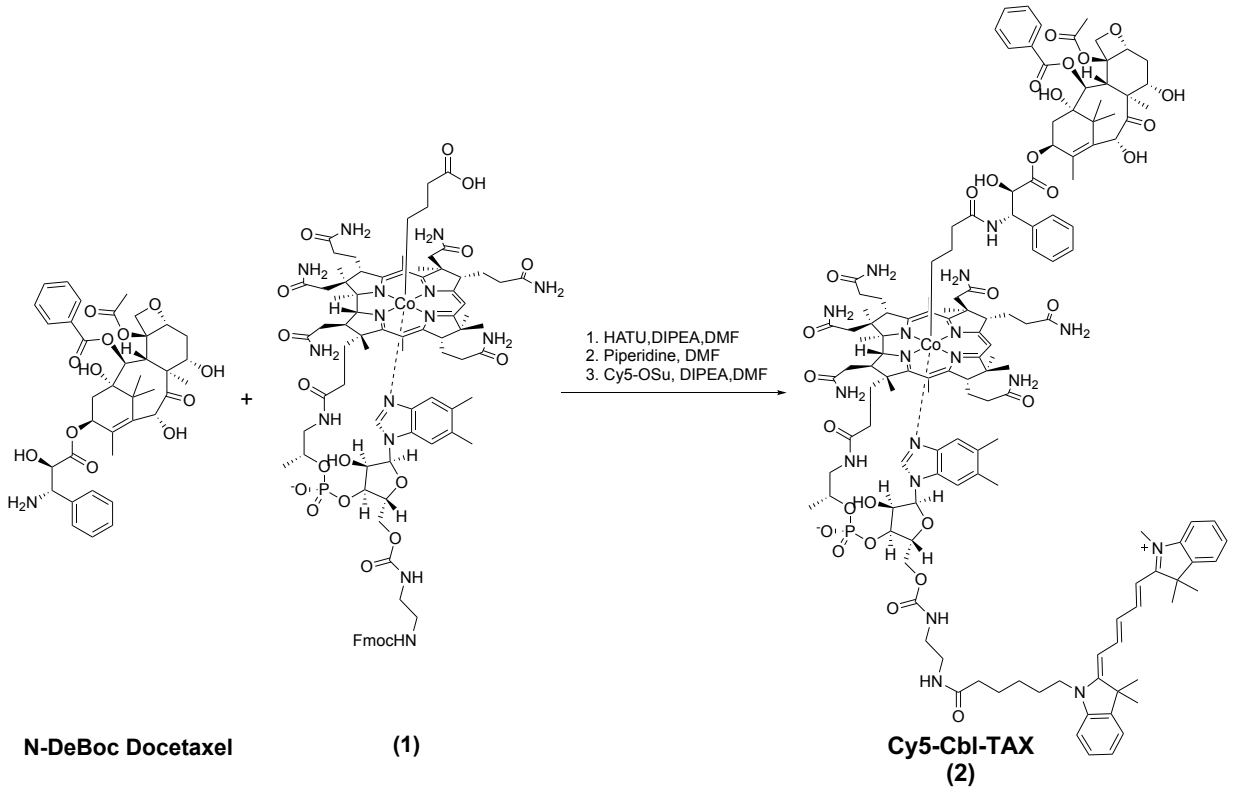

N-DeBoc Docetaxel **(1)** **Cy5-Cbl-TAX (2)**

Scheme 2-1 Synthesis of Cy5-Cbl-TAX (2).

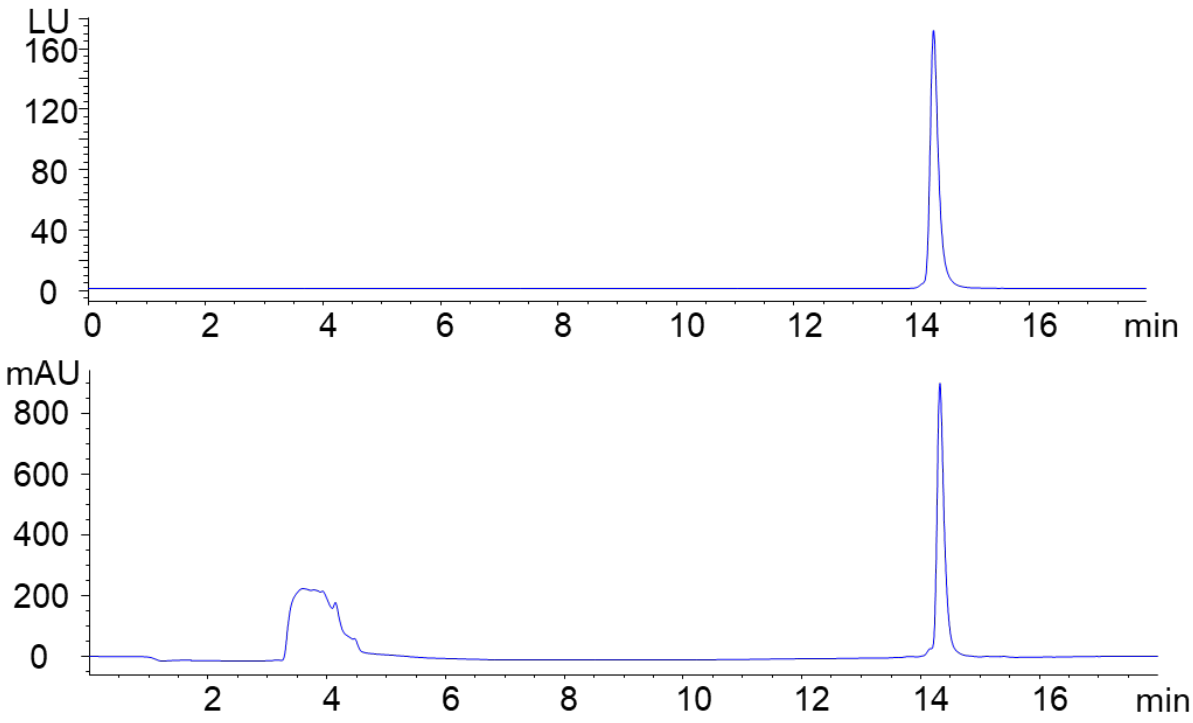

Figure 2.15 LC-MS chromatogram of purified Cy5-Cbl-TAX (**2**) detected by the fluorescent detector (top, λ_{ex} = 640 nm; λ_{em} = 670 nm) and by the UV detector (bottom, monitored at 254 nm).

Synthesis of non-photocleavable conjugate Cbl≡-NH_2, precursor of Cbl≡Cy5

Cbl≡-NH_2 was synthesized following modified procedure from literature.[29] The reaction was carried by stirring using 1 eq of cyanocobalamin, 1 eq of copper (I) acetate (CuOAc), 2 eq of 1,8-diazabicyclo[5.4.0]undec-7-ene (DBU) and 10 eq of 1,1-dimethylpropargylamine in dimethylacetamide (DMA) overnight under N_2. The product was purified via reverse phase chromatography with water-methanol (containing 0.1% TFA) solvent system (Yield 71%; Figure **2.16**). ^{1}H NMR (400 MHz, DMSO-d_6, δ): 7.86 (s, 1H), 7.63 (s, 2H), 7.51 (s, 2H), 7.34 (s, 1H), 7.27 (s, 1H), 7.17 (s, 1H), 7.06 (d, J = 7.6 Hz, 2H), 6.98 (s, 1H), 6.92 (s, 1H), 6.79 (s, 1H), 6.66 (s, 1H), 6.54 (s, 1H), 6.47 (s, 1H), 6.36 (s, 1H), 6.24 (d, J = 2.9 Hz, 1H), 6.02 (d, J = 4.3 Hz, 1H), 5.79 (s, 1H), 4.47 (s, 1H), 4.24 (d, J = 7.4 Hz, 1H), 4.20 (d, J = 11.3 Hz, 1H), 4.11 (d, J = 8.3 Hz, 1H), 3.89 (s, 2H), 3.70 (dd, J = 10.1, 5.4 Hz, 2H), 3.55 (dd, J = 18.4, 11.5 Hz, 3H), 3.03 (d, J = 10.7 Hz, 1H), 2.69 (m, 3H), 2.50-2.30 (m, 11H), 2.30 – 2.22 (m, 2H), 2.16 (d, J = 11.5 Hz, 6H),2.10-2.14 (broad s, 1H), 2.04 (d, J = 14.3 Hz, 1H), 1.88 (s, 4H), 1.80 (t, J = 14.3 Hz, 3H), 1.72 (s, 2H), 1.67 (s, 3H), 1.56 (dt, J = 15.3, 7.7 Hz, 3H), 1.34 (s, 3H), 1.21-1.19 (s, 1H), 1.20 (d, J = 6.2 Hz, 6H), 1.07 (d, J = 6.11 Hz, 3 H), 0.98 (s, 5H), 0.97(s, 3H), 0.27 (s, 3H); HRMS (ESI) m/z: $[M+H]^+$ calcd for $C_{67}H_{96}CoN_{14}O_{14}P$, 1411.6; found, (ESI+, m/z) 706.5 $[M+2H]^{2+}$, 1411.7 $[M+H]^+$.

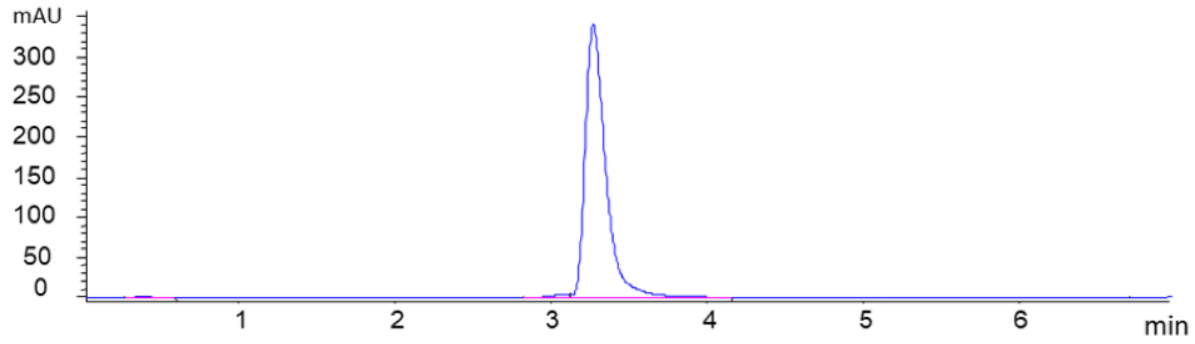

Figure 2.16 LC-MS chromatogram of purified non-photocleavable conjugate Cbl≡-NH2 detected by the UV detector (monitored at 357 nm).

Synthesis of non-photocleavable conjugate Cbl≡Cy5 (**Scheme 2-2**)

Cbl≡Cy5 was synthesized following procedure for Cy5-Cbl-TAX using Cbl≡-NH_2 (1 eq), Cy5-COOH (1 eq), HATU (1 eq) and DIPEA (4 eq) in DMF and mixing for 0.5 h. The product was purified via reverse phase chromatography with water-methanol (containing 0.1% TFA) solvent system (Yield 90%; Figure **2.17**). ^{1}H NMR (400 MHz, DMSO-d_6, δ): 8.33 (t, J = 13.2 Hz, 2H), 7.85 (s, 1H), 7.66 – 7.56 (m, 5H), 7.52 (s, 1H), 7.41 (s, 3H),7.38 – 7.32 (m, 1H), 7.34 (s, 3H), 7.32 – 7.20 (m, 3H), 7.14 (s, 1H), 7.04 (s, 1H), 6.94 (s, 1H), 6.88 (s, 1H), 6.80 (s, 1H), 6.65 (s, 1H), 6.60 – 6.50 (m, 2H), 6.44 (s, 1H), 6.30 – 6.21 (m, 3H), 6.00 (s, 1H), 5.74 (s, 1H), 4.46 (s, 1H), 4.22 (s, 1H), 4.07 (s, 5H), 3.88 (s, 2H), 3.61 (s, 3H), 3.55 (s, 5H), 2.55 (s, 92H), 2.38 (d, J = 16.0 Hz, 9H), 2.27 (s, 1H), 2.15 (d, J = 14.2 Hz, 6H), 2.05 (s, 1H), 1.88 (s, 4H), 1.78 (s, 1H), 1.70 – 1.65 (m, 25H), 1.56 (s, 2H), 1.42 (s, 2H), 1.31 (s, 2H), 1.23 (s, 8H), 1.15 (s, 4H), 1.10 – 1.02 (m, 10H), 1.01 - 0.91 (m, 5H), 0.24 (s, 3H); HRMS (ESI) m/z: M^+ calculated for $(C_{99}H_{133}CoN_{16}O_{15}P)^+$, 1875.9; found (ESI+, m/z) 626.2 $[M^+ + 2H]^{3+}$, 938.7 $[M^+ + H]^{2+}$.

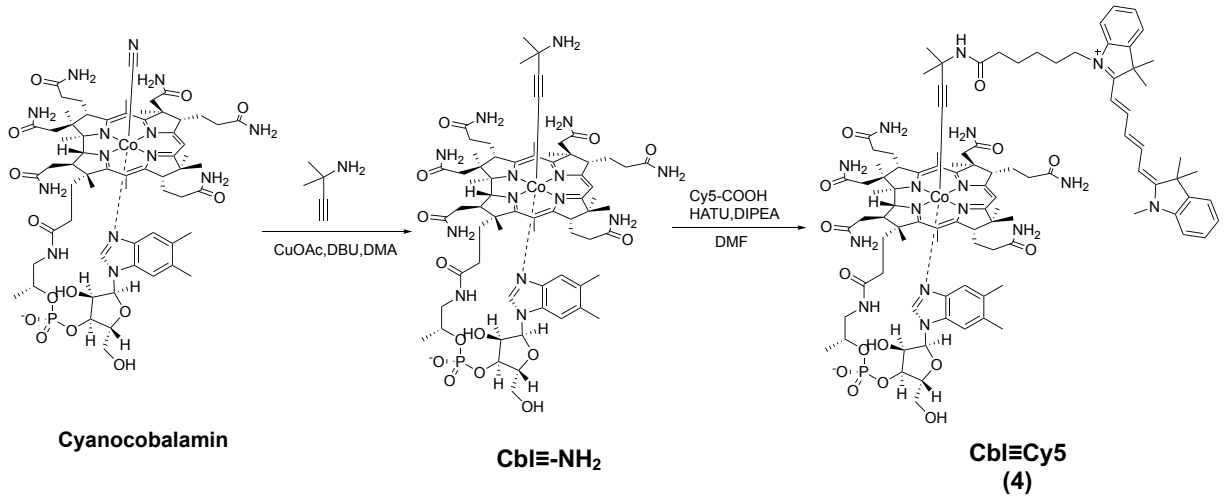

Scheme 2-2 Synthesis of Cbl≡Cy5 (**4**).

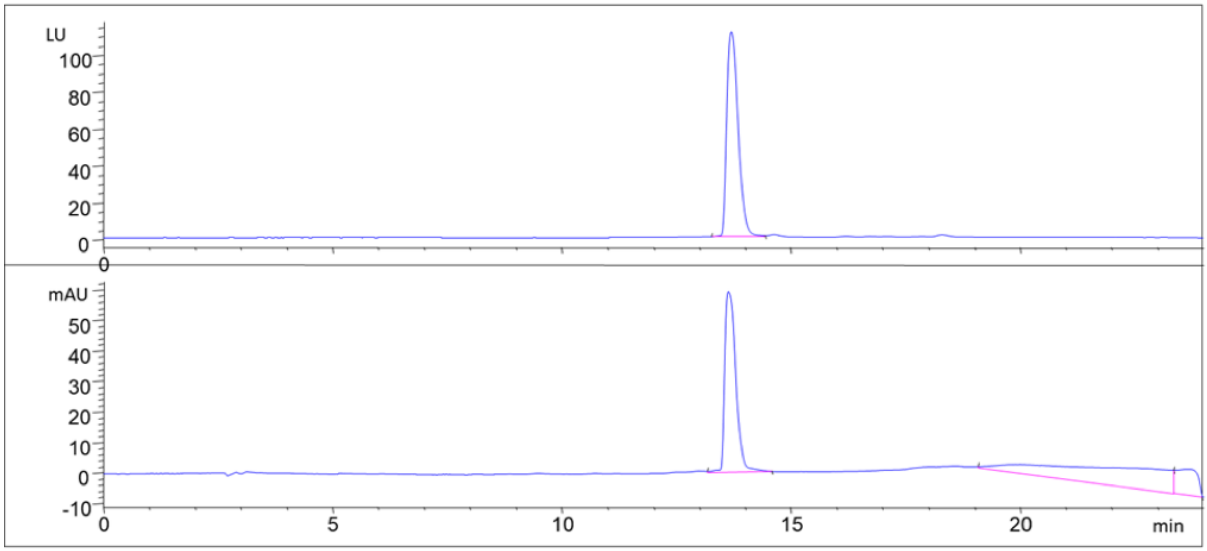

Figure 2.17 LC-MS chromatogram of purified non-photocleavable conjugate Cbl≡Cy5 (**4**) detected by the fluorescent detector (top, λ_{ex} = 645 nm; λ_{em} = 675 nm) and by the UV detector (bottom, monitored at 357 nm).

2.7.2 Loading and Characterization of Cbl RBCs

Red Blood Cell (RBC) Internal Loading Procedure

Whole blood was collected from FVB or Nu/Nu mice via cardiac puncture. RBCs were isolated from whole blood using Ficoll and washed 3x in isotonic PBS (300 mOsm). RBCs were loaded with either Cy5-Cbl-H_2O, Cbl≡Cy5, or Cy5-Cbl-TAX using a modified dialysis procedure.[22-24] The phototherapeutic conjugate was suspended in an 8:1 solution of Diluent C:DMSO and mixed with washed RBC pellets so that the final hematocrit was 70% and the Cbl conjugate concentration was 200 μM. The mixture was placed in a 1 kDa dialysis film and dialyzed against hypotonic buffer (80 mOsm/L PBS containing 6 mM glucose) for 20 min to open pores and allow influx of the Cbl conjugates. The dialysis film was then transferred to isotonic PBS and incubated for 10 min at 37 °C to reseal the cells. The RBCs were washed 3x in isotonic PBS to remove unloaded material and released hemoglobin. Quantitative loading efficiencies were obtained by extracting the conjugate into ethanol and measuring Cy5 absorbance at 645 nm (**Figure 2.18** and **Figure 2.19**).

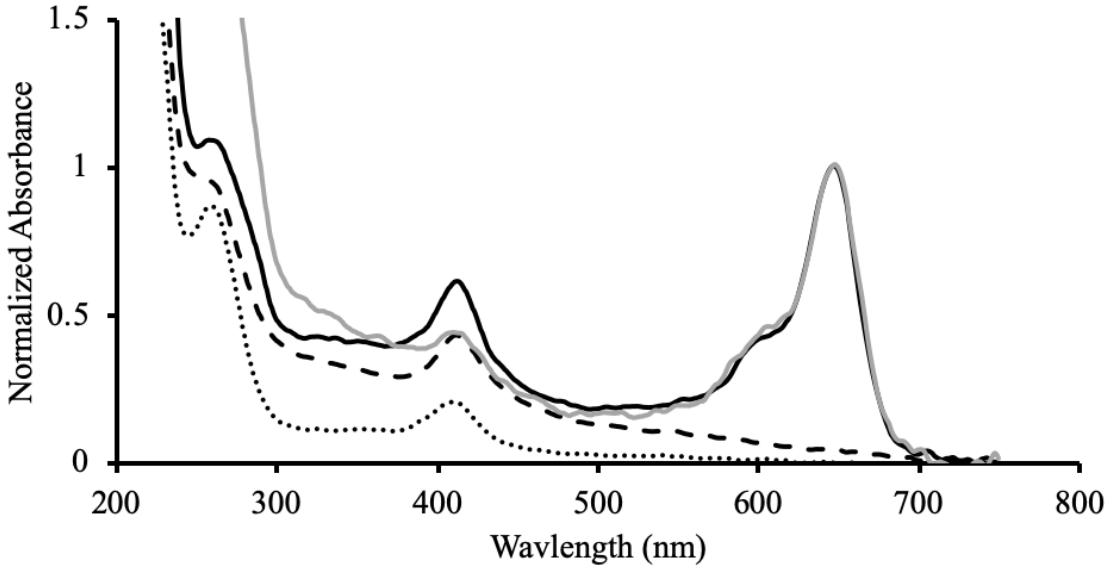

Figure 2.18 UV-Vis absorbance spectra of Cy5-Cbl-TAX (2) (solid black line) and Cy5-Cbl-H_2O (**3**) (solid gray line) extracted from mRBCs with ethanol. The Cy5 peak at 649 nm is absent in the mock loaded (dashed line) and native mRBC samples (dotted line).

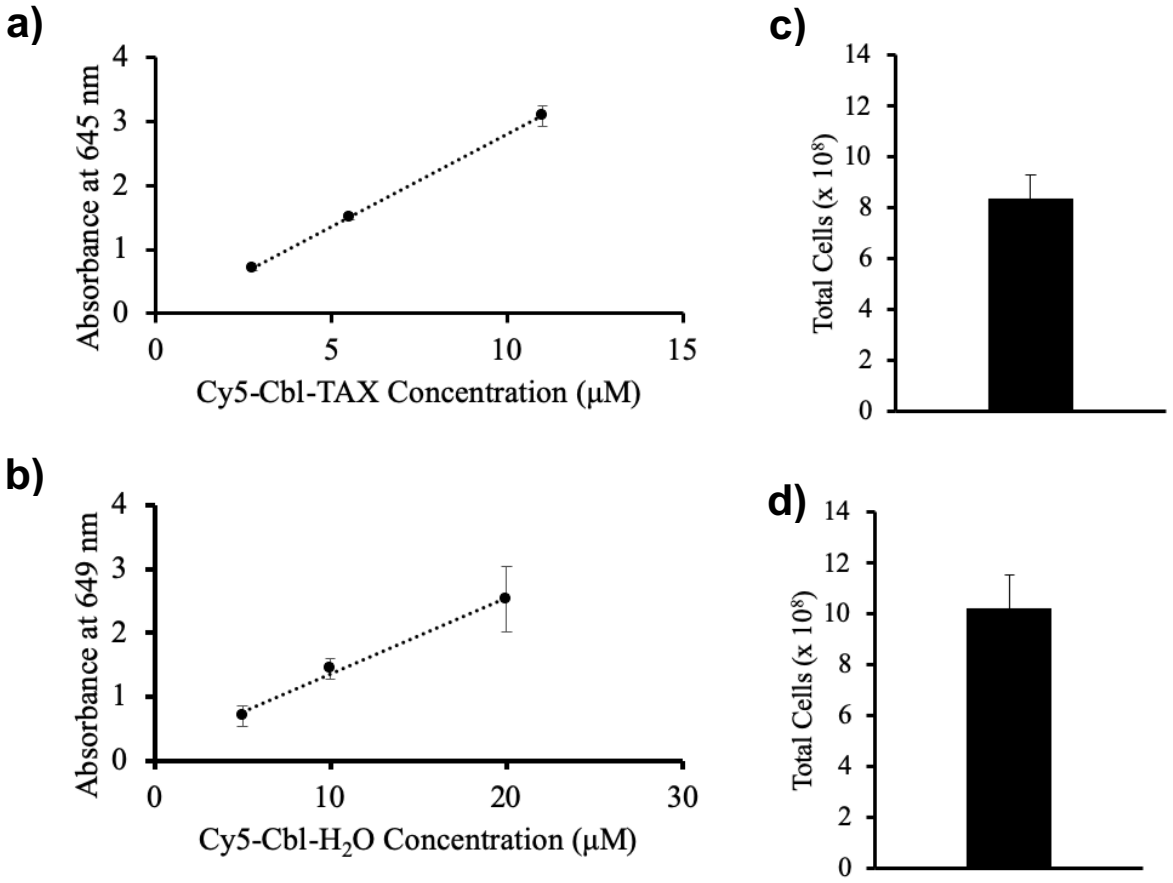

Figure 2.19 Quantification of Concentration of Cy5-Cbl-R/ mRBC. Standard curves at 645 nm for **a)** Cy5-Cbl-TAX (**2**) and **b)** Cy5-Cbl-H_2O (**3**) and cell counts post-loading of **c)** Cy5-Cbl-TAX (**2**) and **d)** Cy5-Cbl-H_2O (**3**).

RBC Surface Loading Procedure

RBCs were prepared from whole blood the same way as in the RBC Internal Loading Procedure. RBCs were suspended to 10% hematocrit in PBS containing 0.02% FBS and mixed with the membrane staining dye DiD (Thermo Fisher Scientific) at a concentration of 10 μM. The mRBCs and dye were incubated at 37 °C with mild vertical rotation for 30 min and then washed 3x in isotonic PBS to remove unloaded material.

Widefield Microscopy

RBCs were diluted to 0.05% hematocrit in PBS, plated on 35 mm MatTek glass bottom dishes, and incubated at room temperature for 15 min to allow the suspended cells to fall to the bottom of the plate. Widefield images were acquired with an inverted Olympus IX81 microscope equipped with a Hamamatsu FLASH 4V3, 60X oil objective and a Cy5 filter cube (Semrock). Multichannel images were split into their respective single channels.

Confocal Microscopy

Confocal microscopy images were taken with an Olympus FV1000 scanning confocal microscope with an IV81 base. Images were acquired using a 60X oil objective. A 635 nm laser was used for excitation of Cy5. All images were acquired at a resolution of 512 x 512 and a pixel dwell time of 10 μs $pixel^{-1}$. All processing was performed using ImageJ software.

Flow Cytometry

Cbl conjugate loading was evaluated by an imaging flow cytometer (Image Stream, Amnis, Seattle, USA) acquiring 2000 - 10000 images of in focus singlets in the bright field channel and the fluorescence emission channel at 660 - 740 nm (Cy5) for each sample. First, a gradient root mean square histogram was used to gate for cells in focus. Then, a scatter plot of aspect

ratio/area was used to gate for single cells. The acquired images were analyzed with IDEAS software (Amnis). Scatter plots of Cy5 intensity/SSC (side scattering) were used to compare and contrast the internal complexity of the cells. For loading quantification, cells with a fluorescent intensity of at least 1 x 10^4 were defined as loaded.

2.7.3 Stability and Photolysis of Cbl RBCs

Mouse and Human in vitro Fragility Tests

Whole blood was collected from DBAIJ mice by cardiac puncture and mRBCs were isolated via a standard Ficoll procedure. Human RBCs were purchased from Zen-Bio. RBCs were internally loaded with Cy5-Cbl-TAX (**2**) using the *RBC Internal Loading Procedure*. All the procedures involving light-sensitive drug were conducted with a minimal light exposure. After the loading procedure, the cells were washed 3x in 1X PBS, the pellet volume was measured, and the cells were diluted to 10% hematocrit in clear DMEM media (Gibco) with 1X GlutaMAX (Gibco) and 1% FBS. The cells were suspended and divided into four equal aliquots and stored at 4 $^{\circ}$C in dark. After 1, 2, 3 and 5 days, the cells were centrifuged, and the supernatant absorbance was measured at 420 nm to determine hemoglobin leakage. A completely lysed pellet was measured at 420 nm to determine the absorbance at 100% lysis. The pellet size was estimated in order to determine the rate of cell lysis. hRBCs were treated the same except that washes were conducted with L-15 media. Storage conditions and analysis were identical for the untreated samples.

Characterization of Photolysis Product of Cy5-Cbl-TAX (**Scheme 2-3**)

Cy5-Cbl-TAX (25 μM) in phosphate-buffered saline (1x PBS) was illuminated for 30 min using an Oriel Xe flash lamp (800 mJ, 62 Hz) as the light source with selective bandpass filters for 646 ± 10 nm. Photolyzed samples were analyzed by LC-MS using a linear gradient binary solvent system (solvent A: 0.1% formic acid/H_2O; solvent B: 0.1% formic acid/methanol) with a ratio of A:B that varied from 95:5 to 5:95 (0 - 18 min) (**Figure 2.20**).

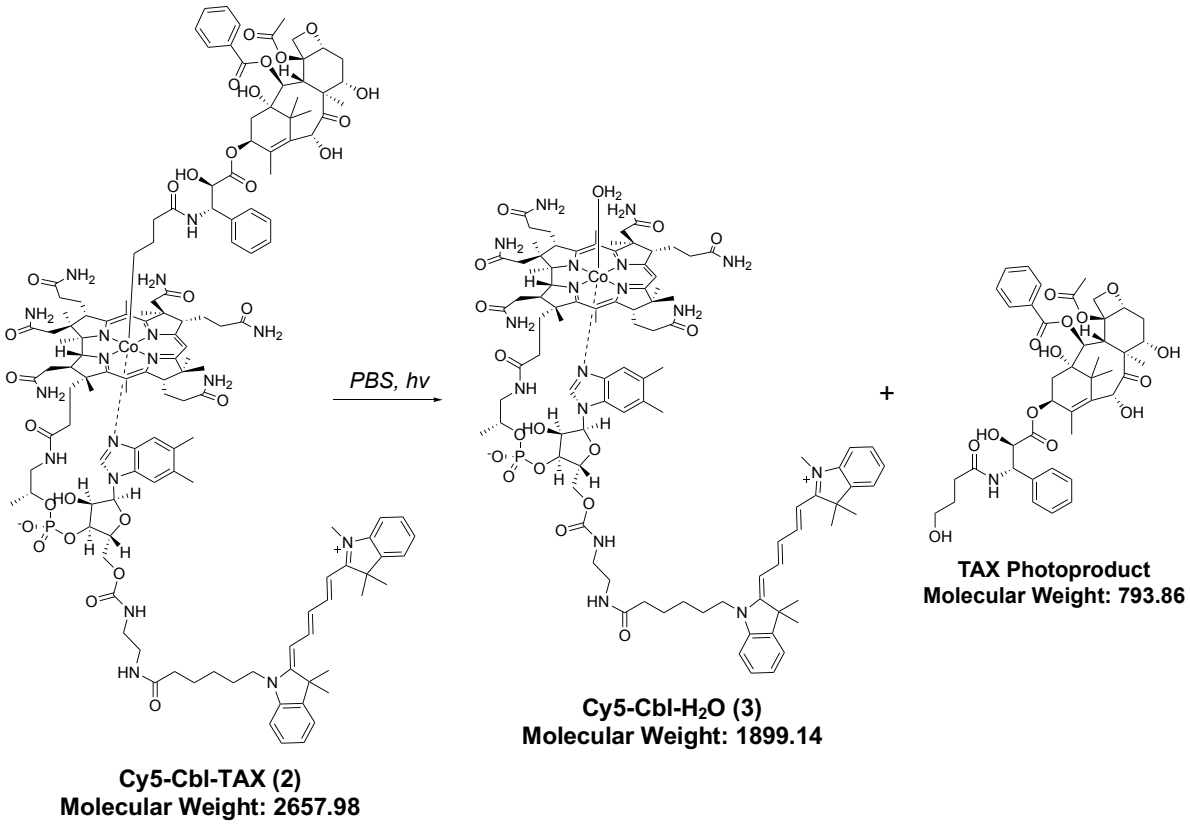

Scheme 2-3 Photolysis of Cy5-Cbl-TAX (**2**) to form photoproducts Cy5-Cbl-H_2O (**3**) and TAX photoproduct.

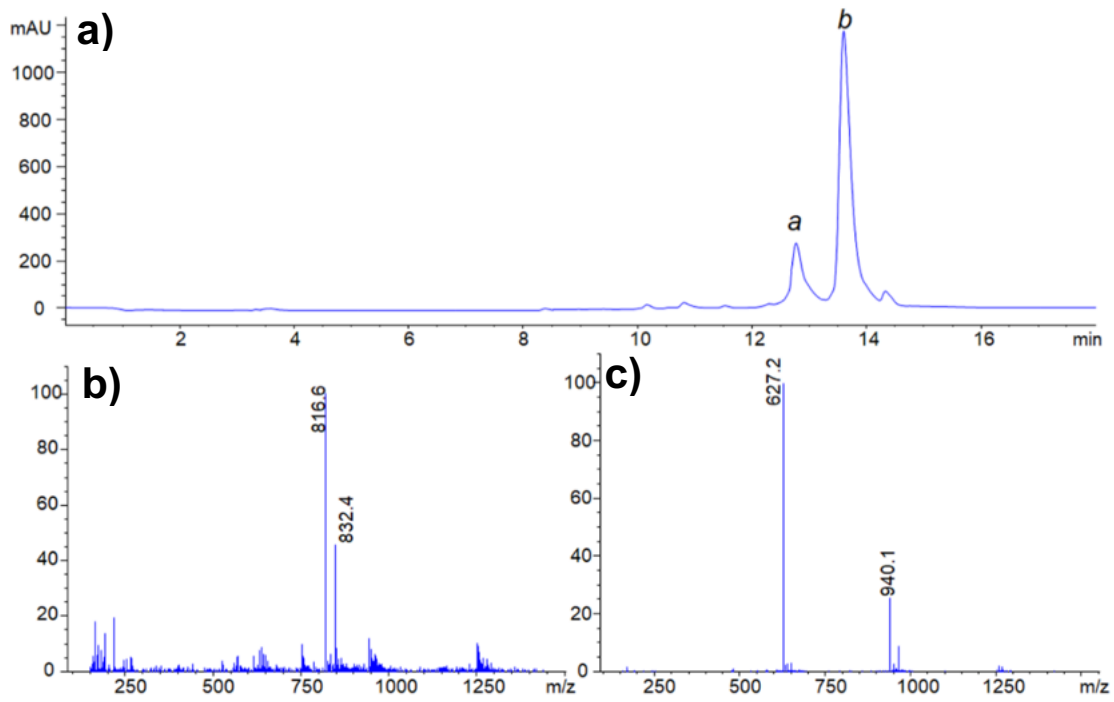

Figure 2.20 Complete photolysis of Cy5-Cbl-TAX (2). a) Reverse-phase HPLC trace of Cy5-Cbl-TAX in PBS (25 μM, pH = 7.4) irradiated at 646 nm for 30 min. The chromatogram was recorded at 254 nm where "peak *a*" = TAX photoproduct (**Scheme 2-3**) and "peak *b*" = Cy5-Cbl-H_2O photoproducts. **b)** ES-MS spectrum of the photolyzed Cy5-Cbl-TAX derivative was recorded in positive ion mode (peak *a*). Characteristic molecular and fragment ions: $[M^+ + Na]^{2+}$ (m/z 816.6), $[M^+ + K]^{2+}$ (m/z 832.4). **c)** ES-MS spectrum of photolyzed Cy5-Cbl-TAX recorded in positive-ion mode (peak *b*). Characteristic molecular and fragment ions: $[M\text{-}H_2O]^{2+}$ (m/z 940.1), $[M\text{-}H_2O^{2+} + H]^{3+}$ (m/z 627.2).

Assessment of TAX Photorelease from RBCs

Cy5-Cbl-TAX loaded hRBCs (100 µL) were added to 1 mL of human platelet rich plasma from Zen-Bio, Inc. Photolysis of the samples was performed using an Oriel Xe flash lamp (800 mJ, 62 Hz) as the light source with selective bandpass filters for 646 ± 10 nm as described above in *Characterization of Photolysis Product of Cy5-Cbl-TAX*. Photolyzed RBC suspensions were incubated at 37 ˚C, subsequently centrifuged at 1000 g for 2 min, and the supernatant removed from the pellet. Acetonitrile was added to the supernatant in a 1:1 ratio, centrifuged at 21,000 g for 10 min, and then analyzed by LCMS (solvent A: 0.1% formic acid/H_2O; solvent B: 0.1% formic acid/isopropanol). The pellet was lysed with 1 mL of acetonitrile and analyzed by LC-MS. The photolyzed TAX product was monitored by its fragment ions 506.8 and 626.8. The percentage of photolyzed TAX present in the supernatant was 98 ± 1%. By contrast, no detectable levels of TAX were found in the supernatant for samples incubated in the dark.

Sensitivity of mRBCs to Hemolysis Under Light Conditions

Whole blood was collected from DBA1J mice by cardiac puncture and isolated via a standard Ficoll procedure. mRBCs were internally loaded with Cy5-Cbl-TAX (**2**) or Cy5-Cbl-H_2O (**3**) using the *RBC Internal Loading Procedure*. All the procedures involving light-sensitive drug were conducted with a minimal light exposure. The loading procedure was performed 3x for each sample to ensure sufficient volume and each sample was pooled and diluted to 5% hematocrit. The cells loaded with each compound were then separated into nine 300 µL aliquots. Three aliquots were completely lysed by adding Triton X-100 to final concentration of 0.05%. Three other aliquots were incubated for 10 min in the dark and the last three aliquots were illuminated for 10 min under 660 nm LED light. The cells from the dark and light experiments were spun down and the supernatant collected. Triton X-100 was added to the recovered supernatants so that the final Triton concentration was 0.05%. The supernatants were analyzed for both Cy5 fluorescence (λ_{ex}

= 645 nm, λ_{em} = 675 nm) and hemoglobin absorbance (λ_{max} = 420 nm). Fluorescence was measured using SpectraMax Gemini EM (Molecular Devices) while absorbance was measured with a DeNovix DS-11 FX+ spectrophotometer/fluorometer, using the microvolume setting.

2.7.4 Cellular Assays Characterizing Cbl-Tax RBC Pharmacological Effects

Microtubule Polymerization Assay

HeLa cells (ATCC) at 50,000 cells/well were plated on MatTek 24-well glass bottom plates pre-coated with gelatin. hRBCs loaded with Cy5-B12-TAX (**2**) [see *Red Blood Cell (RBC) Internal Loading Procedure* method above] were added at 10% hematocrit in 500 µL of complete media in a Millicell Hanging Cell Culture Insert (1 µm, polyethylene terephthalate, Millipore). Control groups include complete media only as well as docetaxel (TAX, 20 nM). Wells for the hRBC + light conditions, complete media, and 20 nM TAX in media, were then exposed to a 660 nm LED board for 30 min at room temperature. Cells were then allowed to incubate for 24 h. Following this treatment time, culture inserts containing HeLa cells were removed from each well, washed once with Dulbecco's PBS (DPBS) and fixed with 4% paraformaldehyde for 10 min at room temperature in the dark. Cells were washed twice with 500 µL DPBS and immediately blocked for 1 h at room temperature in 5% donkey serum (Millipore), 1% BSA, and 0.1% Triton-X 100 in PBS. Cells were incubated with mouse anti-α-Tubulin [DM1A] antibody (Sigma Aldrich, T9026) at 1:1000 in 1% BSA, 0.5% Triton-X 100 in PBS overnight at 4 °C. Cells were washed 3 x 5 min in DPBS before application of Alexa546 anti-mouse secondary antibody at 1:2000 in blocking buffer for 1 h at room temperature. Cells were then washed 3x with PBS. The second wash contained Hoechst 33342 as a nuclear counterstain (1 µL of 5 mg/mL solution per 1 mL PBS). Imaging was performed on an inverted Olympus IX81 microscope equipped with a Hamamatsu ORCA-Flash4.0 camera, 60x oil immersion Plan S-Apo NA 1.35 objective. Images for each condition were captured using Fluoview acquisition software.

Cell Viability Assay

HeLa cells (ATCC Cat. CCL-2) were plated 2,500 cells/well in 96-well tissue culture plates (Corning Costar Cat. #3595) in full growth media following the supplier's recommendations. Human RBCs (ZenBio Cat. SER-10MLRBC) were loaded with Cy5-Cbl-TAX (**2**) following the *RBC Internal Loading Procedure* with minimal light exposure**.** hRBCs were washed with L-15 media (Gibco Cat. #21083-027) 3-5x, then a final wash with 0.22 μm filtered FBS (Millipore-Sigma Cat. #TMS-013-B). hRBCs were resuspended to 20% hematocrit with full HeLa cell growth media. Light treated hRBCs were illuminated with a 660 nm LED light board for 30 min at room temperature. Unilluminated hRBCs were wrapped in aluminum foil at room temperature for 30 min. hRBCs were spun down and the supernatants for the light and dark treatments were collected and put on ice. 24 h after HeLa cells were plated, all media was removed from wells and exposed to the following different conditions in triplicate at 37 ˚C for 24 h: 100 µL of (i) complete media, (ii) 10 nM docetaxel in full media, (iii) 1 μM docetaxel in full media, (iv) supernatant from light-exposed, Cy5-Cbl-TAX (**2**) loaded hRBCs, or (v) supernatant from unilluminated, Cy5-Cbl-TAX (**2**) loaded hRBCs. Cells were incubated at 37 °C for 24 h. Cell viability was assessed using the Calcein AM kit (BioVision #K305-1000) following the manufacturer's instructions.

2.7.5 *In vivo* Biodistribution and Localization Studies

Intravital Imaging

Healthy FVB mice were housed in an approved Division of Comparative Medicine facility until time of imaging. Intravital imaging microscopy experiments were performed using an Olympus IV-100 laser scanning confocal microscope. Images were acquired using a 10x air, 0.4 numerical aperture, working distance 3.1, 13 mm objective and 1.5 zoom value. Images were acquired every 5 s for 90 min at a resolution of 512 x 512 and a pixel dwell time of 10 µs pixel-1. Hair was removed from both ears using hair removal cream and the left ear was immobilized by

two-sided tape on an aluminum block. The mice were anesthetized with 2% isoflurane and placed onto a heated stage (37 °C) to maintain their core body temperature throughout the 90 min imaging procedure. Blood vessels were located in the left ear by illuminating it with a bright white light while imaging in the green fluorescence channel. Tissue autofluorescence appears green, while the vessels appear as dark voids. Suspensions of 100 µL containing RBC pellets at 75 - 90% hematocrit in PBS were injected via tail vein. Prior to injection, RBCs were internally loaded with either Cy5-Cbl-H_2O or Cy5-Cbl-TAX (*n* = 3 animals). As controls, groups of mice were also injected via tail vein with 100 µL RBCs at 75 - 90% hematocrit internally loaded with Cbl≡Cy5, mixed with free Cbl≡Cy5, or externally loaded with DiD (*n* = 6 vessels). Both Cy5 and DiD fluorophores were excited using a 633 nm laser and detected in the 647 nm channel. The image files from each scan were exported to ImageJ software for analysis. Once imaging was completed, mice were euthanized with CO_2 followed by a secondary physical method. All animal imaging performed was approved by the Institutional Animal Care and Use Committee at the University of North Carolina at Chapel Hill.

Measurement of Circulation Time

The quantitative fluorescent intensity of a straight-line region of interest containing vasculature was measured and background fluorescence of an empty vessel was subtracted from each measurement. Selected regions of interest (*n* = 3) for mice in each category were used to calculate the average fluorescence intensity at each time point. Each point in each time series was normalized to the highest fluorescent value to account for random variation between animals on various days. The percent retention data are presented as mean ± SD.

Histology

For histological analysis, ears were harvested less than 5 min after euthanasia at room temperature and the illuminated blood vessels (as well as the corresponding vessel in the non-illuminated ear) were marked with tissue staining dye. Ears were immediately immersion-fixed in 10% neutral buffered formalin in a 1:15 tissue: fixative volume ratio for 48 h at room temperature. The tissue was post-fixed in 70% ethanol at a 1:15 tissue: ethanol volume ratio and embedded in paraffin. 4 μm cross-sections were subsequently stained with H&E and microscopically evaluated. Images were acquired under a 40X objective of a color optical microscope.

Ultrasound Animal Care and Imaging

Homozygous Nu/Nu mice were housed in an approved Division of Comparative Medicine facility until time of imaging. At five weeks old, mice were given a 100 μL subcutaneous injection of 7×10^6 SVR angiosarcoma cells/mL. Tumor measurements were recorded 3x a week and mice were imaged when tumor size was between 5 - 10 mm in the largest dimension. Mice were placed on a heating pad warmed to 37 ˚C and kept under 1.5% isoflurane anesthesia for the duration of the imaging experiment. Ultrasound gel applied to the tumor site helped couple tissue with the transducer used for imaging. Once imaging was completed, mice were euthanized with an overdose of isoflurane followed by a secondary physical method. All animal imaging performed was approved by the Institutional Animal Care and Use Committee at the University of North Carolina at Chapel Hill.

Ultrasound Contrast Agent and RBC Administration

Perfluorocarbon microbubbles made in-house were injected in each animal via a 27G tail-vein catheter. Microbubbles were sized using an AccuSizer 780A (Particle Sizing Systems, Santa Barbara, CA, USA) before administration in order to ensure that an accurate dosing scheme was

maintained throughout the course of the study. Microbubbles (MB) were diluted to 5 x 10^9 MB/ mL and were delivered via a 50 µL volume followed by a 50 µL saline flush. Microbubble doses were administered before each imaging time point. Before the start of treatment, 100 µL of prepared mRBCs were injected followed by 50 µL of heparinized saline.

Ultrasound Imaging Protocol

Mice were imaged with a Vevo 770 imaging system using a custom-built dual frequency transducer (VisualSonics, Toronto, ON, Canada). The ultrasound probe, mounted on a motion stage to allow for 3D data collection, transmits at 4 MHz and receives at 28 MHz. 16 mice were divided into the following four experimental groups: Cy5-Cbl-TAX (**2**) loaded mRBCs with light treatment, Cy5-Cbl-TAX (**2**) loaded mRBCs without light treatment (dark), Cy5-Cbl-H_2O (**3**) loaded mRBCs with light treatment, and vehicle-loaded mRBCs with light treatment. First, a 3D B-mode scan was collected using a 3 Hz frame rate and a 100 µm step size. Scan length varied based on tumor size. Additional 3D acoustic angiography scans were collected before treatment (baseline) and at 5, 15, 25, 35, and 45 min following the beginning of treatment. Light-treated animals were exposed to a 655 nm 100 mW laser that was aligned at the tumor site. The tumor was illuminated for a total of 5 min.

Ultrasound Data Analysis

Data was analyzed using a custom-built MATLAB program (MathWorks, Natick, MA, USA). Individual regions of interest (ROIs) were drawn slice by slice on the B-mode set for each animal. These ROIs were applied to the contrast images and adjusted as necessary to account for animal motion and breathing. Images were binarized using Otsu's method and the area of thresholded signal within the 3D ROI set was calculated. This value was divided by the area of the entire 3D ROI set. Finally, this metric for microbubble retention was normalized to the baseline value for

each animal. A two-factor ANOVA evaluating imaging time points and experimental group was performed to test for statistical significance. This was followed by Dunnett's multiple comparison for imaging time points and Fisher's Least Significant Difference multiple comparison for experimental group.

REFERENCES

1. Raucher, D.; Dragojevic, S.; Ryu, J., Macromolecular Drug Carriers for Targeted Glioblastoma Therapy: Preclinical Studies, Challenges, and Future Perspectives. *Frontiers in Oncology* **2018,** *8* (624).

2. Bonnet, S., Why develop photoactivated chemotherapy? *Dalton Transactions* **2018,** *47* (31), 10330-10343.

3. Kydd, J.; Jadia, R.; Velpurisiva, P.; Gad, A.; Paliwal, S.; Rai, P., Targeting Strategies for the Combination Treatment of Cancer Using Drug Delivery Systems. *Pharmaceutics* **2017,** *9* (4), 46.

4. Ai, D.; Banchs, J.; Owusu-Agyemang, P.; Cata, J. P., Chemotherapy-induced cardiovascular toxicity: beyond anthracyclines. *Minerva Anestesiol* **2014,** *80* (5), 586-94.

5. Ding, S.; O'Banion, C. P.; Welfare, J. G.; Lawrence, D. S., Cellular Cyborgs: On the Precipice of a Drug Delivery Revolution. *Cell Chemical Biology* **2018,** *25* (6), 648-658.

6. Nam, L.; Coll, C.; Erthal, L. C. S.; de la Torre, C.; Serrano, D.; Martínez-Máñez, R.; Santos-Martínez, M. J.; Ruiz-Hernández, E., Drug Delivery Nanosystems for the Localized Treatment of Glioblastoma Multiforme. *Materials (Basel)* **2018,** *11* (5).

7. Linsley, C. S.; Wu, B. M., Recent advances in light-responsive on-demand drug-delivery systems. *Ther Deliv* **2017,** *8* (2), 89-107.

8. Zhang, J.; Tang, H.; Liu, Z.; Chen, B., Effects of major parameters of nanoparticles on their physical and chemical properties and recent application of nanodrug delivery system in targeted chemotherapy. *Int J Nanomedicine* **2017,** *12*, 8483-8493.

9. Shi, J.; Kantoff, P. W.; Wooster, R.; Farokhzad, O. C., Cancer nanomedicine: progress, challenges and opportunities. *Nature Reviews Cancer* **2017,** *17* (1), 20-37.

10. Diamantis, N.; Banerji, U., Antibody-drug conjugates—an emerging class of cancer treatment. *British Journal of Cancer* **2016,** *114* (4), 362-367.

11. Ernsting, M. J.; Murakami, M.; Roy, A.; Li, S.-D., Factors controlling the pharmacokinetics, biodistribution and intratumoral penetration of nanoparticles. *Journal of Controlled Release* **2013,** *172* (3), 782-794.

12. Firer, M. A.; Gellerman, G., Targeted drug delivery for cancer therapy: the other side of antibodies. *Journal of Hematology & Oncology* **2012,** *5* (1), 70.

13. Dawidczyk, C. M.; Kim, C.; Park, J. H.; Russell, L. M.; Lee, K. H.; Pomper, M. G.; Searson, P. C., State-of-the-art in design rules for drug delivery platforms: Lessons learned from FDA-approved nanomedicines. *Journal of Controlled Release* **2014,** *187*, 133-144.

14. Karimi, M.; Sahandi Zangabad, P.; Baghaee-Ravari, S.; Ghazadeh, M.; Mirshekari, H.; Hamblin, M. R., Smart Nanostructures for Cargo Delivery: Uncaging and Activating by Light. *Journal of the American Chemical Society* **2017,** *139* (13), 4584-4610.

15. Yang, Y.; Mu, J.; Xing, B., Photoactivated drug delivery and bioimaging. *Wiley Interdiscip Rev Nanomed Nanobiotechnol* **2017,** *9* (2).

16. Shell, T. A.; Shell, J. R.; Rodgers, Z. L.; Lawrence, D. S., Tunable Visible and Near-IR Photoactivation of Light-Responsive Compounds by Using Fluorophores as Light-Capturing Antennas. *Angewandte Chemie International Edition* **2014,** *53* (3), 875-878.

17. Smith, W. J.; Oien, N. P.; Hughes, R. M.; Marvin, C. M.; Rodgers, Z. L.; Lee, J.; Lawrence, D. S., Cell-Mediated Assembly of Phototherapeutics. *Angewandte Chemie International Edition* **2014,** *53* (41), 10945-10948.

18. Hughes, R. M.; Marvin, C. M.; Rodgers, Z. L.; Ding, S.; Oien, N. P.; Smith, W. J.; Lawrence, D. S., Phototriggered Secretion of Membrane Compartmentalized Bioactive Agents. *Angewandte Chemie International Edition* **2016,** *55* (52), 16080-16083.

19. Sun, B.; Straubinger, R. M.; Lovell, J. F., Current taxane formulations and emerging cabazitaxel delivery systems. *Nano Research* **2018,** *11* (10), 5193-5218.

20. Ganesh, T., Improved biochemical strategies for targeted delivery of taxoids. *Bioorg Med Chem* **2007,** *15* (11), 3597-3623.

21. Jordan, M. A.; Wilson, L., Microtubules as a target for anticancer drugs. *Nature Reviews Cancer* **2004,** *4* (4), 253-265.

22. Dale, G. L.; Villacorte, D. G.; Beutler, E., High-yield entrapment of proteins into erythrocytes. *Biochem Med* **1977,** *18* (2), 220-5.

23. Deloach, J.; Ihler, G., A dialysis procedure for loading erythrocytes with enzymes and lipids. *Biochimica et Biophysica Acta (BBA) - General Subjects* **1977,** *496* (1), 136-145.

24. Pierigè, F.; Bigini, N.; Rossi, L.; Magnani, M., Reengineering red blood cells for cellular therapeutics and diagnostics. *WIREs Nanomedicine and Nanobiotechnology* **2017,** *9* (5), e1454.

25. Bourgeaux, V.; Lanao, J. M.; Bax, B. E.; Godfrin, Y., Drug-loaded erythrocytes: on the road toward marketing approval. *Drug Des Devel Ther* **2016,** *10*, 665-76.

26. Villa, C. H.; Anselmo, A. C.; Mitragotri, S.; Muzykantov, V., Red blood cells: Supercarriers for drugs, biologicals, and nanoparticles and inspiration for advanced delivery systems. *Advanced Drug Delivery Reviews* **2016,** *106*, 88-103.

27. Yan, J.; Yu, J.; Wang, C.; Gu, Z., Red Blood Cells for Drug Delivery. *Small Methods* **2017,** *1* (12), 1700270.

28. Wierzba, A. J.; Hassan, S.; Gryko, D., Synthetic Approaches toward Vitamin B12 Conjugates. *Asian Journal of Organic Chemistry* **2019,** *8* (1), 6-24.

29. Chromiński, M.; Lewalska, A.; Karczewski, M.; Gryko, D., Vitamin B12 Derivatives for Orthogonal Functionalization. *The Journal of Organic Chemistry* **2014,** *79* (16), 7532-7542.

30. Chromiński, M.; Lewalska, A.; Gryko, D., Reduction-free synthesis of stable acetylide cobalamins. *Chemical Communications* **2013,** *49* (97), 11406-11408.

31. Minetti, G.; Egée, S.; Moersdorf, D.; Steffen, P.; Makhro, A.; Achilli, C.; Ciana, A.; Wang, J.; Bouyer, G.; Bernhardt, I.; Wagner, C.; Thomas, S.; Bogdanova, A.; Kaestner, L., Red cell investigations: Art and artefacts. *Blood reviews* **2013,** *27*, 91-101.

32. D'Alessandro, A.; Righetti, P. G.; Zolla, L., The Red Blood Cell Proteome and Interactome: An Update. *Journal of Proteome Research* **2010,** *9* (1), 144-163.

33. Kakhniashvili, D. G.; Griko, N. B.; Bulla, L. A.; Goodman, S. R., The proteomics of sickle cell disease: profiling of erythrocyte membrane proteins by 2D-DIGE and tandem mass spectrometry. *Exp Biol Med (Maywood)* **2005,** *230* (11), 787-792.

34. Shin, S.; Ku, Y.; Babu, N.; Singh, M., Erythrocyte deformability and its variation in diabetes mellitus. *Indian J Exp Biol* **2007,** *45* (1), 121-8.

35. Makley, A. T.; Goodman, M. D.; Friend, L. A. W.; Johannigman, J. A.; Dorlac, W. C.; Lentsch, A. B.; Pritts, T. A., Murine blood banking: characterization and comparisons to human blood. *Shock* **2010,** *34* (1), 40-45.

36. Pan, D.; Vargas-Morales, O.; Zern, B.; Anselmo, A. C.; Gupta, V.; Zakrewsky, M.; Mitragotri, S.; Muzykantov, V., The Effect of Polymeric Nanoparticles on Biocompatibility of Carrier Red Blood Cells. *PLOS ONE* **2016,** *11* (3), e0152074.

37. Stowell, S. R.; Liepkalns, J. S.; Hendrickson, J. E.; Girard-Pierce, K. R.; Smith, N. H.; Arthur, C. M.; Zimring, J. C., Antigen Modulation Confers Protection to Red Blood Cells from Antibody through Fcγ Receptor Ligation. *The Journal of Immunology* **2013,** *191* (10), 5013.

38. McAuliffe, G.; Roberts, L.; Roberts, S., Paclitaxel administration and its effects on clinically relevant human cancer and non cancer cell lines. *Biotechnology Letters* **2002,** *24* (12), 959-964.

39. Soultati, A.; Mountzios, G.; Avgerinou, C.; Papaxoinis, G.; Pectasides, D.; Dimopoulos, M.-A.; Papadimitriou, C., Endothelial vascular toxicity from chemotherapeutic agents: Preclinical evidence and clinical implications. *Cancer Treatment Reviews* **2012,** *38* (5), 473-483.

40. Fung, A. S.; Lee, C.; Yu, M.; Tannock, I. F., The effect of chemotherapeutic agents on tumor vasculature in subcutaneous and orthotopic human tumor xenografts. *BMC Cancer* **2015,** *15* (1), 112.

41. Cameron, A. C.; Touyz, R. M.; Lang, N. N., Vascular Complications of Cancer Chemotherapy. *Canadian Journal of Cardiology* **2016,** *32* (7), 852-862.

42. Sonnichsen, D. S.; Relling, M. V., Clinical Pharmacokinetics of Paclitaxel. *Clinical Pharmacokinetics* **1994,** *27* (4), 256-269.

43. Schrijvers, D., Role of Red Blood Cells in Pharmacokinetics of Chemotherapeutic Agents. *Clinical Pharmacokinetics* **2003,** *42* (9), 779-791.

44. Litvinov, R. I.; Weisel, J. W., Role of red blood cells in haemostasis and thrombosis. *ISBT Sci Ser* **2017,** *12* (1), 176-183.

45. Copple, B. L.; Woolley, B.; Banes, A.; Ganey, P. E.; Roth, R. A., Anticoagulants Prevent Monocrotaline-Induced Hepatic Parenchymal Cell Injury but Not Endothelial Cell Injury in the Rat. *Toxicology and Applied Pharmacology* **2002,** *180* (3), 186-196.

46. George, J. N.; Nester, C. M., Syndromes of Thrombotic Microangiopathy. *New England Journal of Medicine* **2014,** *371* (7), 654-666.

47. Rabah, S. O., Acute Taxol nephrotoxicity: Histological and ultrastructural studies of mice kidney parenchyma. *Saudi Journal of Biological Sciences* **2010,** *17* (2), 105-114.

48. Zheng, Q.; Jockusch, S.; Zhou, Z.; Blanchard, S. C., The Contribution of Reactive Oxygen Species to the Photobleaching of Organic Fluorophores. *Photochemistry and Photobiology* **2014,** *90* (2), 448-454.

49. Huck, J. J.; Zhang, M.; Mettetal, J.; Chakravarty, A.; Venkatakrishnan, K.; Zhou, X.; Kleinfield, R.; Hyer, M. L.; Kannan, K.; Shinde, V.; Dorner, A.; Manfredi, M. G.; Shyu, W. C.; Ecsedy, J. A., Translational Exposure–Efficacy Modeling to Optimize the Dose and Schedule of Taxanes Combined with the Investigational Aurora A Kinase Inhibitor MLN8237 (Alisertib). *Molecular Cancer Therapeutics* **2014,** *13* (9), 2170.

50. Arbiser, J. L.; Moses, M. A.; Fernandez, C. A.; Ghiso, N.; Cao, Y.; Klauber, N.; Frank, D.; Brownlee, M.; Flynn, E.; Parangi, S.; Byers, H. R.; Folkman, J., Oncogenic H-ras stimulates tumor angiogenesis by two distinct pathways. *Proceedings of the National Academy of Sciences* **1997,** *94* (3), 861.

51. Gessner, R. C.; Frederick, C. B.; Foster, F. S.; Dayton, P. A., Acoustic angiography: a new imaging modality for assessing microvasculature architecture. *Int J Biomed Imaging* **2013,** *2013*, 936593.

52. Lin, F.; Shelton, S. E.; Espíndola, D.; Rojas, J. D.; Pinton, G.; Dayton, P. A., 3-D Ultrasound Localization Microscopy for Identifying Microvascular Morphology Features of Tumor Angiogenesis at a Resolution Beyond the Diffraction Limit of Conventional Ultrasound. *Theranostics* **2017,** *7* (1), 196-204.

53. Chen, H.; Sha, H.; Zhang, L.; Qian, H.; Chen, F.; Ding, N.; Ji, L.; Zhu, A.; Xu, Q.; Meng, F.; Yu, L.; Zhou, Y.; Liu, B., Lipid insertion enables targeted functionalization of paclitaxel-loaded erythrocyte membrane nanosystem by tumor-penetrating bispecific recombinant protein. *Int J Nanomedicine* **2018,** *13*, 5347-5359.

54. Fu, Q.; Lv, P.; Chen, Z.; Ni, D.; Zhang, L.; Yue, H.; Yue, Z.; Wei, W.; Ma, G., Programmed co-delivery of paclitaxel and doxorubicin boosted by camouflaging with erythrocyte membrane. *Nanoscale* **2015,** *7* (9), 4020-4030.

55. Gao, L.; Wang, H.; Nan, L.; Peng, T.; Sun, L.; Zhou, J.; Xiao, Y.; Wang, J.; Sun, J.; Lu, W.; Zhang, L.; Yan, Z.; Yu, L.; Wang, Y., Erythrocyte Membrane-Wrapped pH Sensitive Polymeric Nanoparticles for Non-Small Cell Lung Cancer Therapy. *Bioconjugate Chemistry* **2017,** *28* (10), 2591-2598.

56. Jiang, X.; Wang, K.; Zhou, Z.; Zhang, Y.; Sha, H.; Xu, Q.; Wu, J.; Wang, J.; Wu, J.; Hu, Y.; Liu, B., Erythrocyte membrane nanoparticles improve the intestinal absorption of paclitaxel. *Biochemical and Biophysical Research Communications* **2017,** *488* (2), 322-328.

57. Su, J.; Sun, H.; Meng, Q.; Yin, Q.; Tang, S.; Zhang, P.; Chen, Y.; Zhang, Z.; Yu, H.; Li, Y., Long Circulation Red-Blood-Cell-Mimetic Nanoparticles with Peptide-Enhanced Tumor Penetration for Simultaneously Inhibiting Growth and Lung Metastasis of Breast Cancer. *Advanced Functional Materials* **2016,** *26* (8), 1243-1252.

58. Zhu, D. M.; Xie, W.; Xiao, Y. S.; Suo, M.; Zan, M. H.; Liao, Q. Q.; Hu, X. J.; Chen, L. B.; Chen, B.; Wu, W. T.; Ji, L. W.; Huang, H. M.; Guo, S. S.; Zhao, X. Z.; Liu, Q. Y.; Liu, W., Erythrocyte membrane-coated gold nanocages for targeted photothermal and chemical cancer therapy. *Nanotechnology* **2018,** *29* (8), 084002.

59. Harisa, G. I.; Ibrahim, M. F.; Alanazi, F.; Shazly, G. A., Engineering erythrocytes as a novel carrier for the targeted delivery of the anticancer drug paclitaxel. *Saudi Pharmaceutical Journal* **2014,** *22* (3), 223-230.

60. van Tilburg, E. W.; Franssen, E. J. F.; van der Hoeven, J. J. M.; van der Meij, M.; Elshove, D.; Lammertsma, A. A.; Windhorst, A. D., Radiosynthesis of [11C]docetaxel. *Journal of Labelled Compounds and Radiopharmaceuticals* **2004,** *47* (11), 763-777.

CHAPTER 3: *IN VIVO* EFFICACY OF PHOTOACTIVABLE COBALAMIN-DEXAMETHASONE RED BLOOD CELLS

Submitted to *Advanced Therapeutics* **2021.**

The work in this Chapter was a collaboration between the authors Emilia M. Zywot, Natalia Orlova, Song Ding, Rishi R. Rampersad, Emily M. Rabjohns, Victoria A. Wickenheisser, Qunzhao Wang, Joshua G. Welfare, Lauren Haar, Amanda M. Eudy, Teresa K. Tarrant, and David S. Lawrence. Emilia M. Zywot, the author of this dissertation, wrote the publication and contributed the most scientific ideas and experimental effort.

3.1 Introduction to Photoactivated RBCs as Drug Depots for Arthritis

Stimuli-responsive drug delivery systems offer the promise of improved efficacy and reduced toxicity of therapeutic agents. Ultrasound, heat, radiation, and light can be directed at the diseased site and, when coupled with a drug delivery system, can be used to guide the drug to its intended target. An especially compelling case for targeted drug delivery is inflammatory arthritis, a debilitating autoimmune disease with symptoms of extreme pain and cartilage degradation predominantly presenting in the joints of the hands and feet. Current first-line treatments include nonsteroidal anti-inflammatory drugs and corticosteroids, such as dexamethasone (Dex). Unfortunately, the prolonged use of Dex is responsible for a variety of significant side effects, including bone-thinning, weight gain, diabetes, and immunosuppression.[1] Novel therapies designed to maintain Dex's circulatory presence while minimizing its systemic side effects employ slow release carrier-based systems such as liposomes, polymer-drug conjugates, and red blood cells (RBCs).[2] Indeed, RBCs present a potentially elegant solution to the challenge of creating a long term (months) drug depot that circulates throughout the body in an innocuous, dormant form. A variety of RBC-based therapeutic carrier systems have been described, including therapeutic loading strategies that install the drug on the surface or in the

interior of RBCs.[3-6] Most studies reported to date employ an internally loaded prodrug that slowly hydrolyzes to create a membrane permeable parent therapeutic, which subsequently diffuses out of the RBC carrier.[4] This strategy provides a continuous stream of systemically released therapeutic. By contrast, we describe herein the construction and application of engineered RBCs that stably house a Dex derivative that is released upon exposure to long wavelength light. Although light, as a targeting agent, enjoys a number of potential advantages (tight spatial, temporal, and flux control, wavelength modulation),[7, 8] one especially noteworthy attribute is that light can be easily focused on the inflamed and painful joints by the patient.[9] The patient-guided delivery of an anti-inflammatory agent to diseased sites could prove useful in controlling the most devasting aspects of inflammatory arthritis while limiting the consequent side-effects.

A key element of our design strategy is the covalent attachment of Dex to vitamin B12 (cobalamin, Cbl), where Cbl serves three roles.[10] First, Cbl is membrane impermeable, which ensures that the internally loaded Cbl-Drug is retained by the RBC. Second, Dex is appended to the central Co of Cbl via a light responsive Co-C bond. Exposure to the appropriate wavelength cleaves Dex from the Cbl anchor, enabling the drug to freely diffuse from the RBC. Third, although the corrin ring of Cbl absorbs only short wavelength light (330 - 575 nm), installation of fluorophores on the Cbl[11-13] adjusts photo-release of the appended drug to longer, tissue-penetrating wavelengths (650 - 800 nm).[14, 15] With these attributes in mind, we report herein the preparation and characterization of RBC loaded photoactivatable Dex and its application to a mouse model of inflammatory arthritis.

3.2 Synthesis of Cbl-Dex

Both Cy5-Cbl-Dex (**1**) and Cy5-Cbl-H_2O (**2**) (**Figure 3.1**) were synthesized and introduced into RBCs in order to assess drug photo-delivery as a potential therapeutic strategy for the treatment of inflammatory arthritis. Cy5-Cbl-H_2O served as an inactive control that lacks the Dex therapeutic agent. In brief, Dex was appended to the aminopropyl ligand on the Co and Cy5 subsequently coupled to an ethylenediamine linker on the ribose of Cbl (see section 3.8.1). The Cy5 fluorophore extends the light capturing wavelengths of Cbl from 330 - 575 nm to 650 nm, where the latter displays greater tissue penetration than that of the former.[10, 12]

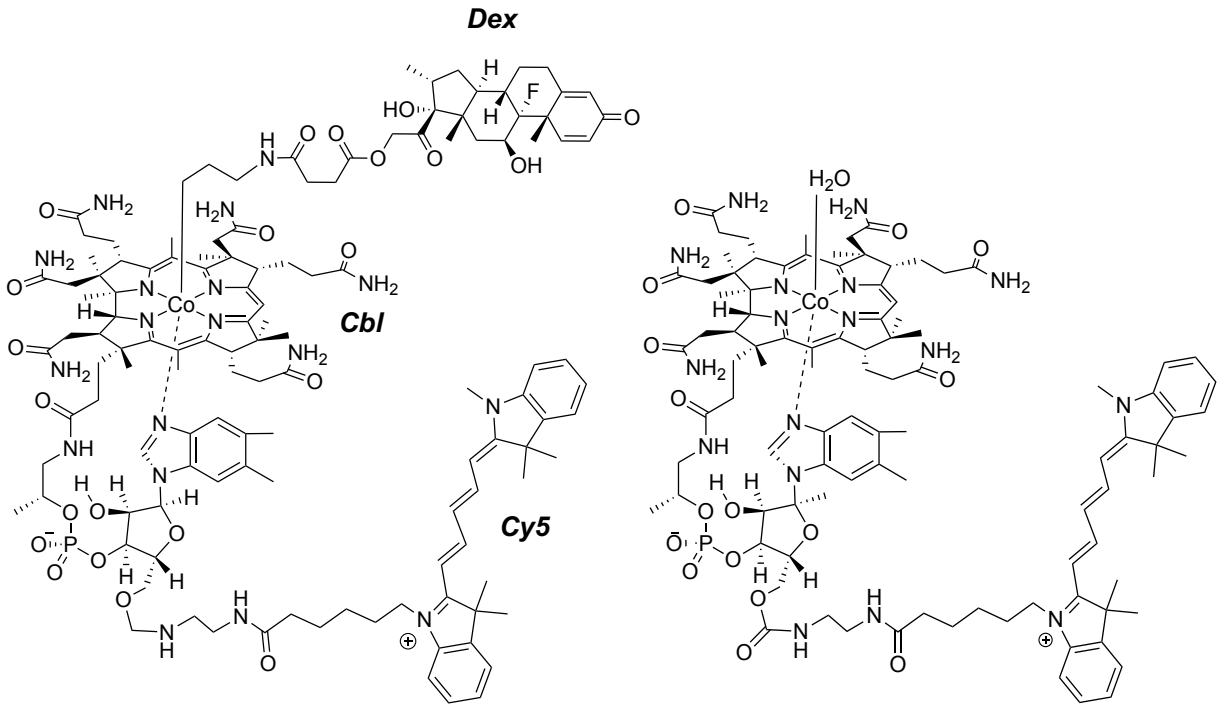

Figure 3.1 Structures of photoactivatable Cy5-Cbl-Dex (1) and control compound Cy5-Cbl-H_2O (2).

3.3 Assembly of Cy5-Cbl-Dex RBCs

RBCs internally loaded with either **1** or **2** were prepared using a hypotonic swelling procedure (**Figure 3.2**).[10, 11, 16] In brief, exposure of RBCs to a low ionic strength buffer solution induces cell swelling and pore formation within the cell membrane, which enables otherwise impermeable compounds to enter RBCs. The pores are subsequently resealed upon exposure to a high salt solution to reestablish an isotonic environment, which internally entraps the molecule of interest inside the RBCs (**Figure 3.3**).[17]

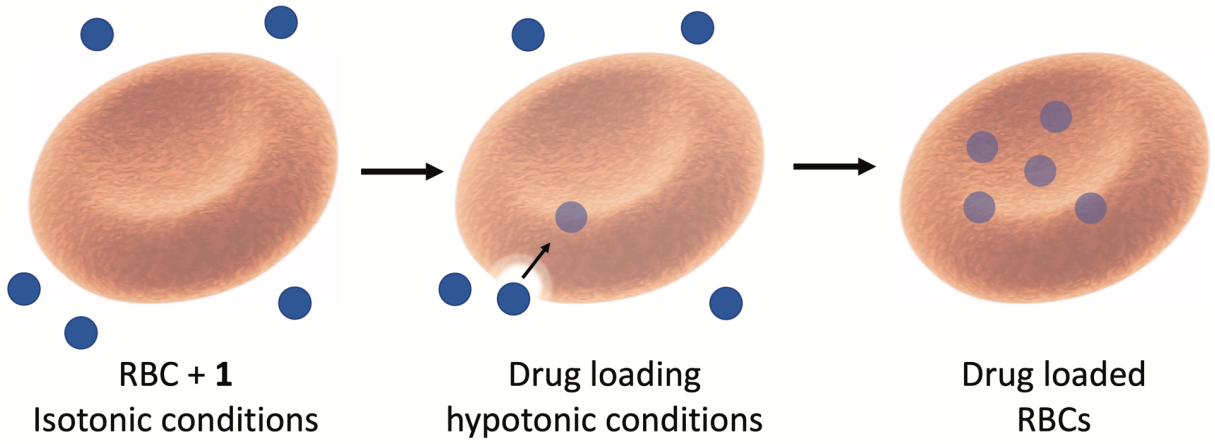

Figure 3.2 Assembly of Cy5-Cbl-Dex RBC Phototherapeutics. Schematic representation of the isotonic-to-hypotonic-to-isotonic method by which phototherapeutics are loaded into RBCs. Pore formation in the RBC membrane occurs in the presence of **1** under hypotonic conditions (4 ˚C for 40 min). Pores are subsequently resealed by direct addition of high salt followed by incubation at 37 ºC for 20 min.

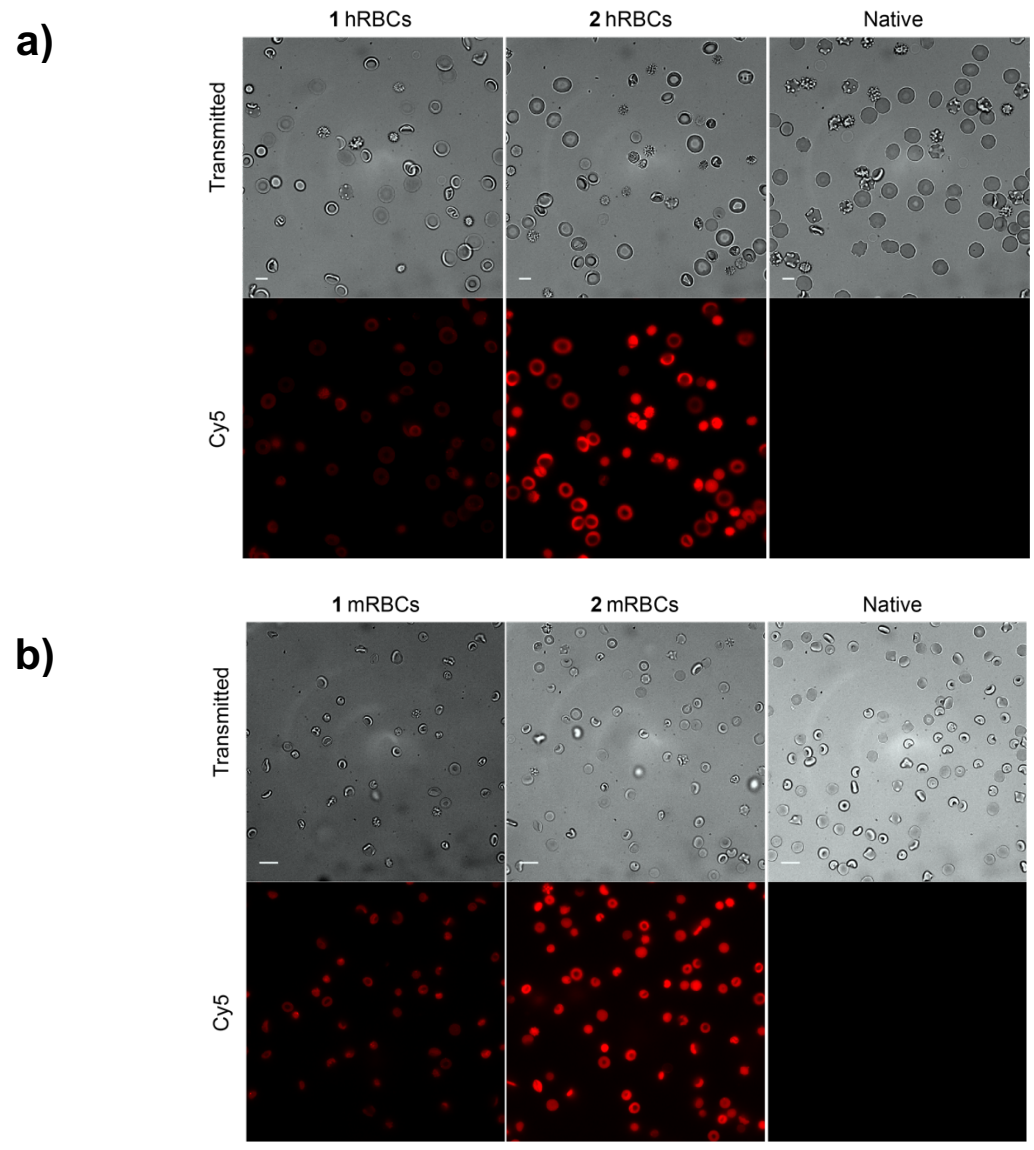

Figure 3.3 Widefield images of loaded RBCs. a) Transmitted (top) and fluorescent Cy5 (bottom) images of internally loaded hRBCs containing **1** or **2**, as well as native hRBCs. Scale bar represents 10 μm. **b)** Transmitted (top) and fluorescent Cy5 (bottom) images of internally loaded mRBCs containing **1** or **2**, as well as native mRBCs. Scale bar represents 10 μm.

The overwhelming majority of RBC drug loading studies have been performed with human erythrocytes (hRBCs). Although loading conditions are well established for hRBCs, mouse RBCs (mRBCs) are less stable than their human counterparts.[10] We found that modification of the established loading protocol improves the stability of the loaded mRBCs.[18-20] Key optimized parameters include lengthening the drug loading and membrane resealing times, the high salt addition to return the RBCs to an isotonic environment, and the presence of ATP (**Figure 3.4**).[21]

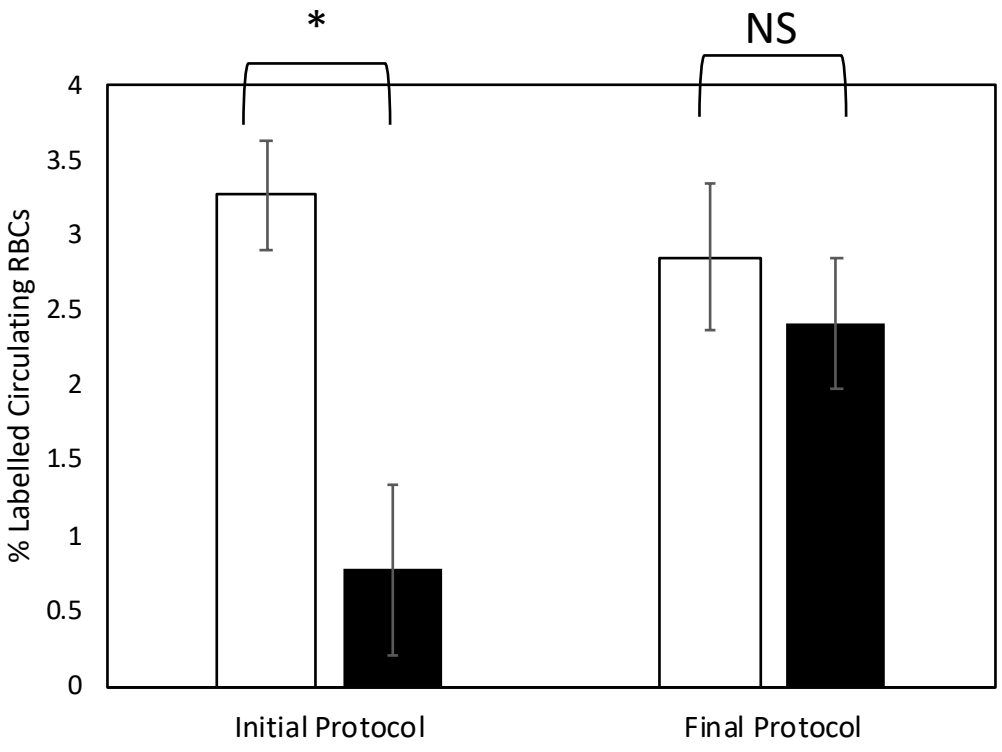

Figure 3.4 ***In vivo*** **circulation of mRBCs** containing **2** (black bars) after 1 h loaded by the initial protocol (hRBC protocol used with mRBCs) and final optimized protocol as compared to control DiI mRBCs (white bars). (n = 3, *P < 0.005)

3.4 *In vitro* Characterization of Cy5-Cbl-Dex RBCs

3.4.1 Morphology and Properties of Cy5-Cbl-Dex RBCs

We characterized both hRBCs and mRBCs loaded with **1** or **2**, including volume and hemoglobin content of the loaded RBCs, cellular distribution of the phototherapeutic, as well as loading homogeneity and quantity of Dex in loaded RBCs. These studies include an examination of native (isolated but unmodified) RBCs, RBCs loaded with **1** or **2**, and RBCs surface modified with the lipidated indocarbocyanine fluorophore DiI (1, 1'-dioctadecyl-3, 3, 3', 3'-tetramethylindocarbocyanine perchlorate; λ_{ex} 550 nm, λ_{em} 570 nm). The DiI loaded cells have been used as a control circulation population and thus are a useful comparison for in vivo studies of internally loaded RBCs.[22] The DiI loaded cells represent a population of RBCs that have undergone a loading procedure (external loading with DiI), but this procedure does not open pores in the membranes of the RBCs, nor does it affect their internal contents. The mean cell volume (MCV), mean cell hemoglobin (MCH), and mean cell hemoglobin concentration (MCHC) of both hRBCs and mRBCs were assessed by automated hemocytometry (**Table 3-1**).[23]

RBCs internally loaded with **1** or **2** are smaller and contain less hemoglobin on average than native RBCs, while RBCs that are externally loaded with DiI display values similar to native RBCs (**Table 3-1**). Trends are comparable for both mRBCs and hRBCs, consistent with the notion that opening and resealing RBCs results in the loss of some of the intracellular contents. In addition, although the recovery of hRBCs following loading is essentially quantitative, a significantly lower recovery was obtained for mRBCs. These results are consistent with the observation that hRBCs are more stable, under ex vivo conditions, than their murine counterparts.[10]

Table 3-1 Automated hemocytometry measurements of *in vitro* properties of human and mouse RBCs. (Data presented as mean ± SD, *n* = 3)

Properties	Native[a)]	DiI[a)]	**1**[a)]	**2**[a)]	Native[b)]	DiI[b)]	**1**[b)]	**2**[b)]
MCV [fl]	98 ± 5	100 ± 1	70 ± 7	76 ± 5	34 ± 1	36 ± 3	29 ± 3	33 ± 4
MCH [pg]	28 ± 2	30 ± 1	18 ± 1	21 ± 2	13 ± 1	14 ± 1	8 ± 1	8 ± 1
MCHC [g/dL]	29 ± 1	30 ± 1	25 ± 3	28 ± 2	38 ± 1	40 ± 1	27 ± 4	23 ± 1
Cell recovery after loading	NA	100%	100%	100%	NA	100%	25-50%	25-50%

[a)] human RBCs; [b)] mouse RBCs

Imaging flow cytometry was used to qualitatively visualize the various RBC populations and to quantitively assess changes in diameter and granularity (side light scattering) (see section 3.8.2). RBCs loaded with **1** or **2** are visually comparable to DiI and native controls (**Figure 3.5**). However, RBCs containing either **1** or **2** exhibit a decrease in both size (diameter) and granularity compared to native or DiI loaded RBCs (**Figure 3.6**). The decrease in diameter of internally loaded RBCs is consistent with hemocytometry MCV analysis and suggests that loss of some of the hemoglobin during the drug loading process is responsible for the smaller cell size. Granularity is commonly related to the internal complexity (microparticles) of the cell. Since RBCs are presumed to have a relatively homogenous refractive index,[24] this implies that the refractive index is altered upon the partial replacement of hemoglobin with the Cbl conjugates **1** or **2**.

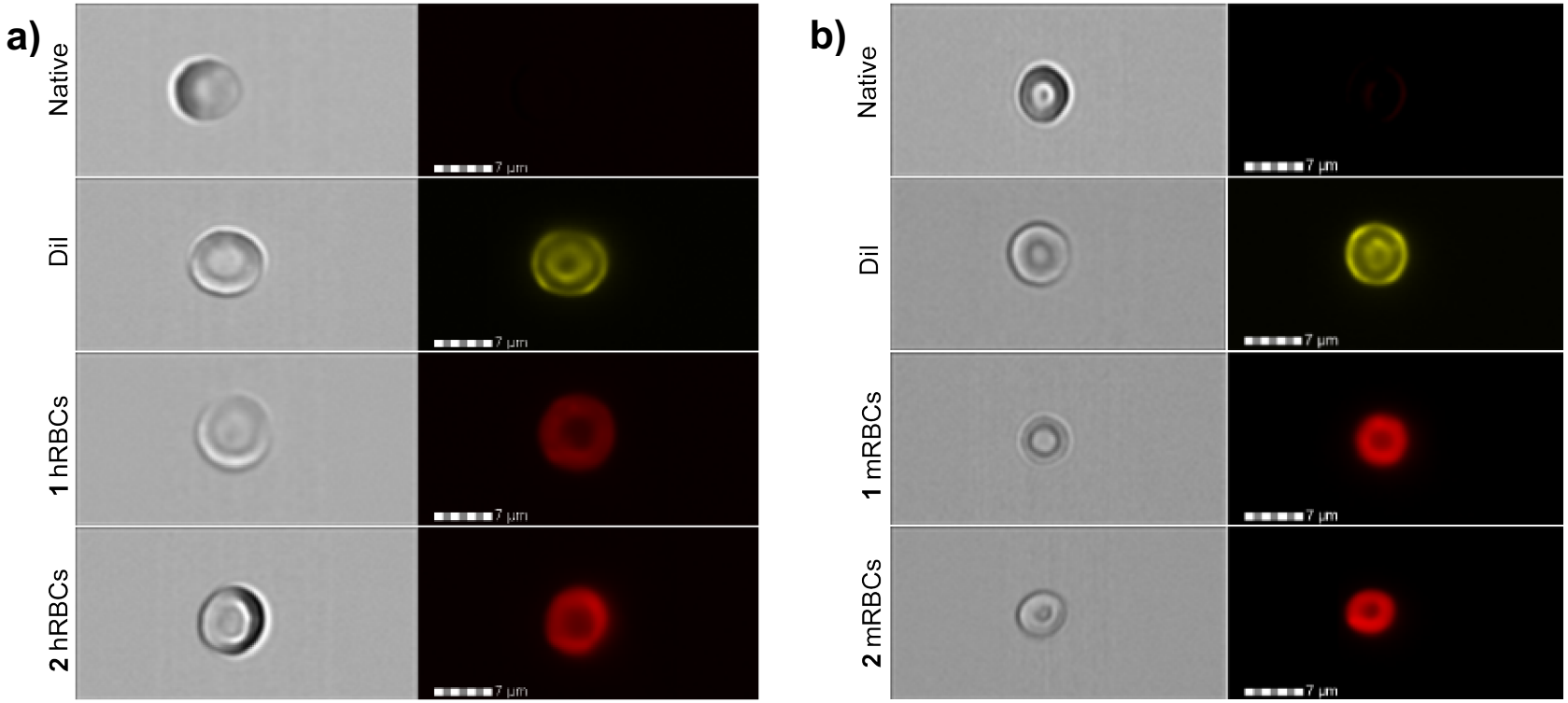

Figure 3.5 Characterization of native and loaded RBCs by imaging flow cytometry. Brightfield images (left) and fluorescent images (right) of native, surface loaded (DiI), and internally loaded (**1**, **2**) RBCs. Scale bar represents 7 µm. **a)** Flow images of hRBCs. **b)** Flow images of mRBCs.

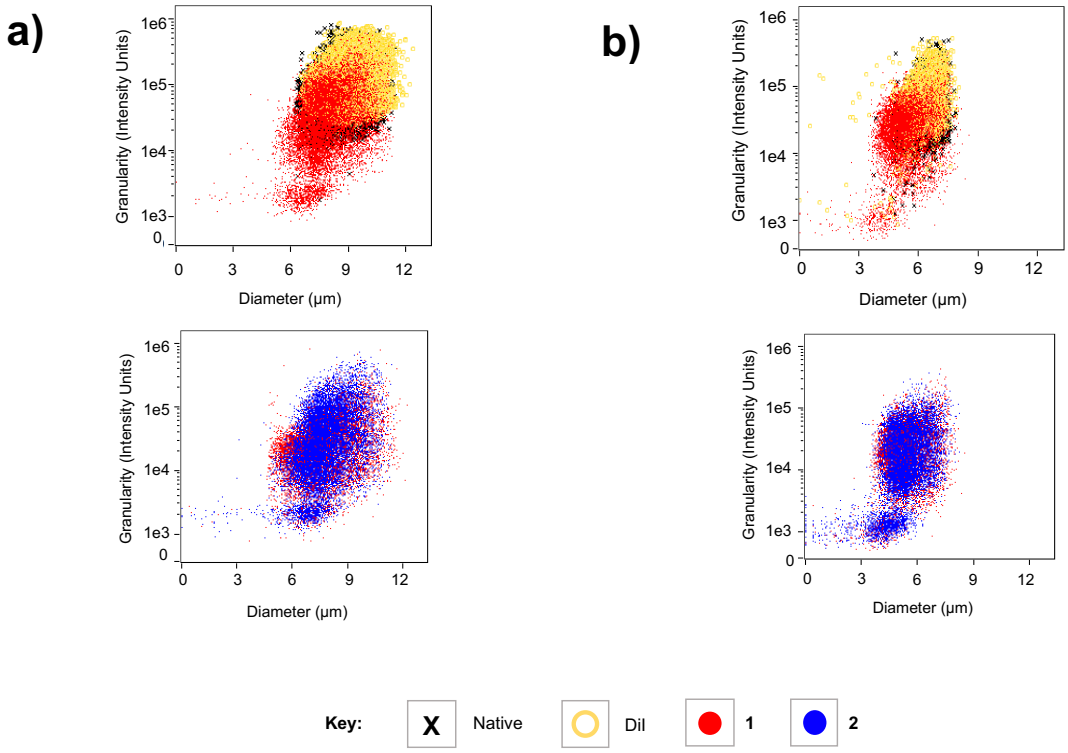

Figure 3.6 Characterization of native and loaded RBCs by flow cytometry diameter versus granularity dot plots. **a)** Plot of granularity versus diameter of loaded hRBCs. hRBCs loaded with **1** (red) display a greater variability in granularity compared to DiI (yellow) and native hRBCs (black x) (top). hRBCs loaded with **2** (blue) exhibit morphological changes comparable to those displayed by hRBCs containing **1** (red) (bottom). **b)** Plot of granularity versus diameter of loaded mRBCs. mRBCs loaded with **1** (red) display a greater variability in granularity compared to DiI (yellow) and native mRBCs (black x) (top). mRBCs loaded with **2** (blue) exhibit morphological changes comparable to those displayed by mRBCs containing **1** (red) (bottom).

We also assessed the uniformity of drug loading in RBCs as well as quantifying the amount of Dex loaded. Fluorescent imaging flow cytometry revealed a uniform peak of loaded **1** and slightly less uniform **2** in hRBCs and mRBCs (**Figure 3.7**). The amount of Cy5-Cbl-Dex and Cy5-Cbl-H_2O loaded was quantified by ethanol extraction of loaded RBC pellets and subsequent measurement of the absorbance of Cy5 at 649 nm (see section 3.8.2). mRBCs contain 0.4 mg Dex/100 µL of mRBCs while their human counterparts possess a comparable 0.5 mg Dex/100 µL of hRBCs.

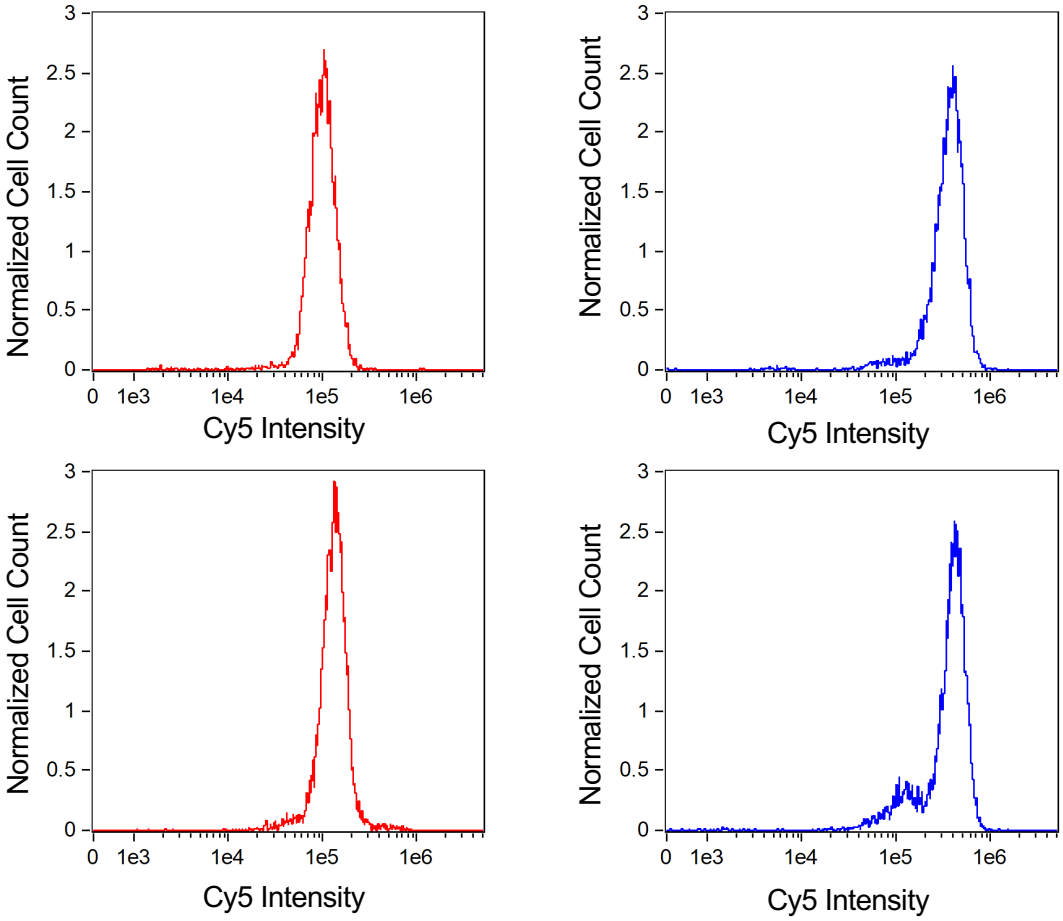

Figure 3.7 ImageStream flow cytometry representative fluorescence histograms of RBCs containing **1** (red) and **2** (blue): loaded hRBCs (top row) and mRBCs (bottom row).

3.4.2 Photolysis of Dex from Cbl-Dex hRBCs

We subsequently examined the light-triggered release of Dex from loaded hRBCs. Given that the phototherapeutic is designed to respond to 645 nm photons, which penetrates tissue to greater depths than shorter wavelengths, we explored Dex release in the presence of the Fitzpatrick series of tissue phantoms. The latter are devised to mimic the tissue absorbing properties of human skin color, from lightly to heavily pigmented.[25] The photo-release of Dex from hRBCs containing **1** was quantified by LC-MS (see section 3.8.3). Furthermore, following treatment, the RBC-containing solution was centrifuged and the presence of free Dex examined in both the pellet and the supernatant. We did not detect free Dex in the absence of 645 nm illumination (**Figure 3.8a**). By contrast, 5 min exposure to 645 nm light generated the vast majority (90 ± 5.8%) of free Dex in the supernatant, consistent with the notion that Dex, once released from the membrane impermeable Cbl, is free to diffuse out of the RBC (**Figure 3.8a**).

We also examined the photolysis of **1** filtered through Fitzpatrick skin phantom solutions in order to mimic tissue absorption and scattering of light (**Figure 3.8b,c**).[26] The phantoms employed are designed to reproduce the properties of light (Type I-II; [melanin] = 8.8 μg/mL), brown (Type III-IV; [melanin] = 66 μg/mL), and dark (Type V-VI; [melanin] = 130 μg/mL) skin.[26] Illumination (510 nm) through the Fitzpatrick phantoms fails to produce significant photolysis of a buffered solution of Cbl-Dex (see section 3.8.1). Nearly 90% of Cbl-Dex is unphotolyzed upon 6 min of illumination in the presence of type I/II Fitzpatrick phantom (**Figure 3.8b**). As expected, tissue phantoms containing greater melanin concentrations are even more effective at blocking photolysis. By contrast, analogous experiments performed at 645 nm with **1** results in nearly complete photolysis after only 3 min (**Figure 3.8c**). Finally, we examined the photorelease (645 nm) of Dex from hRBCs containing **1** in the presence of the tissue phantoms (**Figure 3.8d**). Reassuringly, illumination triggers the rapid photolysis of **1** and subsequent release of Dex from RBCs.

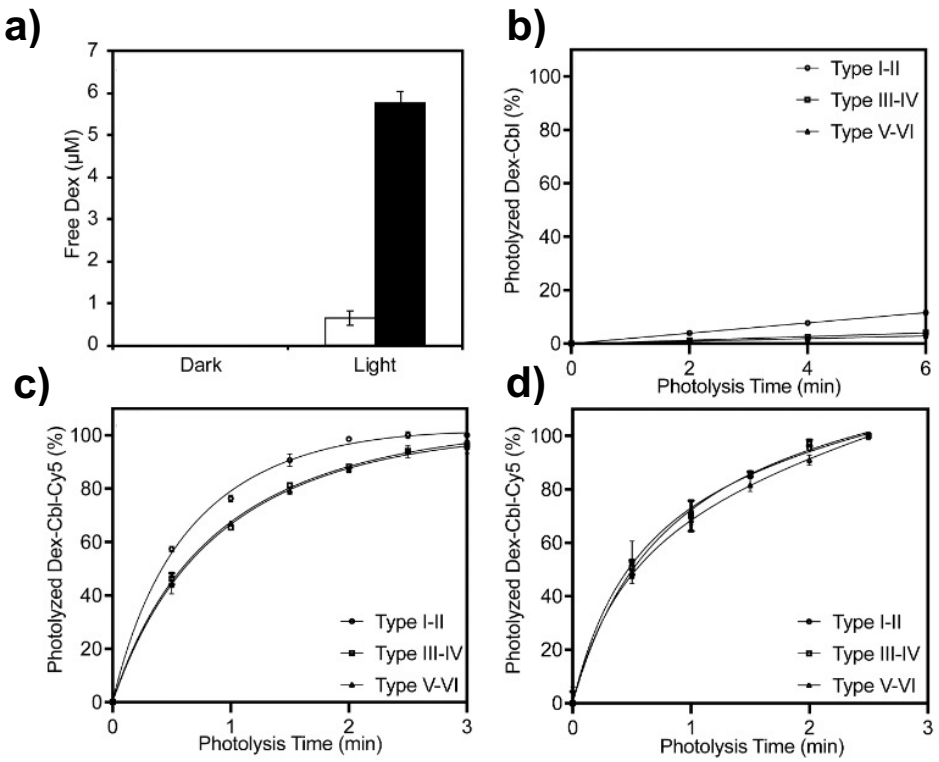

Figure 3.8 Photolysis of Cbl-Dex derivatives and release from hRBCs. **a)** hRBCs containing **1** were kept in the dark or exposed to 645 nm light for 5 min. Following illumination, the RBCs were centrifuged and the presence of free Dex in the supernatant (white bars) and pellet (black bars) quantified via LC-MS. Free Dex is not detected in the absence of illumination whereas, upon illumination, 90 ± 5.8% of free Dex is present in the supernatant. **b)** Illumination (510 nm) of Cbl-Dex in solution in the presence of Fitzpatrick phantom solutions: light (Type I/II, circle), brown (Type III/IV, square), and dark skin (Type V/VI, triangle). **c)** Illumination (645 nm) of **1** in solution in the presence of Fitzpatrick phantom solutions. **d)** Illumination (645 nm) of **1** in hRBCs in the presence of Fitzpatrick phantom solutions. All samples were illuminated with a light intensity of 1.0 mW/cm^2 for up to 6 min.

3.4.3 Impact of Photoreleased Dex from Cy5-Cbl-Dex hRBCs on Human Cells

Our initial studies on the potential therapeutic efficacy of photoactivatable Dex were performed on a variety of cultured human cells. Dex mediates its therapeutic action via the glucocorticoid receptor α (GRα), which is normally found in the cytoplasm but localizes to the nucleus in response to glucocorticoid binding.[27] Upon entry into the nucleus, GRα associates with glucocorticoid responsive elements and stimulates or represses target gene expression.[27, 28] We assessed the ability of Dex, photoreleased from RBCs bearing **1**, to trigger GRα in HeLa cells and primary fibroblast-like synoviocytes (FLS). HeLa cells were used as a model cell line due to their established sensitivity to conventional Dex (**Figure 3.9**).[29] In contrast, FLS are non-immune cells that have been demonstrated to participate in rheumatoid arthritis (RA) pathogenesis. The FLS employed in this study were collected and cultured from RA patients.

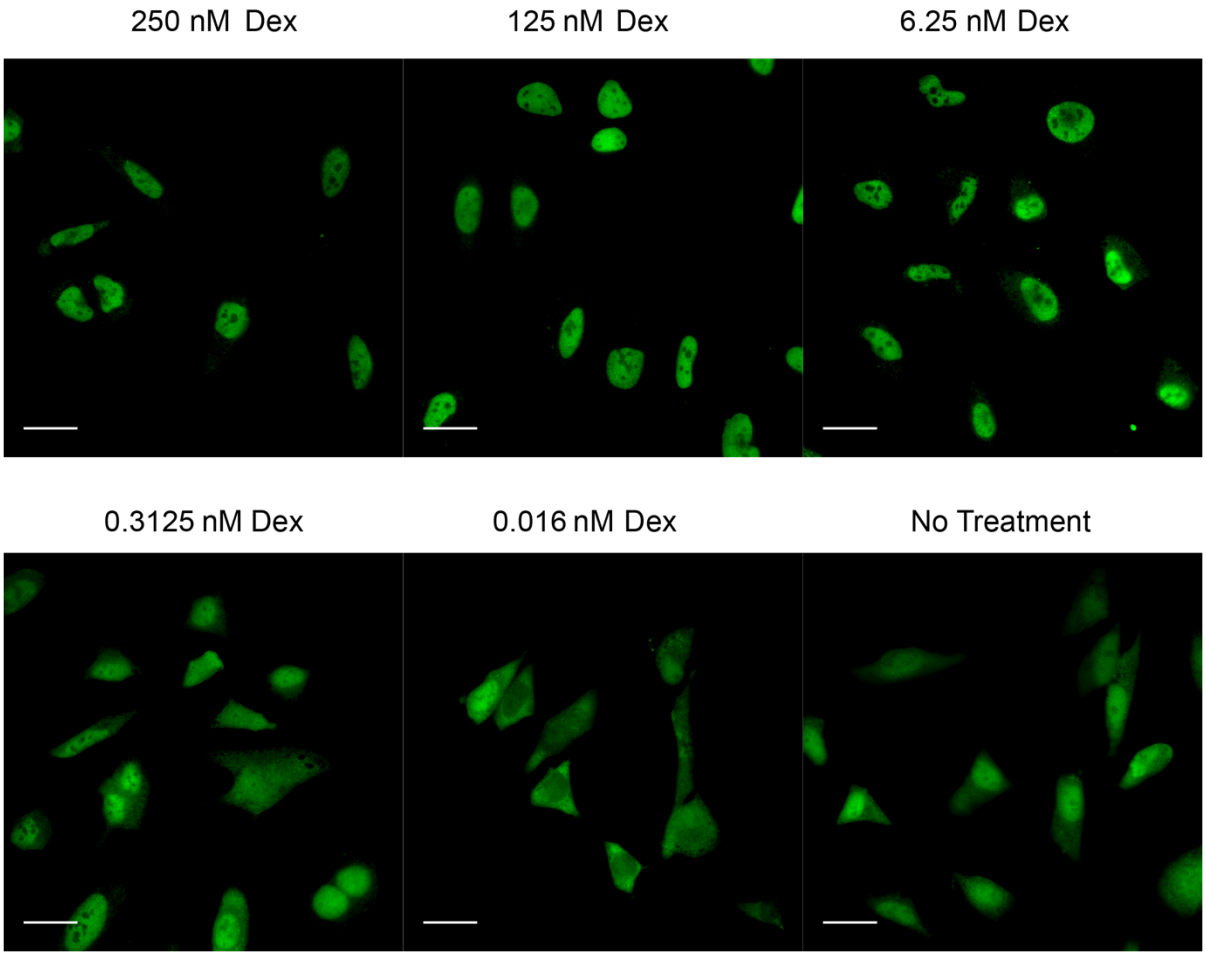

Figure 3.9 Immunohistological analysis of HeLa cells responding to a gradient of Dex concentrations. Labeled with 488 anti-GRα. Scale bars represent 30 μm.

Both HeLa and FLS cells were exposed to hRBCs bearing **1** in the dark and at 660 nm. In addition, RBCs containing **2** (i.e., no Dex) was used as a negative control and Dex itself was employed as a positive control. HeLa cells respond in a manner consistent with literature precedent (**Figure 3.10**).[29] In the absence of 660 nm exposure, GRα is primarily retained in the cytoplasm in untreated HeLa cells and in cells co-incubated with hRBCs containing either **1** or **2**. By contrast, robust GRα nuclear localization is clear in Dex exposed HeLa cells. Analogous experiments were performed in the presence of 660 nm light. Untreated HeLa cells, as well as those co-incubated with hRBCs containing **2** (negative control), fail to display a nuclear GRα migration. However, hRBCs loaded with **1** trigger the anticipated GRα migration in a fashion consistent with that observed with the parent glucocorticoid. These experiments were recapitulated using primary FLS cells from RA patients (**Figure 3.11**). We do note that FLS cells are phenotypically heterogeneous and do not display the near 100% uniform GRα nuclear migration observed with HeLa cells. However, both 660 nm-exposed hRBCs bearing **1**, and Dex itself, trigger the same degree of GRα relocation in FLS cells (**Figure 3.12**).

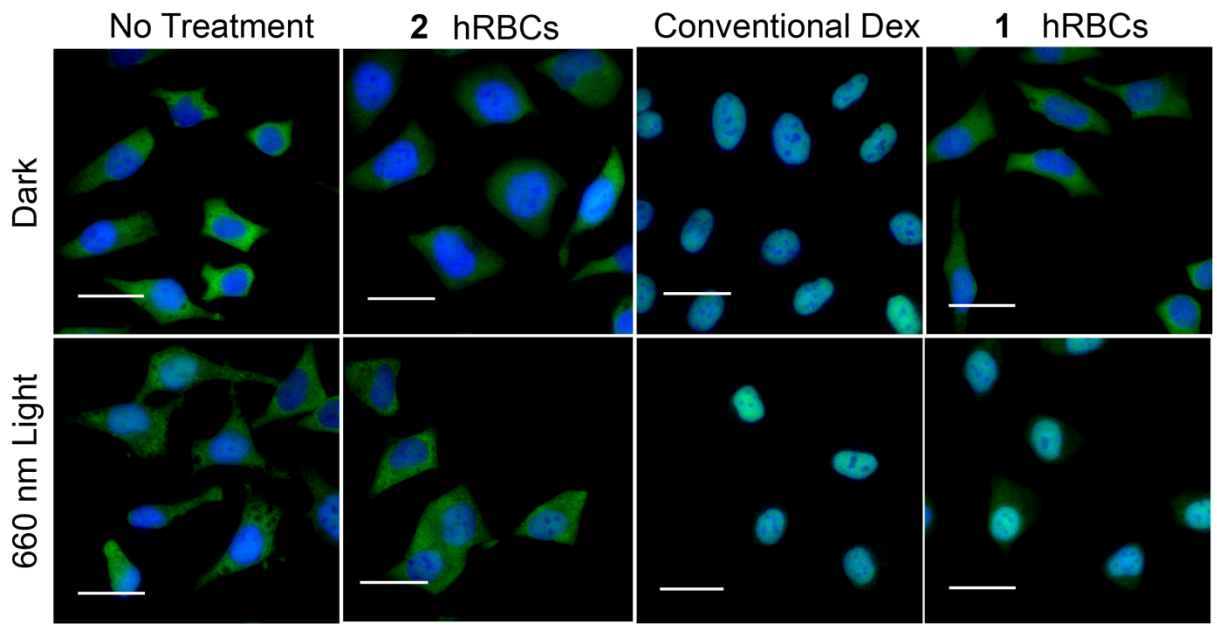

Figure 3.10 Immunocytochemical analysis of GRα nuclear localization in HeLa cells. HeLa cells were cultured in serum free media for 24 h and then left untreated (column 1), exposed to hRBCs containing **2** (column 2), Dex (250 nM) (column 3), or hRBCs containing **1** (column 4) in the absence (row 1) or presence of 660 nm light (row 2). Cells were fixed and permeabilized, exposed to anti-GRα, and subsequently anti-rabbit secondary antibodies conjugated to Alexa Fluor 488 (green). Cells were also labeled with the nuclear Hoechst 33342 stain (blue). Images display merged green and blue channels where scale bars represent 30 μm (Representative 1 of 5).

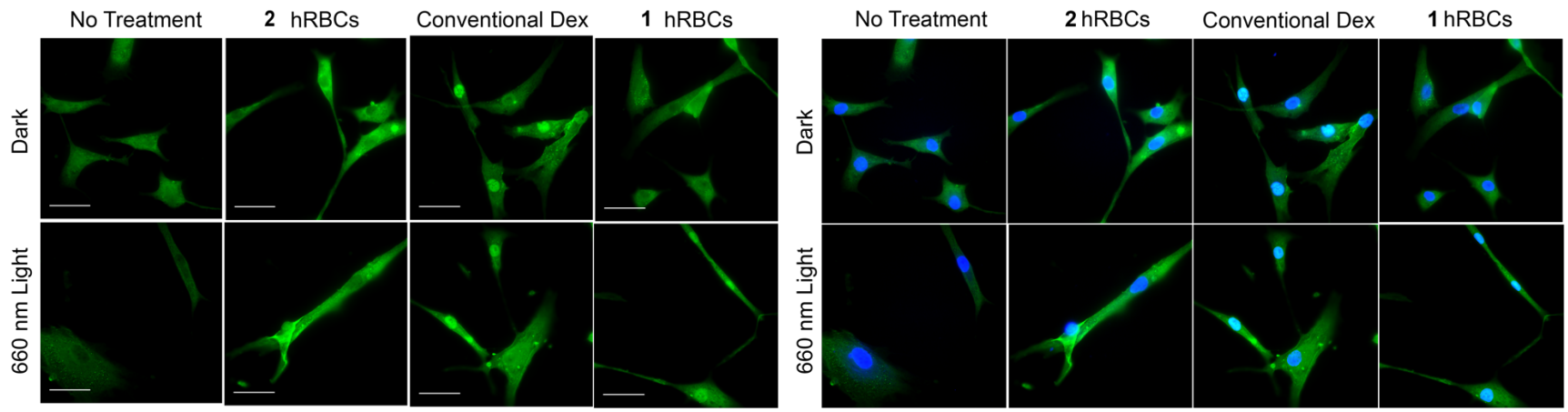

Figure 3.11 Immunocytochemical analysis of GRα nuclear localization in FLS cells. FLS cells were left untreated (column 1), exposed to hRBCs containing **2** (column 2), Dex (250 nM; column 3), or hRBCs containing **1** (column 4) in the absence (row 1) or presence of 660 nm light (row 2). Cells were fixed and permeabilized, exposed to anti-GRα, and subsequently anti-rabbit secondary antibodies conjugated to Alexa Fluor 488 (green; left). Cells were also labeled with the nuclear Hoechst 33342 stain (blue; composite; right).

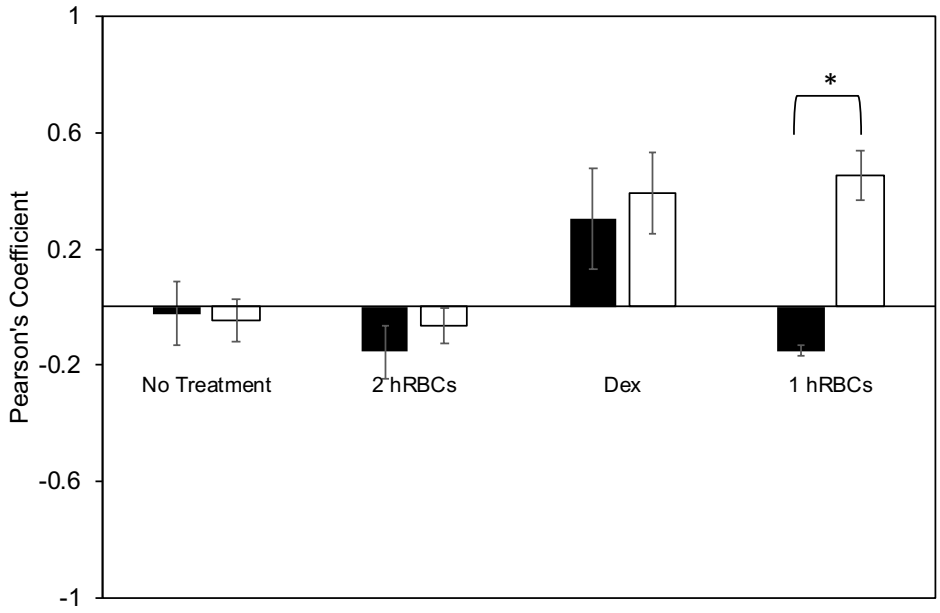

Figure 3.12 Pearson's coefficient quantification of co-localization in anti-GRα and Hoechst stained primary FLS cells. -1 represents anti-localization while 1 represents complete co-localization. GRα is not nuclear localized in FLS cells exposed to hRBCs loaded with **1** (Cy5-Cbl-Dex) in the dark (black bar), whereas GRα is nuclear localized under identical conditions upon illumination at 660 nm (white bar). (n = 4, *P < 0.0005)

Glucocorticoids are known to induce apoptosis in certain cell types, which has been shown to serve as both a mechanism of action for anti-inflammatory effects as well as a contributor to certain negative side effects (such as osteoporosis).[27] With this in mind, we examined the impact that free Dex, or hRBCs containing **1** or **2**, on Dex resistant and sensitive cells (see section 3.8.4). FLS cells experience minimal growth inhibition in response to treatment with Dex (**Figure 3.13a**). The viability of FLS cells is likewise minimally impacted upon exposure to illuminated hRBCs bearing either **1** or **2** (**Figure 3.13b**)**.** However, unlike synoviocytes, B cells are known to be sensitive to Dex (**Figure 3.13a**).[30, 31] We examined the effect of hRBCs loaded with either **1** or **2**, in the presence of 660 nm light, on Sup-B15 lymphoma B cell viability. As expected, both Dex photo-released from Cy5-Cbl-Dex hRBCs, as well as the parent drug (Dex), impact B cell viability (**Figure 3.13b**). These results suggest that Dex, delivered to the site of inflammation, should reduce the localized immune response responsible for symptoms associated with arthritis. Furthermore, since synoviocytes play a key role in producing extracellular components of the synovial fluid, it is reassuring that the photorelease of Dex from RBCs does not impact FLS viability.

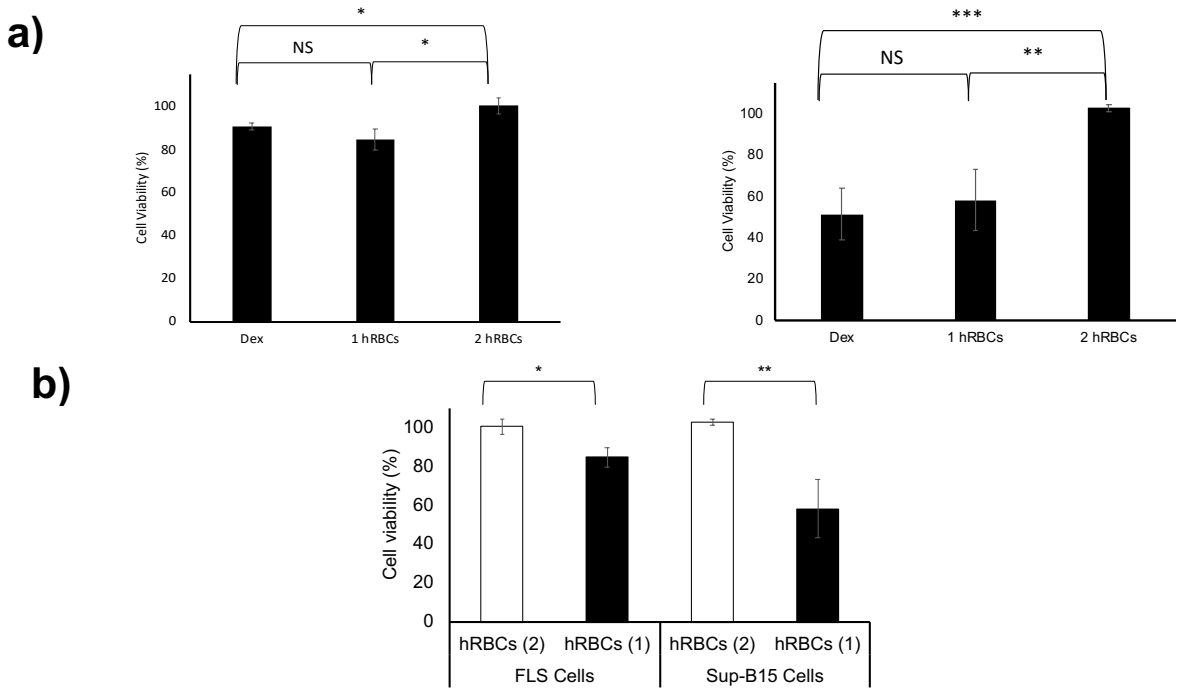

Figure 3.13 Viability of cells exposed to Dex and Cbl-RBCs. a) Viability of FLS cells at a density of 5,000 cells/cm^2 (left). FLS cells display a comparable, yet minimal, response to Dex (2 mM) and **1** hRBCs (Cy5-Cbl-Dex) illuminated at 660 nm (30 min). By contrast, the viability of FLS cells is not impacted by **2** hRBCs (Cy5-Cbl-H_2O) in the presence of 660 nm. Viability of Sup-B15 cells in the presence of Dex (2 mM), **1** hRBCs, and **2** hRBCs following 30 min of 660 nm illumination (right). The toxicity of illuminated **1** hRBCs (Cy5-Cbl-Dex) is similar to that of 2 mM Dex, thereby demonstrating that both treatments have an analogous effect. By contrast, 660 nm exposed **2** hRBCs have no cytotoxic effect on Sup-B15 cells, indicating that the cytotoxic effect is Dex-dependent. (n = 3, *P < 0.05, **P < 0.01, ***P < 0.005, NS = not significant). **b)** The effect of 660 nm illuminated hRBCs loaded with **1** or **2** on the viability of FLS and Sup-B15 B cells. hRBC treatments with **1** have a minimal impact on FLS cell viability, but a more substantial effect on Sup-B15 cells (n = 3, *P < 0.05, **P < 0.01).

3.5 *In vivo* ADME of Cbl-Dex Red Blood Cells

The circulatory integrity of modified RBCs was examined with a 1:1 mixture of two mRBC populations: (i) internally loaded with Cy5-Cbl-H_2O (**2**) and (ii) externally loaded with DiI (**Figure 3.14a**). A mixture of the two populations were tail vein injected into mice and a blood sample was subsequently acquired after 20 min. Flow cytometry revealed that both cell types constitute approximately 3% of all circulating RBCs. Subsequent blood sampling after 1 h revealed minimal loss of circulating modified RBCs. These results indicate that the loaded mRBCs were circulating during illumination.

The distribution of mRBCs loaded with **1** in the kidneys, liver, and spleen of treated animals at 0 min, 30 min, and 24 h was visualized via histology (**Figure 3.14b,c**). Damaged RBCs are predominantly cleared by the spleen, which filters the blood through cords. Aged or damaged RBCs which have stiffer membranes cannot pass through these cords and are then cleared by splenic macrophages.[32] Evidence of intracellular Cy5 RBCs in the blood (**Figure 3.14a**) and within the red pulp of the spleen after was observed 30 min and 24 h (**Figure 3.14b,c**). Cy5 was also present in the liver and renal tubules after 24 h (**Figure 3.14d**) suggesting hepatic clearance and urinary excretion of freed Cy5-Cbl, respectively. Mice from preliminary studies of 90% hematocrit Cy5-Cbl-Dex injections micturated blue urine further supporting urinary excretion of freed Cy5-Cbl.

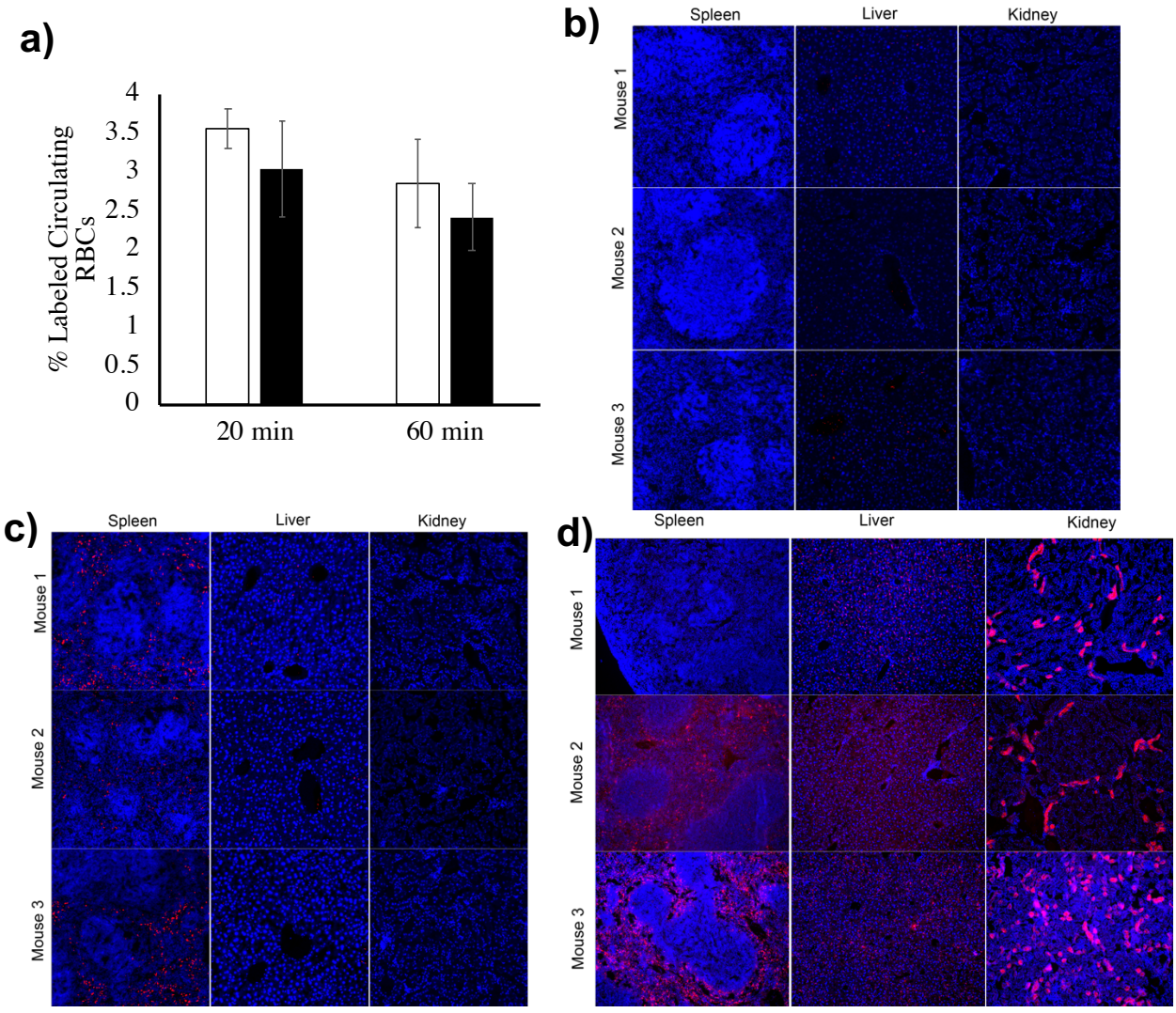

Figure 3.14 Circulatory Integrity of Modified mRBCs. a) Percent of loaded mRBCs circulating in mice (*n* = 3) at 20 min and 60 min. **b)** and **c)** RBCs containing **1** are not noticeably cleared in the liver or kidney within the first 0 (b) or 30 min (c). **d)** Renal histopathology shows evidence of extracellular Cy5 in the renal tubules, suggesting urinary excretion from the body after 24 h.

3.6 *In vivo* Photoactivated Treatment of Collagen Antibody-Induced Arthritis in a Mouse Model

The phototherapeutic efficacy of mRBCs containing **1** was evaluated using the collagen-antibody induced arthritis (CAIA) mouse model. CAIA is an accepted animal model of inflammatory arthritis in general and of RA in particular.[33-36] CAIA shares several features with human RA, including a dependence on inflammatory mononuclear cells in acute inflammation, the presence of anti-collagen antibodies during disease expression, and joint erosion in end-stage disease.[37] Particular advantages to the CAIA model include its rapid onset and highly consistent penetrance of disease with minimal inter-experimental variability.[38]

In brief, CAIA was induced by an intraperitoneal (i.p.) injection of arthrogenic mAb 5-clone cocktail into DBA1/J mice on day 0 followed by i.p. injection of lipopolysaccharide (LPS) on day 2 according to manufacturer instructions. Arthritis was measured daily by a blinded observer using a clinical disease score index 0 – 4, where 0 = normal paw; 1 = mild but definite swelling of the ankle or digits; 2 = moderate redness and swelling of an ankle ± any number of digits; 3 = moderate redness and swelling of the entire paw; and 4 = maximal redness and swelling of the entire paw and digits, with or without ankylosis.[39] CAIA mice were tail vein injected with a 90% hematocrit of allogenic, strain-specific quality controlled mRBCs containing **1** or **2** (negative control). A single arthritic paw was illuminated with a 3 mW 635 nm laser for 5 min (see section 3.8.6). In addition, a positive control treatment group was treated with (0.5 mg/kg) dexamethasone sodium phosphate i.p. (“IP Dex”). Within 24 h following treatment, only mice exposed to mRBCs containing **1**, with illumination of the inflamed paw, displayed statistically diminished arthritic severity relative to animals treated with mRBCs containing **2** (P = 0.01*)*. By contrast, there is no statistical difference in arthritic severity of laser treated paws of animals receiving IP Dex at 24 h compared to inactive control **2** mRBC treatment (**Figure 3.15a**). If clinical paw swelling was still present in an IP Dex-treated mouse, IP Dex treatment was continued until clinical remission was

achieved. Thus, IP Dex mice received between one to four doses of steroid, depending on persisting severity of disease (**Figure 3.15b**). Specifically, on the second day of treatment, 8 of 11 IP Dex mice had clinical inflammation and were treated with a second dose of IP Dex. Similarly, mice treated with photoresponsive **1** or **2** mRBCs continued to receive daily laser treatments on the arthritic paw until clinical inflammation was resolved or study end. All mice were terminated after 4 days of treatment for all groups. The disease curves of both serially dosed IP Dex and serially lasered mRBCs containing **1** achieve statistical difference in arthritis severity when compared to the serially lasered inactive **2** mRBCs control (P = 0.0001 and P = 0.0002 respectively) and are comparable to each other (P = 0.9). 78% less Dex was administered in the single **1** mRBC treatment dose with serial laser treatments as compared to the average IP Dex treatments required to achieve comparable remission (**Figure 3.15c**).

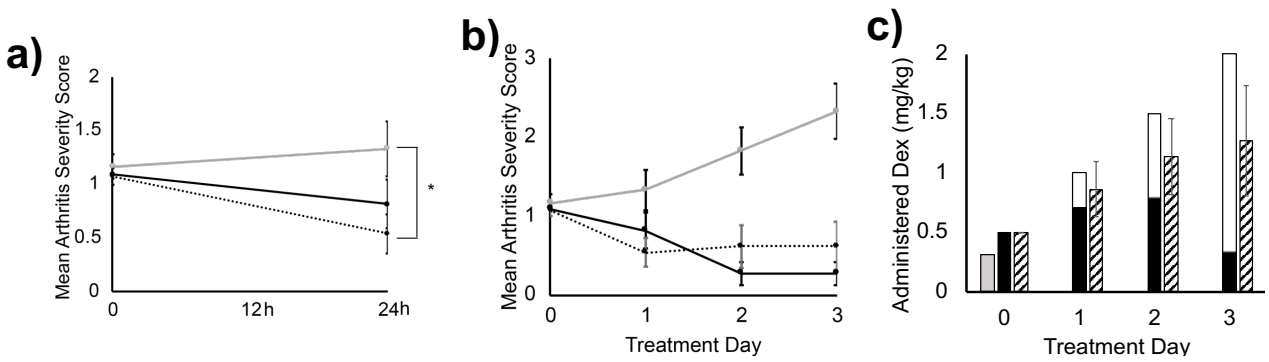

Figure 3.15 Light stimulated Dex treatment of CAIA mice. a) There is significantly less inflammation (*P = 0.01) in mice treated with RBCs containing **1** (dotted line) than mice exposed to RBCs loaded with **2** (gray line) after the first 24 h of treatment. IP Dex serves as a positive treatment control (black line), but does not achieve a statistically significant improvement at 24 h. **b)** Mice treated with mRBCs loaded with **1** and illuminated daily (dotted line, n = 13, P = 0.0002) continued to maintain remission of inflammation while arthritis in IP Dex treated mice (black line, n = 11, P = 0.0001) continued to improve after 1 - 4 injections, depending on the persisting severity in the arthritic paw. Both treatments are significantly different over time when compared to the illuminated daily inactive control (**2**) loaded mRBCs which continued to worsen (gray line, n = 12), despite daily laser treatment, but are comparable to each other (P = 0.9). **c)** Administered Dex from loaded mRBCs (gray, n = 13) compared to average IP Dex (hatched, n = 11). Shaded bars furnish the ratio of mice that received additional doses (black) of IP Dex over the treatment course to achieve remission and the total dose received. Mice treated with **1** loaded mRBCs only required 1 intravenous infusion on day 0 followed by daily illumination of the arthritic paw to achieve remission of inflammation (gray). Mice treated with **1** mRBCs received 78% less Dex (mg/kg) than mice treated with IP Dex to achieve similar clinical remission of inflammation (P < 0.0001).

3.7 Conclusion

Arthritis therapies are constrained by (1) the failure to deliver sufficient quantities of drug to the inflamed site to achieve the desired therapeutic effect, (2) the range of moderate to severe side effects associated with long-term systemic exposure, and (3) the inability of the patient to self-administer therapeutics in a site-targeted as-needed fashion. There is a compelling biomedical need to develop a technology to address these issues, especially given the chronic nature and prevalence of arthritis, the capricious acute episodes of pain and inflammation, and different disease subtypes of arthritis that affect a broad swath of the population. We have developed a light activation strategy that triggers the delivery of the anti-inflammatory agent, Dex, in a site-specific fashion. RBCs conveying the photoactivatable therapeutic offer the means to employ the circulatory system as a drug depot, which offers the opportunity to target inflamed diseased sites in a patient-directed fashion. We have shown that RBCs harboring the phototherapeutic agent display properties similar to those of native and surface labelled erythrocytes. Furthermore, given the long wavelength responsiveness of the carrier system, drug release is efficiently triggered through tissue phantoms that mimic the entire range of pale to dark skin types. Finally, we have demonstrated that the RBC-conveyed photo-anti-inflammatory agent not only induces the desired reduction in inflammation but does so at a dose that is significantly lower than the standard of care for the parent drug.

3.8 Supporting Information, Figures, and Methods

Chemicals and Materials

All chemical reagents were purchased from suppliers as noted below and used as received. Spectra/ Por 1 kDa dialysis tubing, Fisher Bioreagents 10X PBS, Gibco DMEM, Vybrant DiI, and Enzymax LLC mini-spin columns were purchased from Thermo Fisher Scientific (Waltham, MA). Ficoll-Paque Premium 1.084, Absolute ethanol, dexamethasone, and fetal bovine serum were purchased from MilliporeSigma (St. Louis, MO); Arthrogen-CIA 5 Clone Cocktail Kit and e. coli LPS were purchased from Chondrex (Redmond, WA, USA), dexamethasone sodium phosphate Injection from USP Mylan (IL, USA), and Isothesia Isoflurane from Henry Schein Animal (India). All water was filtered using Milli-Q Reference water purification system.

Animals

Male DBA/1J mice aged 8-10 weeks were purchased from Jackson Laboratories (Bar Harbor, ME, USA) and housed at UNC-CH or Duke University under the care of the respective institutions Division of Laboratory Animal Resources. All procedures performed were approved by the Institutional Animal Care and Use Committees of UNC-CH (#19-048.0) and Duke University Medical Center (#A185-17-08).

Cell Culture

Human fibroblast-like synoviocytes (FLS) from the Tarrant lab were previously obtained by Mainz et al.[40] Briefly, cells were collected from 6 individuals who fulfilled the American College of Rheumatology 1987 criteria for the diagnosis of RA during a synovectomy or total joint replacement.[41] FLS were de-identified and existed in a repository, thus making them exempt from IRB approval (Study #14-1569). FLS were isolated from samples and cells were grown in DMEM, 10% BCS, and 1% Penicillin Streptomycin at 37 °C under a humidified atmosphere containing

5.0% CO_2. Cells were used from the 6th to the 10th passage. Human HeLa cells were purchased from ATCC (ATCC®CLL-2™). Cells were grown in DMEM, 10% FBS, 1% Penicillin Streptomycin and 1% GlutaMAX at 37 °C under a humidified atmosphere containing 5.0% CO_2. Human Sup-B15 cells were purchased from ATCC (ATCC®CRL-1929™). Cells were grown in Iscove's Modified Dulbecco's medium, 20% FBS, 2% GlutaMAX, and 0.05 mM 2-mercaptoethanol at 37 °C under a humidified atmosphere containing 5.0% CO_2. Human RBCs stored in acid citrate dextrose were purchased from ZenBio.

3.8.1 Synthesis of Cbl Conjugates

Synthesis of Fmoc-Cbl-CN

Fmoc-Cbl-CN was synthesized per previously published protocols.[42] Briefly, cyanocobalamin (Cbl-CN, 0.5 g, 0.35 mmol) was dissolved in dry DMSO (10 mL) to form a dark red solution. To the solution was added 1,1-carbonyldiiimidazole (CDT, 1.4 mmol) to activate the 5' ribose hydroxyl group of the nucleotide loop. The solution was allowed to stir for 4 h, at which time ethylenediamine (EDA, 2.9 mmol) was added to the solution. The reaction mixture was stirred for an additional 4 h. Upon LC-MS confirmation of the formation of the desired amide bond, the solution was diluted to 50 mL with a 2:1 solution of diethyl ether:DCM, which induced precipitation of the Cbl derivative. The mixture was centrifuged for 4 min to pellet the modified Cbl, decanted, and the pellet was allowed to dry. The pellet was dissolved in dry DMF (10 mL). 9-fluorenylmethyl N-succinimidyl carbonate (Fmoc-OSu, 492 mg, 1.5 mmol) was added to the solution and stirred for 4 h. The solution was split into two 5 mL aliquots and both aliquots were diluted with diethyl ether (to 50 mL). The solutions were centrifuged to pellet the Fmoc-linker-Cbl and decanted, leaving red pellets. The pellets were allowed to dry, dissolved in MeOH (10 mL each), and re-centrifuged. Unreacted Fmoc-OSu and trace Cbl formed light pink pellets. The MeOH supernatants containing the majority of the Cbl conjugate were decanted, combined, and

diluted to 40% MeOH with DI water. A 12 g Biotage C18 column with sample was prepped with 5:95 MeOH:H_2O (0.1% TFA) and the solution was eluted using an MeOH:H_2O (0.1%TFA) gradient from 5% to 80% MeOH. Fractions were analyzed for purity via LC-MS and combined, concentrated under reduced pressure, and lyophilized to yield a powdered red solid (59.5% yield).

Synthesis of Fmoc-Cbl-Propylamine

Fmoc-Cbl-Propylamine was synthesized per previous protocols.[42] Briefly, Fmoc-Cbl-CN (0.2 mmol) was dissolved in MeOH (20 mL). NH_4Br (5% w/v, 1 g) was dissolved in the solution, and Zn (0.022 mol) was added to the solution. The solution was shaken vigorously by hand for 30 s, then placed on a shake plate for 30 min. The solution turned black, indicating reduction of Co^{+3} to Co^{+}. 3-bromopropylamine hydrobromide (0.9 mmol) was added to the solution, and it was returned to the shake plate for 4 h. The mixture was spun to pellet the Zn, then decanted. A 30 g Biotage C18 column with the orange sample was prepped with 5:95 MeOH:H_2O (0.1% TFA) and the solution was eluted using an MeOH:H_2O (0.1%TFA) gradient from 5% to 60% MeOH. Fractions were analyzed for purity via LC-MS and combined, concentrated under reduced pressure, and lyophilized to yield a powdered orange solid (45% yield).

Synthesis of Ethylenediamine-Cbl-Dex (EDA-Cbl-Dex, **Scheme 3-1**)

Succinyl-Dex[43] (0.041 mmol) was dissolved in dry DMF (5 mL) along with DIPEA (0.32 mmol) and HATU (0.047 mmol). The solution was stirred for 5 min to activate the carboxylic acid. After 5 min, Fmoc-Cbl-Propylamine (0.041 mmol) was added to the solution, and the reaction vessel was placed on a shake plate for 4 h. After 4 h, the solution was diluted with diethyl ether (to 50 mL) and spun down to pellet the product. Then the supernatant was decanted. The Fmoc-Cbl-Dex pellet was allowed to dry for 4 h, then dissolved in dry DMF (5 mL). Piperidine (0.29 mmol) was added to the solution to deprotect the Fmoc group. The solution was stirred for 4 h,

then diluted with diether ethyl (to 50 mL) to precipitate the product, which was pelleted via centrifugation. The pellet was dissolved in MeOH (10 mL) and then diluted with DI water (to 40 mL). A 12 g Biotage C18 column with sample was prepped with 5:95 MeOH:H_2O (0.1% TFA) and the solution was eluted using an MeOH:H_2O (0.1%TFA) gradient from 10% to 80% MeOH. Fractions were analyzed for purity via LC-MS (**Figure 3.16**) and combined, concentrated under reduced pressure, and lyophilized to yield a powdered orange solid. ^{1}H NMR (**Figure 3.17**; 500 MHz, MeOD) δ 9.34 (s, 1H), 7.68 (s, 1H), 7.54 (s, 1H), 7.44 (d, *J* = 10.1 Hz, 1H), 6.89 (s, 1H), 6.53 (d, *J* = 5.2 Hz, 1H), 6.31 (dd, *J* = 10.1, 1.9 Hz, 1H), 6.10 (t, *J* = 1.7 Hz, 1H), 5.05 (d, *J* = 17.7 Hz, 1H), 4.83 (s, 1H), 4.57 (d, *J* = 10.7 Hz, 1H), 4.36 – 4.22 (m, 5H), 3.93 (dd, *J* = 9.1, 5.0 Hz, 1H), 3.53 – 3.35 (m, 2H), 3.25 (dd, *J* = 13.7, 4.9 Hz, 1H), 3.14 – 3.00 (m, 3H), 2.84 – 2.75 (m, 2H), 2.77 – 2.67 (m, 1H), 2.67 – 2.54 (m, 3H), 2.54 (s, 3H), 2.53 – 2.44 (m, 10H), 2.40 (s, 1H), 2.40 – 2.28 (m, 3H), 2.25 (t, *J* = 10.0 Hz, 1H), 2.24 – 2.09 (m, 1H), 2.06 – 2.00 (m, 2H), 1.98 (d, *J* = 10.5 Hz, 2H), 1.87 (s, 3H), 1.86 – 1.70 (m, 2H), 1.68 (d, *J* = 5.4 Hz, 3H), 1.68 – 1.62 (m, 1H), 1.61 (s, 3H), 1.53 (s, 3H), 1.45 (s, 3H), 1.38 – 1.30 (m, 1H), 1.27 – 1.19 (m, 5H), 1.09 (s, 3H), 0.99 (d, *J* = 27.6 Hz, 6H), 0.88 (d, *J* = 7.2 Hz, 3H), 0.29 (dt, *J* = 10.5, 4.9 Hz, 1H), 0.14 – 0.04 (m, 1H), -0.47 (dd, *J* = 12.3, 6.9 Hz, 1H). (ESI) m/z: $[M+2H]^{2+}$ calculated for $C_{94}H_{133}CoFN_{16}O_{22}P$, 975.0; found, (ESI+, m/z) 974.5 $[M+2H]^{2+}$.

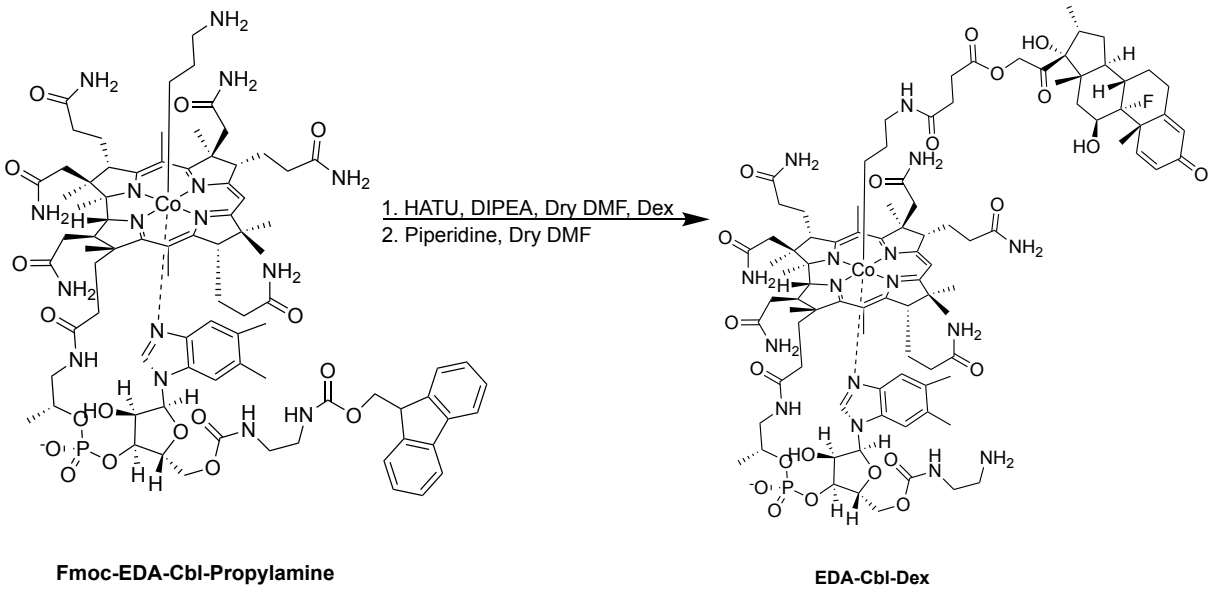

Scheme 3-1 Synthesis of EDA-Cbl-Dex.

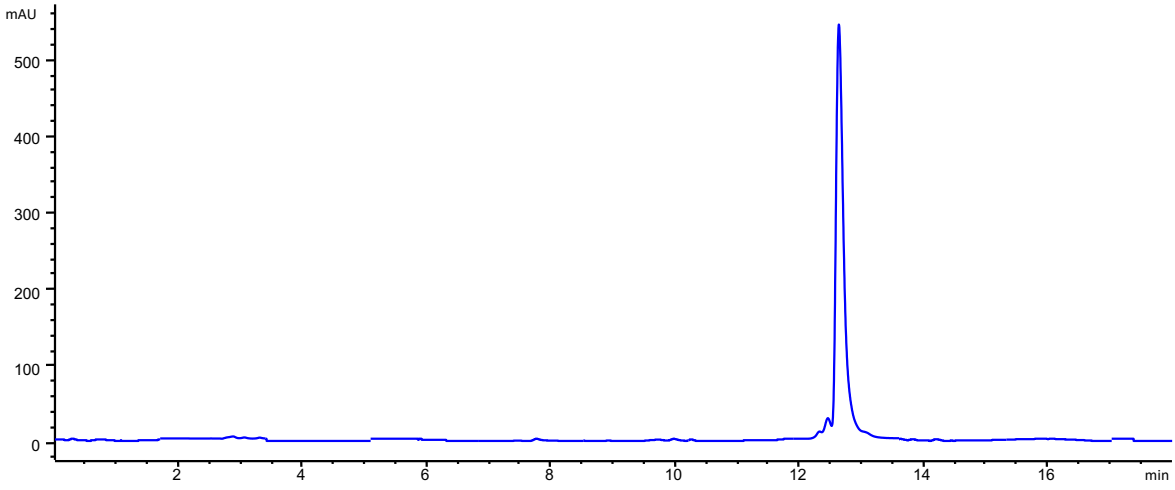

Figure 3.16 LC-MS chromatogram of purified EDA-Cbl-Dex detected by the UV detector (monitored at 360 nm).

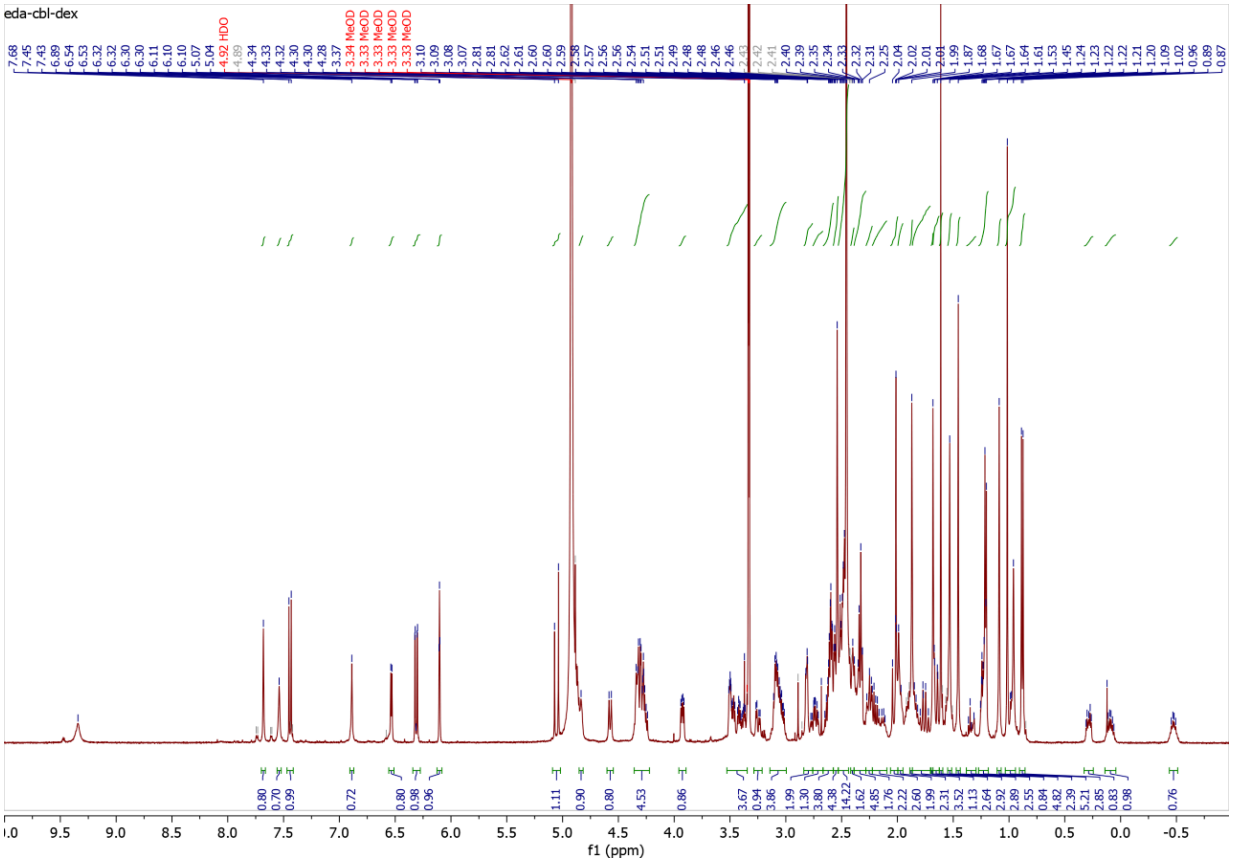

Figure 3.17 ^{1}H NMR of EDA-Cbl-Dex.

Synthesis of Cy5-Cbl-Dex (**1**, **Scheme 3-2**)

Cy5 (0.0204 g, 0.04 mmol) was dissolved in dry DMF (5 mL) creating a dark blue solution. DIPEA (0.0481 g, 0.37 mmol) and HATU (0.0113 g, 0.03 mmol) were added to solution and the reaction mixture was placed on a shake plate for 10 min. EDA-Cbl-Dex (0.0495 g, 0.025 mmol) was then added to the solution and the reaction vessel shaken for an additional 2.5 h. The solution was diluted with diethyl ether (to 50 mL) and centrifuged to pellet the Cbl conjugate. Residual ether was removed by "air drying" for 4 h in the dark. The pellet was then dissolved in MeOH (4 mL) and diluted with DI water (to 15 mL). A 30 g Biotage C18 column with sample was prepped with MeOH:H_2O (0.1% TFA) and the solution was eluted using an MeOH:H_2O (0.1%TFA) gradient from 0% to 80% MeOH. Fractions were analyzed for purity via LC-MS (**Figure 3.18**) and combined, concentrated under reduced pressure, and lyophilized to yield a blue solid (49.2 g, 80.2% yield). ^{1}H NMR (**Figure 3.19**; 500 MHz, MeOH-d4): 8.26 (td, J=13.03 Hz, 3H), 7.68 (s, 1H), 7.50 (dd, J=4.94, 3H), 7.42 (m, 4H), 7.28 (dq, J=7.66, 5H), 6.85 (s, 1H), 6.63 (t, J=12.35, 2H) 6.53 (d, J=5.26, 1H) 6.30 (t, J=10.52, 4H) 6.10 (s, 1H), 5.07 (s, 1H), 5.07, (s, 1H), 4.89 (s, 3H) 4.82 (s, 1H), 4.55 (d, J= 10.71, 1H), 4.37 (s, 1H), 4.33 (t, J=9.61, 3H), 4.29 (d, J=10.39, 2H), 4.22 (m, 1H), 4.11 (t, J= 7.58, 2H), 3.92 (dd, J=5.00, 1H), 3.67 (s, 1H), 3.64 (s, 3H), 3.49 (t, J=5.07, 1H), 3.29 (t, J=5.91, 3H), 3.21 (q, J=5.53, 2H), 3.04 (m, 2H), 2.80 (s, 2H), 2.32 (t of d, 2H), 2.68 (s, 5H), 2.64 (d, J=5.96, 1H), 2.60 (dt, J=3.89, 4H), 2.56 (d, J=2.56, 1H), 2.53 (s, 3H), 2.51 (s, 2H) 2.48 (m, 3H), 2.46 (s, 4H), 2.43 (s, 4H), 2.42 (s, 4H), 3.40 (s, 1H), 2.36 (m, 3H), 2.33 (t, J=7.65, 5H), 2.25 (t, J=7.65, 5H), 2.19 (m, 2H) 2.11 (m, 2H), 2.02 (d, J=9.91, 2H), 2.00 (d, J= 6.61, 2H) 1.96 (d, 3H), 1.89 (s, J=7.16, 3H), 1.82 (q, J=7.89 4H), 1.74 (s, 7H), 1.73, (s, 7H) 1.70 (t, J= 7.57, 3H), 1.67 (dd, J=6.23, 4H), 1.63 (t, 2H), 1.61 (s, 4H), 1.52 (s, 3H), 1.47 (quart, 4H) 1.44 (s, 3H), 1.33 (m, 5H), 1.31 (s, 4H), 1.24 (m, 2H), 1.20 (d, J=6.36, 5H), 1.08 (s, 3H), 1.01 (s, 4H), 0.94 (t. 3H), 0.92 (t, J=6.99, 2H), 0.88 (d, J=7.24, 5H), 0.27 (m, 1H), 0.10 (m, 1H), -0.47 (s, 1H).

(ESI) *m/z*: $[M+3H]^{3+}$ calculated for $C_{126}H_{170}CoFN_{18}O_{23}P$, 805.6; found, (ESI+3, m/z) 805.1 $[M+3H]^{3+}$.

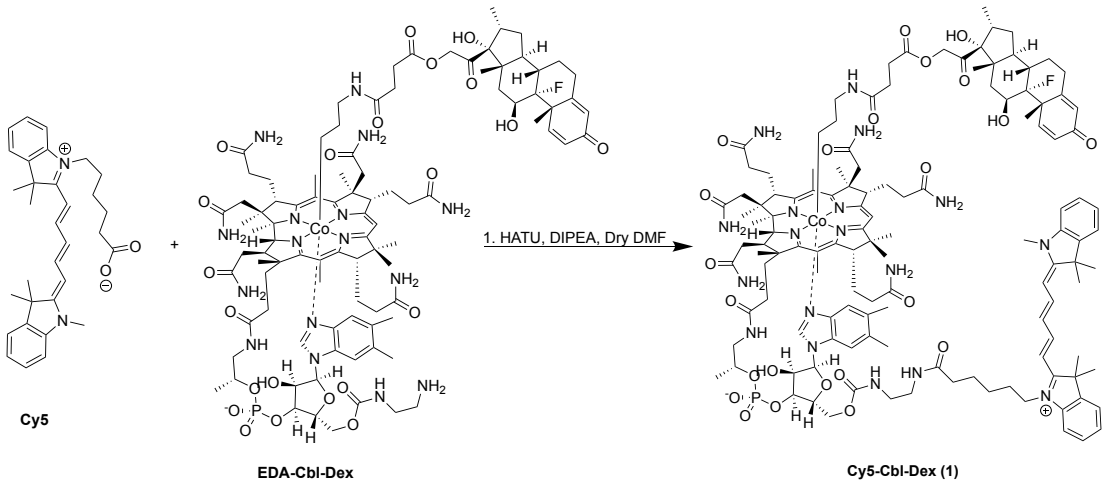

Scheme 3-2 Synthesis of Cy5-Cbl-Dex (1).

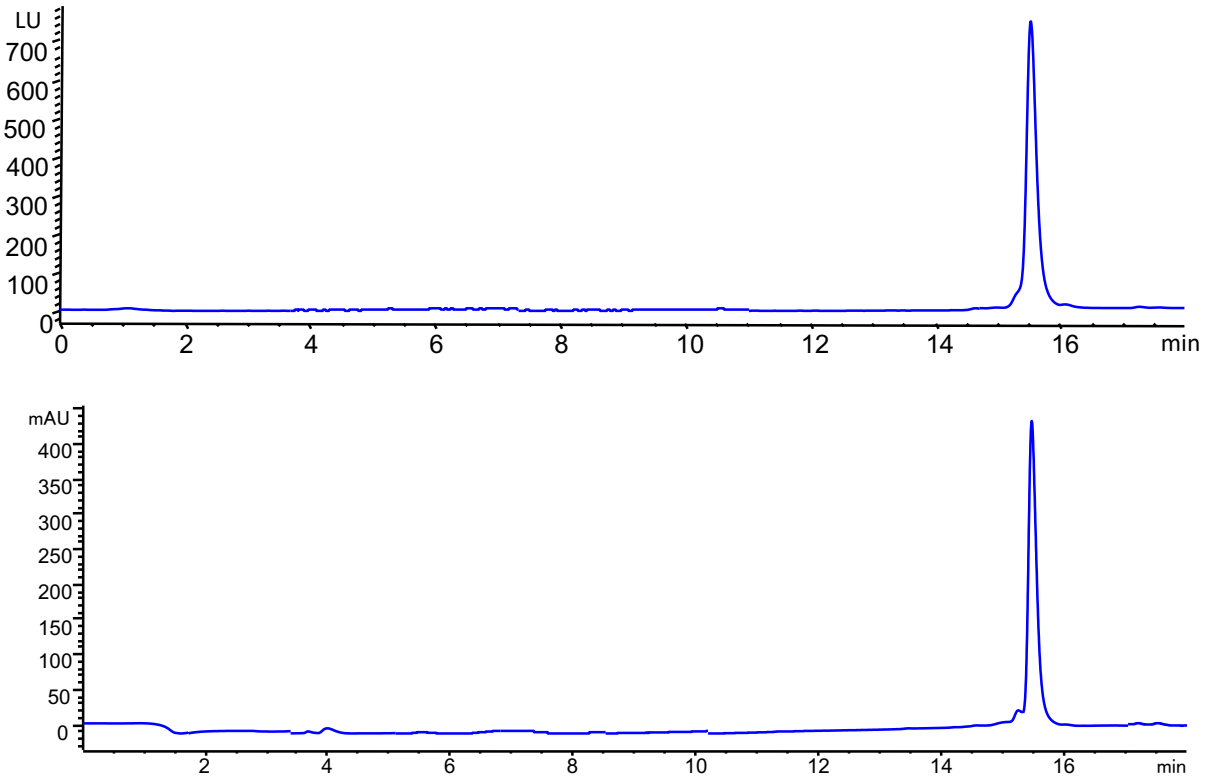

Figure 3.18 LC-MS chromatogram of purified Cy5-CbI-Dex (**1**) detected by the fluorescent detector (top, λ_{ex} = 640 nm; λ_{em} = 670 nm) and by the UV detector (bottom, monitored at 254 nm).

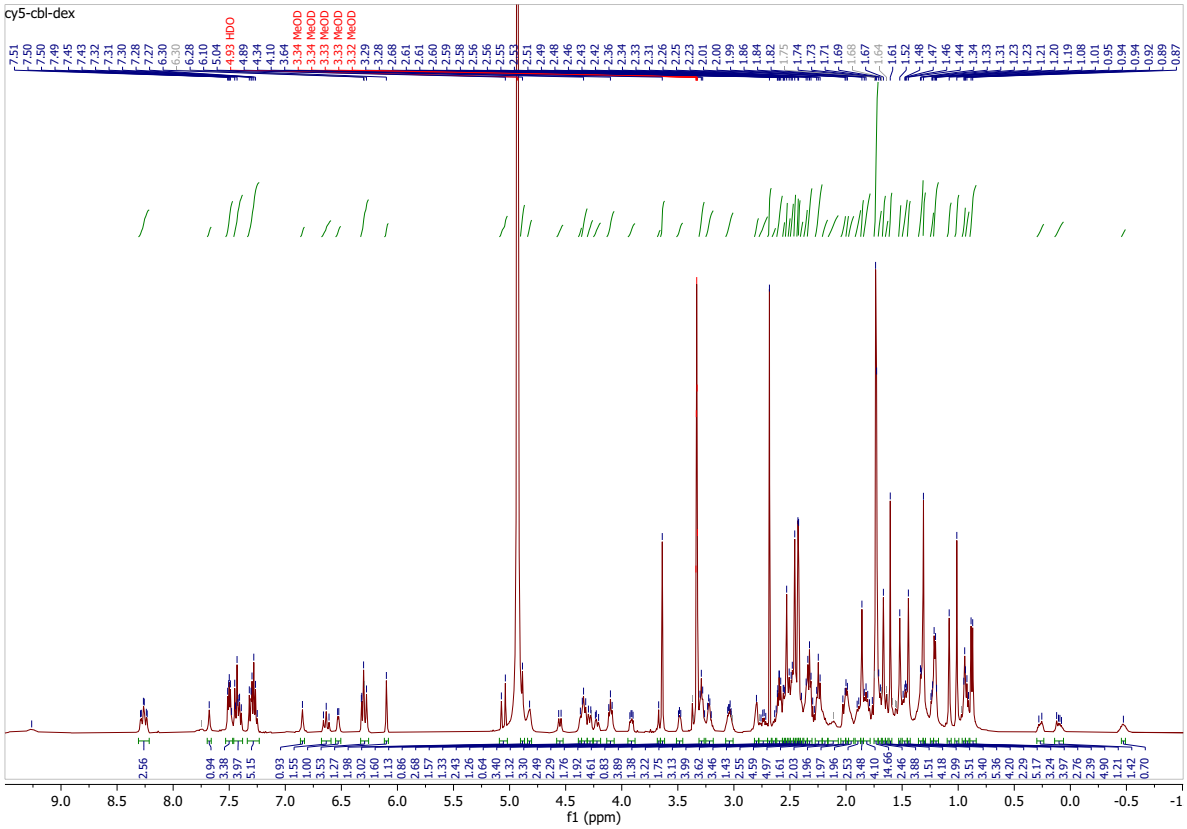

Figure 3.19 ^{1}H NMR of Cy5-Cbl-Dex (1).

Synthesis of Cbl-Dex (**Scheme 3-3**)

Succinyl-Dex[44] (100 mM, 37.2 µL in DMF), HCTU (100 mM, 37.2 µL in DMF), DIPEA (200 mM, 37.2 µL in DMF) were mixed for 1 min. The mixture was then added to a solution of β-(3-aminopropyl)cobalamin[13] (4.3 mg, 3.1 µmol) in DMF (0.5 mL) and stirred for 0.5 h. The mixture was then added to a solution of Cbl-NH_2 β-(3-aminopropyl)cobalamin[13] (4.3 mg, 3.1 µmol) in DMF (0.5 mL) and stirred for 0.5 h. The reaction mixture was purified via a 12 g Biotage C18 column with a Acetonitrile:H_2O (0.1% TFA) binary solvent system and the solution was eluted. Fractions were analyzed for purity via LC-MS and combined, concentrated under reduced pressure, and lyophilized to yield the final product (**Figure 3.20**). ^{1}H NMR (500 MHz, DMSO-d_6): δ 7.84 (s, 1H), 7.68 (s, 2H), 7.61 (s, 1H), 7.54 (s, 1H), 7.36 (s, 1H), 7.31 (d, *J* = 10.1 Hz, 1H), 7.22 (d, *J* = 16.3 Hz, 2H), 7.14 (s, 1H), 6.98 (s, 1H), 6.92 (s, 1H), 6.80 (s, 1H), 6.70 (s, 1H), 6.61 (s, 1H), 6.41 (s, 1H), 6.24 (dd, *J* = 10.1, 1.9 Hz, 1H), 6.17 (d, *J* = 3.6 Hz, 1H), 6.07 (s, 1H), 6.02 (s, 1H), 5.42 (d, *J* = 4.8 Hz, 1H), 5.17 (s, 1H), 5.03 (d, *J* = 17.7 Hz, 1H), 4.76 (d, *J* = 17.6 Hz, 1H), 4.51 (s, 1H), 4.29 (d, *J* = 8.7 Hz, 1H), 4.16 (s, 1H), 4.03 (s, 1H), 3.96 (d, *J* = 8.7 Hz, 2H), 3.66 (s, 1H), 3.54 (s, 1H), 3.41 – 3.38 (m, 6H), 3.14 (d, *J* = 10.1 Hz, 1H), 2.86 (s, 1H), 2.55 (s, 18H), 2.45 (d, *J* = 9.8 Hz, 9H), 2.40 (s, 4H), 2.32 (s, 2H), 2.22 – 2.16 (m, 9H), 2.15 – 2.09 (m, 2H), 2.01 (t, *J* = 14.9 Hz, 3H), 1.84 (s, 1H), 1.77 – 1.73 (m, 3H), 1.70 (s, 3H), 1.63 (d, *J* = 11.7 Hz, 2H), 1.54 (d, *J* = 13.5 Hz, 2H), 1.49 (s, 3H), 1.45 (s, 1H), 1.39 (s, 3H), 1.35 (d, *J* = 11.0 Hz, 1H), 1.24 (d, *J* = 8.9 Hz, 5H), 1.22 – 1.18 (m, 1H), 1.03 (d, *J* = 15.5 Hz, 4H), 0.87 (s, 3H), 0.79 (d, *J* = 7.2 Hz, 3H), 0.40 (s, 2H), 0.07 (s, 1H), -0.38 (1H). Mass spec (ESI) *m/z*: $[M+2H]^{2+}$ calculated for $C_{91}H_{127}CoFN_{14}O_{21}P$, 931.9; found (ESI+, m/z) 931.6 $[M+2H]^{2+}$.

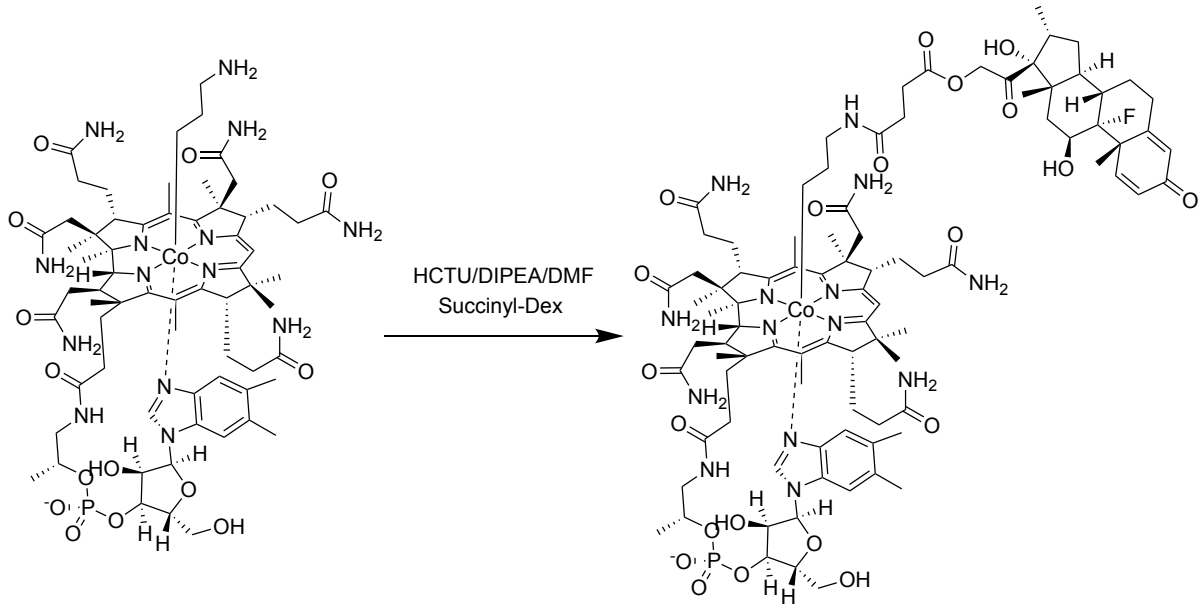

Cbl-Propylamine **Cbl-Dex**

Scheme 3-3 Synthesis of Cbl-Dex.

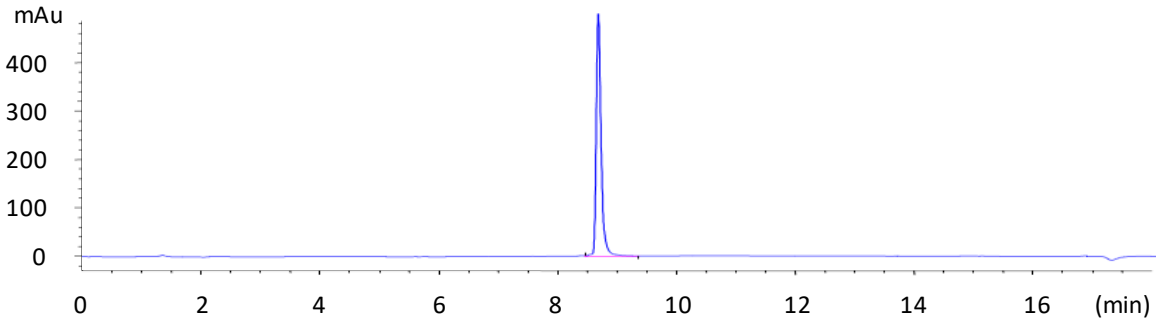

Figure 3.20 LC-MS chromatogram of purified Cbl-Dex detected by the UV detector (monitored at 357 nm).

3.8.2 Loading and *in vitro* Characterization of Cbl RBCs

*Encapsulation of **1** and **2** in mRBCs*

Mouse blood was collected from DBA-1J mice. mRBCs were isolated by filtering through Ficoll-Paque at 400 g for 30 min. The serum and white blood cells were removed and packed mRBCs were washed 3 times with 1X PBS at 500 g for 4 min. RBCs were loaded as previously described with slight modifications to allow for stable loading of larger RBC pellets.[10] Most commonly, mRBC pellets (400 µL, 100% hematocrit) were prepared for loading by addition of a solution of **1** (13.8 mM, 8 µL) or **2** (19 mM, 6 µL) in DMSO and diluent C (164 µL) to create a mixture of mRBCs (70% hematocrit) and Cbl conjugate (200 µM). The RBC/Cbl mixture was dialyzed for 40 min in 400 mL of dialysis buffer (80 mOSm/L PBS, 0.25% glycerol, 10 mM glucose, 2 mM ATP) at 4 °C. RBCs were removed from dialysis tubing and resealed by adding 0.1 volume 10X PBS per vol of dialyzed RBCs and by incubating for 20 min at 37 °C. Loaded, resealed RBCs were washed 5x with 1X PBS or 3x with 1X PBS and 2x with FBS. All manipulations of light responsive compounds occurred in the dark room to prevent exposure to ambient light.

Imaging Flow Cytometry

RBCs loaded with the Cbl conjugates **1** or **2** or externally loaded with DiI were washed with 1X PBS and then diluted 1,000-fold with 1X PBS to achieve a concentration of 9 x 10^7 RBCs/mL. Loaded cells were then evaluated using the ImageStreamX Mark II (Amnis, Seattle, USA). Samples were run at a speed of 25 µL/min and 100,000 unique cells were imaged in two brightfield channels (intensities of 64.6 mW and 93.94 mW), a side scatter channel (785 nm laser at an intensity of 2 mW with a 740 - 800 nm filter), a DiI channel (488 nm solid state laser at an intensity of 200 mW with a 560 - 595 nm filter), and a Cy5 Channel (658 nm diode laser at an intensity of 150 mW with a 660 - 740 nm filter) at 60X magnification. Cells were gated, first filtering for focus by requiring a gradient root mean square greater than 60, then analyzing for singlet cells using a gate within an Area vs Aspect Ratio scatter plot (**Figure 3.21**). The fluorescence of the

cells was then analyzed using an intensity histogram of the appropriate fluorescence channel. General morphology of cells was analyzed by comparing cells using the diameter feature (Erode mask, pixel 03) as established in previous methods and intensity of channel 6 (the granularity channel).[45] Images were analyzed using the IDEAS Software.

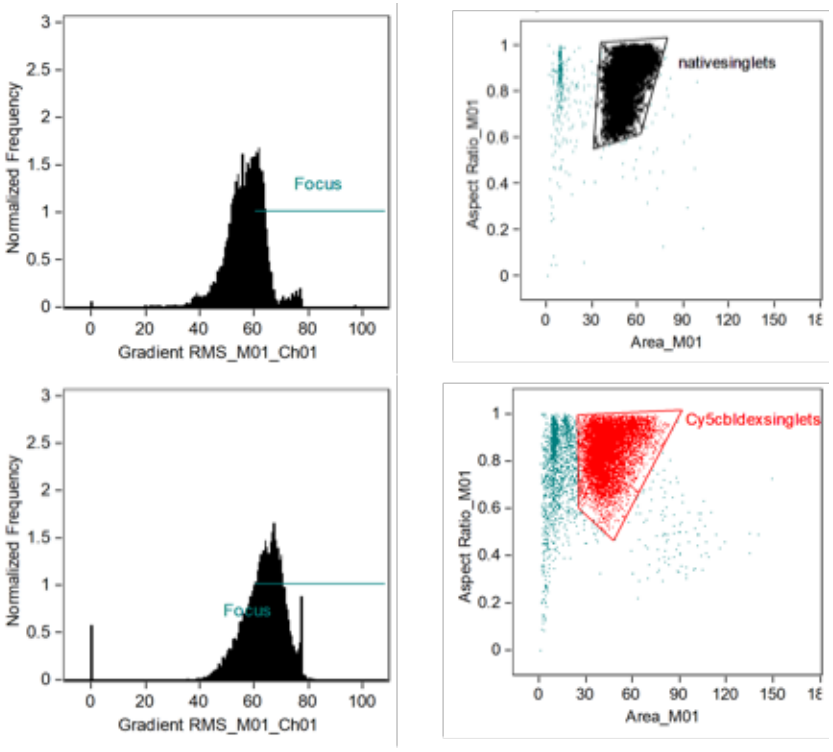

Figure 3.21 Imaging flow analysis gating for RBC populations. Representative analysis of native mRBCs (top) and mRBCs containing **1** (bottom). RBCs were first selected for in focus images (gradient RMS >60) and then selected for singlet cells using area versus aspect ratio.

Ethanol Extraction of Cbl Conjugates from RBCs

Loaded RBCs were extracted using ethanol to detect the amount of Cbl conjugates **1** or **2** loaded. Post loading, RBCs were separated into 100 µL 100% hematocrit pellets. Loaded RBCs were transferred to Enzymax LLC mini-spin columns and two equivalents by volume of ethanol were added to extract the Cbl conjugate. After sitting for 15 min, the extract was filtered from the RBC membranes and residual cell components at 13,000 g for 5 min. The extract was left overnight at 4 °C. The next day residual precipitate was removed by filtering in a mini-spin column at 13,000 g for 5 min. The extract was subsequently diluted to 1 mL with ethanol and the absorbance of the sample at 649 nm was measured using a DeNovix DS-11 FX+ spectrophotometer/fluorometer (Wilmington, DE, USA). Loaded Dex was calculated from a standard curve of the stock Cbl conjugate **(Figure 3.22** and **Figure 3.23)**.

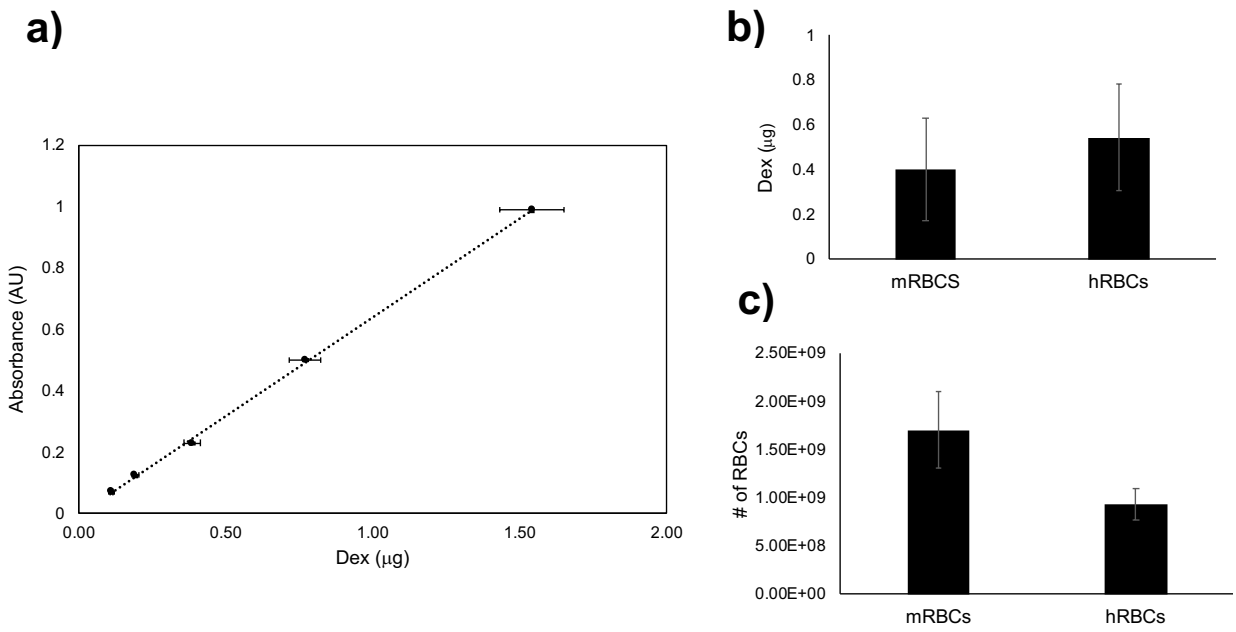

Figure 3.22 Quantification of RBCs containing 1 by ethanol extraction of a loaded RBC pellet and Cy5 absorbance measurement. a) Standard curve of **1** stock in ethanol. **b)** Quantified μg of Dex loaded in a 100 μL pellet at 100% hematocrit. **c)** Number of RBCs in a 100 μL pellet at 100% hematocrit.

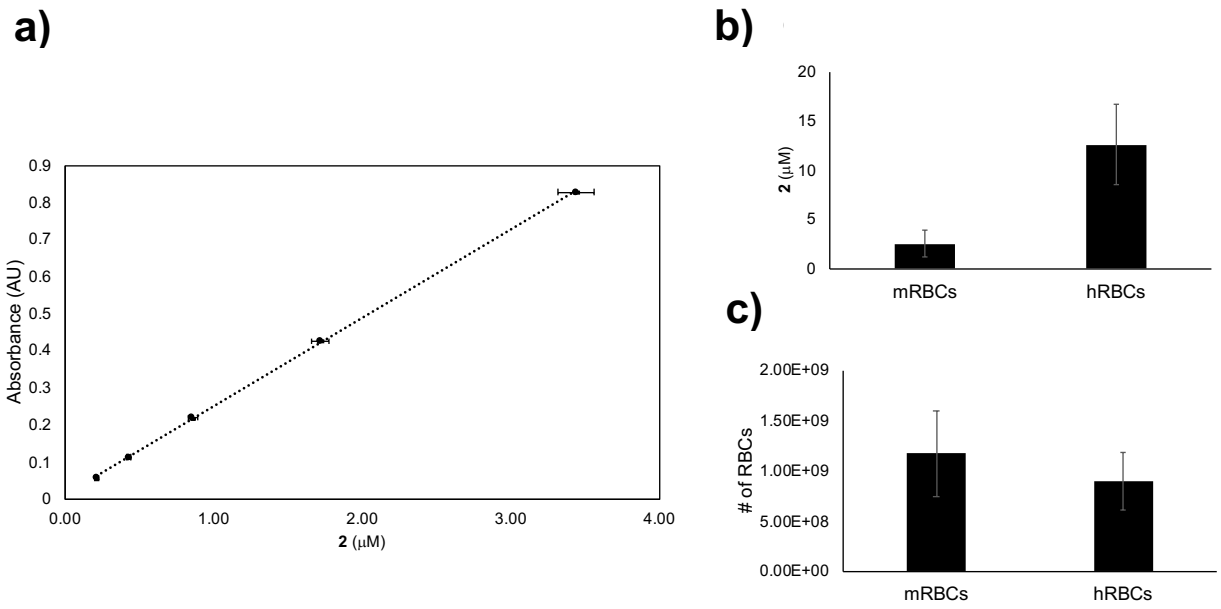

Figure 3.23 Quantification of RBCs containing 2 by ethanol extraction of a loaded RBC pellet and UV-Vis absorbance measurement of Cy5. a) Representative standard curve of **2** stock in ethanol. **b)** Quantified μg of Dex loaded in a 100 μL pellet at 100% hematocrit. **c)** Number of RBCs in a 100 μL pellet at 100% hematocrit.

Automated Hemocytometry

hRBCs were prepared as 10% hematocrit hRBC samples as described above and then analyzed via the Siemens Advia 2120i – automated CBC. RBCs were sphered and fixed and then automatically processed through a Flowcell where RBC Count, MCV and hemoglobin content were measured using a laser diode. Hemoglobin was measured in a colorimeter by lysing all RBCs to free hemoglobin. The free hemoglobin was converted to methemoglobin and then porphyrin and the color change was measured at 546 nm. MCH was calculated by the analyzer using the following equation: MCH = Hgb x 10/RBC. mRBCs were prepared as 10% hematocrit mRBC samples as described above. Samples were then analyzed using the IDEXX ProCyte Dx automated hematology instrument (software version 00-34 Build57) using settings for mouse whole blood.

3.8.3 Photolysis of Cbl-Dex from Solution RBCs

*Photorelease of Dex from Cy5-Cbl-Dex (**1**) hRBCs* (**Scheme 3-4**)

Cy5-Cbl-Dex (Loaded into hRBCs, 20% hematocrit in human platelet rich plasma, 500 µL) were photolyzed as described below. Release of Dex into supernatant after photolysis was assessed by extracting Dex from plasma and pellet with acetonitrile followed by LC-MS analysis, comparing photolyzed product fragment ion 510 and 373 in the supernatant and pellet. Exposure to the light source was performed 5 - 10 min so that Cy5-Cbl-Dex was fully photolyzed, as revealed by the absence of un-photolyzed starting material via LC-MS (**Figure 3.24**).

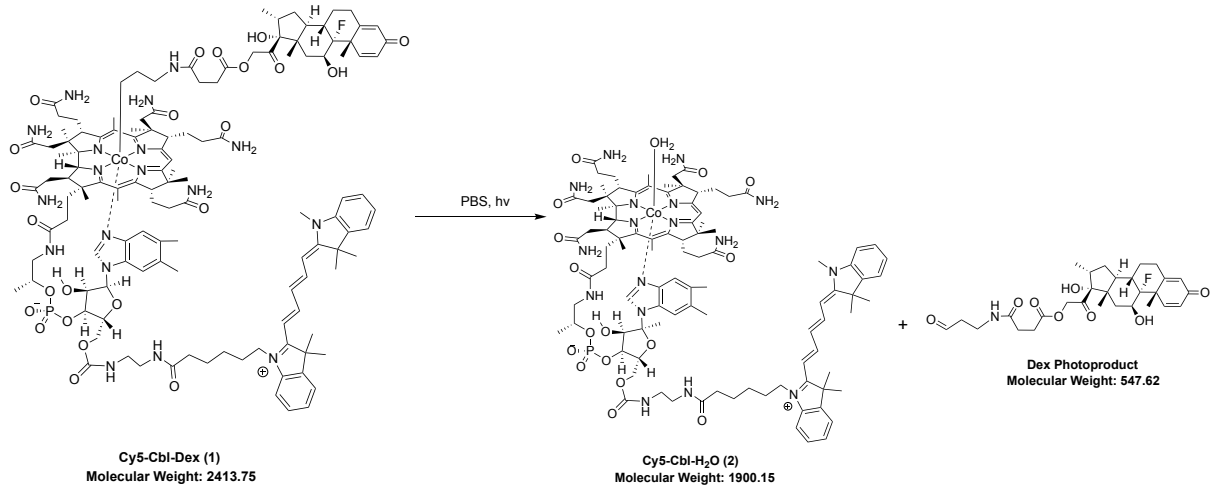

Scheme 3-4 Photolysis of Cy5-Cbl-Dex (**1**) in PBS to form photoproducts Cy5-Cbl-H_2O (**2**) and Dex aldehyde photoproducts.

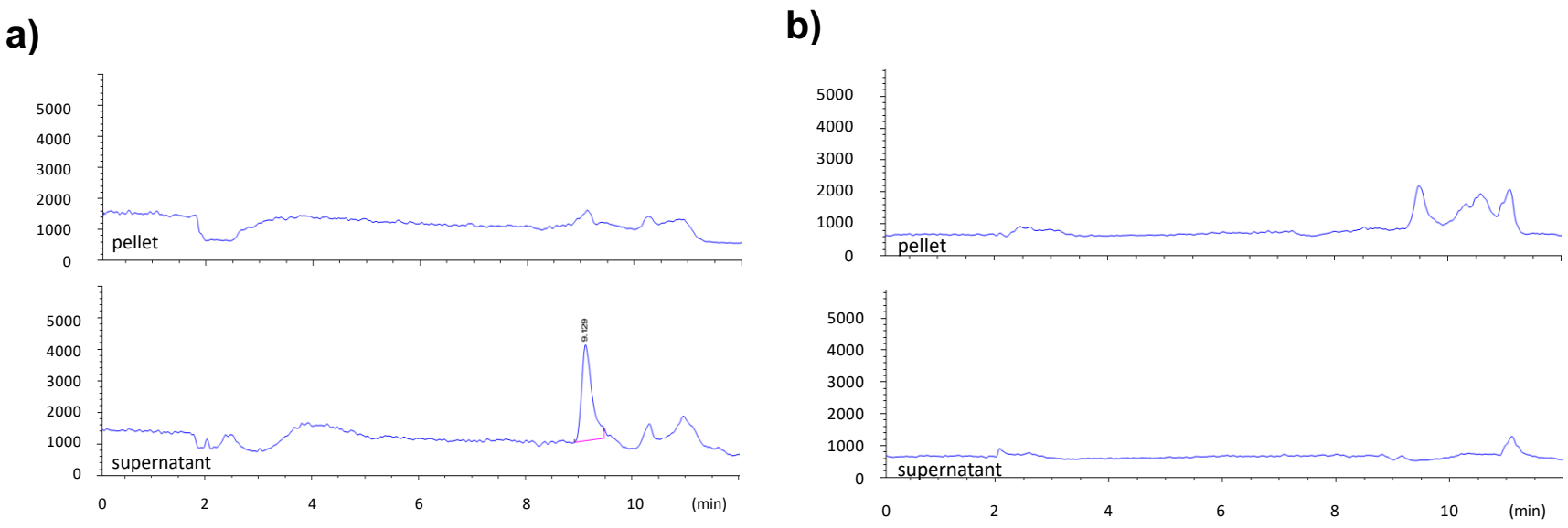

Figure 3.24 Photolysis of 1 from loaded hRBCs. Following incubation, and light/dark exposure, the solution was centrifuged, and the supernatant and pellet processed. **a)** hRBCs loaded with **1** in human platelet rich plasma were photolyzed at 645 ± 10 nm using an Oriel Xe flash lamp (800 mJ, 62 Hz) and appropriate bandpass filters. Analysis by LC-MS revealed that the overwhelming majority (90 ± 5.8%) of the photolyzed Dex product was present in the supernatant (bottom) and not the pellet (top). **b)** hRBCs loaded with **1** in human platelet rich plasma were kept in the dark before analysis. Analysis by LC-MS revealed that the overwhelming majority of Cy5-Cbl-Dex was present in the pellet (top) and not the supernatant (bottom).

*Photolysis of Cy5-Cbl-Dex (**1**) and Cbl-Dex with Fitzpatrick Skin Phantom Solutions*

Fitzpatrick skin phantom solutions were prepared following a previously reported protocol.[26] Hematocrit lysate stock solution (25% hematocrit) was prepared via sonicated lysis of RBCs in water followed by centrifuge to remove residual membranes. All skin phantom solutions contained 0.3% v/v Intralipid®, 1% hemoglobin, and erythrocyte lysate solution (1% v/v) in PBS. Melanin stock solution (3 mg/mL in 100 mM NH_4OH solution) was added at varying concentrations depending on Fitzpatrick skin type (I – II ~8.8 µg/mL; III – IV ~66 µg/mL; V – VI ~130 µg/mL). The skin phantom solution was inserted between the sample and the light source before illumination. Cbl-Dex (20 µM in MeOH/PBS 1:1, 200 µL) or Cy5-Cbl-Dex (20 µM in MeOH/PBS 1:1, 100 µL) were placed in a cuvette and illuminated with a Xe Lamp with a 510 nm Newport filter for Cbl-Dex and a 645 nm Newport filter for Cy5-Cbl-Dex. The sample was exposed to a light intensity of 1.0 mW/cm^2. For Cbl-Dex, the progress of photolysis was monitored by observing an absorbance increase at 350 nm as previously described.[46] For Cy5-Cbl-Dex, the progress of photolysis was monitored by observing the fluorescence decrease using at 675 nm (with λ_{ex} at 645 nm). Completion of photolysis was confirmed by LC-MS (**Figure 3.25**). Analogous experiments were conducted using Cy5-Cbl-Dex loaded human RBCs (20% hematocrit in human platelet rich plasma, 100 µL), which were added to 0.5 mL of human platelet rich plasma (Zen-Bio, Inc). Photolysis of the samples was performed using an Oriel Xe flash lamp (800 mJ, 62 Hz) as the light source with selective bandpass filters for 645 ± 10 for 5 min (dark samples were incubated in the dark for 5 min). Photolyzed RBC suspensions were centrifuged at 1000 g for 3 min, and the supernatant removed from the pellet. Acetonitrile was added to the supernatant in a 1:1 ratio, centrifuged at 21,000 g for 5 min, and then analyzed by LC-MS (solvent A: 0.1% formic acid/H_2O; solvent B: 0.1% formic acid/methanol). The pellet was extracted with 0.5 mL of acetonitrile and analyzed by LC-MS as well. The photolyzed Dex product was monitored by its fragment ions 510

(Dex-aldehyde) and 373 (hydrolyzed Dex) and compared with standard photolyzed product from photolysis in PBS/MeOH (1:1).

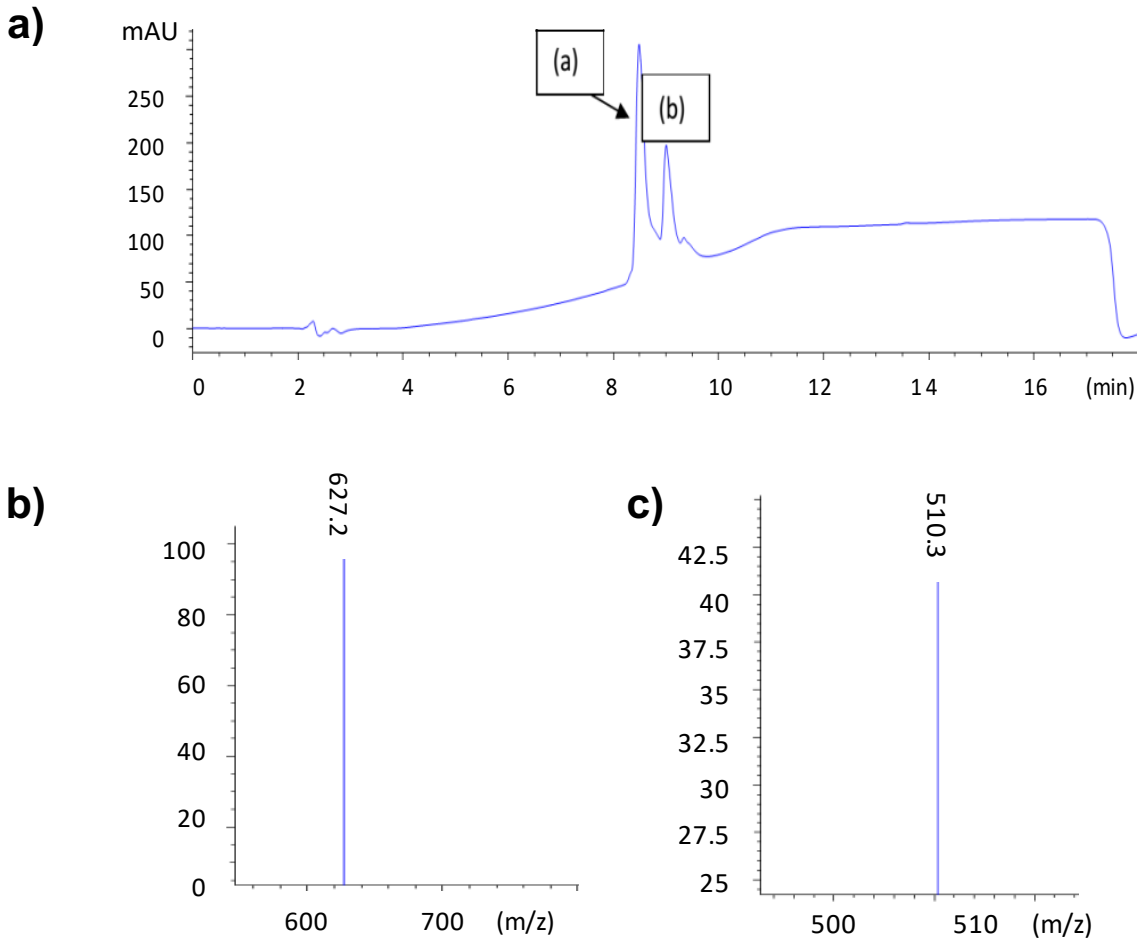

Figure 3.25 Complete photolysis of Cy5-Cbl-Dex after illumination at 645 nm for 30 min. **a)** Reverse-phase HPLC trace of Cy5-Cbl-Dex in PBS (25 μM, pH = 7.4) illuminated at 645 nm for 30 min. The chromatogram was recorded at 251 nm where "peak a" = Cy5-Cbl-H_2O photoproduct and "peak b" = Dex photoproducts (**Scheme 3-4**). **b)** ES-MS spectrum of the photolyzed Cy5-Cbl-Dex was recorded in positive ion mode (peak a). Characteristic molecular and fragment ion: $[(M - H_2O) + H]^{+3}$ (m/z 627.2). **c)** ES-MS spectrum of photolyzed Cy5-Cbl-Dex recorded in positive-ion mode (peak b). Characteristic molecular and fragment ion: $[M - F - H_2O]^{+1}$ (m/z 510.3).

3.8.4 Cy5-Cbl-Dex hRBC Impact on Human Cells

GRα Localization in Human Cells

Human HeLa or FLS cells were seeded in 24-well glass-bottom plates treated with polylysine at a density of 5 x 10^4 cells/mL and allowed to adhere overnight. HeLa cells were then serum starved for 24 h while FLS cells were immediately treated after adhering overnight. The cell cultures were subsequently exposed to 100 µL of **1** RBCs at 10% hematocrit (7.9 x 10^8 cells/mL), or 100 µL of **2** RBCs at 10% hematocrit (8.5 x 10^8 cells/mL), or 500 µL Dex at 250 nM, or 500 µL ethanol vehicle in plain DMEM using Millicell Hanging Cell Culture Inserts (1 µm, polyethylene terephthalate, Millipore). Light treated samples had been exposed to a 660 nm LED board for 30 min at RT. After 30 min of exposure, hanging wells were removed and cells were incubated for an additional 30 min at 37 °C in a humidified environment at 5% CO_2. Cells were then washed 3x with 1X PBS, fixed with 4% PFA in PBS for 10 min, washed with 2x 1X PBS (1 mL), and treated with methanol for 5 min. Fixed cells were treated with a blocking buffer (5% Donkey serum; 0.1% Triton X-100; PBS) and stained for GRα using monoclonal rabbit anti-GRα antibody (Abcam 181327) at 1:200 dilution in antibody dilution buffer (1% BSA; 0.1% Triton-X-100; PBS). Cells were then washed with PBS (3 x 5 min) while stirring before incubation with anti-rabbit AlexaFluor 488 secondary antibody (Life Technologies A11034) at 1:500 dilution in antibody dilution buffer for 1 h at room temperature. Cells were washed (1 x 5 min) with PBS and imaged on an inverted Olympus IX81 microscope equipped with a Hamamatsu FLASH 4V3, 60X oil objective, and a FITC filter cube (Semrock). Images were analyzed using ImageJ. FLS cells and quantified using ImageJ's Coloc 2 program. Regions of Interest (created from the Hoechst nuclear stain) were analyzed for colocalization between the Hoechst nuclear stain and anti-GRα 488 fluorescence in the nuclear space. Pearson's coefficients without thresholding were analyzed from four replicates.

Cell Viability Upon Exposure to Dex

Sup-B15 and FLS cell seeding densities were optimized to ensure cells linearly responded to MTS (**Figure 3.26**). Sup-B15 were then seeded in 24-well glass-bottom plates at a density of $1.7x10^6$ cells/mL and allowed to settle for 1 h, while primary FLS cells were plated at a density of $1x10^4$ cells/mL and allowed to adhere overnight. Cells were then treated with 100 µL of **1** RBCs at 50% hematocrit (4.45×10^9 cells/mL), or 100 µL of **2** RBCs at 50% hematocrit (4.3×10^9 cells/mL), or 500 µL free Dex at 2 mM, or 500 µL plain DMEM which was added to wells in Millicell Hanging Cell Culture Inserts (1 µm, polyethylene terephthalate, Millipore). Samples were exposed to a 660 nm LED board for 30 min at RT. After 30 min of exposure, hanging wells were removed and cells were incubated for 24 h at 37 °C in a humidified environment at 5% CO_2. Cells were then treated with 100 µL MTS/1 mL media for 2 h (Abcam 197010) after which absorption at 492 nm was measured using a HTS 7000 BioAssay Reader (Perkin Elmer, Waltham, Ma).

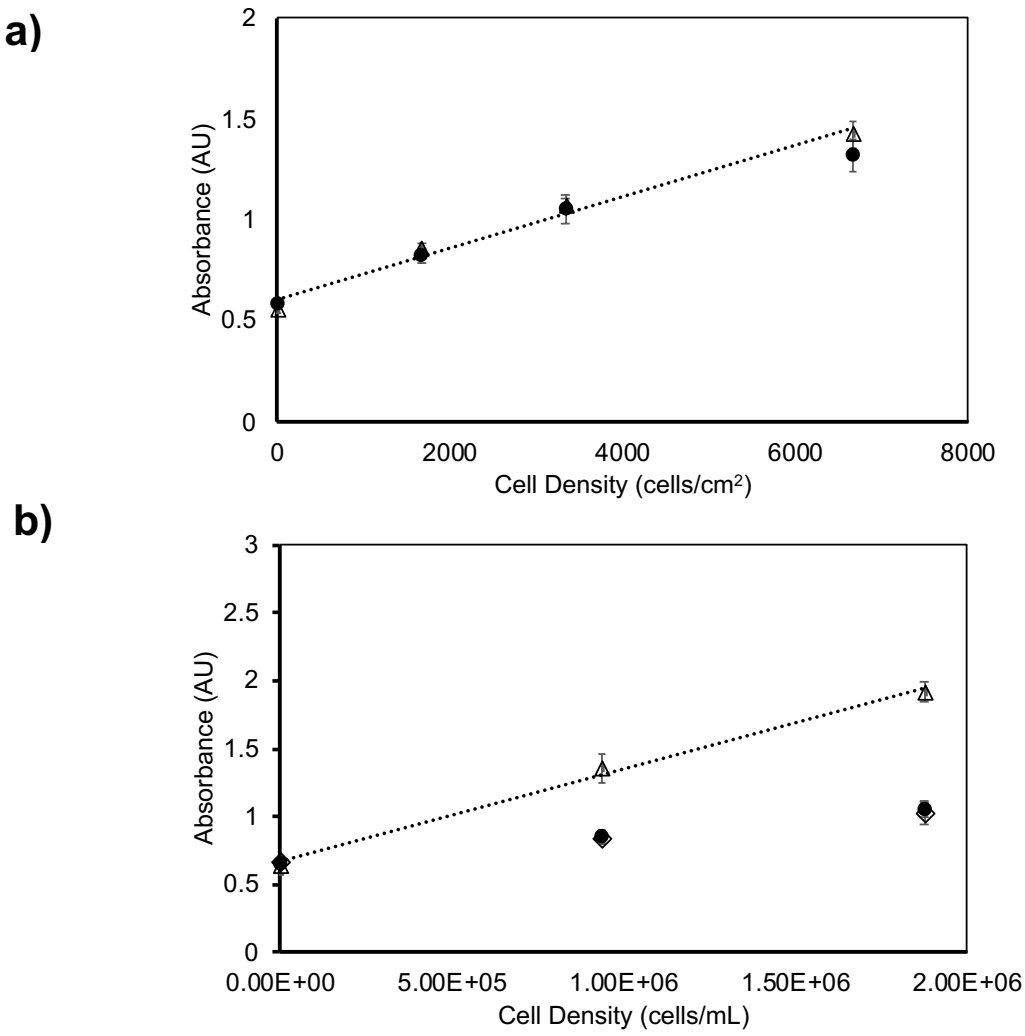

Figure 3.26 Optimization of cell densities for cell viability (MTS) assays. a) FLS cells plated up to a density of 7,000 cells/cm^2 display a linear response in media (triangle, dotted line) and are their viability is not affected by 100 mM Dex (filled circle). **b)** The MTS viability assay is linear up to 2 x 10^6 cells/mL in media (triangle, dotted line) for Sup-B15 cells. The viability of Sup-B15 cells is compromised in the presence of 2 mM Dex (filled circle) and 20 mM Dex (diamond).

3.8.5 *In vivo* Assessment of ADME

Assessment of Circulatory Viability of Modified mRBCs

Whole blood of DBA-1J, 8 - 10 week, male donors was harvested on the day of loading by cardiac puncture. Internally loaded and control RBCs were prepared as described above. mRBCs loaded with **2** were resuspended in PBS at 50% hematocrit and 100 µL of cell suspension was drawn into syringes circumferentially covered with tape to block light. Externally loaded control mRBCs (DiI) and internally (**2**) loaded mRBCs were mixed together 1:1 v/v and 100 µL of the mixture was loaded in a syringe at 90% hematocrit and circumferentially taped to block light. Samples were injected into DBA-1J mice via the tail vein. At the described time points, blood was collected from mice via tail nicks. Mice were euthanized via CO_2 inhalation according to approved UNC IACUC protocol #19-048.0. Whole blood was diluted approximately 1,000 - 1,500-fold and analyzed on the Attune NxT flow cytometer as described below.

Histology

Soft tissues including liver, spleen, kidneys and tail were harvested for frozen sectioning to assess circulation and clearance pathways of phototherapeutics as these organs are most commonly involved in RBC, drug, and toxin clearance. Tissues were placed in 4% paraformaldehyde overnight and rinsed in PBS at 24 h, at which point the samples were placed in increasing concentrations of sucrose in PBS to achieve a 30% sucrose solution for prevention of ice crystallization during cryopreservation. Samples were placed in 15% sucrose in PBS for 24 h. The samples were then transferred to 30% sucrose in PBS until freezing, when samples were covered with OCT in cryomolds and frozen via dry ice. The samples were then stored in -80 ºC until sectioning by cryostat. Frozen sections were obtained at 5 μm using the Thermo Scientific Cryostar NX70 Cryostat (Waltham, MA) and stored at -80 ºC. Immunofluorescence nuclear stain of frozen sections was carried out on the Bond fully automated slide staining system (Leica

Microsystems Inc., Norwell, MA) using the Bond Research Detection System kit (Leica, DS9455). Slides were removed from -80 ºC and equilibrated to room temperature for 60 min before transferring to Bond Wash solution (AR9590). Nuclei were incubated with Hoechst 33258 (Invitrogen, Carlsbad, CA) at 1:5000 dilution for 20 min. The stained slides were mounted with ProLong Gold antifade reagent (Life Technologies, P36930).

3.8.6 *In vivo* Assessment of Efficacy

Attune NxT Flow Cytometry

mRBCs loaded with the Cbl conjugates **1** or **2**, or externally loaded with DiI, or unmodified were diluted 1,000-fold with 1X PBS to achieve a concentration of 1 x 10^7 RBCs/mL. Diluted samples were analyzed using the Attune NxT (ThermoFisher). First, a scatter plot of side scatter area (SSC-A) to side scatter height (SSC-H) was used to gate for single cells. Then, Cy5 from **2** was excited and measured using the 637 nm 100 mW laser and the RL1 detector (Mirror 654LP, Filter 670/14). Data was processed using FCS Express v.7.04 ensuring even flow of sample through the instrument by plotting time vs forward scatter area (FSC-A). Final data allowed for RBC size characterization via scatter plots of FSC-A vs SSC-A and loading uniformity via Cy5 fluorescence-RL1-area and DiI/ CFDA-SE fluorescence-BL1-area (**Figure 3.27**).

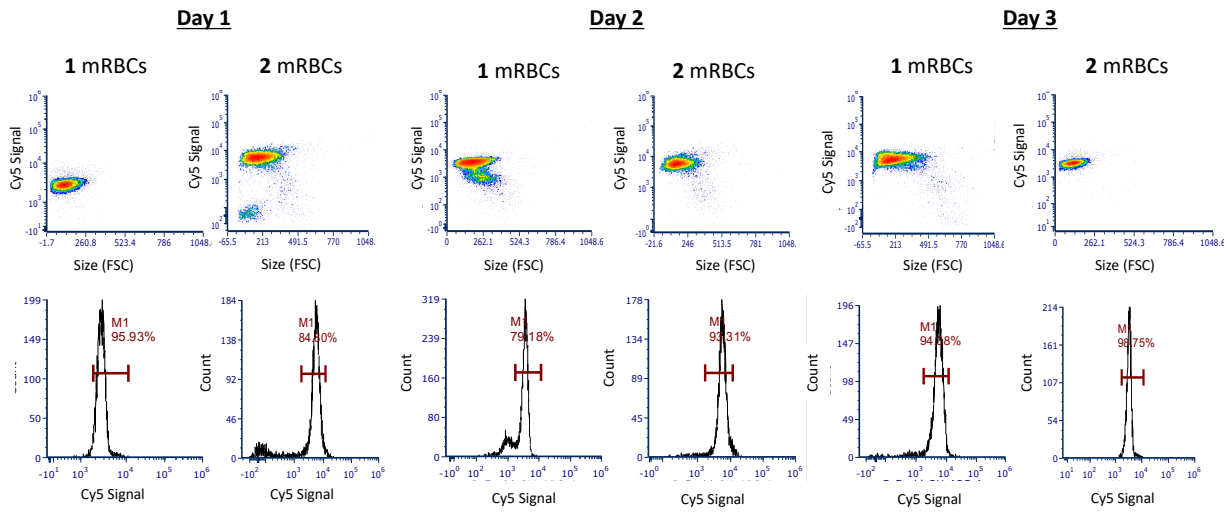

Figure 3.27 Quality control of mRBCs loaded for animal experiments. Representative flow cytometry analysis of mRBCs prepared on multiple days loaded with **1** or **2** mRBCs and subsequently injected into mice. Cy5 signal versus size (FSC) is presented in the top row, whereas the Cy5 fluorescence signal histogram is presented in the bottom row. The M1 gate was used to establish the percentage of Cbl-loaded RBCs.

Collagen Antibody Induced Arthritis (CAIA) Animal Model

Collagen Antibody Induced Arthritis (CAIA) was induced in forty-five 8 - 10 week-old male DBA/IJ mice via the i.p. injection of Chondrex Arthrogen-CIA 5-Clone Cocktail (1.6 mg/mouse) followed by an i.p. injection of lipopolysaccharide from *E. coli* (25 mg) 3 days later, as per the manufacturer's instructions. Arthritis was measured daily by a blinded observer with a clinical disease score index and measurement of paw swelling. The clinical disease score index is performed with the following scoring system: 0 = normal paw; 1 = mild but definite swelling of the ankle or digits; 2 = moderate redness and swelling of an ankle ± any number of digits; 3 = moderate redness and swelling of the entire paw; and 4 = moderate redness and swelling of all three joints in the paw.[47, 48] The maximum score/paw is 4. This method has been previously validated in inflammatory arthritis models.[47, 48] Assessment of disease occurred while the mouse was anesthetized using isoflurane.

*Treatment of Mice with IP Dex or RBCs Containing **1** or **2*** (**Scheme 3-5**)

Mice were randomized after symptom onset in at least one paw with a clinical score ≥ 1 to one of three groups that received the following injections: RBCs containing **1** delivered intravenously (**1** mRBC; experimental treatment); RBCs containing **2** delivered intravenously (**2** mRBC; inactive control, no drug); or Dex sodium phosphate solution delivered i.p. (IP Dex; positive control). The **1** mRBC group (90% hematocrit, 100 µL) received mRBCs internally loaded with approximately 0.0065 mg Cy5-Cbl-Dex (**1**), equivalent to 0.31 mg/kg/mouse, and the IP Dex group received 0.5 mg/kg/mouse. The IP Dex group required additional injections of 0.5 mg/kg daily to achieve a clinical score of 0 in the arthritic paw that was receiving laser. Injections of loaded RBCs were performed via the tail vein by a single, blinded technician using a 27G needle. A laser was applied to the first observed affected joint (only one paw per mouse) in all groups for 5 min immediately following injection and each day until experiment termination at day 4. Mice

were euthanized via CO_2 inhalation according to approved Duke IACUC protocol #A1851708. An RS laser diode (Power Technology Inc., Alexander AR, USA), 635 nm, 3 mW (**Figure 3.28**) was used for laser treatment of the arthritic paw (clinical score ≥ 1). If two or more joints were simultaneously affected, then the laser-treated paw was selected at random. A single, blinded experimenter performed all laser treatments and both lower and upper extremity paws were treated in the study. The laser was applied to the selected joint at an angle that allowed for illumination of the entire joint and paw and was held in position for a total of 5 min per animal. Mice were anesthetized using isoflurane during laser treatment. Treatment was applied to the same paw daily from day of injection until termination.

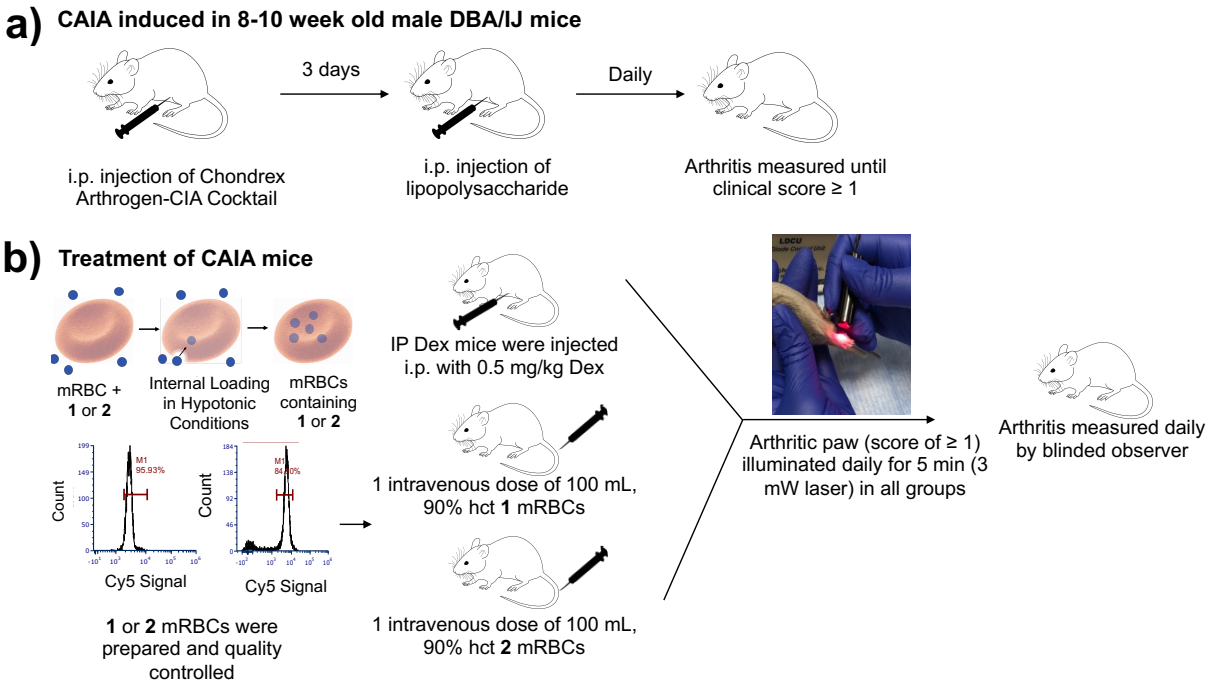

Scheme 3-5 Scheme of treatment of arthritic animals with Dex (delivered intraperitoneally; "IP Dex") and 90% hematocrit (hct) 100 µL mRBCs containing **1** or **2** (delivered via tail vein injection). **a)** CAIA was induced per the Chondrex protocol, and the animals exposed to one of three treatment protocols upon developing at least one arthritic paw (clinical score ≥ 1). **b)** Arthritic mice were treated with IP Dex or mRBCs containing **1** or **2** followed by daily 3 mW laser, 5 min illumination. IP Dex mice continued to receive treatment until complete remission of the arthritic paw.

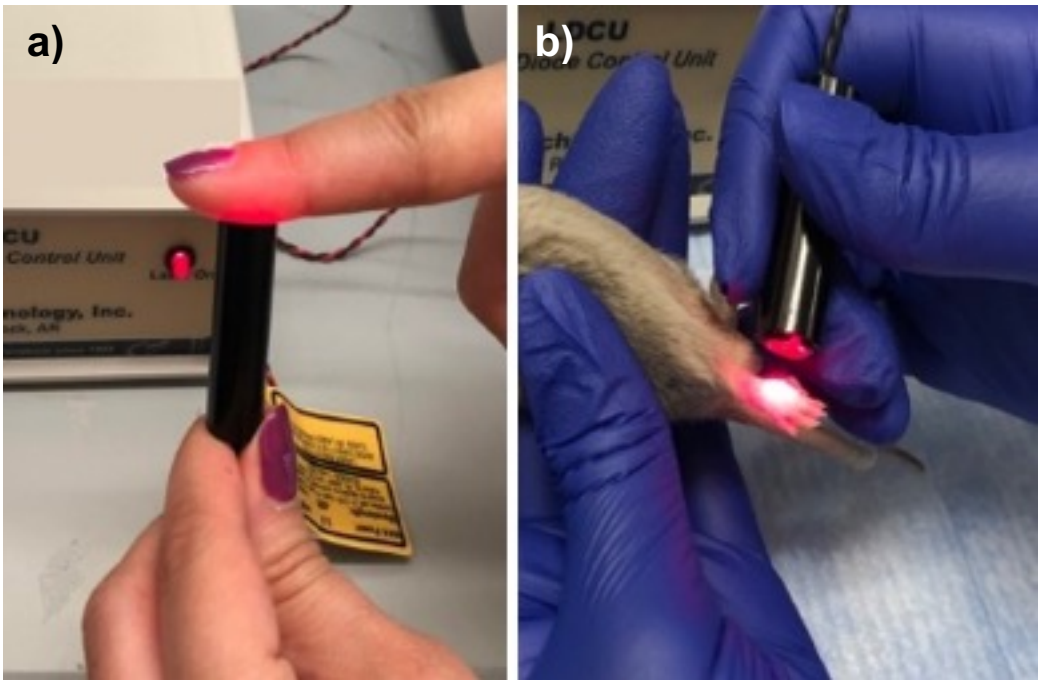

Figure 3.28 RS laser diode (Power Technology Inc., Alexander AR, USA) employed for photorelease (635 nm, 3 mW) of Dex from RBCs in the mouse hindlimb at an angle that allowed for illumination of the entire joint and paw. The RS laser diode was able to penetrate deep into the tissue of the **a)** human distal interphalangeal joint and the **b)** mouse hindlimb at an angle that allowed for illumination of the entire joint and paw.

Statistical Analysis

All plots are presented as the mean ± standard deviation. Data was analyzed by an unpaired Student's *t* test. GraphPad Prism software was used for statistical analysis. A *P* value of less than 0.05 is considered to be statistically significant. We have previously demonstrated that 10 animals per group are needed to achieve 80% power to detect a medium effect size (0.22) at a 0.05 level of significance in the CAIA model.[47, 48] There were >10 animals per group for each of the three experimental groups in this study. The area under the curve (AUC) of the arthritis severity score-time curve was calculated for laser paws in each treatment group. AUC differences were estimated by ANOVA. Comparisons were made across all three treatment groups, and pairwise comparisons were performed using Tukey's test based on the LSMEANS statement. All analyses were conducted using SAS 9.4 (Cary, North Carolina). A one-way ANOVA was used for comparing laser-paw treatment groups at 24 h and was found to be significant (*P* = 0.05). A subsequent Mann Whitney U test comparing laser-paw Cy5-Cbl-Dex (**1**) RBCs (*n* = 13) with Cy5-Cbl-H_2O (**2**) RBC control (*n* = 12) identified significant difference (*P* = 0.01) at 24 h, whereas IP Dex (*n* = 11) did not achieve statistical significance from the control. An unpaired T test was used to analyze the cumulative steroid dose used to achieve clinical remission of the laser-treated paw between IP Dex (*n* = 11) mice and Cy5-Cbl-Dex (**1**) RBCs (*n* = 13) mice, where IP Dex mice were treated daily with 0.5 mg/kg IP until the arthritis subsided (ranging between 1 - 4 steroid doses + laser) and **1** RBC mice received a single dose (0.31 mg/kg intracellularly loaded within 50% Hct) injected intravenously followed by daily laser for 3 additional days.

REFERENCES

1. Bullock, J.; Rizvi, S. A. A.; Saleh, A. M.; Ahmed, S. S.; Do, D. P.; Ansari, R. A.; Ahmed, J., Rheumatoid Arthritis: A Brief Overview of the Treatment. *Med Princ Pract* **2018,** *27* (6), 501-507.

2. Luhder, F.; Reichardt, H. M., Novel Drug Delivery Systems Tailored for Improved Administration of Glucocorticoids. *Int J Mol Sci* **2017,** *18* (9).

3. Koleva, L.; Bovt, E.; Ataullakhanov, F.; Sinauridze, E., Erythrocytes as Carriers: From Drug Delivery to Biosensors. *Pharmaceutics* **2020,** *12* (3).

4. Rossi, L.; Pierige, F.; Aliano, M. P.; Magnani, M., Ongoing Developments and Clinical Progress in Drug-Loaded Red Blood Cell Technologies. *BioDrugs* **2020,** *34* (3), 265-272.

5. Ding, S.; O'Banion, C. P.; Welfare, J. G.; Lawrence, D. S., Cellular Cyborgs: On the Precipice of a Drug Delivery Revolution. *Cell Chem Biol* **2018,** *25* (6), 648-658.

6. Glassman, P. M.; Villa, C. H.; Ukidve, A.; Zhao, Z.; Smith, P.; Mitragotri, S.; Russell, A. J.; Brenner, J. S.; Muzykantov, V. R., Vascular Drug Delivery Using Carrier Red Blood Cells: Focus on RBC Surface Loading and Pharmacokinetics. *Pharmaceutics* **2020,** *12* (5).

7. Karimi, M.; Sahandi Zangabad, P.; Baghaee-Ravari, S.; Ghazadeh, M.; Mirshekari, H.; Hamblin, M. R., Smart Nanostructures for Cargo Delivery: Uncaging and Activating by Light. *J Am Chem Soc* **2017,** *139* (13), 4584-4610.

8. Ankenbruck, N.; Courtney, T.; Naro, Y.; Deiters, A., Optochemical Control of Biological Processes in Cells and Animals. *Angew Chem Int Ed Engl* **2018,** *57* (11), 2768-2798.

9. Wickenheisser, V. A.; Zywot, E. M.; Rabjohns, E. M.; Lee, H. H.; Lawrence, D. S.; Tarrant, T. K., Laser Light Therapy in Inflammatory, Musculoskeletal, and Autoimmune Disease. *Curr Allergy Asthma Rep* **2019,** *19* (8), 37.

10. Marvin, C. M.; Ding, S.; White, R. E.; Orlova, N.; Wang, Q.; Zywot, E. M.; Vickerman, B. M.; Harr, L.; Tarrant, T. K.; Dayton, P. A.; Lawrence, D. S., On Command Drug Delivery via Cell-Conveyed Phototherapeutics. *Small* **2019,** *15* (37), e1901442.

11. Hughes, R. M.; Marvin, C. M.; Rodgers, Z. L.; Ding, S.; Oien, N. P.; Smith, W. J.; Lawrence, D. S., Phototriggered Secretion of Membrane Compartmentalized Bioactive Agents. *Angew Chem Int Ed Engl* **2016,** *55* (52), 16080-16083.

12. Shell, T. A.; Lawrence, D. S., Vitamin B12: a tunable, long wavelength, light-responsive platform for launching therapeutic agents. *Acc Chem Res* **2015,** *48* (11), 2866-74.

13. Shell, T. A.; Shell, J. R.; Rodgers, Z. L.; Lawrence, D. S., Tunable visible and near-IR photoactivation of light-responsive compounds by using fluorophores as light-capturing antennas. *Angew Chem Int Ed Engl* **2014,** *53* (3), 875-8.

14. Weinstain, R.; Slanina, T.; Kand, D.; Klan, P., Visible-to-NIR-Light Activated Release: From Small Molecules to Nanomaterials. *Chem Rev* **2020,** *120* (24), 13135-13272.

15. Kobayashi, H.; Ogawa, M.; Alford, R.; Choyke, P. L.; Urano, Y., New strategies for fluorescent probe design in medical diagnostic imaging. *Chem Rev* **2010,** *110* (5), 2620-40.

16. Bourgeaux, V.; Lanao, J. M.; Bax, B. E.; Godfrin, Y., Drug-loaded erythrocytes: on the road toward marketing approval. *Drug Des Devel Ther* **2016,** *10*, 665-76.

17. Gothoskar, A. V., Resealed Erythrocytes: A Review. *Pharmaceutical Technology* **2004**, 140-158.

18. Pierige, F.; Bigini, N.; Rossi, L.; Magnani, M., Reengineering red blood cells for cellular therapeutics and diagnostics. *Wiley Interdiscip Rev Nanomed Nanobiotechnol* **2017,** *9* (5).

19. Dale, G. L.; Villacorte, D. G.; Beutler, E., High-yield entrapment of proteins into erythrocytes. *Biochem Med* **1977,** *18* (2), 220-5.

20. Deloach, J.; Ihler, G., A dialysis procedure for loading erythrocytes with enzymes and lipids. *Biochim Biophys Acta* **1977,** *496* (1), 136-45.

21. Aujla, H.; Wozniak, M.; Kumar, T.; Murphy, G. J.; REJUVENATE Investigators, Rejuvenation of allogenic red cells: benefits and risks. *Vox Sang* **2018**.

22. Stowell, S. R.; Liepkalns, J. S.; Hendrickson, J. E.; Girard-Pierce, K. R.; Smith, N. H.; Arthur, C. M.; Zimring, J. C., Antigen modulation confers protection to red blood cells from antibody through Fcgamma receptor ligation. *J Immunol* **2013,** *191* (10), 5013-25.

23. Doig, K.; Zhang, B., A Methodical Approach to Interpreting the Red Blood Cell Parameters of the Complete Blood Count. *Clinical Laboratory Science* **2017,** *30* (3), 174-185.

24. Martinez-Torres, C.; Laperrousaz, B.; Berguiga, L.; Boyer-Provera, E.; Elezgaray, J.; Nicolini, F. E.; Maguer-Satta, V.; Arneodo, A.; Argoul, F., Deciphering the internal complexity of living cells with quantitative phase microscopy: a multiscale approach. *J Biomed Opt* **2015,** *20* (9), 096005.

25. Sharma, A. N.; Patel, B. C., Laser Fitzpatrick Skin Type Recommendations. In *StatPearls*, Treasure Island (FL), 2021.

26. Rodgers, Z. L.; Hughes, R. M.; Doherty, L. M.; Shell, J. R.; Molesky, B. P.; Brugh, A. M.; Forbes, M. D.; Moran, A. M.; Lawrence, D. S., B(12)-mediated, long wavelength photopolymerization of hydrogels. *J Am Chem Soc* **2015,** *137* (9), 3372-8.

27. Hardy, R. S.; Raza, K.; Cooper, M. S., Therapeutic glucocorticoids: mechanisms of actions in rheumatic diseases. *Nat Rev Rheumatol* **2020,** *16* (3), 133-144.

28. Ramamoorthy, S.; Cidlowski, J. A., Corticosteroids: Mechanisms of Action in Health and Disease. *Rheum Dis Clin North Am* **2016,** *42* (1), 15-31, vii.

29. Karra, A. G.; Konstantinou, M.; Tzortziou, M.; Tsialtas, I.; Kalousi, F. D.; Garagounis, C.; Hayes, J. M.; Psarra, A. G., Potential Dissociative Glucocorticoid Receptor Activity for Protopanaxadiol and Protopanaxatriol. *Int J Mol Sci* **2018,** *20* (1).

30. Andreau, K.; Lemaire, C.; Souvannavong, V.; Adam, A., Induction of apoptosis by dexamethasone in the B cell lineage. *Immunopharmacology* **1998,** *40* (1), 67-76.

31. Lill-Elghanian, D.; Schwartz, K.; King, L.; Fraker, P., Glucocorticoid-induced apoptosis in early B cells from human bone marrow. *Exp Biol Med (Maywood)* **2002,** *227* (9), 763-70.

32. Mebius, R. E.; Kraal, G., Structure and function of the spleen. *Nature Reviews Immunology* **2005,** *5* (8), 606-616.

33. Kollias, G.; Papadaki, P.; Apparailly, F.; Vervoordeldonk, M. J.; Holmdahl, R.; Baumans, V.; Desaintes, C.; Di Santo, J.; Distler, J.; Garside, P.; Hegen, M.; Huizinga, T. W.; Jungel, A.; Klareskog, L.; McInnes, I.; Ragoussis, I.; Schett, G.; Hart, B.; Tak, P. P.; Toes, R.; van den Berg, W.; Wurst, W.; Gay, S., Animal models for arthritis: innovative tools for prevention and treatment. *Annals of the rheumatic diseases* **2011,** *70* (8), 1357-62.

34. Dinser, R., Animal models for arthritis. *Best practice & research. Clinical rheumatology* **2008,** *22* (2), 253-67.

35. Keller, K. K.; Lindgaard, L. M.; Wogensen, L.; Dagnaes-Hansen, F.; Thomsen, J. S.; Sakaguchi, S.; Stengaard-Pedersen, K.; Hauge, E. M., SKG arthritis as a model for evaluating therapies in rheumatoid arthritis with special focus on bone changes. *Rheumatol Int* **2013,** *33* (5), 1127-33.

36. Sakaguchi, N.; Takahashi, T.; Hata, H.; Nomura, T.; Tagami, T.; Yamazaki, S.; Sakihama, T.; Matsutani, T.; Negishi, I.; Nakatsuru, S.; Sakaguchi, S., Altered thymic T-cell selection due to a mutation of the ZAP-70 gene causes autoimmune arthritis in mice. *Nature* **2003,** *426* (6965), 454-60.

37. Nandakumar, K. S.; Holmdahl, R., Antibody-induced arthritis: disease mechanisms and genes involved at the effector phase of arthritis. *Arthritis research & therapy* **2006,** *8* (6), 223.

38. Tarrant, T. K.; Liu, P.; Rampersad, R. R.; Esserman, D.; Rothlein, L. R.; Timoshchenko, R. G.; McGinnis, M. W.; Fitzhugh, D. J.; Patel, D. D.; Fong, A. M., Decreased Th17 and antigen-specific humoral responses in CX(3) CR1-deficient mice in the collagen-induced arthritis model. *Arthritis Rheum* **2012,** *64* (5), 1379-87.

39. Khachigian, L. M., Collagen antibody-induced arthritis. *Nat Protoc* **2006,** *1* (5), 2512-6.

40. Mainz, E. R.; Serafin, D. S.; Nguyen, T. T.; Tarrant, T. K.; Sims, C. E.; Allbritton, N. L., Single Cell Chemical Cytometry of Akt Activity in Rheumatoid Arthritis and Normal Fibroblast-like Synoviocytes in Response to Tumor Necrosis Factor alpha. *Anal Chem* **2016,** *88* (15), 7786-92.

41. Arnett, F. C.; Edworthy, S. M.; Bloch, D. A.; McShane, D. J.; Fries, J. F.; Cooper, N. S.; Healey, L. A.; Kaplan, S. R.; Liang, M. H.; Luthra, H. S.; et al., The American Rheumatism Association 1987 revised criteria for the classification of rheumatoid arthritis. *Arthritis Rheum* **1988,** *31* (3), 315-24.

42. Shell, T. A.; Shell, J. R.; Rodgers, Z. L.; Lawrence, D. S., Tunable Visible and Near-IR Photoactivation of Light-Responsive Compounds by Using Fluorophores as Light-Capturing Antennas. *Angewandte Chemie International Edition* **2014,** *53* (3), 875-878.

43. McLeod, A. D.; Friend, D. R.; Tozer, T. N., Glucocorticoid-dextran conjugates as potential prodrugs for colon-specific delivery: hydrolysis in rat gastrointestinal tract contents. *J Pharm Sci* **1994,** *83* (9), 1284-8.

44. Mao, L.; Wang, H.; Tan, M.; Ou, L.; Kong, D.; Yang, Z., Conjugation of two complementary anti-cancer drugs confers molecular hydrogels as a co-delivery system. *Chem Commun (Camb)* **2012,** *48* (3), 395-7.

45. Johnson, S. M.; Banyard, A.; Smith, C.; Mironov, A.; McCabe, M. G., Large Extracellular Vesicles Can be Characterised by Multiplex Labelling Using Imaging Flow Cytometry. *Int J Mol Sci* **2020,** *21* (22).

46. Juzeniene, A.; Nizauskaite, Z., Photodegradation of cobalamins in aqueous solutions and in human blood. *J Photochem Photobiol B* **2013,** *122*, 7-14.

47. Giguere, P. M.; Billard, M. J.; Laroche, G.; Buckley, B. K.; Timoshchenko, R. G.; McGinnis, M. W.; Esserman, D.; Foreman, O.; Liu, P.; Siderovski, D. P.; Tarrant, T. K., G-protein signaling modulator-3, a gene linked to autoimmune diseases, regulates monocyte function and its deficiency protects from inflammatory arthritis. *Mol Immunol* **2013,** *54* (2), 193-8.

48. Tarrant, T. K.; Billard, M. J.; Timoshchenko, R. G.; McGinnis, M. W.; Serafin, D. S.; Foreman, O.; Esserman, D. A.; Chao, N. J.; Lento, W. E.; Lee, D. M.; Patel, D.; Siderovski, D. P., G protein-coupled receptor kinase-3-deficient mice exhibit WHIM syndrome features and attenuated inflammatory responses. *J Leukoc Biol* **2013,** *94* (6), 1243-51.

CHAPTER 4: PRE-CLINICAL DEVELOPMENT OF COBALAMIN PHOTOACTIVATABLE THERAPEUTICS: EXTENSIVE PROGRESS AND REMAINING CHALLENGES

The photochemistry of cobalamin (Cbl) derivatives has been the subject of intensive investigations since the 1950s. Cbl's photoresponsivity was first discovered when stored cyanocobalamin, a treatment for pernicious anemia since the 1920s, degraded in a lit environment.[1-3] In general, Cbl derivatives are currently under development as targeting agents for cancer, as well as photoactivatable therapeutics.[4, 5] The Lawrence group, specifically, has made extensive progress in developing Cbl as a photoactivatable therapeutic since the early 2000's. Cbl derivatives are promising photoactivatable therapeutics as their scaffold is derived from vitamin B12 and thus expected to introduce minimal toxicity but still maintain the inherent photoresponsivity to 330 - 575 nm wavelengths. This Chapter will review the progress the lab has made pre-clinically developing this photoresponsive moiety into a feasible photoactivatable therapeutic and the challenges that remain. The development path is shown in **Figure 4.1**, a modified version of **Figure 1.12** originally introduced in Chapter 1.

Initial investigations of Cbl focused on novel cancer treatments. Given the precedent of photodynamic therapy and targeted drug delivery systems (DDSs), cancer is an indication with numerous unmet clinical needs that localized delivery and treatment have begun to address. Photoactivatable Cbl, specifically, provides a means of localizing chemotherapeutic release, and thus minimizing systemic toxicity, by external light stimulation. By introducing carriers, we were able to expand the relevance of Cbl therapeutics beyond cancer into other indications, such as arthritis. Arthritis is an inflammatory disease with a prevalence of 5 patients per 1000 adults with symptoms of pain, inflammation, and eventually physical deformation of joints commonly in the

hands and the feet.[6, 7] Due to arthritis' chronic nature, close monitoring for strict treat-to-target is required for successful remission. Given the treatment needs, as well as negative side effects of chronic use of glucocorticoid drugs (e.g., prednisone or dexamethasone), patient-directed targeted delivery of anti-inflammatory drugs may both support treatment adherence and efficacy while diminishing adverse effects of these therapeutics.[8, 9] Thus, with a team of chemical, biological, and clinical experts, the Lawrence group has continued to make significant progress on Cbl phototherapeutics in preparation for first in human studies.

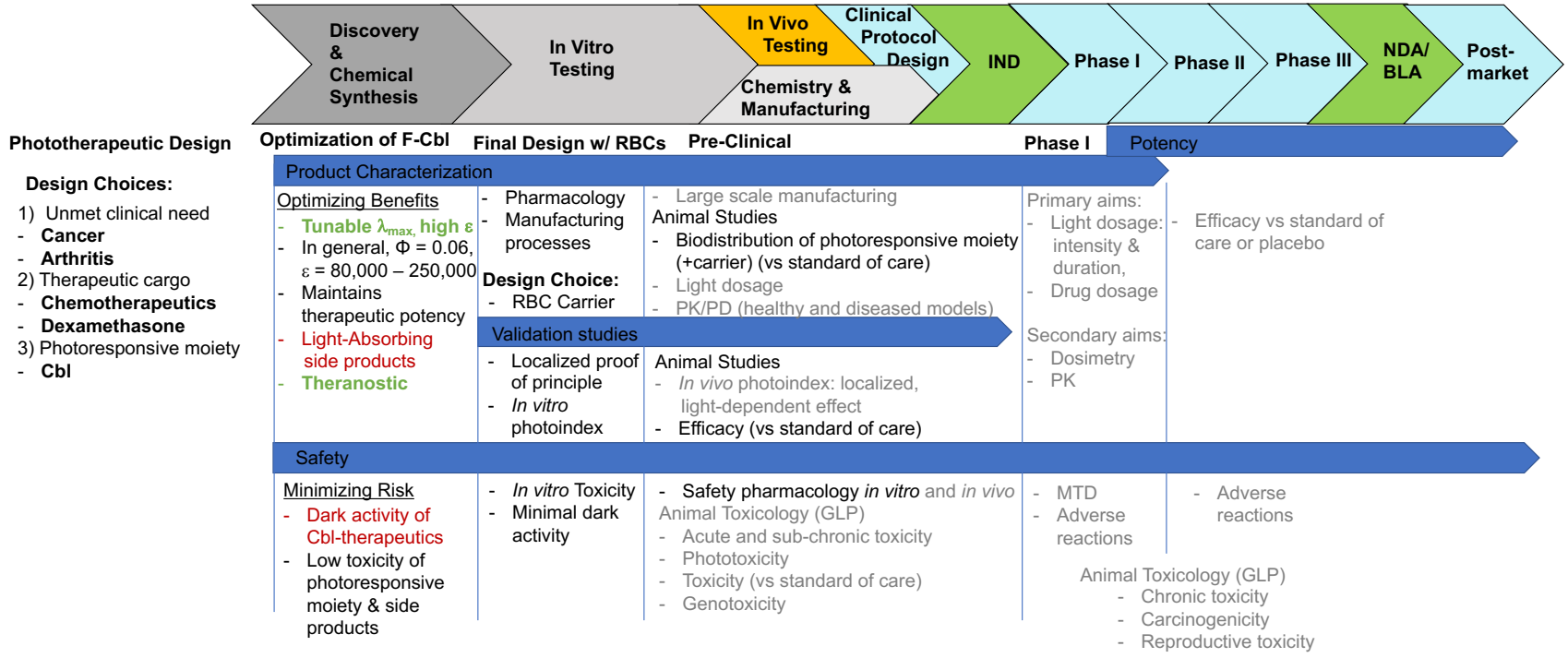

Figure 4.1 Development of Cy5-Cbl-Dex RBCs. The path initially introduced in Chapter 1 is modified for the development of Cy5-Cbl therapeutics. In green are additional benefits of Cy5-Cbl while in red are discovered risks. Gray studies have yet to be conducted.

4.1 Cbl: Initial Characterization and Optimization

Photophysical Properties (λ_{max}, ε, and Φ) and Rates of Photolysis

The capacity of a photoactivatable therapeutic to release therapeutic in response to illumination is defined by its photophysical properties, which are most easily measured *in vitro*. These properties include: the maximum wavelength (λ_{max}) of photoresponsiveness, the ability to absorb photons of light (ε), and the ability of the therapeutic to use the absorbed energy for therapeutic cargo release (Φ). Under *in vivo* conditions, the rate of photolysis will also significantly affect whether the therapeutic is locally released upon stimulation. For example, if the rate of photolysis is too slow the therapeutic could diffuse away from the treatment site before photorelease occurs.

Long-wavelength photoresponsiveness within the optical window of tissue (600 - 950 nm) is required for any non-superficial indications to penetrate tissue beyond 1 - 2 mm of depth.[10] In 2014, the Lawrence group discovered that synthetically appending a fluorophore to the 5'-OH of the Cbl ribose modulates the photoresponsivity of Cbl. The fluorophore acts as an antenna by both introducing the fluorophore's λ_{max} which is capable of causing photorelease and accelerating rates of photolysis.[11] Studies of the appended fluorophore on Cbl demonstrated improved photolysis rates of TAMRA-Cbl-Adenosine ($0.89 \pm 0.32\ s^{-1}$) as compared to Cbl-Adenosine ($0.38 \pm 0.04\ s^{-1}$) at an illumination of 546 ± 10 nm (< 15 mW/ cm^2) (**Figure 4.2**). Interestingly, the Φ for adenosine release of TAMRA-Cbl-Adenosine (0.066) is significantly lower when compared to Cbl-Adenosine (0.3). The increase in rate is thus attributed to an increase in photon absorption: the ε at 546 nm increases by more than 10-fold by appending the TAMRA antenna (Cbl-Adenosine's 8,100 $M^{-1}\ cm^{-1}$ vs TAMRA-Cbl-Adenosine's 86,000 $M^{-1}\ cm^{-1}$). The dramatic increase in ε, but less extreme increase in rates suggests that energy is still lost by other means, such as fluorescence.[12] Similarly, studies testing photolysis through Fitzpatrick tissue phantoms (solutions which include pigments that induce scattering and absorption of light similar to tissue) of Cbl-Dex versus Cy5-

Cbl-Dex with illumination near their respective λ_{max} (510 nm vs 645 nm) demonstrated significantly improved rates of photolysis of the Cy5 derivative. Cy5-Cbl-Dex is completely photolyzed in 3 min while minimal photolysis of Cbl-Dex occurs in that time as discussed in Chapter 3 (**Figure 3.8**).[13] Thus, the fluorophore antenna introduces photoresponsivity of Cbl into the tissue-penetrating long-wavelength range and improves the photolysis rate. However, a significant energy loss is still observed as indicated by the decreased Φ of TAMRA-Cbl-Adenosine and fluorescence of Cy5-Cbl species tracked in Chapter 2 (**Figure 2.3**).[14]

Although fluorophore antennas introduce photoresponsivity in the optical window of tissue to Cbl, the diminished Φ of therapeutic release may affect therapeutic efficacy *in vivo*. Since light is significantly scattered as it diffuses through tissue (even at long wavelengths), ensuring high Φ is important for achieving therapeutic efficacy in thicker tissue. Further, the photoproducts of Cbl continue to absorb light further diminishing the available photons for therapeutic release. In general, Cbl's Φ has also been found to depend on pH, the axial species attached, and solvent.[3] Fortunately, the joints of the hands and feet for arthritis treatment are superficially accessible and can easily be illuminated for extended periods of time. Thus, treating this more accessible tissue avoids the feasibility challenges of deeper tissue indications in potentially acidic environments (such as cancer), that may be exposed for more limited durations during surgery. *In vivo* quantification of therapeutic photorelease has yet to be performed.

Fluorophore-Cbl species responsive in the optical window of tissue also present unique benefits. TAMRA, Cy5, Atto725, and DyLight 800 fluorophores have all been appended to Cbl and act as antennas that induce photocleavage from λ_{max} of 546 through 800 nm. This tunability allows for preparing multiple therapeutics for wavelength-specific localized release employing the spatial and temporal benefits external laser-stimulation Cbl provides. Further, the persistent fluorescence of fluorophore-Cbl species may be applied for theranostic uses as described in Chapter 2, as well as in other tests of Cbl biodistribution.[4]

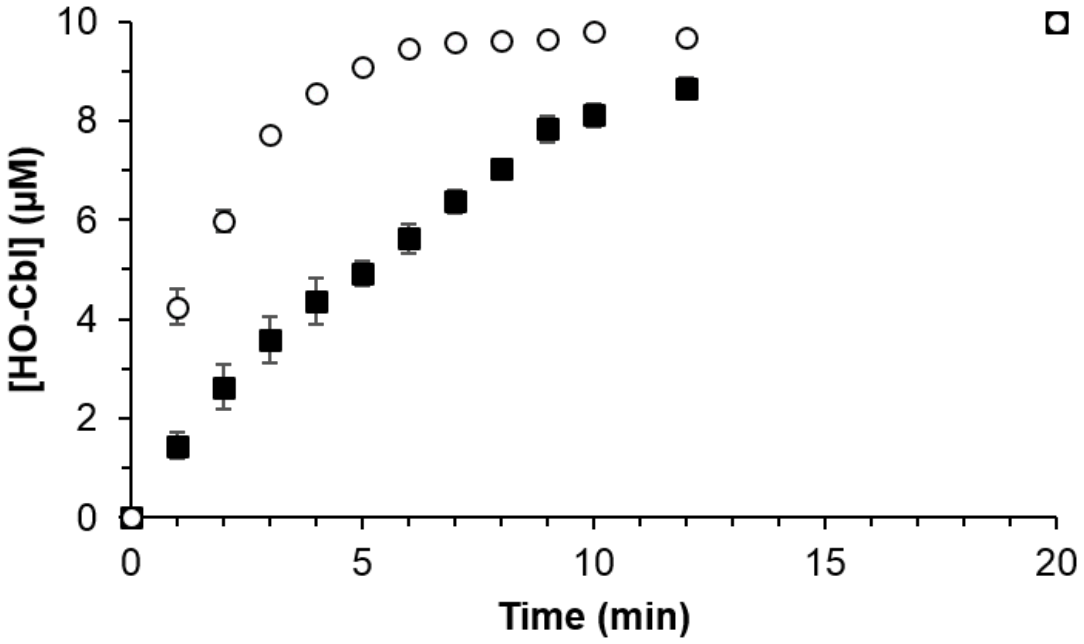

Figure 4.2 Photolysis rates of TAMRA-Cbl (circles) versus Cbl (squares) as measured by production of the HO-Cbl photoproduct. The rate of photolysis is determined from the initial slope from 0 to 3 min. Reprinted with Permission.[12]

Dark Activity

Previously published research on vitamin B12 described how the body and cells absorb natural cyanocobalamins and alkylcobalamins. Specifically, Cbl bound to transcobalamin protein is recognized by CD320 receptors on the cell, which leads to endocytosis of the Cbl-transcobalamin conjugate. These endosomes then transform into lysosomes within which Cbl is disassociated from the transcobalamin transporter protein. The pH change that occurs during endosomal transformation into lysosomes, as well as tumor overexpression of transcobalamin receptors has been exploited with a targeted Cbl-colchicine with an acid-labile linker.[5] After release, Cbl is then transported into the cellular cytosol and associates with cytosolic cobalamin C. Cobalamin C can then decyanate cyanocobalamins or dealkylate alkylcobalamins. The processed Cbl remains in the cytosol or is trafficked into the mitochondria where it contributes as a co-enzyme role in nucleotide synthesis and the tricarboxylic acid cycle, respectively.[15] Thus, there are multiple methods that photoresponsive Cbl-therapeutics could be inadvertently activated within the cell: 1) the lysosomal environment could cause hydrolysis of the axial bond, 2) cobalamin C can cleave the Co-C bond releasing the therapeutic, and 3) the Cbl-therapeutic conjugate may maintain therapeutic activity even in its conjugated state, thus not requiring cleavage for therapeutic activity.[12, 15]

Similar to the described literary findings of vitamin B12, cellular studies of Cbl-BODIPY demonstrated that Cbl can be endosomally sequestered until photolysis in cells (**Figure 4.3**).[11] However, subsequent studies with Cbl-monomethyl auristatin E (MMAE) exposed the potential inadvertent activity of Cbl appended therapeutics, especially potent cytotoxic therapeutics (**Figure 4.4**). To target Cbl chemotherapeutic to glioblastoma cells, the photoindex of Cbl-MMAE treatment in the light and dark on glioblastoma cells and non-target neural stem cells was measured.

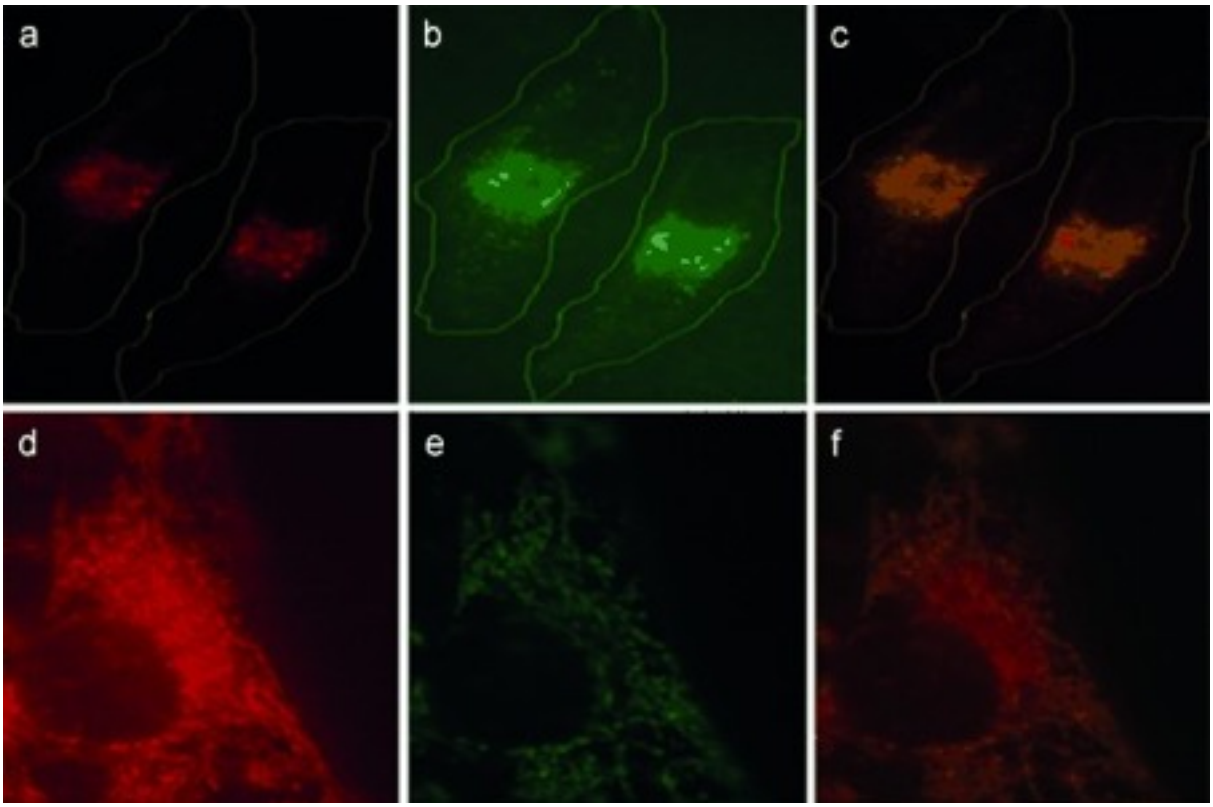

Figure 4.3 Endosomal sequestration of Cbl-BODIPY in HeLa cells. a) HeLa cells treated with 125 nM Cbl-BODIPY kept in the dark. **b)** Rhodamine B-dextran endosomal staining of dark treated HeLa cells. **c)** Overlay a and b. **d)** HeLa cells treated with 125 nM Cbl-BODIPY and illuminated for 15 min with light from an argon lamp filtered through a Cy5 filter cube (500 or 1000 ms every min) **e)** Illuminated cells treated with Mito-Tracker Green mitochondrial staining. **f)** Overlay of d and e. Reprinted with permission.[11]

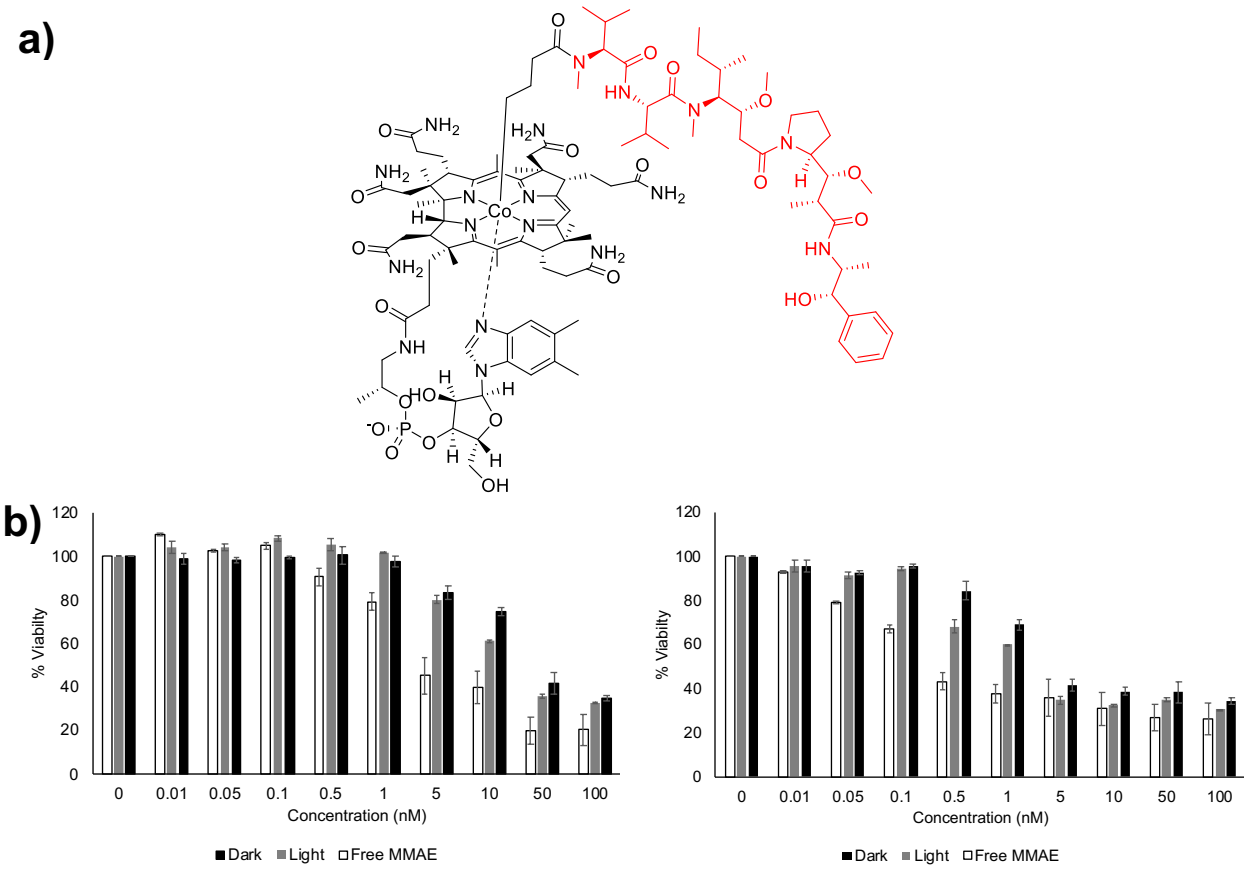

Figure 4.4 Dark Activity of Cbl-MMAE. a) Structure of Cbl-MMAE. **b)** Percentage cell viability of neural stem cells (left) or glioblastoma cells (right) after 72 h of exposure to a range of concentrations (nM) of Cbl-MMAE (black or gray) or control free MMAE (white). Cbl-MMAE was either kept in the dark (black) or illuminated for 30 min at 488 nm (gray) and then incubated for 72 h at 37 ºC.

Table 4-1 EC_{50}'s of Cbl-MMAE or MMAE treating Neural Stem Cells and Glioblastoma.

Cell Type	EC_{50}		
	Dark Cbl-MMAE	Light Cbl-MMAE	Free MMAE
Neural Stem Cell	16 ± 4 nM	7.6 ± 0.9 nM	2.4 ± 0.3 nM
Glioblastoma	1.2 ± 0.1 nM	0.72 ± 0.07 nM	0.12 ± 0.04 nM

The effective concentration that inhibited 50% cell growth (EC_{50}) was calculated for the tested conditions (**Table 4-1**). Although illumination and photorelease improves cytotoxicity of Cbl-MMAE by 2-fold, the nM cytotoxic levels of dark Cbl-MMAE, which only achieve a 10-fold diminished cytotoxicity when compared to free MMAE, suggests potent dark activity of Cbl-MMAE. Although, Cbl could be developed to counter cellular cleavage of therapeutic attachments, these modifications could also eliminate photoresponsivity to long-wavelength light. Thus, a means of sheltering Cbl is required to inhibit the dark therapeutic activity.

The biodistribution of Cbl further underscores the need for a carrier. Initial studies with Cbl-BODIPY highlighted both the enhanced Cbl uptake of tumors, as well as Cbl distribution into the heart, brain, and lungs.[4] More thorough pharmacokinetic (PK) studies observed similar distribution of Cy5-Cbl-Docetaxel (TAX) into the brain and tumor of a xenografted breast cancer mouse model (**Figure 4.5**). The PK of Cy5-Cbl-TAX was also compared to other TAX based DDSs conducted with similar methods in tumor-bearing mice.[16-18] Similar to these other DDSs, Cy5-Cbl-TAX was detected in the tumor at high concentrations up to 3 days. However, Cy5-Cbl-TAX was also detected in brain tissue for 3 days following injection. Unlike Cy5-Cbl-TAX, free TAX is completely cleared from the brain in 2 hours.[16] The localization of a potent TAX derivative into the brain, and potentially other sensitive tissue such as the heart, raises concern for unintended toxicity and severe adverse events. Further, unlike free TAX, Cy5-Cbl-TAX is rapidly cleared from circulation. Cbl≡Cy5 is also similarly cleared as described in Chapter 2 (**Figure 2.10**). Thus, given Cbl's potential dark activity, a strategy is required for sheltering photoactivatable Cbl, diminishing its distribution into sensitive tissue, and improving its circulation time for localized therapeutic release.

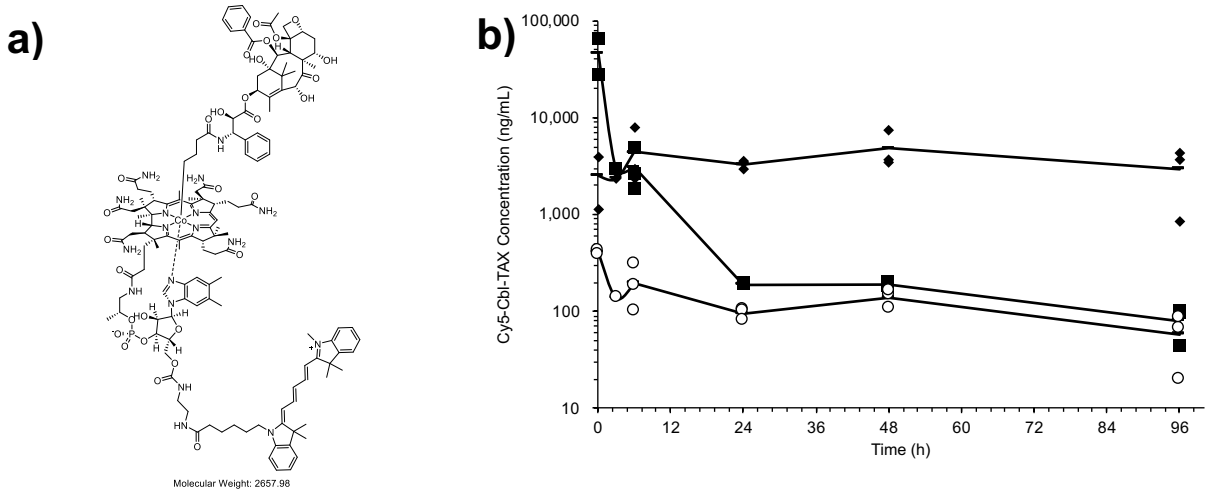

Figure 4.5 Biodistribution of Cy5-Cbl-TAX. a) The structure of Cy5-Cbl-TAX. **b)** Concentration of Cy5-Cbl-TAX over 96 h in MDA-MB-231 xenografted mice brains (circles), plasma (squares), and tumor (diamonds).

4.2 Sheltering Cy5-Cbl Photoactivatable Therapeutics within Carriers

Potential DDSs for arthritis should be able to target the joints. Cbl photoactivatable therapeutics can target therapeutic release to the joints by external stimulation of laser light. However, as discussed in section 4.1 we realized the need to shelter Cbl and modify its biodistribution to improve Cbl-therapeutic bioavailable for targeting to the joints. We preferred a long-circulating carrier to diminish the amount of infusions required during treatment of this chronic disease, which eliminated many NPs as potential options. Further, although direct injection of slow-release hydrogels has been approved for arthritis, we preferred avoiding painful injections into the joints.[19] Thus, when considering potential carriers to shelter Cbl therapeutics, we considered a membrane-based carrier which could take advantage of Cbl's inherent non-cell permeable properties. Given the carriers discussed in Chapter 1, internally loaded long-circulating red blood cells (RBCs) provide multiple benefits as a carrier. Not only can RBCs shelter and improve circulation of Cbl species (clinically tested internally loaded RBCs circulate up to ~25 days) diminishing the number of intravenous infusions, but also the availability of home laser devices provides the opportunity for patient-directed therapeutic release.[20, 21]

4.2.1 Optimization and Validation of RBC carriers

Initial optimization studies of RBC carriers with already synthesized Cy5-Cbl-chemotherapeutic species focused on ensuring internally loaded RBCs preserve the light-dependent activity of Cbl and minimize the previously observed dark activity discussed in section 4.1. Methotrexate (MTX), colchicine, paclitaxel, and docetaxel (TAX) were appended to Cy5-Cbl or FL800-Cbl which were subsequently loaded into RBCs. Initial studies with Cbl-BODIPY RBCs confirmed BODIPY release and escape from RBCs after 3 min of LED illumination. Subsequent *in vitro* photoindex studies of photoreleased MTX confirmed a 3-fold increase in the activity of MTX after illumination. Qualitative microtubule images further validated a light-dependent effect

of colchicine, paclitaxel, and TAX photorelease.[14, 22] The potential orthogonal benefits of Cbl species were also preserved as tested by co-loaded RBCs carrying FL800-Cbl-colchine and Cbl-BODIPY (**Figure 4.6**).[22] Thus, internally loaded Cy5-Cbl RBCs were validated as a method of sheltering Cbl and inhibiting dark activity of multiple chemotherapeutics until light-triggered release by both qualitative HeLa microtubule studies and a quantified effect of MTX in HeLa cells.

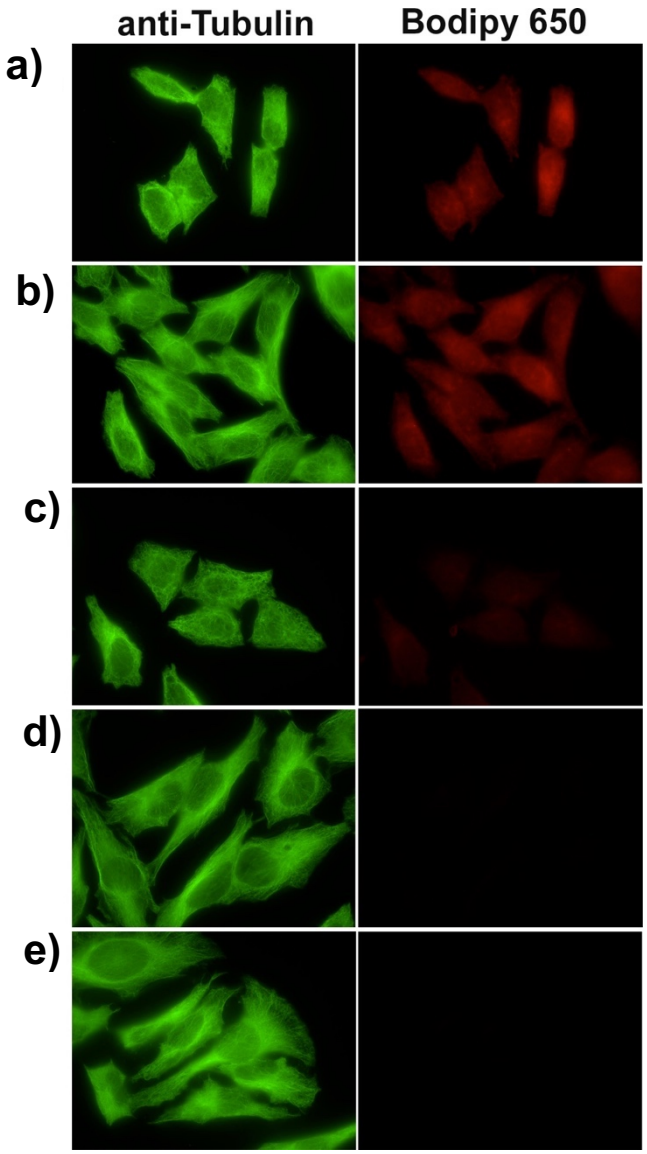

Figure 4.6 Effects of BODIPY or Colchicine orthogonally released from co-loaded FL800-Cbl-Colchicine Cbl-BODIPY RBCs on HeLa cells. The left column shows immunostaining with an anti-tubulin antibody while the right column shows BODIPY fluorescence. **a)** Release of both colchicine (which disrupts the microtubules) and BODIPY (which is uptaken by HeLa cells endosomally) by illumination with 780 nm and 660 nm light respectively. **b)** Release of BODIPY with 660 nm illumination only. **c)** Release of colchicine with 780 nm illumination only. **d)** HeLa cells kept in the dark. **e)** HeLa cells not exposed to RBCs. Reprinted with Permission.[22]

After validating RBCs can shelter and preserve the light-dependent and orthogonal benefits of Cbl PACTs, the RBC Cbl therapeutic system was prepared for *in vivo* validation of chemotherapeutic activity as discussed in Chapter 2.[14] In preparation for animal studies the loading protocol was tested on and optimized for mouse RBCs (mRBCs). Briefly, results demonstrated loaded mRBCs do not affect Cy5 fluorescence of Cy5-Cbl species thus preserving their theranostic potential. Further, a high concentration of Cy5-Cbl-TAX is uniformly loaded into mRBCs (**Figure 2.4**; **Figure 2.5**). Although mRBCs do display significantly diminished integrity as compared to human RBCs (hRBCs), *in vivo* studies were still able to validate that RBCs improve the biodistribution of non-photocleavable Cbl≡Cy5 by localizing the Cbl to the circulation for extended periods of time as compared to free Cbl≡Cy5 (**Figure 2.10**). Further, a localized effect of TAX release is observed in both healthy mouse vasculature and in SVR angiosarcoma mice tumor vasculature (**Figure 2.11**; **Figure 2.13**). The localized *in vivo* effects and general improved biodistribution solidified RBCs as an ideal carrier for Cbl photoactivatable therapeutics. RBSs successfully retain (and potentially enhance) the benefits of Cbl phototherapeutics while overcoming the toxicity risks of dark activity and distribution throughout the body.

4.2.2 Neural Stem Cell-RBC Backpacks

Given the initial success of RBCs to shelter Cy5-Cbl-chemotherapeutics, we also considered the development of neural stem cells (NSCs) as carriers for targeted Cy5-Cbl PACT delivery to gliomas. NSCs have been observed to migrate towards malignant brain tumors.[23, 24] We had initially sought to use NSCs as a means of targeting Cy5-Cbl-MMAE directly to cancerous cells, however, the noted dark activity and high levels of cytotoxicity of MMAE to the NSC posed a challenge to this approach (**Figure 4.4**). Thus, we instead introduced human RBC (hRBC) “backpacks” onto the NSCs as a means of sheltering and inactivating Cy5-Cbl-MMAE while also preserving the inherent migratory capacity of NSCs. hRBCs and NSCs were conjugated to each

other by covalently linking biotin to their surfaces (via an amine-reactive sulfo-NHS-biotin), followed by exposure to tetrameric avidin which has a 1 x 10^{-15} M dissociation constant from biotin (**Figure 4.7a**). Initial optimization of the biotin-avidin linkage resulted in successful biotinylation and avidinylation and further investigation of ideal RBC concentrations showed the degree of backpacking possible (from 1:1 to >10:1 hRBCs:NSCs) (**Figure 4.7b,c**). Both bovine serum albumin - Texas Red fluorophore (BSA-TxRed) internally loaded hRBCs and 1,1-dioctadecyl-3,3,3,3-tetra-methylindodicarbocyanine (DiD) externally loaded hRBCs were successfully adhered to NSCs (**Figure 4.7d**). Further, studies of NSC-RBC migration towards glioblastoma (GBM) confirmed NSCs carrying backpacks retain their migratory capacity (**Figure 4.8**).

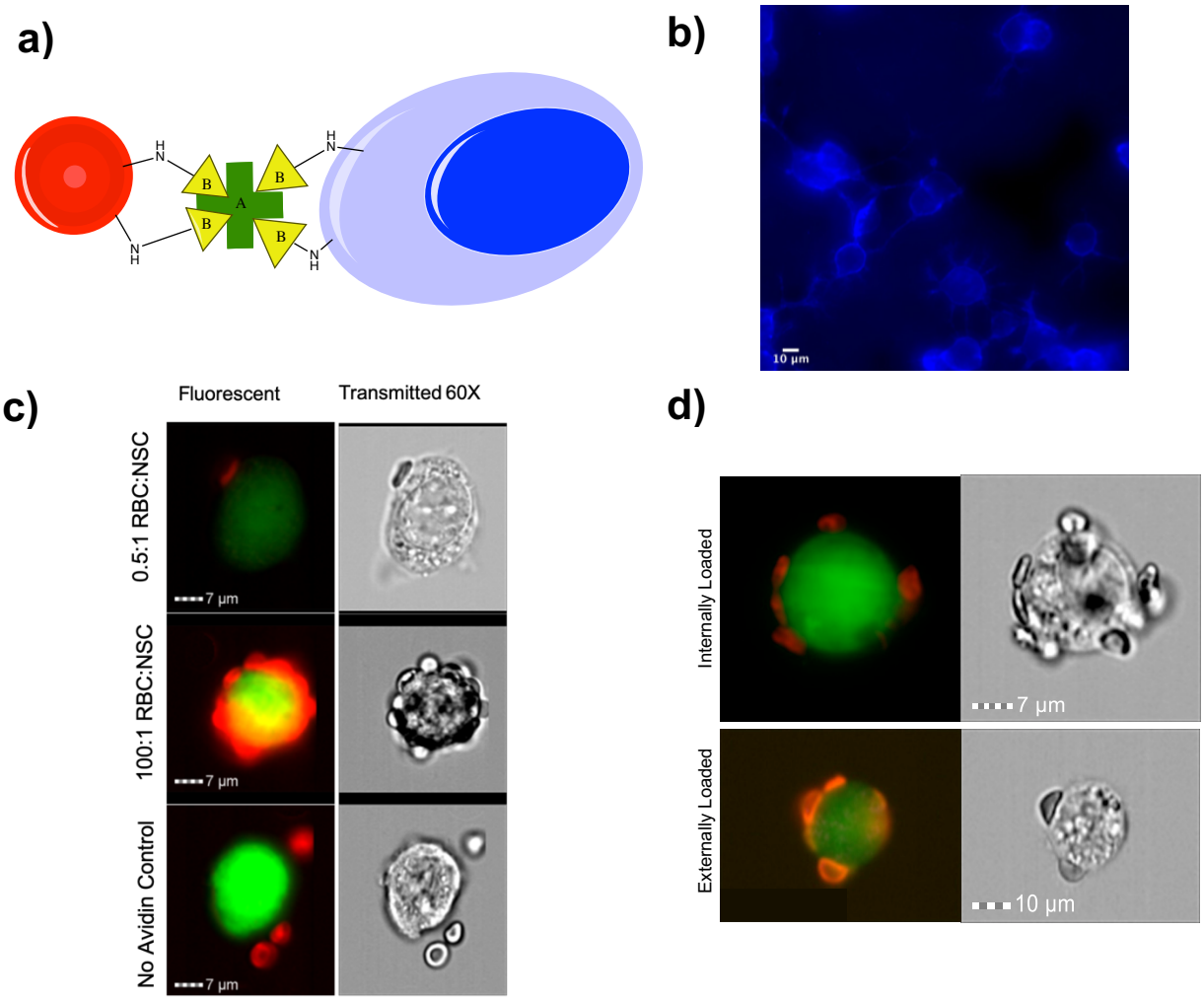

Figure 4.7 Construction of NSC-RBC backpacks. a) Scheme of RBC (red) conjugated to NSC (blue) via a biotin (B) avidin (A) linkage. **b)** Alexafluor555-streptavidin binding to the NSC surface shows successful biotinylation. **c)** and **d)** ImageStream images of composite Cy5 and green fluorescent protein (GFP) images are shown in the left column and transmitted in the right. **c)** hRBCs internally loaded with BSA-TxRed were conjugated to GFP expressing NSCs. A 0.5:1 or 100:1 hRBC: NSC mixture generates 1:1 or >10:1 RBC:NSC conjugates respectively. The No-Avidin control shows non-conjugated hRBCs to an NSC. **d)** Both BSA-TxRed internally loaded hRBCs and DiD externally loaded hRBCs conjugate to NSCs.

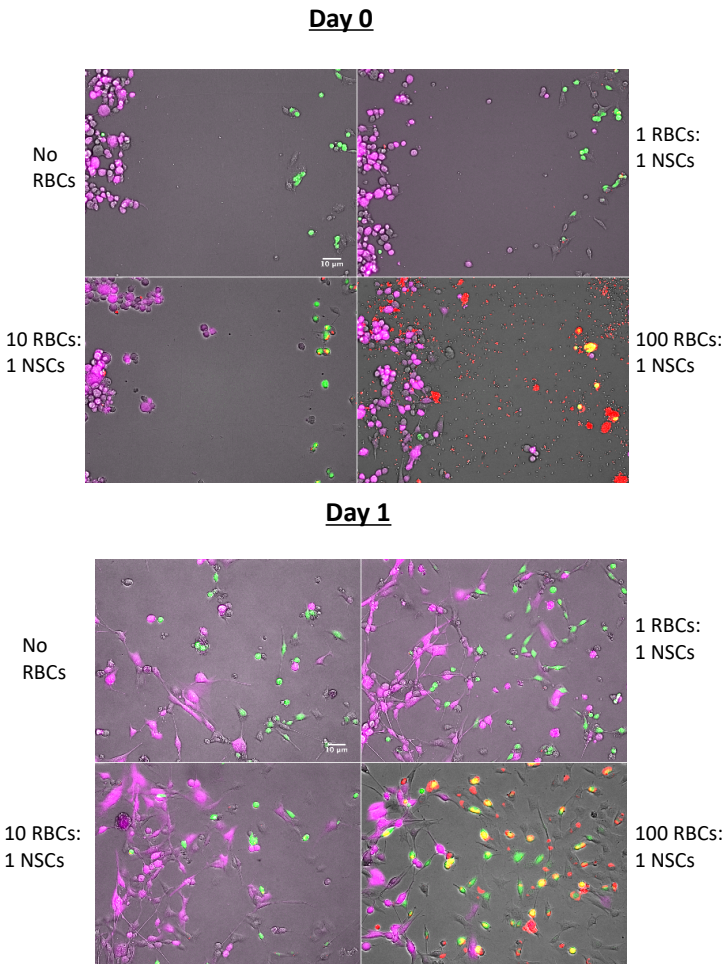

Figure 4.8 Migration of NSC-hRBC backpacks. 10X Olympus widefield images of externally loaded DiD hRBCs were conjugated to GFP expressing NSCs and then plated and allowed to migrate for 24 h toward mCherry expressing GBMs. On day 0 (top) NSC groups were not interspersed with GBM cells. On day 1 (bottom) NSCs (green) or live NSC-RBCs (yellow) migrate toward GBM cells. Mixtures of 100:1 RBC:NSCs show clear, persistent conjugation during migration.

In preparation for multi-day *in vivo* studies of NSC migration to GBM across the mouse brain, the attachment of hRBCs and NSCs over multiple days was assessed with widefield microscopy and ImageStream flow cytometry. While both externally loaded and internally loaded hRBCs (with external biotinylation and streptavidinylation) display minimal lysis and leakage at 37 °C over multiple days (**Figure 4.9**), breakdown of the attachment was qualitatively observed after 3 days at 37 °C for both internally and externally loaded hRBCs (**Figure 4.10a,b**). ImageStream analysis of backpacked NSCs confirmed the loss of adhered RBCs after a 3 day period, potentially due to endosomal uptake of biotin labeling and release of attached hRBCs which then cluster with each other (**Figure 4.10c**). Although RBCs are a solution to shelter chemotherapeutics, backpack linkages face challenges with multi-day *in vitro* and *in vivo* studies with endosomally active and replicating NSCs.

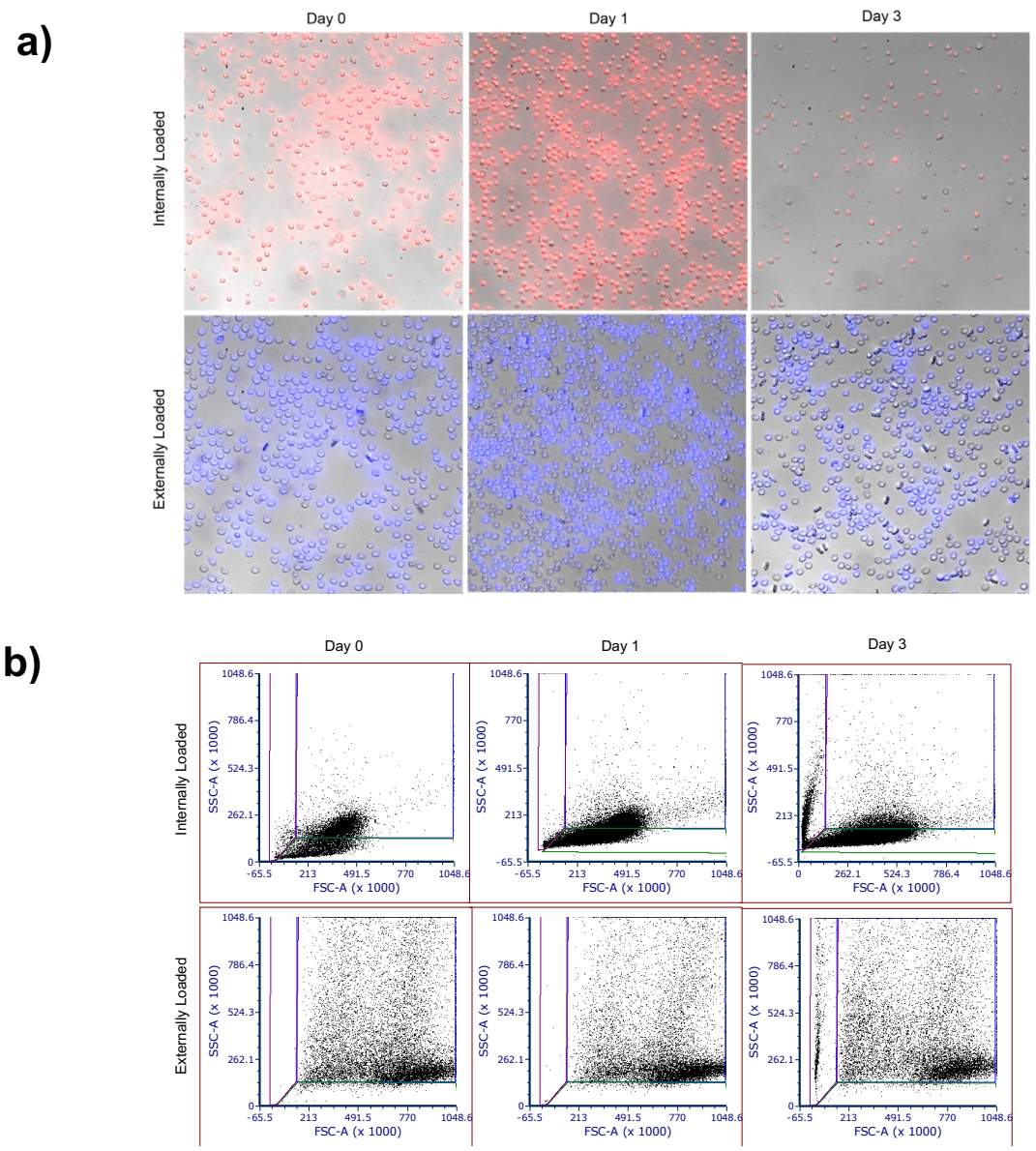

Figure 4.9 Internally loaded BSA-TxRed and externally loaded DiD hRBC integrity after incubating for 0, 1, and 3 days at 37 °C. a) Widefield images of internally loaded (top) and externally loaded hRBCs (bottom). **b)** Flow cytometry dot plots of forward light scatter (FSC) reflecting cell shape versus side light scatter (SSC) reflecting cell granularity over time.

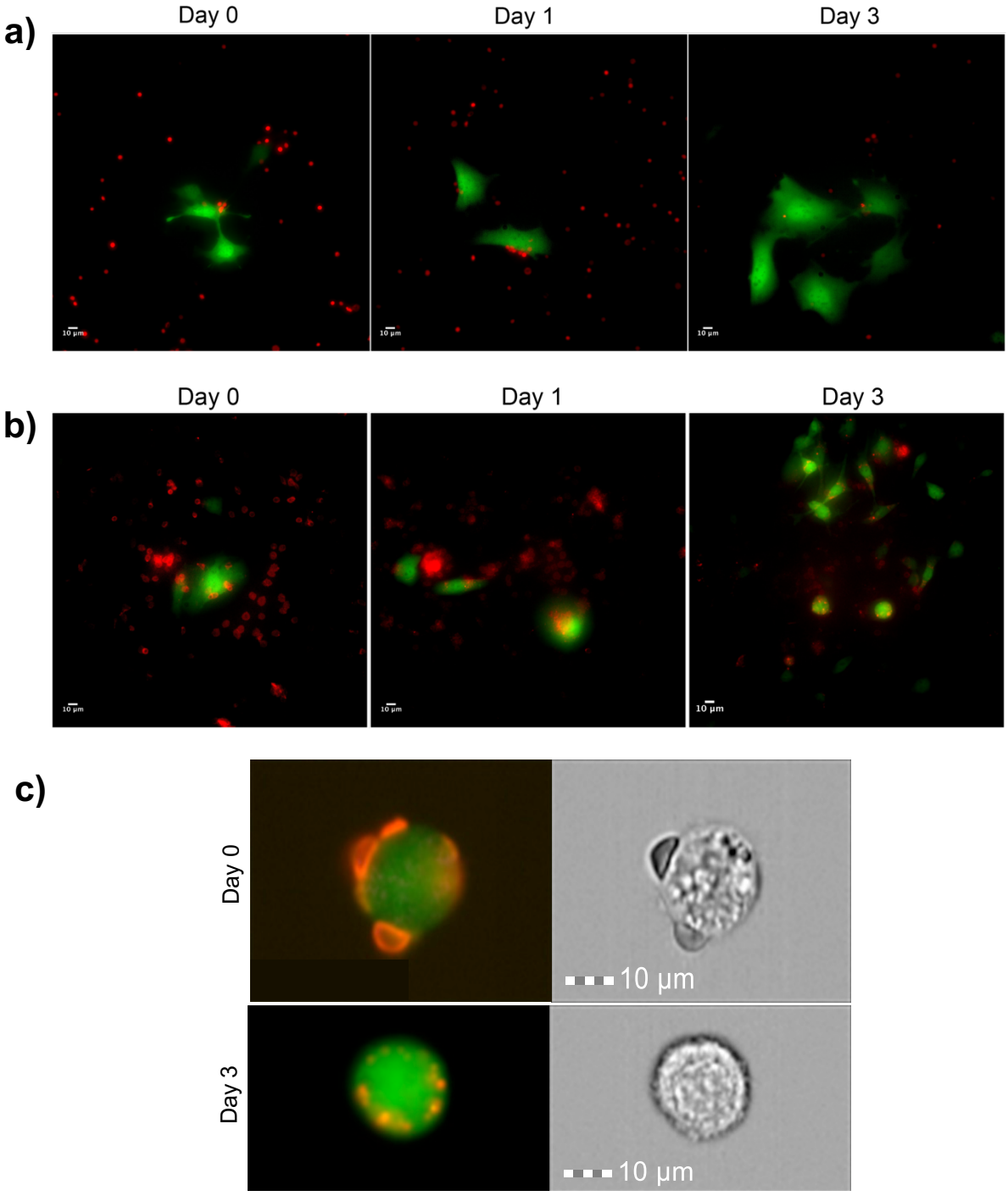

Figure 4.10 Breakdown of RBC-NSC backpacks over time. GFP expressing NSCs were conjugated to a) internally loaded BSA-TxRed RBCs or **b)** and **c)** externally loaded DiD RBCs. **a)** and **b)** Widefield images of conjugated cells over 3 days show breakdown of conjugation. **c)** ImageStream images of NSCs do not show conjugation to RBCs after 3 days.

4.3 Pre-Clinical Development of Cy5-Cbl-Dex RBCs

Thus, having validated Cbl RBCs as a photoactivatable therapeutic with localized delivery, we shifted development towards the arthritis indication. Cbl RBCs have the potential to address multiple unmet clinical needs in this indication including improving safety of chronically used drugs and providing a means for patient-directed treatment. We specifically decided to move forward with dexamethasone (Dex) a glucocorticoid. Glucocorticoids are often employed in the short-term transition to and establishment of disease modifying anti-rheumatic drug treatment.[25] Although glucocorticoids are extremely effective at reducing symptoms of inflammation, pain, and disability, their chronic use is associated with severe adverse effects, including osteoporosis, fractures, diabetes, infections, and more.[26] Since at least one-third of patients persistently use glucocorticoids as part of their treatment there is an unmet medical need to diminish the adverse effects of these potent drugs.[27, 28] Many novel carrier-based delivery methods for glucocorticoids are under development, but only a few have been tested in clinic including delayed-release prednisone tablets, long-circulating liposomal prednisone, and slow-release Dex RBCs.[28-31] Photoactivatable Cy5-Cbl-Dex RBCs can expand current treatments by offering a means of patient-directed localized release to treatment sites, diminishing systemic adverse effects. Further, the long-circulation time of internally loaded RBCs (~25 days) will allow for chronic localized treatment over a month.

My thesis work focused on finalizing the *in vitro* development of Cy5-Cbl-Dex RBCs and transitioning to *in vivo* pre-clinical development as discussed in Chapter 3. I first characterized loaded human RBCs (hRBCs), finding that although loaded mRBCs and hRBCs are similar to each other, the loading process dramatically decreases the mean cell hemoglobin and also affects the mean cell volume when compared to non-modified native RBCs (**Table 3-1**). Although these changes do not meet the pre-requisite of <20% changes in physical characteristics for long-term transfusion, they were sufficient for our initial pre-clinical tests. More rigorous *in vitro* assays were

also conducted to assess the light-dependent nature and safety of Cy5-Cbl species. Illuminated Cy5-Cbl-Dex hRBCs had a comparable effect to similar concentrations of conventional Dex on HeLa cells, primary fibroblast like synoviocytes (FLS), and Sup-B15 cells. HeLa and FLS immunocytochemical studies further confirmed that Cy5-Cbl-Dex RBCs have a minimal effect on the Dex-target glucocorticoid receptor α (GRα) in the dark, but comparable to conventional Dex after illumination. Thus, Cy5-Cbl-Dex RBCs retain Dex's pharmacological activity. *In vitro* toxicity studies confirmed that the illuminated control Cy5-Cbl-H_2O hRBC has no effect on cell viability while illuminated Cy5-Cbl-Dex RBCs have a comparable effect to conventional Dex on Sup-B15 and FLS cell viability (**Figure 3.10**; **Figure 3.11**; **Figure 3.13**). FLS and Sup-B15 were specifically investigated since FLS and B cells are crucial mediators of the inflammatory arthritic response and targets of Dex activity.[32, 33]

In vivo studies were performed to quantify the bioavailability of Cy5-Cbl-Dex mRBCs. Cy5-Cbl-Dex mRBCs loaded by an optimized protocol as compared to the protocol employed in Chapter 2, do circulate for at least 1 h, the required amount of time for illumination and therapeutic release. However, clearance is observed within 24 h (**Figure 3.14**). Excitingly, intravenously injected loaded Cy5-Cbl-Dex RBCs achieve the remission of arthritis in the acute collagen antibody induced arthritis (CAIA) model similar to that of conventional Dex injected intraperitoneally (**Figure 3.15**). Moreover, loaded RBCs produce a more efficient and persistent response as compared to conventional Dex. However, the exact cause of the difference is not yet clear due to differences in injection method (and thus bioavailability) along with treatment.

Thus, both *in vitro* and *in vivo* studies served to characterize Cy5-Cbl-Dex RBCs. Specifically, studies demonstrated their *in vitro* properties, confirmed *in vitro* safety of Cy5-Cbl RBCs, and confirmed minimal dark activity in the nM sensitive HeLa immunohistochemical assay. Further, initial animal studies demonstrated similar efficacy of Cy5-Cbl-Dex RBCs to standard of care.

4.4 Next Steps for Cy5-Cbl RBC Development

As demonstrated by the exciting pre-clinical results, Cy5-Cbl-Dex RBCs are poised for a more thorough pre-clinical investigation (see **Figure 4.1**). Although experiments with Cy5-Cbl-TAX have demonstrated localized release in both tumor and healthy vasculature, the localized effect of Dex needs to be similarly assessed. In both the acute CAIA model, as well as in a more chronic but less aggressive mouse model, Dex could be locally released from Cy5-Cbl-Dex RBCs in mice who present inflammation in more than one paw.[34, 35] In such models, the efficacy should be limited to only the illuminated paw. However, such studies require long-term circulation of mRBCs. If the therapeutic is systemically released within 24 h, these studies will not properly assess long-term Cy5-Cbl-Dex efficacy for more chronic treatment and subsequent chronic indications. The in-depth discussion in section 4.4.1 describes the current status of Cy5-Cbl-Dex mRBC integrity, PK, and clearance studies. Another control that should be included in future animal studies is a dark mouse control, which receives Cy5-Cbl-Dex RBCs but is not illuminated. Such a control will help assess for dark activity and begin to establish an *in vivo* photoindex of spatial and temporal delivery of Dex from circulating Cy5-Cbl-Dex mRBCs. Along with an *in vivo* photoindex, a more rigorously quantified *in vitro* photoindex could support *in vivo* findings. Multiple *in vitro* studies have already validated light-dependent efficacy and consistently indicated an improved photoindex. However, quantification of the photoindex is still required and can be performed by quantifying GRα localization in sensitive GRα cell lines in response to Cy5-Cbl-Dex RBCs.[36]

Another facet that should be thoroughly investigated before conducting more rigorous animal studies is ensuring the light dosage is sufficiently high to photoactivate Dex in mouse paws. Although thorough PK studies of the joint tissue and vasculature would be the ideal method to quantify and ensure therapeutic release after the 5 mW 5 min treatment, previous groups have conducted cyanine bleaching studies as measured by optical imaging to ensure that sufficient

light penetrates tissue and activates the photoactivatable therapeutic.[37] Another option is employing Cbl-BODIPY650 similar to its previous use in assessing biodistribution of Cbl in tumors.[4] BODIPY650 is highly cell permeable and when conjugated to Cbl should still activate photocleavage in response to near infrared wavelengths similar to previous results from studies of Cbl-BODIPY. Initial studies with Cbl-BODIPY650 RBCs, or ideally FL800-Cbl-BODIPY650, would provide a means of measuring "therapeutic" release, distribution, and localization for both *in vivo* light dosage and localization studies.[38] Of course, this system is only an imaging control and preliminary findings with the BODIPY derivative would need to be quantified with rigorous PK studies of the Dex derivative.

Once these initial studies validate the *in vivo* localized efficacy of Cy5-Cbl-Dex RBCs, it is important to initiate toxicology studies and the optimization of manufacturing techniques for scaling up synthesis to clinical needs and meeting good manufacturing practice (GMP) requirements. Specifically, good laboratory practice (GLP) toxicology studies should thoroughly quantify the extent of therapeutic exposure as well as follow-up on the potential damage from Cy5-generated reactive oxygen species noted in Chapter 2 (**Figure 2.12**). Since Cy5-Cbl-Dex RBCs will be a chronic "slow-release" treatment, longer-term toxicity studies will need to be performed to account for the extended 28-day circulation of these modified RBCs. Manufacturing studies will require optimization of the light-sensitive Cbl syntheses as well as development of technology for loading RBCs. Conversely, a partnership with EryDel and their Red Cell Loader may minimize the RBC manufacturing required before clinical translation.[39] However, initial pre-clinical validation and characterization are required before considering GMP manufacturing and GLP toxicology studies are underway.

4.4.1 Cy5-Cbl mRBC Integrity Challenges

Although extensive *in vitro* and *in vivo* investigations into mRBC loading processes have already been conducted, circulation of mRBCs from our current methods is still limited to at-most to 24 h. Initially, with the clinical precedent set by the Red Cell Loader, a hypotonic dialysis method was selected and optimized.[39] As discussed in Chapter 2, mouse RBCs (mRBCs) display significant instability *in vitro* which is further decreased upon dialysis loading (**Figure 2.6**).[14] Thus, in preparation for the animal efficacy studies conducted in Chapter 3, optimization of mRBC stability was further conducted. The dialysis and reseal conditions were optimized, supplemental stabilizing components were added, and a high-salt reseal step was introduced. Although these changes did extend circulation as noted in Chapter 3 (**Figure 3.4**), the current optimized protocol established still displays significant clearance from circulation within 3 h (**Figure 4.11**). Based on the histology results discussed in Chapter 3, a noted increase in fluorescence within the spleen occurs over 24 h and significant fluorescence emerges in the kidney at 24 h (**Figure 3.14**). The loaded mRBCs may be cleared from circulation by initial capture within the spleen, wherein they are broken down, and the remaining Cy5-Cbl species further processed in the liver and cleared through the kidney after 24 h.[40]

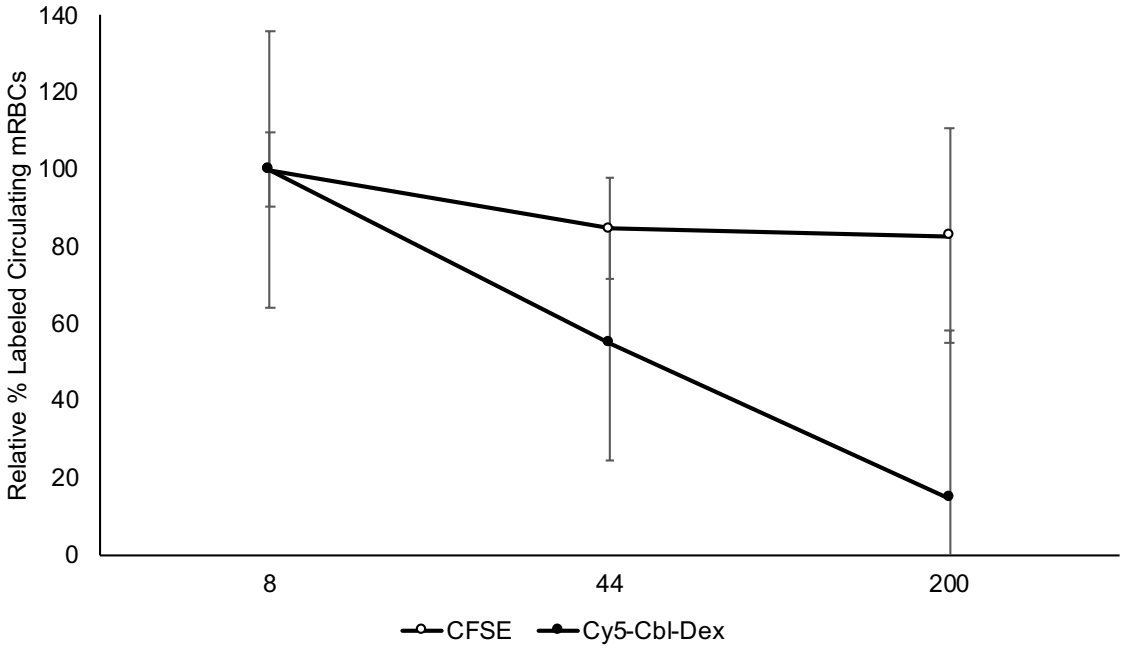

Figure 4.11 Clearance of loaded mRBCs within 3 h. A mixture of internally stained carboxyfluorescein succinimidyl ester (CFSE) mRBCs and internally loaded Cy5-Cbl-Dex mRBCs were intravenously injected into healthy DBA1J mice. Circulation over 3 h was monitored by sacking and collecting blood from mice via cardiac puncture. Over 3 h, internally loaded Cy5-Cbl-Dex mRBCs (filled circle) are cleared from circulation while control CFSE-stained mRBCs (open circle) continue circulating.

Thus, I investigated alternate methods of internally loading mRBCs in preparation for multi-day animal studies. Specifically, a previously published method that further improved upon the high-salt loading protocol employed in Chapter 3 and successfully achieved 9 days of circulation with loaded mRBCs was tested. The protocol requires doubling the circulation and resealing times and addition of stabilizing factors (including ATP, adenine, inosine, glucose, etc.) to all solutions of the original protocol employed in Chapter 3.[41, 42] Widefield images show morphologically similar loaded mRBCs from both the Chapter 3 protocol and the extended loading protocol. However, the extended loading produces less fluorescent mRBCs (**Figure 4.12a**). Semi-qualitative analysis with flow cytometry confirms these findings, as the extended protocol produces non-uniformly fluorescent mRBCs unlike the original protocol which uniformly loads the mRBCs (**Figure 4.12b**). The morphology of native mRBCs, of mRBCs loaded with the Chapter 3 protocol, and mRBCs loaded with the extended protocol was assessed by flow cytometry forward light scatter (FSC; which assesses mRBC shape) and side light scatter (SSC; which assess the granularity of the mRBC interior). Overlay of a native mRBC population gate onto the loaded mRBCs estimates nearly 3-fold more mRBCs from the extended loading fall within the native gate as compared to mRBCs loaded by the Chapter 3 protocol (**Figure 4.12b**). As previously discussed in Chapter 1, loaded RBCs should ideally demonstrate only a 20% change in characteristics from native RBCs to maintain necessary long-term circulation stability.[20, 43] Thus, although the efficiency of therapeutic loading is decreased during the extended loading, the improved preservation of shape and granularity may improve circulation. Further, the loss in drug loading efficiency may be more in line with the Red Cell Loader, which only encapsulates 30 ± 3% drug.[44] Of course, animal circulation studies are the true standard by which an ideal loading protocol should be optimized. Future studies should continue to assess and optimize *in vivo* circulation in preparation for longer-term efficacy and toxicity studies in chronic treatment models.

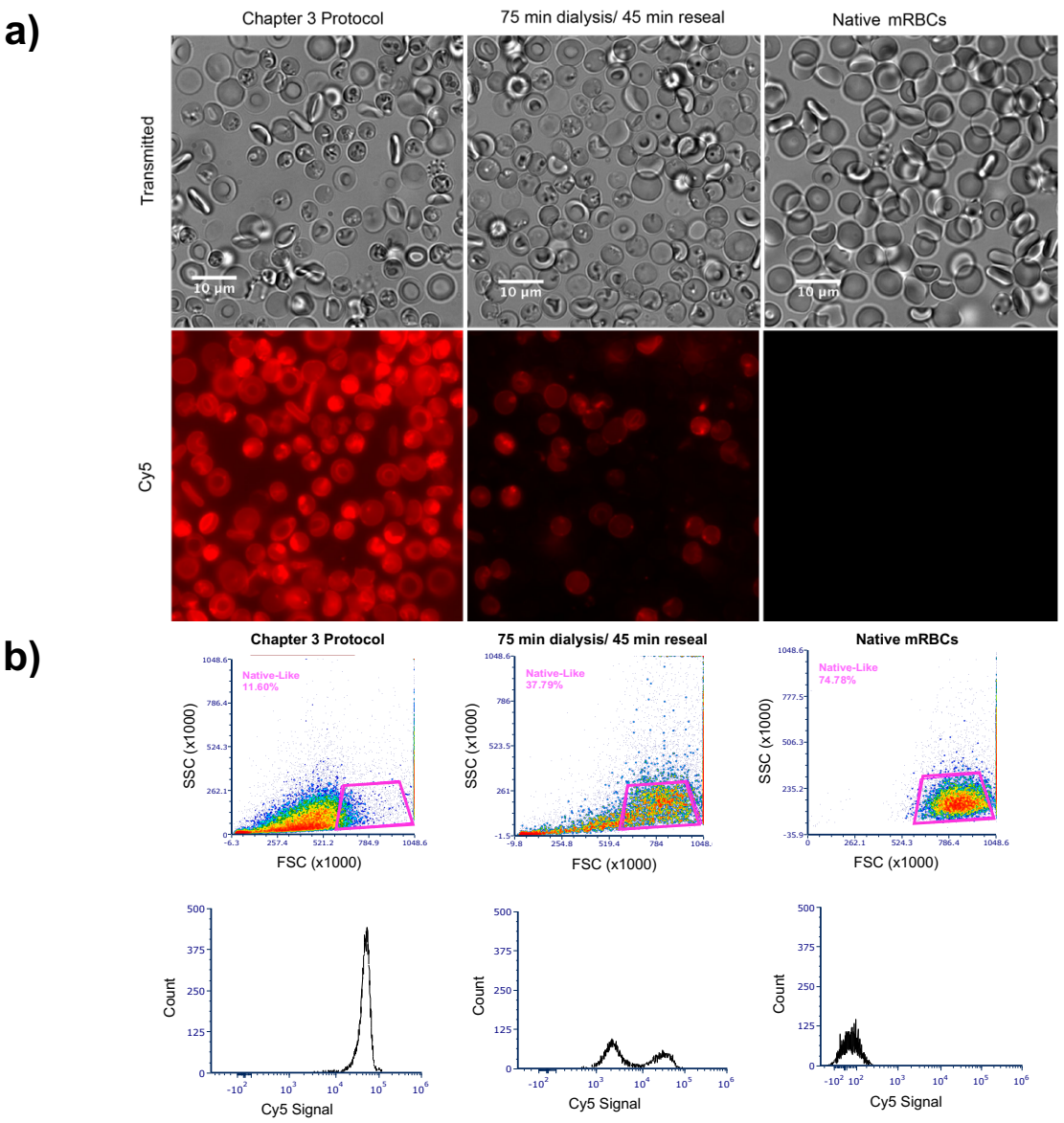

Figure 4.12 Analysis of two lead loading protocols for stabilizing mRBCs *in vivo*. a) Widefield images of mRBCs loaded by the protocol from Chapter 3 (left column), the experimental protocol (middle column), and native mRBCs (right column). **b)** Flow cytometry dot plots of forward light scatter (FSC) reflecting cell shape versus side light scatter (SSC) reflecting cell granularity over time of the protocol from Chapter 3, experimental protocol, and native mRBCs (top). Histogram of Cy5 signal of loaded mRBCs (bottom).

4.5 Conclusion

Since the initial development of long-wavelength photoresponsive Cbl moieties in 2014, an array of Cy5-Cbl photoactivatable therapeutics have been described and multiple therapies have entered pre-clinical testing.[11] Starting with the development of cancer treatments, Cbl derivatives maintain the pharmacological activity of appended chemotherapeutics and release chemotherapeutics in response to light. However, Cbl derivatives also significantly distribute throughout the body and display dark activity *in vitro*. Thus, RBCs were introduced as potential carriers for Cy5-Cbl therapeutics.[22] Since then, these Cy5-Cbl RBC therapeutic DDSs have been shown to shelter Cy5-Cbl therapeutics, extend their circulation time, locally release the therapeutic, and achieve comparable efficacy to a standard of care control. Specifically, both Cy5-Cbl-TAX and Cy5-Cbl-Dex RBCs have been tested *in vivo*.

Currently, arthritis is our lead indication due to the persistent unmet clinical need to make glucocorticoids less toxic.[28, 30] Cy5-Cbl-Dex RBCs can improve efficacy and safety as compared to these clinical therapeutics, as well as provide a novel means for patient-directed therapeutic release. In general, the Cbl RBC system has proven safe *in vitro* and *in vivo*. Further GLP studies are needed to assess potential toxicity from reactive oxygen species generated by Cy5. In addition, a long-term (weeks for rodents, months for primates) circulating system is required to validate the extent of directed treatment in small and large chronic arthritis animal models. Further controls showing light-dependent and localized efficacy *in vivo* need to be conducted before shifting into large-scale GLP toxicology and GMP manufacturing studies. The work conducted herein has established the required assays for quality assurance, poised Cy5-Cbl-Dex RBCs for further pre-clinical testing and eventual GXP studies, and set a path to the clinic for photoactivatable Cy5-Cbl RBC therapeutics.

REFERENCES

1. Brown, K. L., Chemistry and Enzymology of Vitamin B12. *Chemical Reviews* **2005,** *105* (6), 2075-2150.

2. Rickes, E. L.; Brink, N. G.; Koniuszy, F. R.; Wood, T. R.; Folkers, K., Crystalline Vitamin B12. *Science* **1948,** *107* (2781), 396-397.

3. Jones, A. R., The photochemistry and photobiology of vitamin B12. *Photochemical & Photobiological Sciences* **2017,** *16* (6), 820-834.

4. Gendron, L. N.; Zites, D. C.; LaRochelle, E. P. M.; Gunn, J. R.; Pogue, B. W.; Shell, T. A.; Shell, J. R., Tumor targeting vitamin B12 derivatives for X-ray induced treatment of pancreatic adenocarcinoma. *Photodiagnosis and Photodynamic Therapy* **2020,** *30*, 101637.

5. Bagnato, J. D.; Eilers, A. L.; Horton, R. A.; Grissom, C. B., Synthesis and Characterization of a Cobalamin−Colchicine Conjugate as a Novel Tumor-Targeted Cytotoxin. *The Journal of Organic Chemistry* **2004,** *69* (26), 8987-8996.

6. Firestein, G. S., Evolving concepts of rheumatoid arthritis. *Nature* **2003,** *423* (6937), 356-361.

7. Aletaha, D.; Smolen, J. S., Diagnosis and Management of Rheumatoid Arthritis: A Review. *JAMA* **2018,** *320* (13), 1360-1372.

8. Burmester, G. R.; Pope, J. E., Novel treatment strategies in rheumatoid arthritis. *The Lancet* **2017,** *389* (10086), 2338-2348.

9. Gibofsky, A.; Galloway, J.; Kekow, J.; Zerbini, C.; de la Vega, M.; Lee, G.; Lee, E. Y.; Codreanu, C.; Koehn, C.; Steinberg, K.; Bananis, E.; de Leon, D. P.; Maniccia, A.; Dikranian, A.; for the, R. A. N. g. a. p., Comparison of patient and physician perspectives in the management of rheumatoid arthritis: results from global physician- and patient-based surveys. *Health and Quality of Life Outcomes* **2018,** *16* (1), 211.

10. Kobayashi, H.; Ogawa, M.; Alford, R.; Choyke, P. L.; Urano, Y., New Strategies for Fluorescent Probe Design in Medical Diagnostic Imaging. *Chemical Reviews* **2010,** *110* (5), 2620-2640.

11. Shell, T. A.; Shell, J. R.; Rodgers, Z. L.; Lawrence, D. S., Tunable Visible and Near-IR Photoactivation of Light-Responsive Compounds by Using Fluorophores as Light-Capturing Antennas. *Angewandte Chemie International Edition* **2014,** *53* (3), 875-878.

12. Rodgers, Z. L. COBALAMIN-FLUOROPHORES' PHOTOCHEMISTRY AND BIOMEDICAL APPLICATIONS. Dissertation, The University of North Carolina at Chapel Hill, 2016.

13. Zywot, E. M.; Orlova, N.; Ding, S.; Rampersad, R. R.; Rabjohns, E. M.; Wickenheisser, V. A.; Wang, Q.; Welfare, J. G.; Haar, L.; Eudy, A. M.; Tarrant, T. K.; Lawrence, D. S., Light Directed Therapeutic Delivery to Arthritic Joints. *Science Advances* **2021**.

14. Marvin, C. M.; Ding, S.; White, R. E.; Orlova, N.; Wang, Q.; Zywot, E. M.; Vickerman, B. M.; Harr, L.; Tarrant, T. K.; Dayton, P. A.; Lawrence, D. S., On Command Drug Delivery via Cell-Conveyed Phototherapeutics. *Small* **2019,** *15* (37), 1901442.

15. Nielsen, M. J.; Rasmussen, M. R.; Andersen, C. B. F.; Nexø, E.; Moestrup, S. K., Vitamin B12 transport from food to the body's cells—a sophisticated, multistep pathway. *Nature Reviews Gastroenterology & Hepatology* **2012,** *9* (6), 345-354.

16. Sambade, M.; Deal, A.; Schorzman, A.; Luft, J. C.; Bowerman, C.; Chu, K.; Karginova, O.; Swearingen, A. V.; Zamboni, W.; DeSimone, J.; Anders, C. K., Efficacy and pharmacokinetics of a modified acid-labile docetaxel-PRINT(®) nanoparticle formulation against non-small-cell lung cancer brain metastases. *Nanomedicine (Lond)* **2016,** *11* (15), 1947-1955.

17. Peng, L.; Schorzman, A. N.; Ma, P.; Madden, A. J.; Zamboni, W. C.; Benhabbour, S. R.; Mumper, R. J., 2'-(2-bromohexadecanoyl)-paclitaxel conjugate nanoparticles for the treatment of non-small cell lung cancer in an orthotopic xenograft mouse model. *Int J Nanomedicine* **2014,** *9*, 3601-3610.

18. Chu, K. S.; Schorzman, A. N.; Finniss, M. C.; Bowerman, C. J.; Peng, L.; Luft, J. C.; Madden, A. J.; Wang, A. Z.; Zamboni, W. C.; DeSimone, J. M., Nanoparticle drug loading as a design parameter to improve docetaxel pharmacokinetics and efficacy. *Biomaterials* **2013,** *34* (33), 8424-8429.

19. Ocular Therapeutix, I. Dextenza [Labelling]. Drugs@FDA Database. U.S. Food and Drug Administration. https://www.accessdata.fda.gov/drugsatfda_docs/label/2019/208742s001lbl.pdf (accessed June 16 2021).

20. Bourgeaux, V.; Lanao, J. M.; Bax, B. E.; Godfrin, Y., Drug-loaded erythrocytes: on the road toward marketing approval. *Drug Des Devel Ther* **2016,** *10*, 665-76.

21. Juhász, M. L. W.; Levin, M. K.; Marmur, E. S., A review of available laser and intense light source home devices: A dermatologist's perspective. *Journal of Cosmetic Dermatology* **2017,** *16* (4), 438-443.

22. Hughes, R. M.; Marvin, C. M.; Rodgers, Z. L.; Ding, S.; Oien, N. P.; Smith, W. J.; Lawrence, D. S., Phototriggered Secretion of Membrane Compartmentalized Bioactive Agents. *Angewandte Chemie International Edition* **2016,** *55* (52), 16080-16083.

23. Jeon, J. Y.; An, J. H.; Kim, S. U.; Park, H. G.; Lee, M. A., Migration of human neural stem cells toward an intracranial glioma. *Experimental & Molecular Medicine* **2008,** *40* (1), 84-91.

24. Bagó, J. R.; Alfonso-Pecchio, A.; Okolie, O.; Dumitru, R.; Rinkenbaugh, A.; Baldwin, A. S.; Miller, C. R.; Magness, S. T.; Hingtgen, S. D., Therapeutically engineered induced neural stem cells are tumour-homing and inhibit progression of glioblastoma. *Nature communications* **2016,** *7*, 10593-10593.

25. Allen, A.; Carville, S.; McKenna, F., Diagnosis and management of rheumatoid arthritis in adults: summary of updated NICE guidance. *BMJ* **2018,** *362*, k3015.

26. O'Dell, J. R.; Matteson, E. L. Use of glucocorticoids in the treatment of rheumatoid arthritis. UpToDate. https://www-uptodate-com.libproxy.lib.unc.edu/contents/use-of-glucocorticoids-in-the-treatment-of-rheumatoid-arthritis?search=Use%20of%20glucocorticoids%20in%20the%20treatment%20of%20rheumatoid%20arthritis&source=search_result&selectedTitle=1~150&usage_type=default&display_rank=1 (accessed June 16 2021).

27. Caplan, L.; Wolfe, F.; Russell, A. S.; Michaud, K., Corticosteroid use in rheumatoid arthritis: prevalence, predictors, correlates, and outcomes. *The Journal of Rheumatology* **2007,** *34* (4), 696.

28. Strehl, C.; van der Goes, M. C.; Bijlsma, J. W. J.; Jacobs, J. W. G.; Buttgereit, F., Glucocorticoid-targeted therapies for the treatment of rheumatoid arthritis. *Expert Opinion on Investigational Drugs* **2017,** *26* (2), 187-195.

29. Alten, R.; Holt, R.; Grahn, A.; Rice, P.; Kent, J.; Buttgereit, F.; Gibofsky, A., Morning stiffness response with delayed-release prednisone after ineffective course of immediate-release prednisone. *Scand J Rheumatol* **2015,** *44* (5), 354-8.

30. Lühder, F.; Reichardt, H. M., Novel Drug Delivery Systems Tailored for Improved Administration of Glucocorticoids. *Int J Mol Sci* **2017,** *18* (9), 1836.

31. Castro, M.; Rossi, L.; Papadatou, B.; Bracci, F.; Knafelz, D.; Ambrosini, M. I.; Calce, A.; Serafini, S.; Isacchi, G.; D'Orio, F.; Mambrini, G.; Magnani, M., Long-term Treatment With Autologous Red Blood Cells Loaded With Dexamethasone 21–Phosphate in Pediatric Patients Affected by Steroid-dependent Crohn Disease. *Journal of Pediatric Gastroenterology and Nutrition* **2007,** *44* (4).

32. Hardy, R.; Cooper, M. S., Unravelling how glucocorticoids work in rheumatoid arthritis. *Nature Reviews Rheumatology* **2018,** *14* (10), 566-567.

33. Hardy, R. S.; Raza, K.; Cooper, M. S., Therapeutic glucocorticoids: mechanisms of actions in rheumatic diseases. *Nature Reviews Rheumatology* **2020,** *16* (3), 133-144.

34. Bevaart, L.; Vervoordeldonk, M. J.; Tak, P. P., Evaluation of therapeutic targets in animal models of arthritis: how does it relate to rheumatoid arthritis? *Arthritis Rheum* **2010,** *62* (8), 2192-205.

35. Caplazi, P.; Baca, M.; Barck, K.; Carano, R. A. D.; DeVoss, J.; Lee, W. P.; Bolon, B.; Diehl, L., Mouse Models of Rheumatoid Arthritis. *Veterinary Pathology* **2015,** *52* (5), 819-826.

36. Karra, A. G.; Konstantinou, M.; Tzortziou, M.; Tsialtas, I.; Kalousi, F. D.; Garagounis, C.; Hayes, J. M.; Psarra, A.-M. G., Potential Dissociative Glucocorticoid Receptor Activity for Protopanaxadiol and Protopanaxatriol. *Int J Mol Sci* **2019,** *20* (1), 94.

37. Nani, R. R.; Gorka, A. P.; Nagaya, T.; Yamamoto, T.; Ivanic, J.; Kobayashi, H.; Schnermann, M. J., In Vivo Activation of Duocarmycin–Antibody Conjugates by Near-Infrared Light. *ACS Central Science* **2017,** *3* (4), 329-337.

38. Myochin, T.; Hanaoka, K.; Komatsu, T.; Terai, T.; Nagano, T., Design Strategy for a Near-Infrared Fluorescence Probe for Matrix Metalloproteinase Utilizing Highly Cell Permeable Boron Dipyrromethene. *Journal of the American Chemical Society* **2012,** *134* (33), 13730-13737.

39. Magnani, M.; Rossi, L.; D'Ascenzo, M.; Panzani, I.; Bigi, L.; Zanella, A., Erythrocyte engineering for drug delivery and targeting. *Biotechnology and Applied Biochemistry* **1998,** *28* (1), 1-6.

40. Mebius, R. E.; Kraal, G., Structure and function of the spleen. *Nature Reviews Immunology* **2005,** *5* (8), 606-616.

41. Antonelli, A.; Sfara, C.; Mosca, L.; Manuali, E.; Magnani, M., New Biomimetic Constructs for Improved In Vivo Circulation of Superparamagnetic Nanoparticles. *Journal of nanoscience and nanotechnology* **2008,** *8*, 2270-8.

42. Antonelli, A.; Sfara, C.; Weber, O.; Pison, U.; Manuali, E.; Salamida, S.; Magnani, M., Characterization of ferucarbotran-loaded RBCs as long circulating magnetic contrast agents. *Nanomedicine* **2016,** *11* (21), 2781-2795.

43. Gothoskar, A. V., Resealed Erythrocytes: A Review. *Pharmaceutical Technology* **2004**, 140-158.

44. Magnani, M., Engineered red blood cells as therapeutic agents. *American Journal of Hematology* **2017,** *92* (10), 979-980.